

The University of Maine

DigitalCommons@UMaine

Electronic Theses and Dissertations

Fogler Library

Spring 5-2022

Development of Thermoplastic Composite External Reinforcing of Concrete Decking System

Jackman A. Mickiewicz

University of Maine, jackman.mickiewicz@maine.edu

Follow this and additional works at: <https://digitalcommons.library.umaine.edu/etd>



Part of the [Civil Engineering Commons](#), [Manufacturing Commons](#), and the [Structural Engineering Commons](#)

Recommended Citation

Mickiewicz, Jackman A., "Development of Thermoplastic Composite External Reinforcing of Concrete Decking System" (2022). *Electronic Theses and Dissertations*. 3562.

<https://digitalcommons.library.umaine.edu/etd/3562>

This Open-Access Thesis is brought to you for free and open access by DigitalCommons@UMaine. It has been accepted for inclusion in Electronic Theses and Dissertations by an authorized administrator of DigitalCommons@UMaine. For more information, please contact um.library.technical.services@maine.edu.

**DEVELOPMENT OF THERMOPLASTIC COMPOSITE EXTERNAL REINFORCING OF
CONCRETE DECKING SYSTEM**

By

Jackman Andrew Mickiewicz

B.S. University of Maine, 2019

A THESIS

Submitted in Partial Fulfillment of the

Requirements for the Degree of

Master of Science

(in Civil Engineering)

The Graduate School

The University of Maine

May 2022

Advisory Committee:

Dr. William Davids, Professor of Civil Engineering, Co-Advisor

Dr. Roberto A. Lopez-Anido, Professor of Civil Engineering, Co-Advisor

Dr. Eric Landis, Professor of Civil Engineering

Copyright 2022 Jackman Andrew Mickiewicz

**DEVELOPMENT OF THERMOPLASTIC COMPOSITE EXTERNAL REINFORCING OF
CONCRETE DECKING SYSTEM**

By

Jackman Andrew Mickiewicz

Thesis Advisors: Dr. William Davids and Dr. Roberto A. Lopez-Anido

An Abstract of the Thesis Presented

in Partial Fulfillment of the Requirements for the

Degree of Master of Science

(in Civil Engineering)

May 2022

The use of reinforced concrete is very common in the construction of a wide variety of structures. In buildings it is used for floors, beams, columns, and walls. It can also be used in infrastructure as parts of bridges, dams, pavements, etc. Typically, concrete is reinforced with steel, primarily rebar, to carry tensile stresses.

Like every other industry, construction is always looking at ways to advance its technology. The work outlined in this thesis looks to assist in that goal, primarily by looking at options for using a different material than the traditional steel reinforcements to create a reinforced concrete system. Steel-reinforced concrete is susceptible to corrosion from being exposed to the elements and

chemicals, like salts. Which reinforced concrete structures frequently experience, and in turn jeopardizes the strength and safety of the structure. Ideal reinforcing materials and methods would give a more durable structure without sacrificing any strength. The material determined to best meet these requirements was a continuous fiber-reinforced thermoplastic (CFRTP), the material selected was a polyethylene terephthalate glycol (PETg) thermoplastic reinforced with E-Glass fibers. The work primarily revolved around ways to enhance the reinforcement of concrete bridge decking. This work could easily be adapted for building floors and slabs. In this thesis, the load requirements adopted were for reinforced concrete bridge decking with a stay-in-place formwork, as provided by the American Association of State Highway and Transportation Officials (AASHTO) LRFD Bridge Design Specifications.

This thesis outlines the work done towards building a prototype thermoplastic plate that could be used for stay-in-place concrete and contribute towards the tensile reinforcement of the structure. There were three main stages of work that went into this; the first was the creation of a prototype beam that was a hybrid section of concrete, thermoplastic formed as a closed-corrugation section, and rebar. The second stage looked into the secondary processes of bonding already consolidated thermoplastic plates, as well as ways to manipulate the surface. And the final stage was creating a spliced plate of closed-corrugations, resembling a prototype of a stay-in-place formwork for a reinforced concrete bridge deck.

ACKNOWLEDGEMENTS

I would first like to give a substantial thank you to my advisors Dr. William Davids and Dr. Roberto Lopez-Anido, for their constant support and guidance through my graduate studies both in the classroom and in the research lab. I greatly appreciate all they have done for me so far in my engineering career and all I'm sure they will do for the years to come.

I would next like to thank the U.S. Army Engineer Research and Development Center (ERDC) for providing the funding for my research work, allowing me to continue my education and expose me to the world of research. Having the opportunity to expose myself to such a unique and modern research topic in the world of structural engineering advancement is something I deeply appreciate.

I would also like to thank Dr. Eric Landis for serving as a member on my defense committee and the recommendations and guidance he provided. Additionally I would like to thank all the members at the Advanced Structures and Composites Center (ASCC); from the undergrads to the lab technicians to the ERDC employees that were a constant resources and provided extraordinary assistance throughout my time at the ASCC.

Finally and possibly most importantly I would like to thank my family and friends for all the support, assistance and some timely research breaks they all provided me as I worked towards life goals of mine both academically and personally.

TABLE OF CONTENTS

ACKNOWLEDGEMENTS	iii
LIST OF TABLES	ix
LIST OF FIGURES	x
CHAPTER 1: INTRODUCTION	1
1.1 Project Background	1
1.2 Objective of the Thesis	8
1.3 Thesis Outline	10
CHAPTER 2: HYBRID CLOSED-CORRUGATION SECTION DESIGN AND MANUFACTURING	12
2.1 Introduction	12
2.2 Design of Thermoplastic Section	14
2.2.1 Classical Laminate Theory	14
2.2.2 Single Closed-Corrugation Failure Prediction	21
2.3 Manufacturing of Hybrid Beams	27
2.3.1 Tape Layup Placement and Orientation	27
2.3.2 Consolidation Method	28
2.3.3 Corrugation Shape Stamp Forming	30
2.3.4 Secondary Bonding of Closed-Corrugation Section	32
2.3.5 Constructing Hybrid Closed-Corrugation Specimen	37

CHAPTER 3: SINGLE CLOSED-CORRUGATION TESTING AND ANALYSIS	40
3.1 Testing Setup.....	40
3.2 Test Procedures	41
3.3 Test Results	43
3.3.1 Construction Loading Test.....	43
3.3.2 Hybrid Beam Failure Test.....	47
3.3.3 Analysis of Data.....	51
3.4 Advancement Options – Secondary Bonding	59
CHAPTER 4: SECONDARY BONDING MANUFACTURING TRIALS	60
4.1 Introduction	60
4.1.1 Secondary Bonding.....	60
4.1.2 Surface Manipulation.....	61
4.2 Manufacturing of Secondary Bonding Coupon Specimen.....	62
4.2.1 Tape Layup Orientation	62
4.2.2 Consolidation of Control Specimen.....	62
4.2.3 Consolidation of Test Specimen	65
4.2.4 Secondary Bonding Process.....	66
4.3 Secondary Bonding Coupon Testing.....	69
4.3.1 Test Setup and Procedure.....	69
4.3.2 Test Results.....	70

4.3.3	Discussion of Results	74
4.4	Prototype Rebar Surface Manipulation	84
4.4.1	Material Used.....	85
4.4.2	Manufacturing the CSM-PETg Layer.....	85
4.4.3	Manufacturing the Grooved Plate.....	91
4.4.4	Adaptions to Stay-In-Place Formwork	95
4.5	Summary and Conclusions	96
CHAPTER 5: CLOSED-CORRUGATION SPLICED PLATE.....		97
5.1	Introduction	97
5.1.1	Splicing Options for Closed-Corrugations.....	97
5.2	Design of Thermoplastic Section	100
5.2.1	Design of Thermoplastic Section.....	100
5.2.2	Failure Prediction.....	102
5.3	Manufacturing of Spliced Panel.....	107
5.3.1	Initial Manufacturing Process	107
5.3.2	Secondary Bonding Mold Manufacturing	108
5.3.3	3D Printed Mold Manufacturing Trials	112
5.3.4	Secondary Bonding of Closed-Corrugation Panel.....	114
5.3.5	Instrumentation of Closed-Corrugation Panel	118
5.4	Spliced Closed-Corrugation Panel Testing	120

5.4.1	Test Setup.....	120
5.4.2	Test Procedure	121
5.4.3	Discussion of Results	122
5.5	Advancement Options	138
5.5.1	Takeaways from Spliced Closed-Corrugation Manufacturing and Testing	138
5.5.2	Improvements of Splicing Methods.....	139
CHAPTER 6: CONCLUSIONS AND RECOMMENDATION FOR FUTURE WORK.....		140
6.1	Hybrid Closed-Corrugation Beam	140
6.2	Secondary Bonding and Surface Manipulation.....	141
6.2.1	Secondary Bonding.....	141
6.2.2	Exterior Surface Manipulation.....	142
6.3	Spliced Closed-Corrugation Panel Fabrication and Assessment	142
6.4	Recommendations for Future Work.....	144
6.4.1	Advancement of Thermoplastic Stay-In-Place Formwork	144
6.4.2	Advancement of Internal Reinforcement.....	145
REFERENCES		147
APPENDIX A:.....		148
APPENDIX B:		149
APPENDIX C:.....		162
APPENDIX D:.....		172

APPENDIX E:	184
APPENDIX F:	186
APPENDIX G:	188
BIOGRAPHY OF THE AUTHOR.....	190

LIST OF TABLES

Table 1: Longitudinal E-Glass/PETg Material Properties [3]	5
Table 2: Transverse E-Glass/PETg Material Properties [3]	6
Table 3: Corrugated Plate Laminate Layup Schedule	15
Table 4: Laminate Strength – Corrugation Top Flange and Web / Cover Plate.....	22
Table 5: Laminate Strength – Corrugation Bottom Flange	22
Table 6: Geometric Properties of Single Closed-Corrugation.....	23
Table 7: Strength and Stiffness of Hybrid Closed-Corrugation Specimen.....	51
Table 8: Summary of Strain Data – Readings at 20 kips.....	58
Table 9: Tested Secondary Bonding Settings with Success Rate.....	68
Table 10: Labeling System with Full Manufacturing Settings.....	68
Table 11: Lap Shear Coupon Testing Raw Data	71
Table 12: Failure Loads and Lap Shear Strength Calculations.....	75
Table 13: MNR Outlier Check in Data Sets	76
Table 14: Control – PETg Spacer Specimen Data Set with MNR Calculation.....	77
Table 15: Corrugated Plate Laminate Layup Schedule	101
Table 16: Laminate Strength – Corrugation Top Flange and Web / Cover Plate.....	103
Table 17: Laminate Strength – Corrugation Bottom Flange	103
Table 18: Geometric Properties of Multi-Corrugation Panel	104
Table 19: Failure, Maximum Deflection, Stiffness of Failure Test.....	129
Table 20: Closed-Corrugation Panel Midspan Strain Gauge Regions.....	134
Table 21: Closed-Corrugation Panel Outer Strain Gauge Regions	135

LIST OF FIGURES

Figure 1: Temporary Formwork for Concrete during Bridge Construction [1].....	2
Figure 2: Stay-in-Place Steel Formwork [2].....	3
Figure 3: Periodic Table of Thermoplastics [5].....	4
Figure 4: Flat Panel Beam Model with Shear Studs and Concrete [4].....	7
Figure 5: Corrugated Panel Corrugation with Tentative Dimensioning [4].....	8
Figure 6: Stiffened Panel Configuration with Tentative Dimensioning [4].....	8
Figure 7: Single Closed-Corrugation Rendering.....	9
Figure 8: Multi Closed-Corrugation Spliced Panel Rendering.....	10
Figure 9: Rendering of Bare Closed-Corrugation Specimen.....	12
Figure 10: Rendering of Concrete-CFRTP Closed-Corrugation Hybrid Specimen.....	13
Figure 11: Closed-Corrugation Approximate Dimensioning and Section Labels.....	14
Figure 12: Positioning of Layups on Corrugated Plate.....	17
Figure 13: CLT Conversion Flow Chart [7].....	18
Figure 14: Stress-Strain Through-Thickness in 12-Direction (+1 Nx Applied).....	19
Figure 15: Stress-Strain Through-Thickness in XY-Direction (+1 Nx Applied).....	20
Figure 16: Completed Hybrid Closed-Corrugation Specimen.....	21
Figure 17: Shear Flow at Bond of Single Closed-Corrugation.....	26
Figure 18: Stacking Positioning of Corrugated Plates for Consolidation.....	29
Figure 19: Fully Consolidated Flat Plate.....	30
Figure 20: Stamp Forming Mold Positioned in the Press.....	31
Figure 21: Dimensioning of Formed Corrugated Sections with Tentative Dimensioning.....	32
Figure 22: Rendering of Mold Modifications for Secondary Bonding.....	33
Figure 23: Rendering of Spring Table Supporting Cover Plate for Secondary Bonding.....	34

Figure 24: Temperature of Parts during Secondary Bonding Process	36
Figure 25: Completed Closed-Corrugation Part	37
Figure 26: Rebar Cage and Formwork Prepared for Concrete	38
Figure 27: Completed Hybrid Closed-Corrugation Specimen.....	39
Figure 28: Free-Body Diagram of Closed-Corrugation Testing.....	40
Figure 29: Test Setup for Single Closed-Corrugation Specimen.....	41
Figure 30: Strain Gauge Positioning on Closed-Corrugation Specimen	42
Figure 31: Load-Deflection Plot of Specimen 1 – Construction Loading	45
Figure 32: Load-Deflection Plot of Specimen 2 – Construction Loading	45
Figure 33: Failure of Specimen 1 – End Cross Section	47
Figure 34: Failure of Specimen 2 – End Cross Section	47
Figure 35: Failure of Specimen 4 – End and Side View.....	48
Figure 36: Failure of Specimen 5 – Side View.....	48
Figure 37: Web Failure of Specimen 4.....	49
Figure 38: Load-Deflection Plot for Hybrid Closed-Corrugation Specimen.....	50
Figure 39: Strain Gauge Location and Side Definition	51
Figure 40: Specimen 3 Strain-Heights at Midspan and Beyond the Load Head at 5 kips.....	53
Figure 41: Specimen 3 Strain-Heights at Midspan and Beyond the Load Head at 10 kips.....	54
Figure 42: Specimen 3 Strain-Heights at Midspan and Beyond the Load Head at 15 kips.....	55
Figure 43: Specimen 3 Strain-Heights at Midspan and Beyond the Load Head at 20 kips.....	56
Figure 44: Multi Closed-Corrugation Spliced Panel Rendering.....	59
Figure 45: Secondary Bonding Lap Shear Specimen Rendering.....	61
Figure 46: Cross-Sectional View of Stacking Procedure for Control Specimen.....	63

Figure 47: Side View of a PETg Spacer Control Coupon – Highlighted Bond Area.....	64
Figure 48: Side View of an Aluminum Spacer Control Coupon – Highlighted Bond Area	64
Figure 49: Side View of a Secondary Bonded Test Specimen – Highlighted Bond Area.....	66
Figure 50: Cross-Sectional View of Stacking Positioning of Test Specimen	66
Figure 51: Lap Shear Coupon Loading into Instron Machine	70
Figure 52: Failed PETg Spacer Control Coupon	72
Figure 53: Failed Test Specimen – Complete Bond Line Failure	73
Figure 54: Failed Test Specimen – Fibers Present at the Failure Surface	73
Figure 55: Lap Shear Distribution (Substrate 225°F and IR Oven 335°F).....	79
Figure 56: Lap Shear Distribution (Substrate 225°F and IR Oven 360°F).....	80
Figure 57: Lap Shear Distribution (Substrate 280°F and 335°F)	81
Figure 58: Plot of Specimen Series by Average Lap Shear Strength and Forming Pressure	83
Figure 59: Trial CSM Sheet - 350°F / Constant 30 psi / 2 Resin Sheets / Passive Cooling	87
Figure 60: Trial CSM Sheet - 400°F / Initial 30 psi / 2 Resin Sheets / Active Cooling	87
Figure 61: Trial CSM Sheet - 450°F / 0 psi / 2 Resin Sheets / Passive Cooling	88
Figure 62: Trial CSM Sheet - 450°F / Constant 30 psi / 1 Resin Sheet / Active Cooling	88
Figure 63: Trial CSM Sheet - 450°F / Initial 30 psi / 2 Resin Sheets / Passive Cooling.....	89
Figure 64: Stacking Procedure to Form Deformation Layer	90
Figure 65: Forming Settings of the Deformation Layer	91
Figure 66: Schematic of Stacking Procedure of Final Consolidation.....	92
Figure 67: Completed Prototype CFRTP Reinforcing Bar.....	93
Figure 68: Close up View of Unidirectional Core	94
Figure 69: Close up View of CFRTP Rebar Deformation Layer	95

Figure 70: Section View of Closed-Corrugation with Grooved Surfaces	96
Figure 71: CFRTP Tongue-and-Groove Closed-Corrugation Design	97
Figure 72: CFRTP Implanted Corrugation Design.....	98
Figure 73: CFRTP Overlapping Cover Plate Design.....	99
Figure 74: CFRTP Multi-Corrugation Single Cover Plate Design.....	100
Figure 75: 3D Printing of Multi-Corrugation Mold – Single Section	109
Figure 76: 3D Printed Mold Ready for Machining.....	110
Figure 77: Dimensioning of Heating Element Groove	111
Figure 78: Fully Machined 3D Printed Mold	111
Figure 79: Bending and Cracking of Mold during Initial Heating	112
Figure 80: Corrugation Prepared for Secondary Bonding with Spring Table	115
Figure 81: Completed Multi-Corrugation Panel	117
Figure 82: Assumed Poorly Bonded Area of Spliced Panel	118
Figure 83: Location of Strain Gauges at both Center and Outer Locations.....	119
Figure 84: Location of the Center and Outer Sets of Strain Gauges	119
Figure 85: Multi-Corrugation Panel Test Setup.....	120
Figure 86: Free-Body Diagram of Closed-Corrugation Testing.....	121
Figure 87: Load versus Deflection of Panels during Construction Loading	123
Figure 88: Load v. Deflection of Specimen 4 – Construction Loading.....	124
Figure 89: Failure Test Load-Deflection Plot of Multi-Corrugation Panel Specimen	127
Figure 90: Shear Flow at Secondary Bond of Panel 4	130
Figure 91: Inside of Corrugation at Support of Failed Panel 1	131
Figure 92: Photo before Testing of Panel 1 – No Load	132

Figure 93: Photo during Testing of Panel 1 - Loaded.....	132
Figure 94: Photo after Testing of Panel 1 – No Load.....	133
Figure 95: End Cross Section View after Testing of Panel 3	134
Figure 96: Strain Readings in Regions 1-M and Region 2-M at 15 kips.....	135
Figure 97: Strain Readings in Region 1-O and Region 2-O	136
Figure 98: Strain Readings in Region 3-O and Region 4-O	137
Figure 99: Strain v. Load of Midspan Western Edge – Specimen 4.....	138

CHAPTER 1: INTRODUCTION

1.1 Project Background

Advancement is something all fields strive for, attempting to improve on current methods to create an even better system or product. The construction industry is no different, starting with simple stone, lumber, and mud structures and advancing to steel, reinforced concrete, engineered wood composites. Current building methods are able to create structures capable of withstanding incredibly forces. But advancement continues searching for ways to continue to increase the strength capabilities of materials and lifespan of structures.

Current, continuous fiber-reinforced thermoplastic (CFRTP) composites show promise for improving infrastructure construction speed and durability. Thermoplastic composites can be formed using heat, promising more efficient manufacturing and greater field adaptability that thermoset resins typically used in fiber reinforced composites for structural applications. That is exactly the path this research looks to pursue, utilizing thermoplastic materials to enhance reinforced concrete, specifically in the application of bridge decking.

There are two main ways concrete bridges can be constructed, either through prefabricated measures or site placed concrete. Prefabricated sections are created off-site and brought to site and placed into the desired position. This can be desired when there are time or space restrictions on site, but can be affected by transportation limitations. For this reason some sections might have to be placed on site. Both options however will require formwork to be constructed giving concrete its shape and also to support the concrete until it has cured to the desired strength. Temporary formwork is a common method, this formwork is often constructed out of wood, and is removed from the final structure once the concrete is cured and up to strength. An example of temporary formwork in a bridge application is shown in Figure 1.



Figure 1: Temporary Formwork for Concrete during Bridge Construction [1]

In other projects the temporary formwork is replaced by a steel stay-in-place formwork. This formwork provides the same initial curing support as the temporary formwork, but isn't removed and can give the structure extra tensile support. An example of steel stay-in-place formwork is shown in Figure 2.



Figure 2: Stay-in-Place Steel Formwork [2]

Research work for this thesis looks into the concept of stay-in-place formwork for concrete bridge decks, with a goal of utilizing thermoplastic materials to construct this formwork that can also serve as tensile reinforcing for the concrete. This has been an ongoing project at the Advanced Structures and Composites Center (ASCC) at the University of Maine (UMaine), with previous work laying the ground work for this research. Work began with material characterization and initial design iterations from Seigars [3] and continued with further design methods and testing with Smith [4]. Material characterization looked into multiple thermoplastic materials including with more in-depth research being done looking at in-situ polymerized acrylic type Elium from Arkema and Polyethylene Terephthalate Glycol (PETg) unidirectional tapes [3]. With the availability of pre-impregnated unidirectional tapes of PETg with E-Glass fibers as well as the thermoplastics crystallinity balance and being of engineering grade, shown in Figure 3. It was determined PETg would be best for the manufacturing of plate section prototypes that could be utilized for stay-in-place formwork of concrete deck.

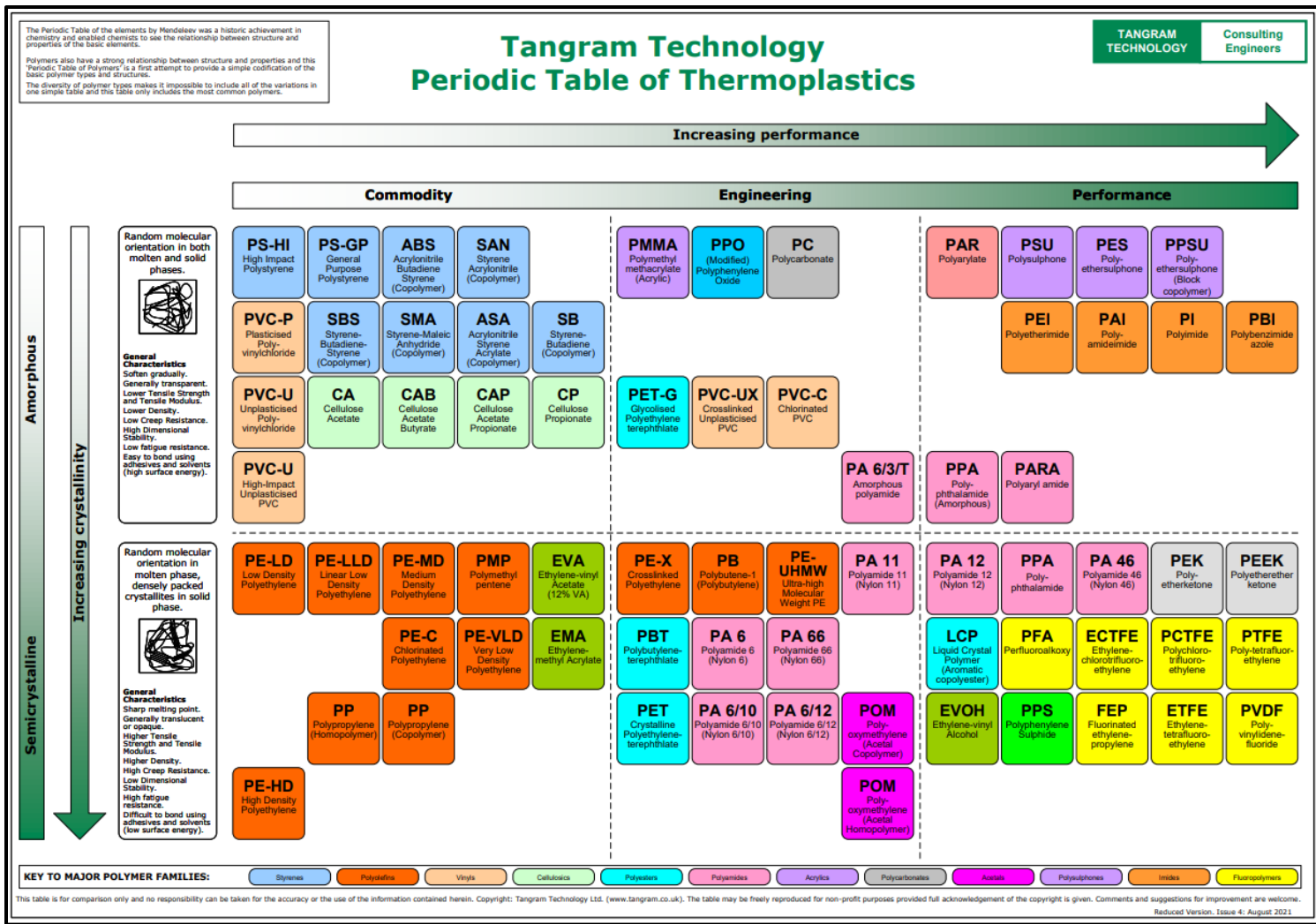


Figure 3: Periodic Table of Thermoplastics [5]

A table of the material properties developed through testing by Seigars [3] is outlined in Table 1 for longitudinal properties and Table 2 for transverse properties. Additionally a material sheet of the PETg pre-impregnated tapes is provided in Appendix A, provided from the supplier PolyOne [6].

Table 1: Longitudinal E-Glass/PETg Material Properties [3]

Properties and COV	E-Glass/PETg
Fiber Volume Fraction, V_f (%)	36.4 (3.0 %)
Tensile Strength, F_{1t} (MPa)	623 (10.2 %)
Tensile Elastic Modulus, E_{1t} (GPa)	28.2 (3.65 %)
Compressive Strength, F_{1c} (MPa)	310 (17.7 %)
Compressive Elastic Modulus, E_{1c} (MPa)	23.5 (14.7 %)
In-Plane Shear Strength, F_6 (MPa)	28.8 (5.25 %)
In-Plane Shear Elastic Modulus, G_{12} (GPa)	1.48 (18.9 %)
Poisson's Ratio, ν_{12} (-)	0.353 (2.52 %)
Ultimate Tensile Strain, ε_{1t}^u ($\mu\varepsilon$)	23,300 (12.8 %)
Ultimate Compressive Strain, ε_{1c}^u ($\mu\varepsilon$)	12,300 (15.2 %)
Ultimate In-Plane Shear Strain, ε_{1y}^u ($\mu\varepsilon$)	49,800 (25.0 %)

Note: COV percentages reported with respective measured value in parenthesis.

Table 2: Transverse E-Glass/PETg Material Properties [3]

Properties and COV	E-Glass/PETg
Tensile Strength, F_{2t} (MPa)	14.5 (17.7 %)
Tensile Elastic Modulus, E_{2t} (GPa)	4.43 (10.9 %)
Compressive Strength, F_{2c} (MPa)	65.0 (6.92 %)
Compressive Elastic Modulus, E_{2c} (MPa)	4.98 (13.9 %)
In-Plane Shear Strength, F_6 (MPa)	31.1 (4.02 %)
In-Plane Shear Elastic Modulus, G_{21} (GPa)	1.53 (6.67 %)
Poisson's Ratio, ν_{21} (-)	0.823 (11.4 %)
Ultimate Tensile Strain, ε_{2t}^u ($\mu\varepsilon$)	3,400 (16.4 %)
Ultimate Compressive Strain, ε_{2c}^u ($\mu\varepsilon$)	24,700 (32.1 %)
Ultimate In-Plane Shear Strain, ε_{2x}^u ($\mu\varepsilon$)	251,000 (23.3 %)
Avg. Composite Panel Thickness, t (mm)	2.4

Note: COV percentages reported with respective measured value in parenthesis.

The first section was a flat Continuous Fiber Reinforced Thermoplastic (CFRTP) PETg panel beam with friction welded shear stud plate developed by Seigars [3] and tested by Smith [4], shown in Figure 4.

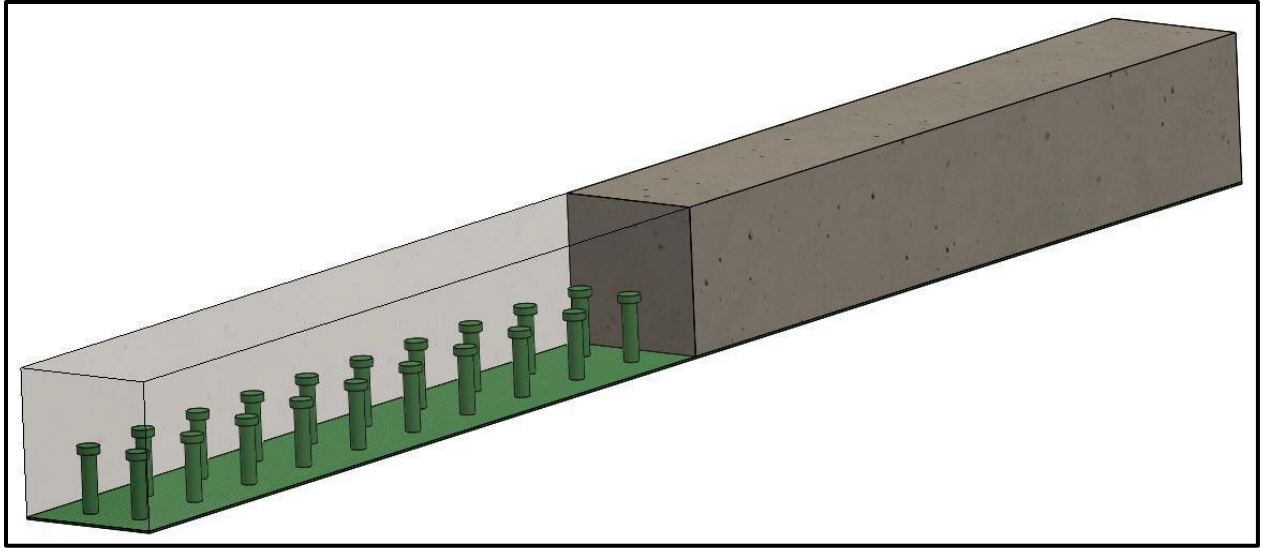


Figure 4: Flat Panel Beam Model with Shear Studs and Concrete [4]

This flat beam with friction welded shear studs appeared to experience low load sharing between studs, resulting in ultimate failure of a beam to occur soon after the first shear stud failed as discussed by Smith [4]. Therefore it was determined the bonding method of friction welding the studs was not a quality method for transferring shear forces. This led to two other cross sections being designed and explored with an attempt to pinpoint a design that could be utilized for the continuation of the research work by looking at full panels to be tested. The first was a corrugation design with crossing bars to provide stiffness, shown in Figure 5. The second was a stiffened panel that was formed with multiple CFRTP plates getting secondarily bonded together to create the formwork, shown in Figure 6.

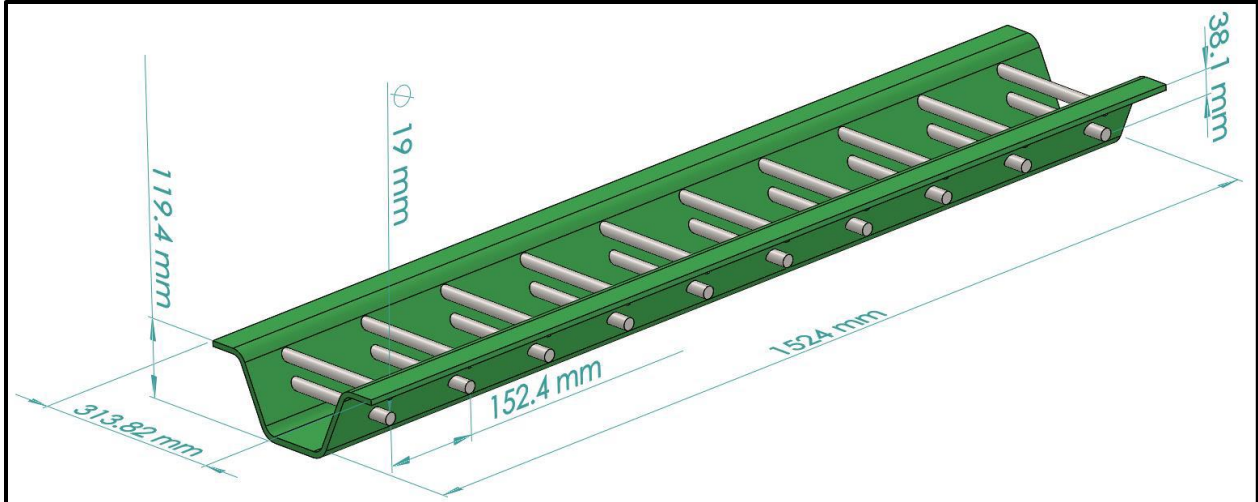


Figure 5: Corrugated Panel Corrugation with Tentative Dimensioning [4]

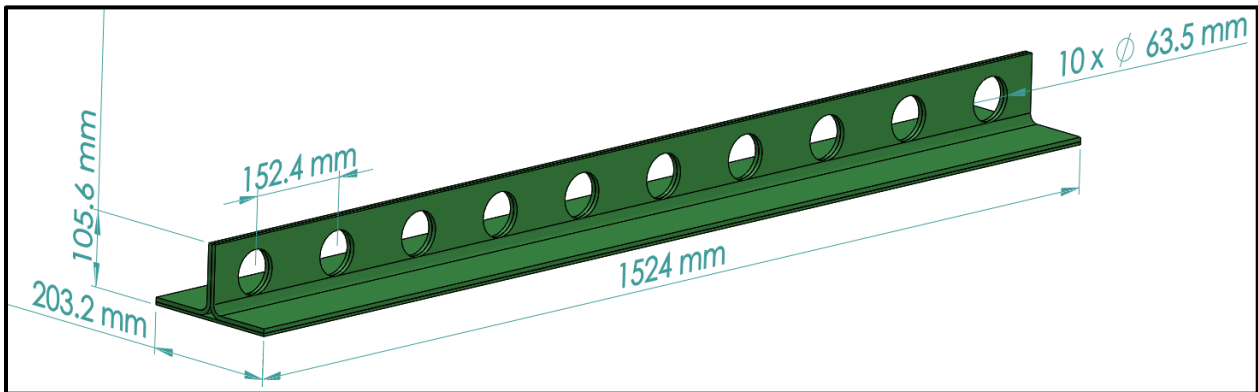


Figure 6: Stiffened Panel Configuration with Tentative Dimensioning [4]

This testing provide insight that the corrugation design would provide the most benefits for future work, and best resembles the materials currently used in bridge construction.

1.2 Objective of the Thesis

There were two main purposes for performing this research, the first was to develop a system made of CFRTP tapes that could be used as a stay-in-place formwork for reinforced concrete decking, with a focus on developing a shear transfer between sections. This would allow the formwork to additionally be utilized as tensile reinforcement for the concrete section. The

second purpose was to further explore the manufacturing capabilities and requirements of CFRTP sections in the ASCC.

Through initial project work previously mentioned, it was determined the corrugation shape was the design that provided the most optimistic results and required additional work to improve on the design. Utilizing the base design for the corrugated shape developed by Smith [4], improvements were developed as an attempt to increase flexural stiffness and shear transfer through a cover plate create the closed-corrugated design displayed in Figure 7.

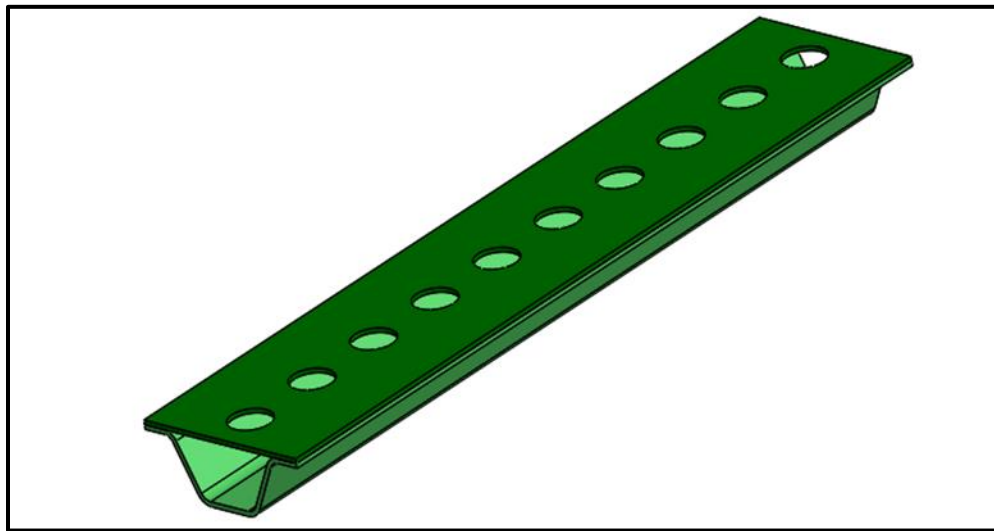


Figure 7: Single Closed-Corrugation Rendering

This cross sectional shape additionally allows for multiple joining methods when looking to attach multiple sections into one panel of formwork. Exploration into the secondary bonding of consolidated CFRTP is a main focus of this work, which will lead to the development of a full thermoplastic panel that could serve as a stay-in-place formwork of a concrete bridge deck. An example of this final panel is shown in Figure 8.

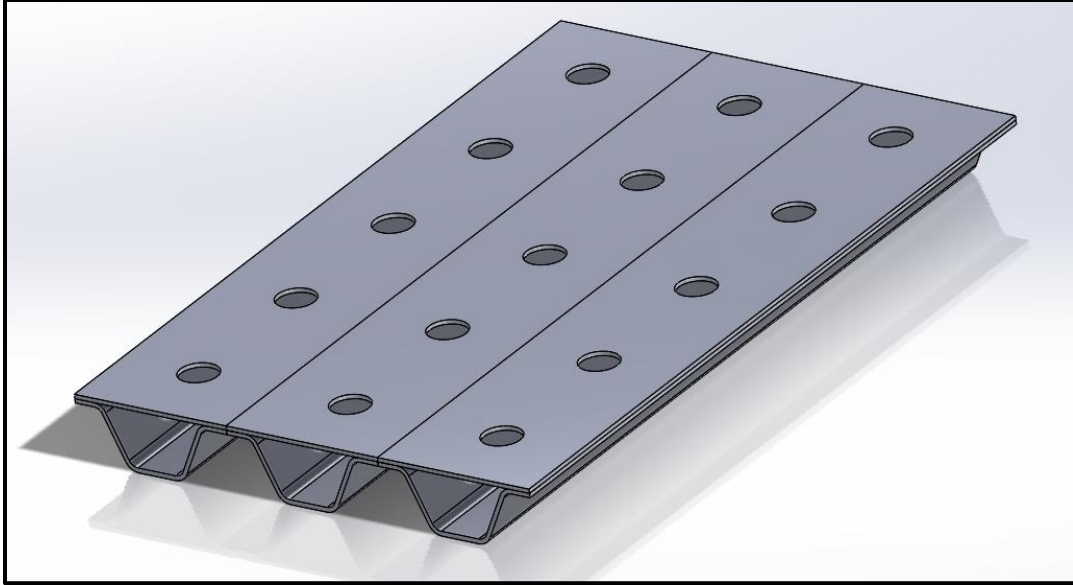


Figure 8: Multi Closed-Corrugation Spliced Panel Rendering

1.3 Thesis Outline

This thesis consists of 6 chapters, the first being the introductory Chapter 1 followed by,

- Chapter 2: Single Closed-Corrugation Manufacturing, details the manufacturing process of single closed-corrugation sections out of CFRTP tapes.
- Chapter 3: Testing of Single Closed-Corrugation Sections, describes the testing procedures and the results of CFRTP closed-corrugation beams and reinforced concrete hybrid beams.
- Chapter 4: Secondary Bonding and External Modification Coupon Testing, covers coupon level manufacturing of specimen to increase knowledge of manufacturing and secondary processes of pre-consolidated CFRTP plates. Includes testing and data analysis of some of the coupons.
- Chapter 5: Closed-Corrugation Panel Testing, discusses the additional manufacturing steps to go from single closed-corrugations to a corrugated panel. Builds off of the previous closed-corrugation manufacturing and highlights the improvements made to the

manufacturing process. Includes testing data and results from the prototype testing of thermoplastic corrugated panels.

- Chapter 6: Conclusion and Recommendations, provides a summary of findings gathered through the work performed and gives brief recommendations for where future research work could be directed to continue advancements.

Additional information is included in Appendices and referenced when applicable in the text.

CHAPTER 2: HYBRID CLOSED-CORRUGATION SECTION DESIGN AND MANUFACTURING

2.1 Introduction

In an attempt to improve the transfer of shear through the concrete into the thermoplastic supportive formwork a closed-corrugation design was created. This design consisted of the corrugation design developed by Smith [4] with the addition of a cover plate over the corrugation valley. This plate had holes down its length allowing for shear studs to be formed out of concrete and vertical rebar, similar to the stiffened panel also developed by Smith [4]. The hope was these shear studs would allow for the concrete section to be connected in both regions, the deck and the corrugation valley, well also proper shear transfer through the system. Renderings of this design can be seen in Figure 9 as a bare specimen and in Figure 10 as a concrete and CFRTP hybrid specimen with internal reinforcement.

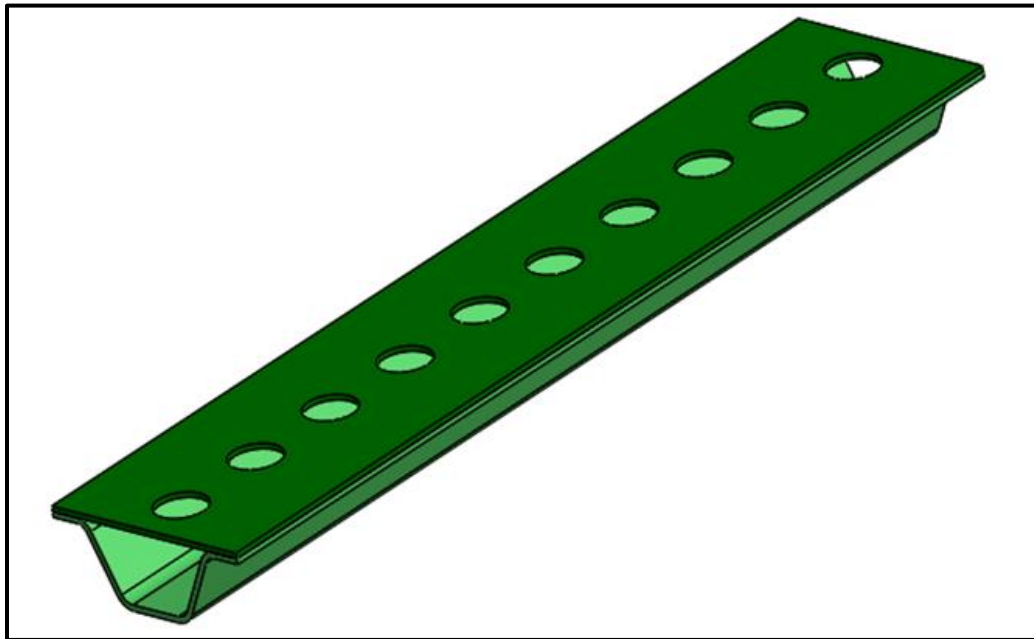


Figure 9: Rendering of Bare Closed-Corrugation Specimen

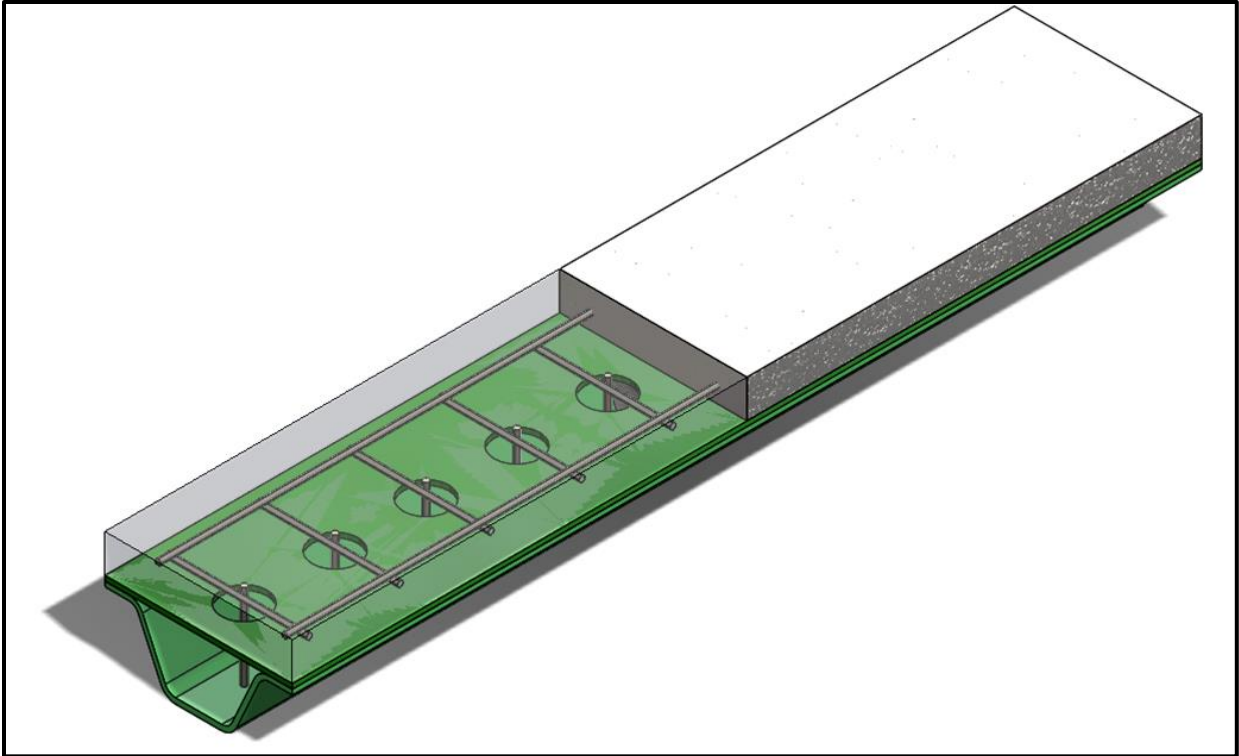


Figure 10: Rendering of Concrete-CFRTP Closed-Corrugation Hybrid Specimen

A fully labeled cross section of the closed-corrugation region names is outlined in Figure 11.

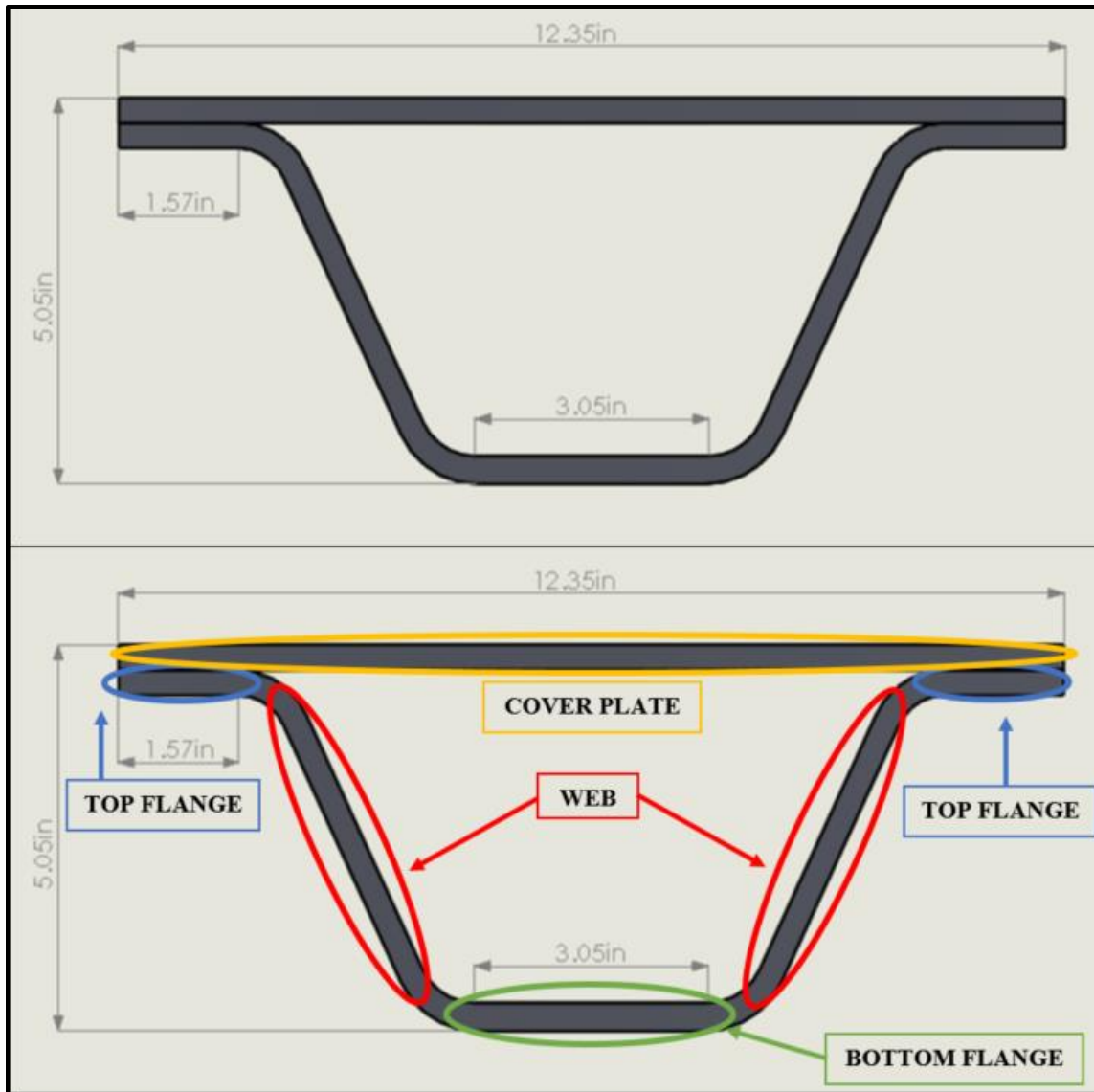


Figure 11: Closed-Corrugation Approximate Dimensioning and Section Labels

2.2 Design of Thermoplastic Section

2.2.1 Classical Laminate Theory

As mentioned the design of corrugation was remaining unchanged from the work performed by Smith, adjustments were simply being made to the shear transfer mechanism. For this reason the laminate layup schedule had layers of the same orientation. Because the cover plate was assumed to experience similar loads to the top flange of the corrugation, it shared the same layup schedule. The layup schedules are as follows,

Corrugation Bottom Flange (Layup #1) =

$$[0_2/\pm 45/0_7/\pm 45/0_7/\pm 45/0_3/\mp 45/0_7/\mp 45/0_7/\mp 45/0_2]$$

Corrugation Web (Layup #2) =

$$[0_2/\pm 45/0_2/\pm 45/0_2/\pm 45/0_2/\pm 45/0_2/\pm 45/0_2/\mp 45/0_2/\mp 45/0_2/\mp 45/0_2/\mp 45/0_2/\mp 45/0_2]$$

Corrugation Top Flange (Layup #2) =

$$[0_2/\pm 45/0_2/\pm 45/0_2/\pm 45/0_2/\pm 45/0_2/\pm 45/0_2/\mp 45/0_2/\mp 45/0_2/\mp 45/0_2/\mp 45/0_2/\mp 45/0_2]$$

Cover Plate (Layup #2) =

$$[0_2/\pm 45/0_2/\pm 45/0_2/\pm 45/0_2/\pm 45/0_2/\pm 45/0_2/\mp 45/0_2/\mp 45/0_2/\mp 45/0_2/\mp 45/0_2/\mp 45/0_2]$$


The layup schedule is displayed in Table 3, the Bottom Flange is represented by “Layup #1” and the Top Flange/Web is represented by “Layup #2”, and is further explained in Section 2.3.1 with the manufacturing of the layups. The positioning of the different layups in the corrugated plates are shown in Figure 12.

Table 3: Corrugated Plate Laminate Layup Schedule

Plate Name: Corrugated Plate			
Layer:	Orientation:		Continuity Across Layups
	Layup #1	Layup #2	
1	0	0	continuous
2	0	0	continuous
3	45	45	continuous
4	-45	-45	continuous
5	0	0	continuous
6	0	0	continuous
7	0	45	
8	0	-45	
9	0	EMPTY	
10	0	0	continuous
11	0	0	continuous
12	45	45	continuous
13	-45	-45	continuous
14	0	0	continuous

Table 3: continued

15	0	0	continuous
16	0	45	
17	0	-45	
18	0	EMPTY	
19	0	0	continuous
20	0	0	continuous
21	45	45	continuous
22	-45	-45	continuous
23	0	0	continuous
24	0	EMPTY	
25	0	0	continuous
26	-45	-45	continuous
27	45	45	continuous
28	0	0	continuous
29	0	0	continuous
30	0	-45	
31	0	45	
32	0	EMPTY	
33	0	0	continuous
34	0	0	continuous
35	-45	-45	continuous
36	45	45	continuous
37	0	0	continuous
38	0	0	continuous
39	0	-45	
40	0	45	
41	0	EMPTY	
42	0	0	continuous
43	0	0	continuous
44	-45	-45	continuous
45	45	45	continuous
46	0	0	continuous
47	0	0	continuous

	Blue Highlighted Layers = Bottom Layup Bundle for Corrugated Plate
	Red Highlighted Layers = Middle Layup Bundle for Corrugated Plate
	Green Highlighted Layers = Top Layup Bundle for Corrugated Plate

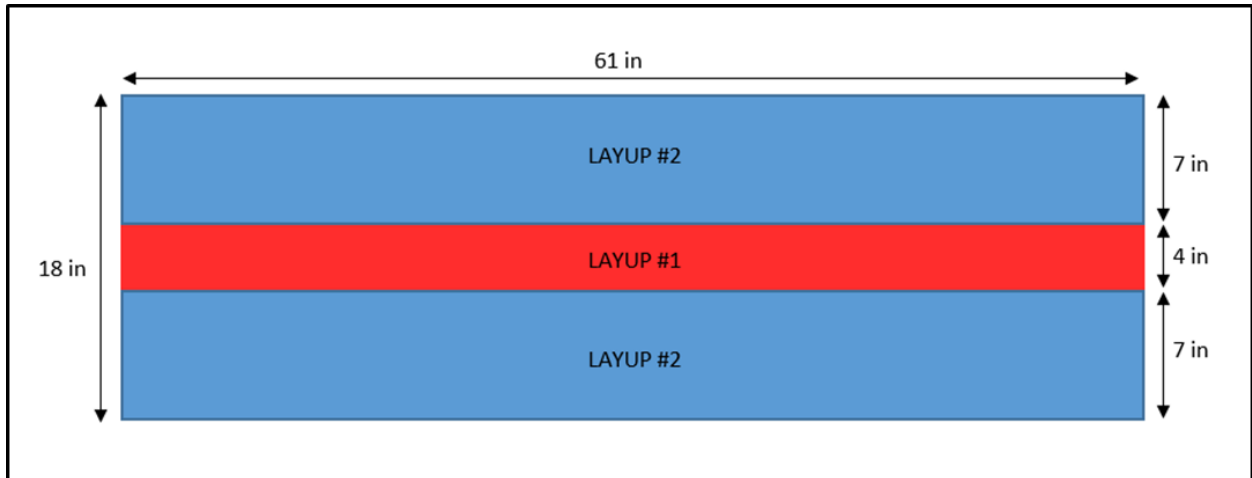


Figure 12: Positioning of Layups on Corrugated Plate

Baseline calculations were made utilizing Classical Lamination Theory (CLT) in order to come up with material properties values, laminate strengths, and reactions to inputted loadings.

Calculations were made using MatLab codes that were constructed following the method outlined in the text by Hyer [7]. The code used is provided in Appendix B. The formulation flow diagram of how properties are used to make calculations is shown in Figure 13.

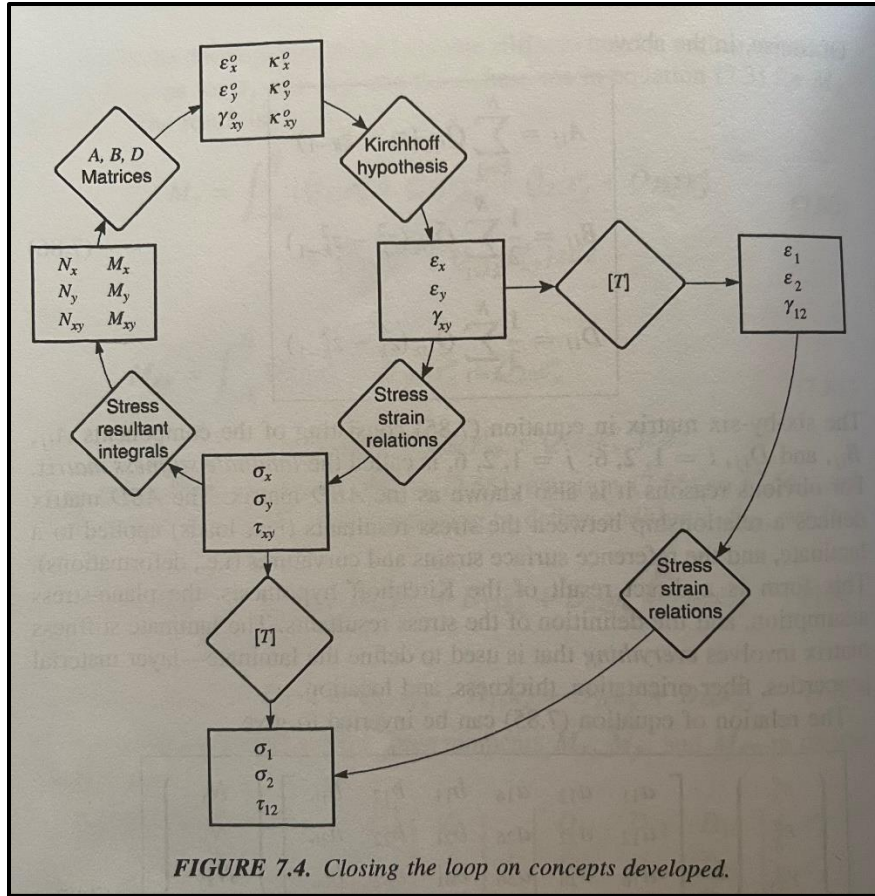


FIGURE 7.4. Closing the loop on concepts developed.

Figure 13: CLT Conversion Flow Chart [7]

Unit forces were inputted for the Force and Moment Resultants and the code displays the through-thickness stress and strain of the laminate in both global and local coordinates. A single unit force was added individually to see how the laminate would react to individual forces. The first scenario was applying a positive unit force to N_x and the remainder resultants were held at zero, and applied to Layup #2 (the layup orientation of the Corrugation Top Flange and Web / Cover Plate). Figures 14 show the stress and strain in the 12-Direction, the local direction of each layer. Figures 15 show the stress and strain in the XY-Direction, the global direction of the entire laminate. The remainder of the scenarios are outlined in Appendix C for Layup #2 and Appendix D for Layup #1.

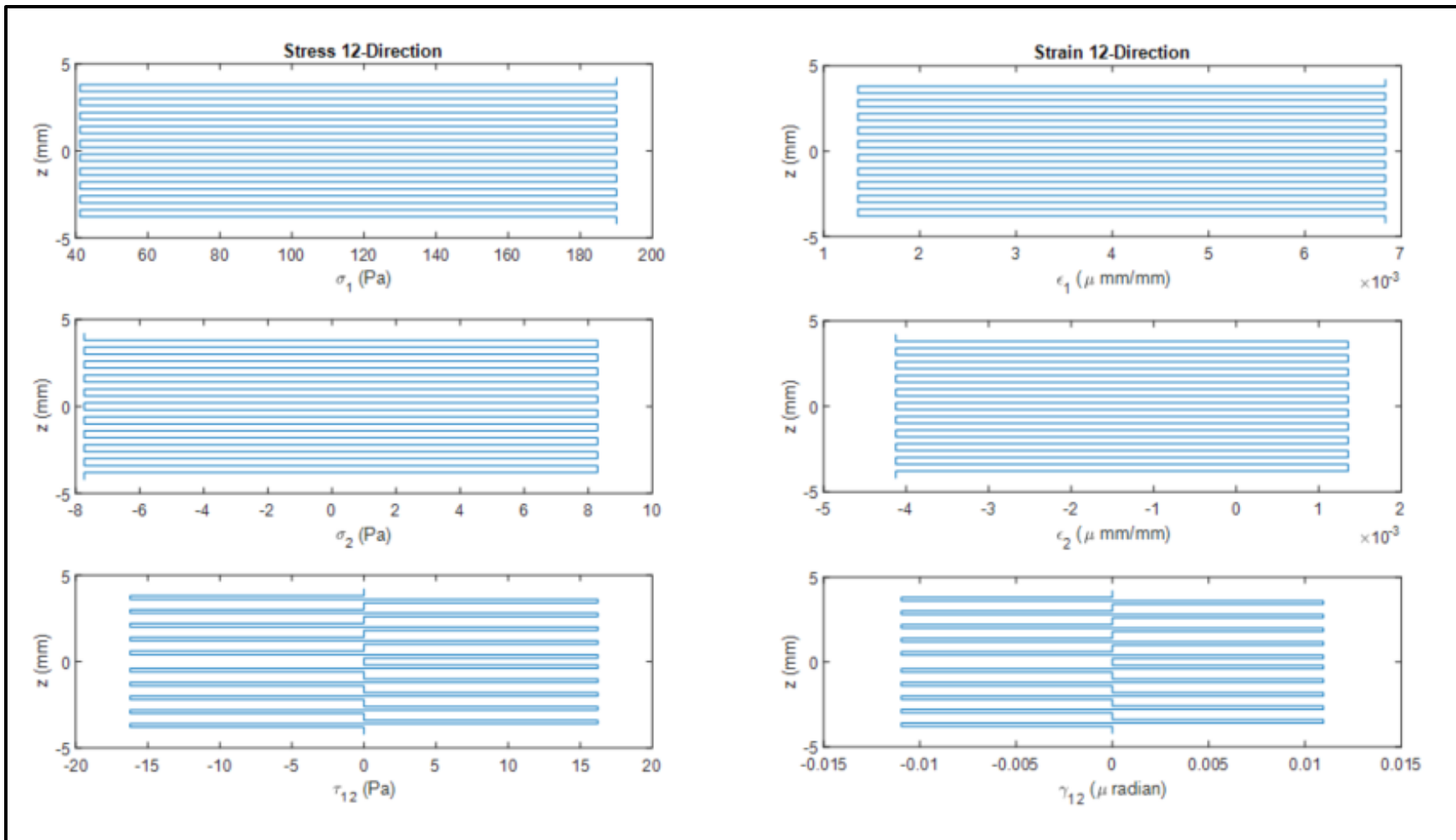


Figure 14: Stress-Strain Through-Thickness in 12-Direction (+1 Nx Applied)

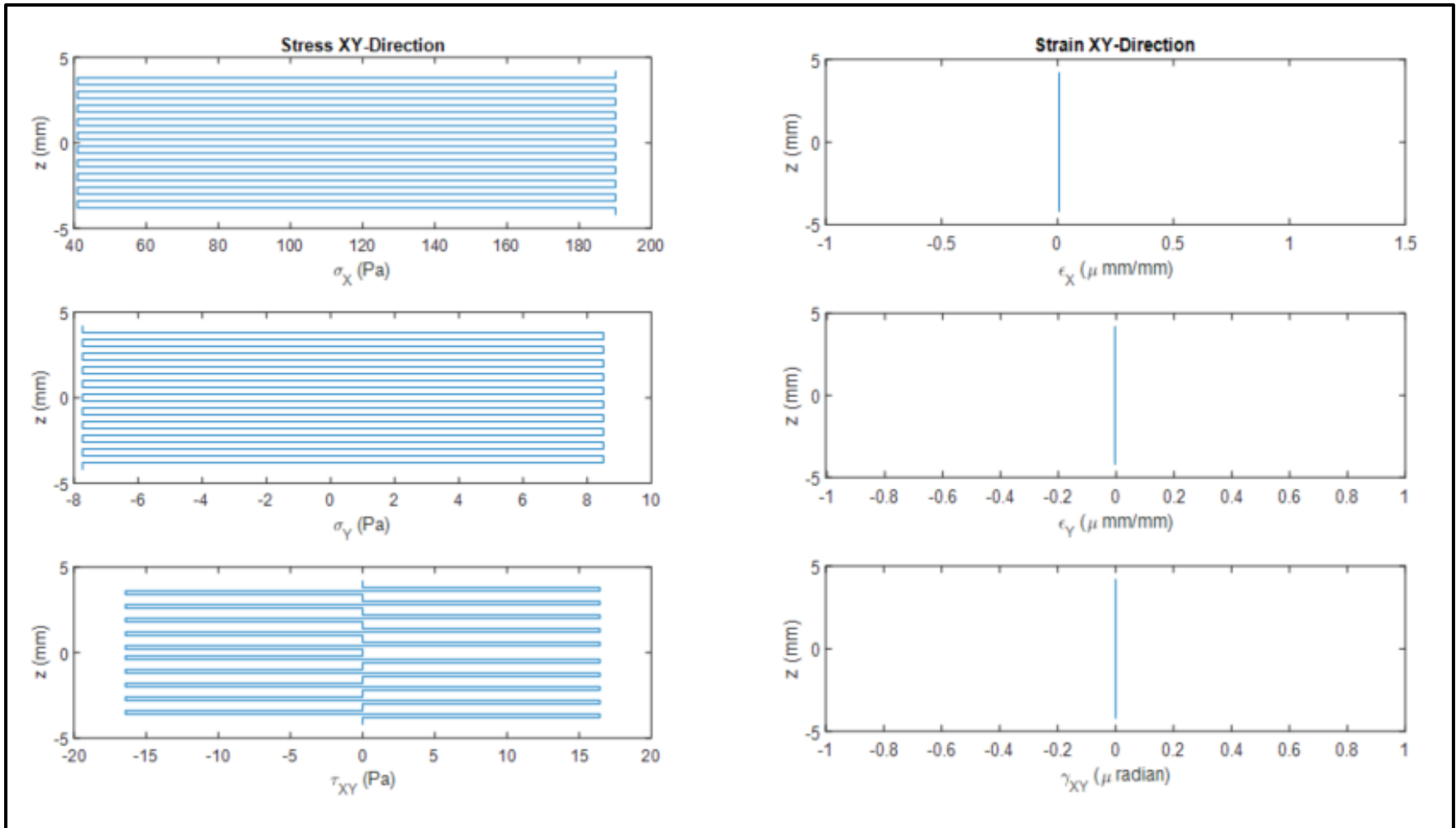


Figure 15: Stress-Strain Through-Thickness in XY-Direction (+1 Nx Applied)

2.2.2 Single Closed-Corrugation Failure Prediction

With previous work being performed on this project at smaller scales, this research was able to continue right where the previous work, Smith [4], left off. This positioned work to begin by looking at prototype beam testing of the closed-corrugation design as both a bare composite beam and a concrete hybrid beam, the concrete hybrid beam is shown in Figure 16.

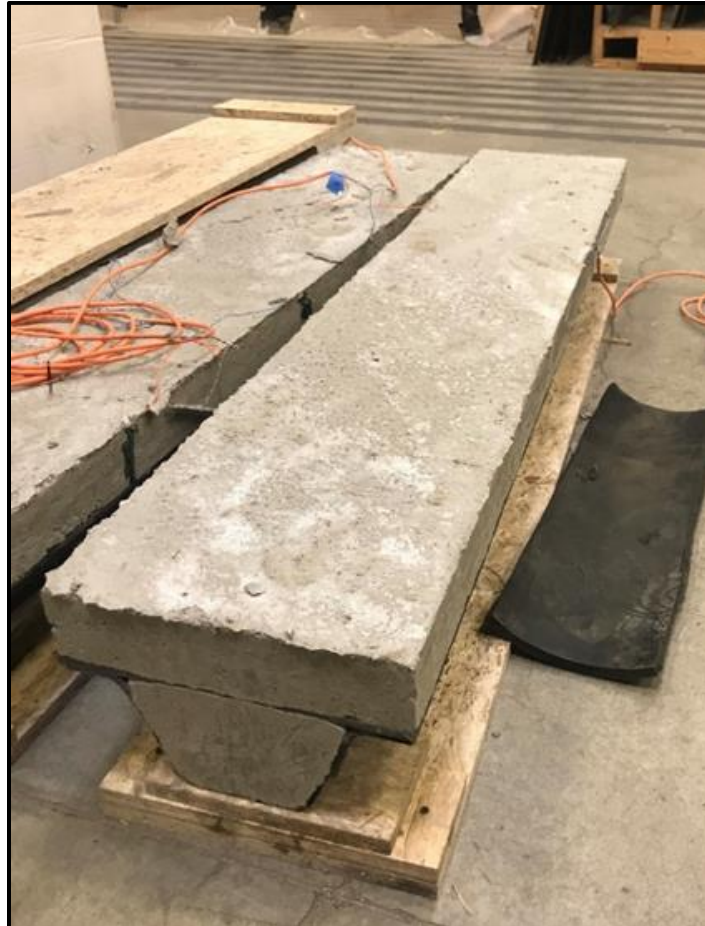


Figure 16: Completed Hybrid Closed-Corrugation Specimen

Preliminary predictions were made utilizing laminate strength calculations allowing for load checks to be calculated and provide a predicted failure load of the thermoplastic closed-corrugation specimen to be used for bare specimen testing. This process began by utilizing code developed on MatLab to calculate the strength of the laminate developed by Smith [4]. The strengths for the two different layups are outlined in Table 4 and Table 5.

Table 4: Laminate Strength – Corrugation Top Flange and Web / Cover Plate

Corrugation Top Flange and Web / Cover Plate		
Material Property	ksi	MPa
Longitudinal Tensile Strength, F_{xt}	30.7	211.9
Longitudinal Compressive Strength, F_{xc}	27.8	191.4
In-Plane Shear Strength, F_{xy}	4.1	28.6

Table 5: Laminate Strength – Corrugation Bottom Flange

Corrugation Bottom Flange		
Material Property	ksi	MPa
Longitudinal Tensile Strength, F_{xt}	42.0	289.4
Longitudinal Compressive Strength, F_{xc}	35.9	247.3
In-Plane Shear Strength, F_{xy}	2.9	19.8

Approximate geometric properties were calculated for the closed-corrugation cross section next using measuring tools in SolidWorks and MatLab Codes, see Appendix E. These properties are displayed in Table 6.

Table 6: Geometric Properties of Single Closed-Corrugation

Geometric Property	Variable	Value	Unit
Total Height of Cross Section	h	5.05	in
Total Width of Cross Section	w	12.35	in
Total Bond Length	b	3.14	in
Diameter of Shear Studs	d	3	in
Cross Sectional Area of Single Corrugation	A_c	5.92	in ²
Cross Sectional Area of Cover Plate	A_{CP}	4.13	in ²
Moment of Inertia	I	31.9	in ⁴
First Moment of Area	Q	6.42	in ³
Centroid Location of Cover Plate – from base	C_{CP}	4.886	in
Centroid Location of Full Panel – from base	Z_1	3.37	in
Centroid Location of Full Panel – from top	Z_2	1.68	in
Spacing between Applied Loads	a	18.67	in

These values allow for three capacity checks: flexural, laminate shear, compression flexure adjusted for shear studs. These checks solve for P , which is the load applied by a single load head and doubled to get the fully applied load. Some force equations pulled from AISC Steel Manuel [8], those equations labeled. For the purposes of these calculations because the section

has two separate layups the lower strengths were used, therefore the tensile and compressive strength are from the top flange/web/cover plate layup (Table 4) and the shear strength from the bottom flange (Table 5).

- Flexural Check:

$$M_{flex} = \min\left(\frac{F_{xt} * I}{Z_1}, \frac{F_{xc} * I}{Z_2}\right)$$

$$M_{flex} = 290.9 \text{ kip} * \text{in}$$

$M_{max} = P * a$ (Simple Beam - Two Equal Concentrated Loads Symmetrically Placed) [8]

$$M_{max} = M_{flex} = P * a \rightarrow P = \frac{M_{flex}}{a} = 15.6 \text{ kip}$$

$$P1_{applied} = 2 * P = 31.2 \text{ kip}$$

- Laminate Shear Check:

$$V_{max} = F_{xy} * \left(\frac{I * b}{Q}\right)$$

$$V_{max} = P = 45.2 \text{ kip}$$

$$P2_{applied} = 2 * P = 90.4 \text{ kip}$$

- Compression Flexure Adjusted for Shear Studs:

$$\text{Width Adjustment: } adj = \frac{w - d}{w} = 0.757$$

$$F'_{xc} = \frac{F_{xc} * adj}{1.3} = 16.1 \text{ ksi}$$

$$M'_{flex} = \frac{F'_{xc} * I}{Z_2} = 305.7 \text{ kip}$$

$$P = \frac{M'_{flex}}{a} = 16.4 \text{ kip}$$

$$P3_{applied} = 2 * P = 32.8 \text{ kip}$$

- Predicted Failure Load:

$$P_{failure} = \min(P1_{applied}, P2_{applied}, P3_{applied}) = P1_{applied} = 31.2 \text{ kip}$$

Another check is looking at the shear flow experienced during testing, and determining if the secondary bond is strong enough to withstand these loads. The shear flow experienced for different loads is shown in Figure 17.

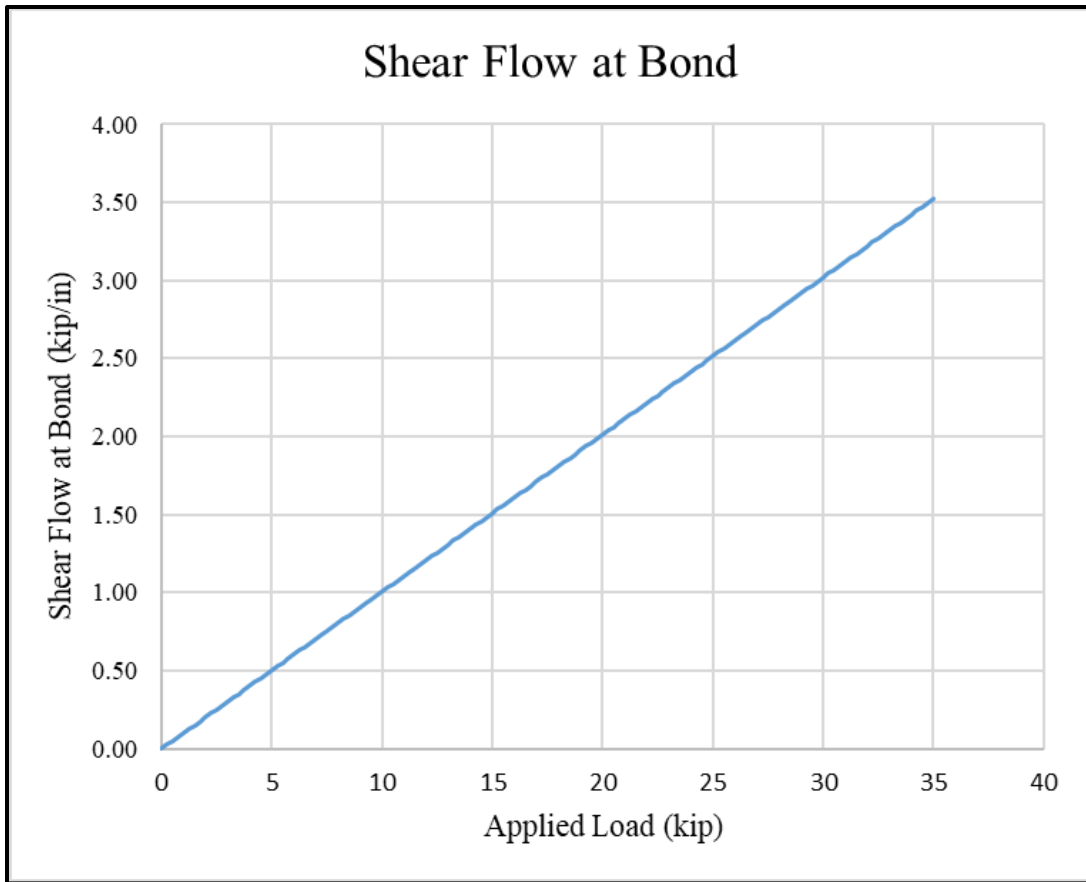


Figure 17: Shear Flow at Bond of Single Closed-Corrugation

With this initial test it was assumed that the secondary bond would be formed would be optimal and be no different than the bonds between layers of consolidated plates, at 3000 psi. With a bond length of about 3.14 in. per specimen, this would mean if an ideal bond was formed then the shear flow that would be able to be withstood by the secondary bond would be about 9.42 kip/in. Which as shown in Figure 16, is well above shear flow expected before other failures occur.

2.3 Manufacturing of Hybrid Beams

The steps to manufacture the closed-corrugation CFRTP specimen are listed below.

1. Creation of the tailored blanks
2. Consolidation of the tailored blanks into flat panels
3. Water jetting panels to desired dimensions and create shear stud holes (alignment holes were also water jetted at this time)
4. Forming of the corrugated shaped panels from flat consolidated plates utilizing a machined mold
5. Secondary bonding flat cover panels to the corrugated panels creating the closed-corrugation specimen

This process through utilizing IR Oven heating and a stamp forming process is very similar to the one outlined in detail by Vanclooster [9]. Additionally measures were taken to prevent wrinkles and buckling of the part during forming discussed by Haanappel [10].

2.3.1 Tape Layup Placement and Orientation

Tailor blanks were manufactured using a Dieffenbacher Fiber Forge Relay 2000 automated tape layup machine by laying 2-inch wide unidirectional E-glass/PETg thermoplastic composite tapes. The tapes are automatically pulled out to the required length and placed in the desired location and orientation on the machine rotating table. Tapes are held in place with vacuum suction until they are secured together through ultrasonic welding. As previously mention in this design an E-glass reinforced PETg tape provided by PolyOne was used, material data sheet is provided in Appendix A. The tape layup machine has a limit on the amount of layers that it is able to successfully connect into a tailored blank. Leading to a careful planning needed on where to split the tailored blanks when creating the dual layup corrugated sections. As

previously mentioned corrugated plates consist of two different layup schedules, one in the center for the bottom flange and the other on the sides for the top flange and web. The layup schedule is outlined in Table 3 of Section 2.2.1. These layups are made into a single tailored blank simultaneously, therefore the table shows when layers in certain sections are left blank well other sections receive another layer and which layers are placed continuously across the entire part.

2.3.2 Consolidation Method

The tailored blanks were all consolidated under the same settings, heated to a forming temperature of 355°F and a pressure of 100 psi. Consolidations were performed in a 650-tonne Utah Hydraulic press. Every consolidation cycle formed four plates, in order to do this a steel caul sheet was used to create two levels and each level allowed for two plates to be consolidated. For the corrugated consolidations thin steel spacers were used to account for the varying thicknesses because of the two different layup regions. These spacers ensured pressure was being appropriately applied to the layup, which along with heat all for the tapes to bond together forming one solid part. Removing the final plates required a release agent to be present on the press surface, caul sheet and corrugation thickness spacers. It is common to use a chemical release agent while consolidating and forming thermoplastic parts. However, since the plates would go through a secondary bonding procedure it was a concern that a chemical release agent could be baked into the part and could weaken or jeopardize success of a secondary bonding process. Because of this a release film was placed onto surfaces that would be used to form the secondary bonds. The stacking procedure for the consolidation of corrugated plates is shown in Figure 18.

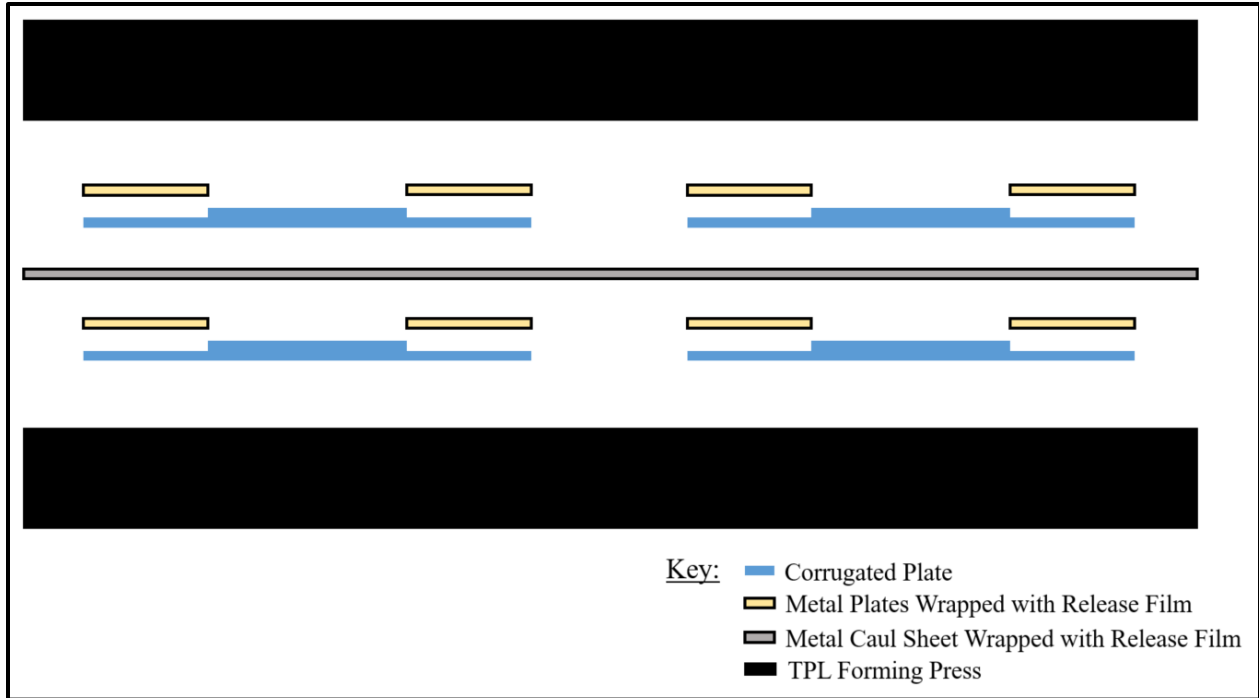


Figure 18: Stacking Positioning of Corrugated Plates for Consolidation

Once consolidated the parts were solid plates that could be cut and formed in order to create the closed-corrugated specimen. An example of the plates after consolidation before final forming procedures is shown in Figure 19.



Figure 19: Fully Consolidated Flat Plate

All panels were oversized to allow for water jetting to bring the dimensions precisely to the correct size. Additionally this allowed ± 45 layers to be trimmed and create a straight edge. For corrugations the only other components water jetted were the alignment pin holes used during stamp forming. Cover plates shear studs were water jetted before the secondary bonding cycle.

2.3.3 Corrugation Shape Stamp Forming

This process utilized an aluminum mold that was manufactured and machined to create the desired geometry for the corrugated sections. This mold, both male and female halves were attached to the forming press in the Thermoplastic Lab (TPL) of the ASCC. The mold was placed with the male end on the fixed bottom of the press with the female end attached to top, shown in Figure 20.



Figure 20: Stamp Forming Mold Positioned in the Press

This orientation along with alignment pins on the male mold ensure the mold and part stay centered during the stamp forming process. The alignment pins additionally help hold the part in the proper position, helping to ensure the desired fiber orientation, geometry and symmetry are all achieved. Due to the temperatures of the process and the speed and accuracy required to successfully form the part, the robotic arm and automated capabilities of the thermoforming cell were utilized. Since the process is automatic parts must be carefully aligned to ensure the part is placed in the correct spot during each trial. The forming process began with the part being placed into the Techni-Modul infrared oven where the corrugation panel was heated to 370°F with a dwell time of 30 seconds. At the conclusion of the heating process the panel was pliable, which allowed it to be formed into the desired corrugated geometry. The robotic arm moved the heated panel from the oven to the press, placing the panel on the alignment pins. The plate was pressed into the corrugated shape at 100 psi, until it cooled below the glass transition temperature

of 178°F. The resulting part is a complete corrugation panel that is 60 inches long and has the geometry outlined in Figure 21.

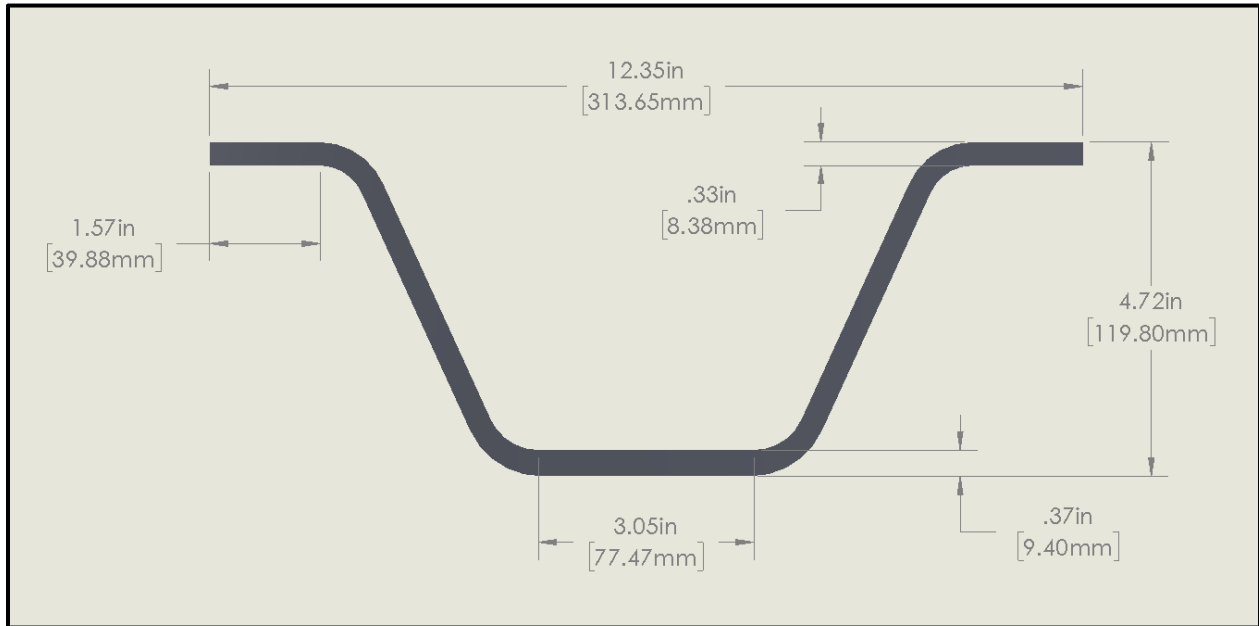


Figure 21: Dimensioning of Formed Corrugated Sections with Tentative Dimensioning

2.3.4 Secondary Bonding of Closed-Corrugation Section

Work up to this point was very similar to previous work performed on research of this project.

The remainder of the manufacturing process further explored options in forming a stay-in-place formwork that is both practical and effective. Specifically as mentioned for this work the closed-corrugation cross section was the targeted design. In order to achieve prototype specimen with this cross section through stamp forming and to attempt to limit the need for additional fasteners a secondary bonding process needed to be completed. The challenge that presented itself for this process was achieving a forming environment (temperature, pressure, time) that would allow two fully consolidated plates to be bonded together.

In order to achieve this it was determined that both the cover plate and the top flanges of the corrugated plate needed to be heated. Since the cover plate was a flat part it could easily be heated in the infrared oven and brought into the press. The corrugated plate couldn't be heated in

the infrared oven due to the need for it to retain its shape during heating and secondary bonding. For this reason it was decided that the corrugated plate would be in the female mold in the press and heated there using a combination of the press heating capabilities as well as cartridge heaters attached to the underside of the mold. These cartridge heaters were attached to the underside of the top flanges of the mold and wired to a control box that allowed the operators to fully control and monitor the heaters to ensure secondary bonding temperature were met. These heaters were strategically placed directly below the top flanges in an attempt to achieve localized heating at the bond area directly and not change overall part geometry. The schematic for the cartridge heater modified mold is shown in Figure 22, with the cartridge heaters shown in dark orange.

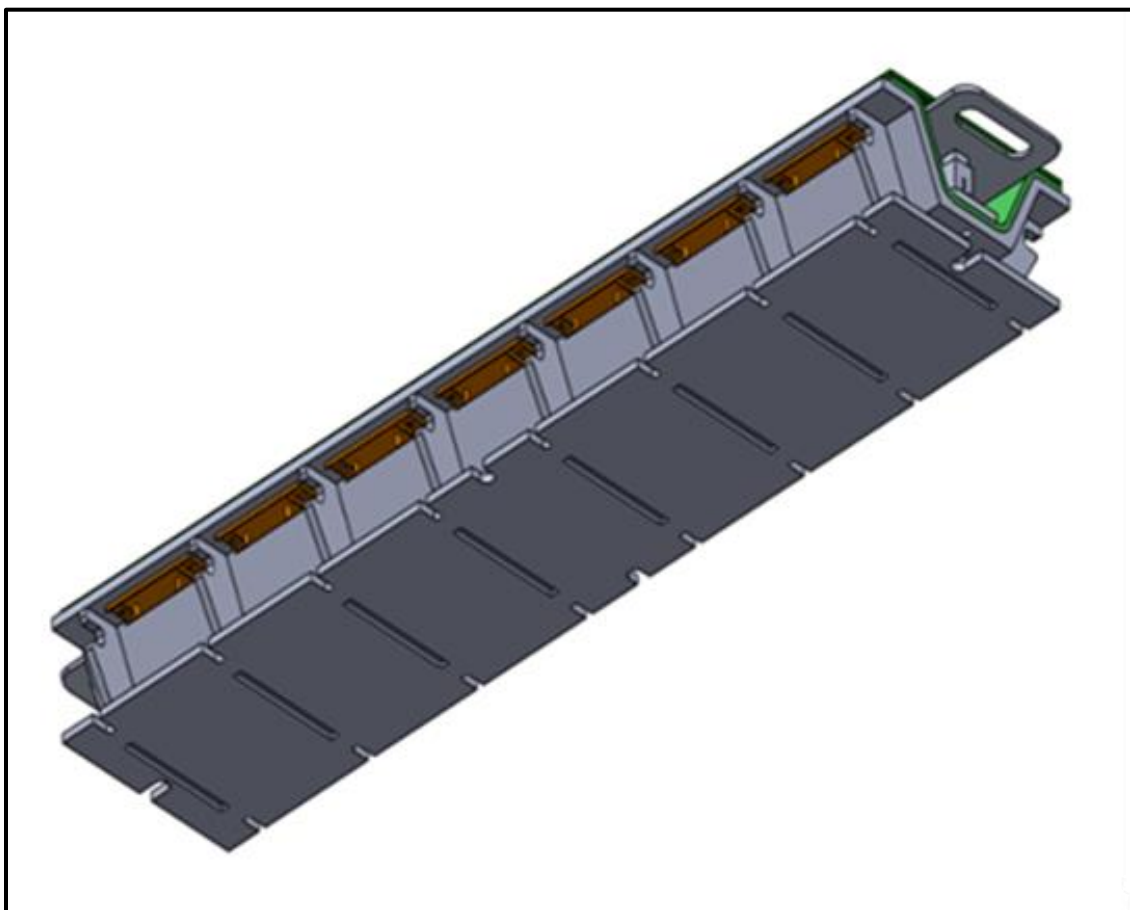


Figure 22: Rendering of Mold Modifications for Secondary Bonding

The other part needed for the secondary bonding process was a spring table for the inner channel of the corrugated panel to provide support to the heated cover plate. Without it the plate would sag throwing off the geometry and strength of the part, and the spring table allow the forming pressure to still be applied fully to the bond area. A cross sectional view of this spring table in the corrugated channel is shown in Figure 23.

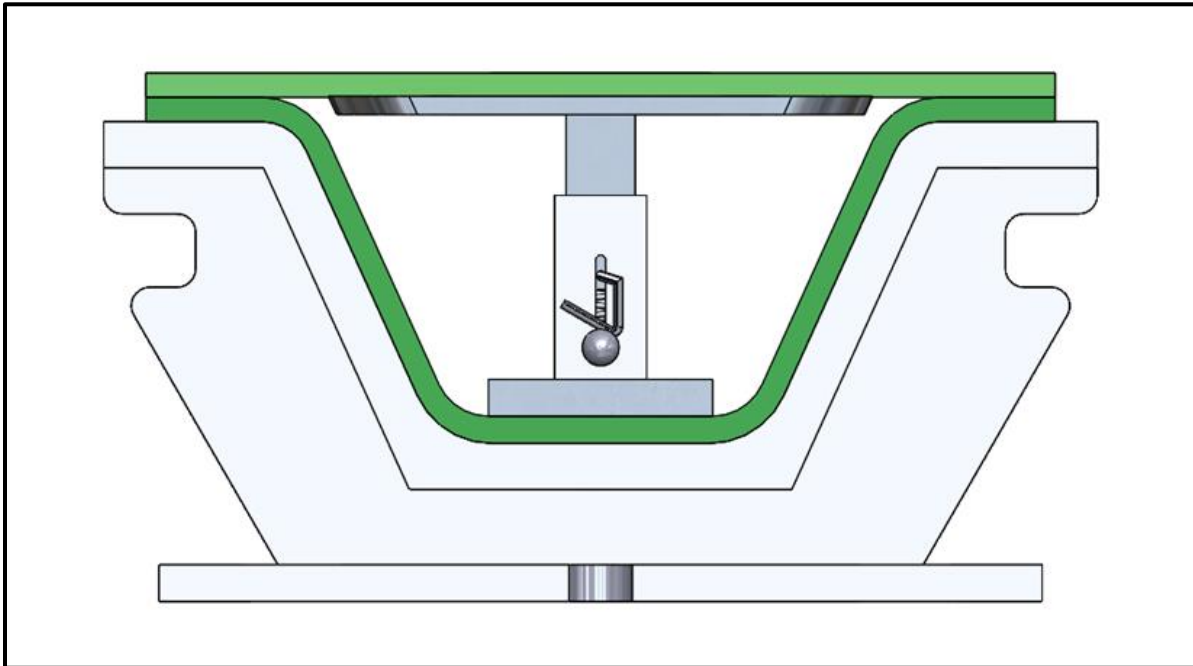


Figure 23: Rendering of Spring Table Supporting Cover Plate for Secondary Bonding

The secondary bonding procedure started with the heating of the corrugated panel in the press. Both press heating and cartridge heaters were used for this process. The press heating was primarily used to help limit the heat loss that was observed during trials. The temperature of the corrugated panel was monitored through thermocouples on both the bond surface of the top flanges and the walls and bottom flange. The bonding temperature of the top flanges was 225°F, and the heaters were adjusted in order for this temperature to be hit. Thermocouples on the non-bonding surfaces were used to monitor the overall temperature of the part and ensures localized heating was being achieved and the final parts strength would be jeopardized. The temperature

of the top flanges was less than the typical consolidation temperature of the PETg tapes of 355°F. It was believed that this process would perform similarly to that of 3D printing, where the material being added and coming out of the nozzle must be at the higher bonding temperature and the substrate part on the table only needs to be heated enough to be accepting of the new material to bond with. Therefore in the case of secondary bonding of closed corrugations, the substrate is the corrugated panel and needs to be heated above the glass transition temperature (T_g) of 178°F in order to be able to be bonded to. Therefore the temperature of 225°F was used for the top flanges. Once this temperature was reached the cover plate was placed into the infrared oven and heated to 370°F with a 30 second dwell time. At the end of the heating cycle the automated robot and system quickly moves the cover plate out of the oven and into position in the press. The press applied 100 psi to the part to form the bonding of the plates, once this pressure was applied the heaters were cut and once the temperature was well below the glass transition temperature the full specimen was removed. Manufacturing temperature and pressure chart is shown in Figure 24 and a completed single closed-corrugation part is shown in Figure 25.

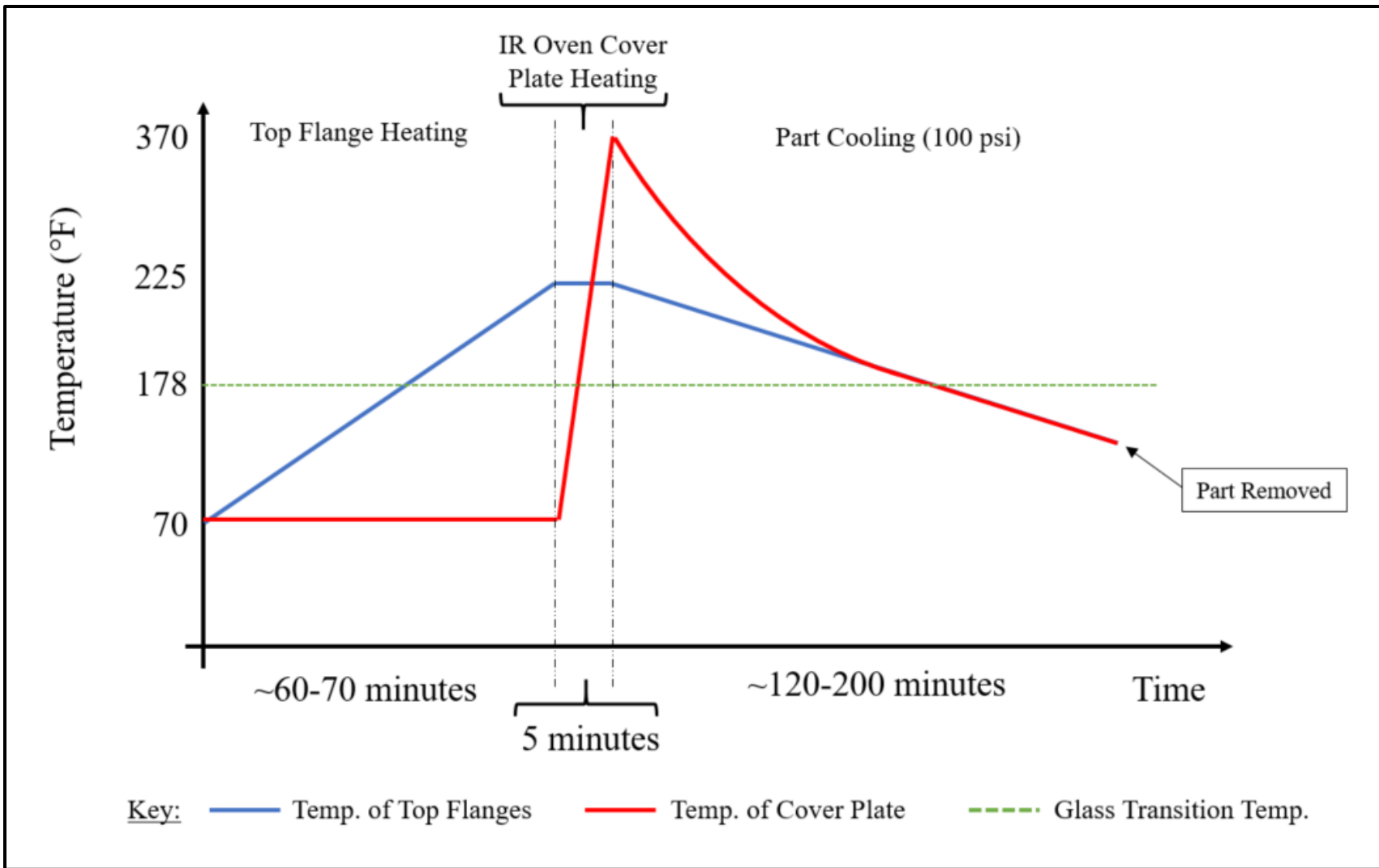


Figure 24: Temperature of Parts during Secondary Bonding Process



Figure 25: Completed Closed-Corrugation Part

2.3.5 Constructing Hybrid Closed-Corrugation Specimen

The final manufacturing step was with the addition of concrete to form a hybrid specimen. This process began by creating a rebar cage that would support the top decking surface as well as strengthen the internal shear studs with the purpose of getting proper shear flow between the concrete and the CFRTP. The rebar cage and #6 rebar going through the shear stud holes of the cover plate and resting on the bottom corrugation. The top deck was reinforced with a rebar cage formed with #3 rebar. An image of this rebar cage placed in the closed-corrugated panel is shown in Figure 26.



Figure 26: Rebar Cage and Formwork Prepared for Concrete

The holes in the cover plate allowed for concrete to be poured and fill the corrugation channel, fill the shear stud holes and then form the top deck. A self-consolidating 6 ksi mix was used to facilitate concrete placement. After initial testing of the hybrid beams it was determined that strengthening the bond of the CFRTP closed-corrugation could help increase the overall strength of the section. For this reason TAPCON concrete screws were used for testing of the final two hybrid specimen, the results of the effect of this modification will be discussed in Section 3.3.2. The complete hybrid specimen is shown again in Figure 27.



Figure 27: Completed Hybrid Closed-Corrugation Specimen

CHAPTER 3: SINGLE CLOSED-CORRUGATION TESTING AND ANALYSIS

3.1 Testing Setup

Plain, closed-corrugated panels were tested initially to assess panel response under construction loads, followed by testing of the hybrid concrete-CFRTP specimen. Four-point bending was applied for both sets of tests, with a 22 kip load cell used for the plain sections and a 110 kip load cell for the hybrid specimen. All testing was performed under a 110 kip Instron frame over a T-Slot table. This table allowed for the tilt table supports to be adjusted and moved exactly to the correct location, and the tilt tables acted as a pin-roller supports. The four point bend tests were run with 18.67 inches between load heads, as well as 18.67 inches between a load head and the near support. Supports were 56 inches center to center, allowing for 2 inches of beam to extend beyond the support and out of the test parameters. This in turn made the tested specimen length also 56 inches. A free-body diagram (FBD) is shown in Figure 28.

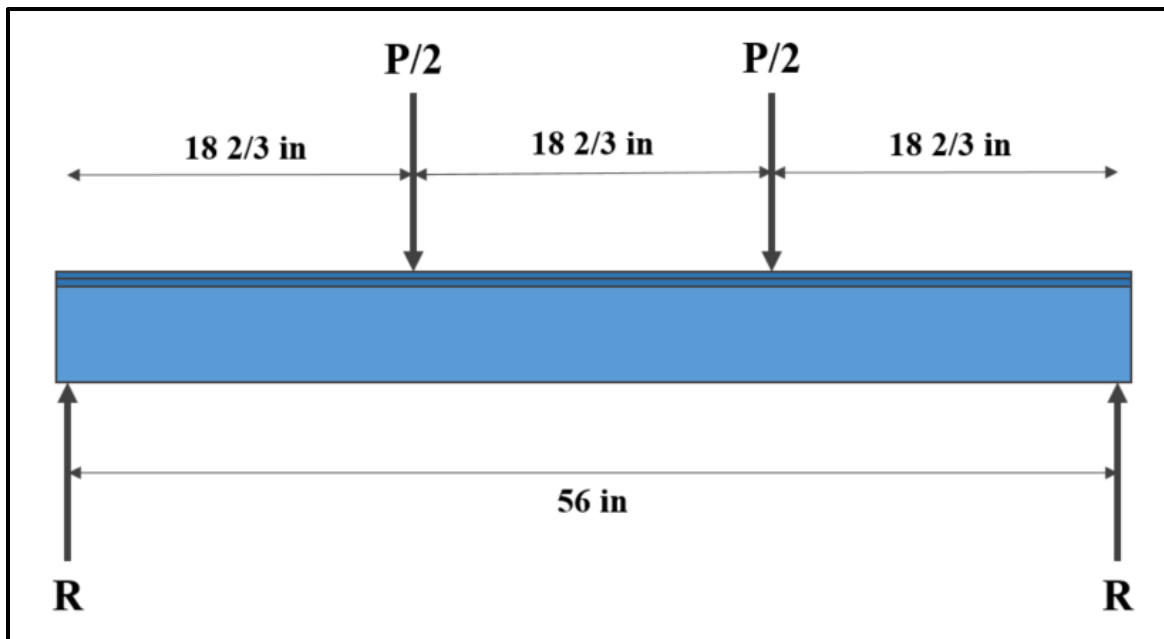


Figure 28: Free-Body Diagram of Closed-Corrugation Testing

Neoprene pads were placed between the support and the specimen, these pads were approximately a 4-inch square. The final component of the test set up was additional neoprene pads placed below the load heads. All neoprene looked to help distribute the loads and prevent stress concentrations. An image of the test set up is shown in Figure 29.



Figure 29: Test Setup for Single Closed-Corrugation Specimen

3.2 Test Procedures

The first step in testing was instrumenting specimen, to monitor strain and deflection of the parts during testing. All specimen had 12 linear strain gauges, 6 at the midspan and 6 between one of the load heads and the support (9.33 inches from the support). For the hybrid sections putty was used to protect the gauges and the wires as concrete was poured. Gauges were placed above and

below the secondary bonds and the very bottom of the specimen at each location. The focus of these gauges was to observe if loads were being appropriately transferred through the secondary bond. The locations of the strain gauges for each set are shown in Figure 30.

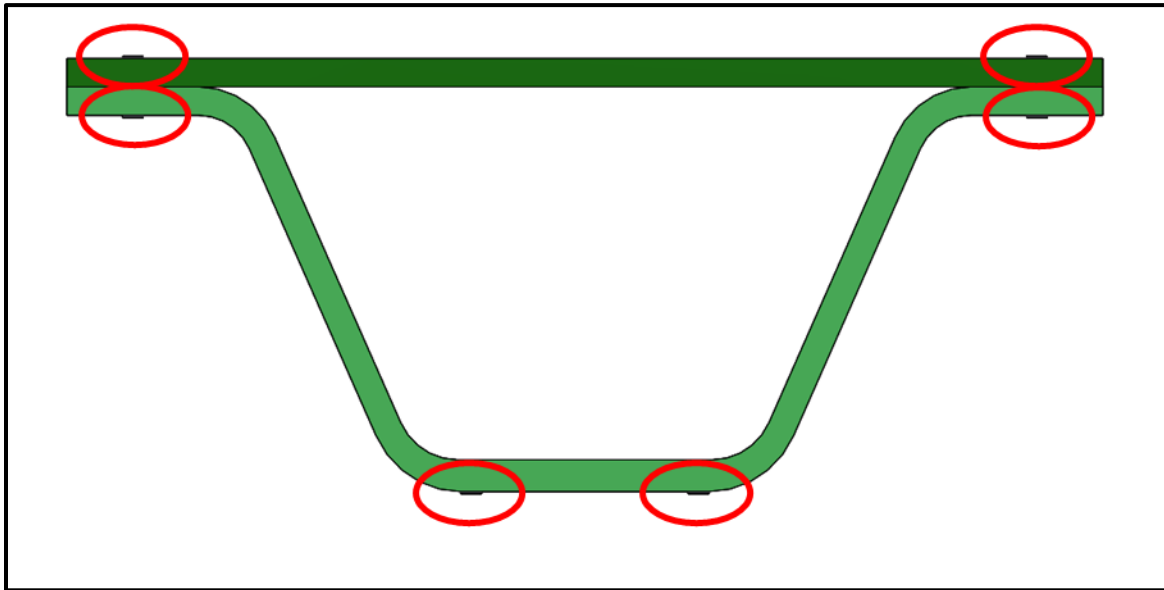


Figure 30: Strain Gauge Positioning on Closed-Corrugation Specimen

String potentiometers placed below the load heads and at the midspan as well as linear displacement transducers (LDTs) at each support were used to record deflection. The only other test prepping required putting some wood blocks into the corrugated channel of the bare specimen directly below the load heads to act as a diaphragm and prevent localized crushing. Once a specimen was fully prepped a series of photographs were taken to help with the visual inspection of the part after failure. Testing began with the bare specimen and the construction loading test. This test was used to confirm that the bare closed-corrugated CFRTP specimen is capable of holding the weight of the wet concrete during construction without excessive deformation which could have negative results for the composite system. The testing procedure included subjecting two specimens to 561 pounds in a four-point bending test followed by unloading. This load-unload process was repeated three times. The load of 561 pounds was

determined through referencing American Association of State Highway and Transportation Officials (AASHTO) LRFD Bridge Design Specifications [11] which outline requirements for stay-in-place formwork of,

- Formwork self-weight
- Weight of Concrete Slab
- Additional 50 pounds per square foot
- Maximum deflections for spans 10 feet or less; span length divided by 180 or 0.5 inches.

After completing the construction loading test, a quick inspection was done of the specimen to ensure it wasn't damaged (neither test displayed damage at this time), then the failure test of a bare specimen was performed. Videos were taken during the failure test with a series of photographs being taken at the conclusion of the test to show locations of failure. Upon completion of the bare specimen, failure tests were performed on the full hybrid specimen. The same camera protocols recording the test and the results were completed for these hybrid specimen.

3.3 Test Results

Two tests were conducted on panel specimens as detailed subsequently: construction loading tests on bare closed corrugated CFRTP specimens, and strength load tests on composite closed corrugated CFRTP specimens. The strength of the concrete was monitored through the testing procedure. The compressive strength of the concrete was approximately of 7000 psi at the time of testing, exceeding the target strength by approximately 1000 psi.

3.3.1 Construction Loading Test

Both of the specimens tested under the construction loading criteria defined by AASHTO successfully withstood the loading with no visible damage, and deflections did not exceed the

AASHTO limit of 0.02 inches. Figure 31 shows the load-midspan deflection plot for Specimen 1 and Figure 32 shows the same plot for Specimen 2.

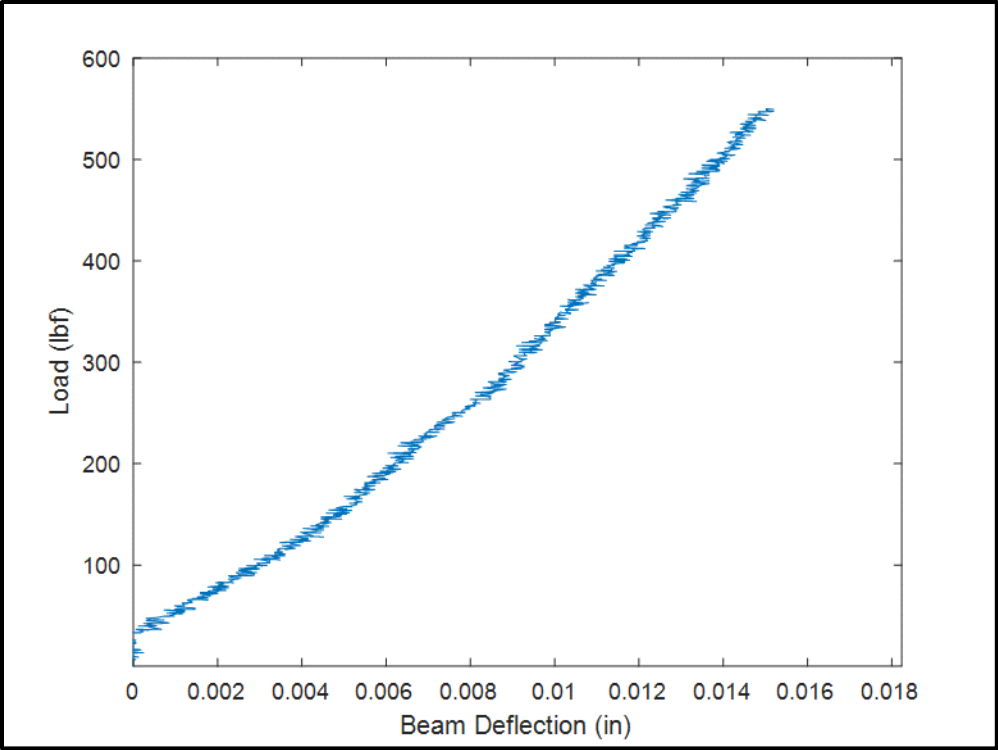


Figure 31: Load-Deflection Plot of Specimen 1 – Construction Loading

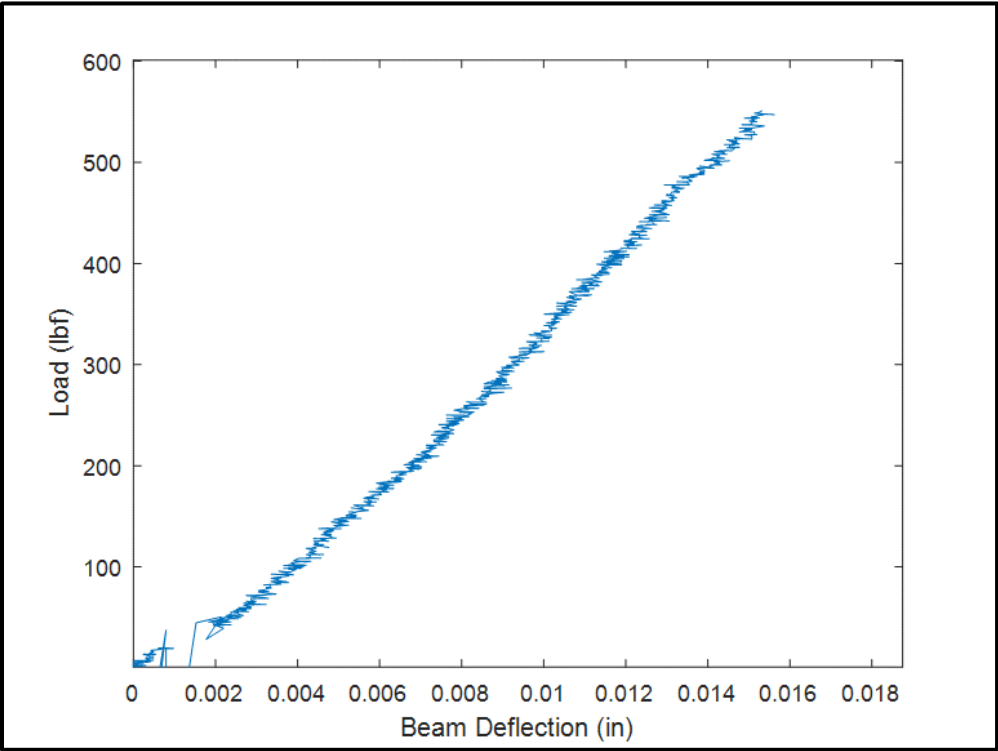


Figure 32: Load-Deflection Plot of Specimen 2 – Construction Loading

In the plot for Specimen 1 there is initially some loading and with no recorded deflection, and the reason for this is unclear. Possible reasoning could be due to the neoprene compressing before readings began or a lag in the data recording devices. In the plot for Specimen 2 the spikes in the plot before 0.002 inches could be due to the load cell being used within the bottom 1% of its capacity. These plots also allow for the experimental stiffness of the beams to be calculated by looking at the slope of a trend line between 100 kips and 500 kips for each plot. For Specimen 1 this experimental stiffness as 37.4 kip/in. Similarly the plot for Specimen 2 also shows the experimental stiffness of the beam to be 38.8 kip/in.

After completing the construction loading cycles, the bare specimens were loaded until failure. Failure predictions were that failure would be at 31.2 kips as a compression failure in the cover plate, as seen in Section 2.2.2. For Specimen 1 failure occurred at a load of 19.8 kips, and for Specimen 2 at a load of 20.5 kips. Specimen 1 had visible failure in the bottom flange and the secondary bond, but there was concern of the wood block working against the specimen and contributing to the failure of the secondary bond. For that reason the diaphragm wood blocks were removed for Specimen 2, which saw a higher failure load and only saw failure in the bottom flange. The failure images of Specimen 1 and Specimen 2 are displayed in Figure 33 and 34 respectively.



Figure 33: Failure of Specimen 1 – End Cross Section



Figure 34: Failure of Specimen 2 – End Cross Section

3.3.2 Hybrid Beam Failure Test

During testing a modification was made to specimens 4 and 6 to mechanically strengthen the secondary bond by installing TAPCON concrete anchors at the locations of the shear studs through the top flange and cover plate and into the concrete deck. Anchors were not installed in

Specimens 3 and 5. All test specimens exhibited failure in the secondary bond, with the cover plate popping off the corrugated section as shown in Figures 35 and 36.



Figure 35: Failure of Specimen 4 – End and Side View



Figure 36: Failure of Specimen 5 – Side View

In specimens 3 and 5, the cover plate started to separate in the middle of the beam between the load heads and spread to the ends, and failure occurred when the splitting extended all the way to the end of the specimen. In specimens 4 and 6, secondary bond failure initiated at the ends of the specimen. In all the tests except Specimen 6, broken fibers were visible as a result of the secondary bond failure, an example of this can be seen in Figure 35. This shows that the quality of the secondary bond was very good, and wasn't failing directly at the surface between the two plates, but rather within the CFRTP. The TAPCON-modified Specimen 4 exhibited an additional failure in the web of the corrugation as shown in Figure 37.



Figure 37: Web Failure of Specimen 4

The failures observed around the secondary bond surface need to be addressed and improved as the project advances. The neutral axis was observed to be very close to that secondary bond level, and could be causing the failure to occur there. Optimization of the cross sectional geometry to manipulate the height of the neutral axis could allow this failure to be avoided.

The load-deflection curves for the four specimen are displayed in Figure 38. Load is recorded with the Instron, and deflection was measured with string potentiometers. The deflection results for Specimen 5 were invalid after a load of approximately 22 kips due to the string potentiometer bottoming out or disconnecting during the test. However, up to that point the data appear valid and can be used to evaluate stiffness of the specimen. The AASHTO Equivalent Factored Load of these specimen was 14.5 kips, and the failure load for all specimens exceeded that value. Stiffness was calculate over the linear portion of the plots for each specimen, this was deemed to be between 5 and 20 kips, this was done to capture response in the linear range. Strength and stiffness results are summarized in Table 7.

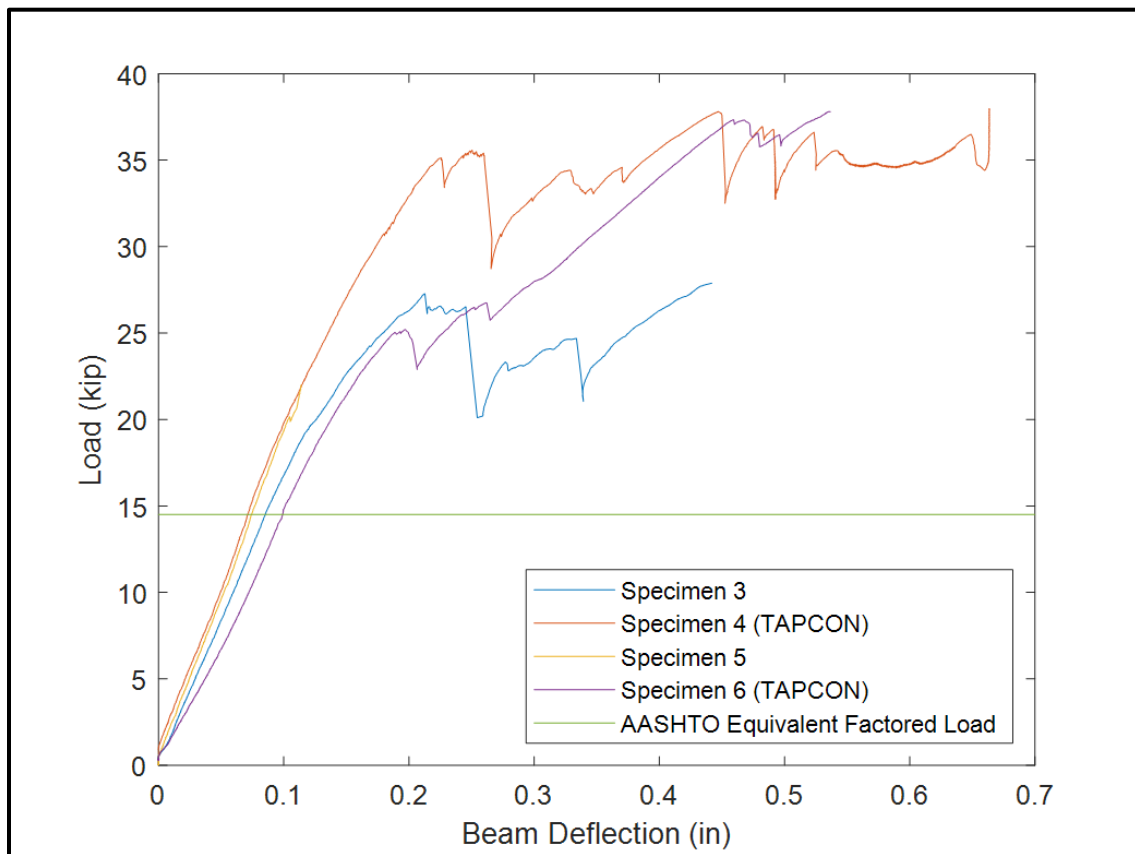


Figure 38: Load-Deflection Plot for Hybrid Closed-Corrugation Specimen

Table 7: Strength and Stiffness of Hybrid Closed-Corrugation Specimen

Specimen	TAPCON Modified	Max Load (kip)	Max Deflection (in)	Stiffness (kip/in)
Specimen 3		27.9	0.442	155.6
Specimen 4	X	38.0	0.664	187.3
Specimen 5		33.8	0.117	184.1
Specimen 6	X	37.8	0.537	149

3.3.3 Analysis of Data

When looking at the flexural strain of the hybrid specimen all 12 longitudinal strain gauges were evaluated and grouped based on the position they are on the beam and the side they are on.

These strain gauge locations are shown in Figure 39.

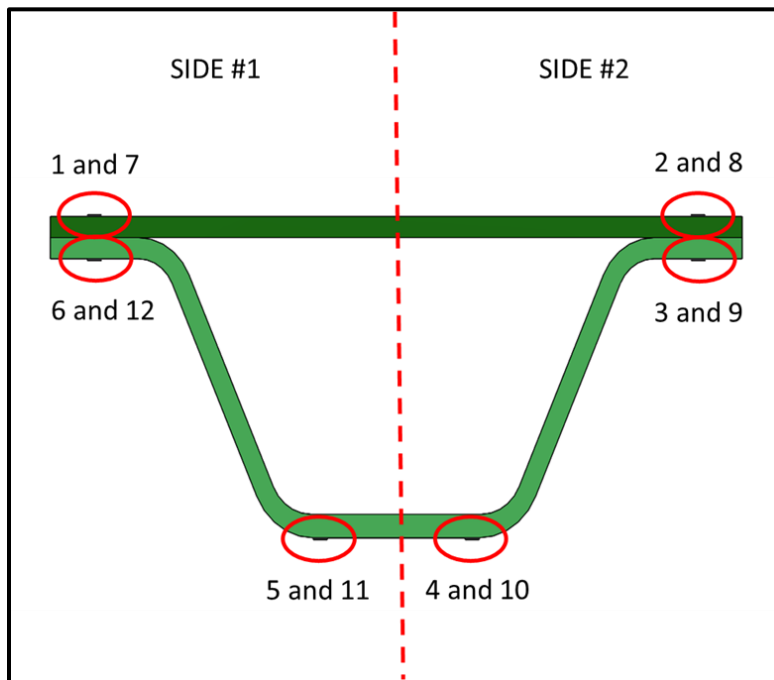


Figure 39: Strain Gauge Location and Side Definition

Figures 40 to Figure 43 show the strain at each height for Specimen 3 where gauges were placed at varying loads; 5 kips, 10 kips, 15 kips, and 20 kips. The maximum load strain measurements were evaluated at was at 20 kips, at which point the specimen load-deflection was linear and shear cracks hadn't formed on any of the specimens. A summary of available strain data is shown in Table 8 for all specimen. The addition of the TAPCON concrete anchors after the installation of the strain gauges caused some of the strain gauges to be compromised and not provide accurate readings, which is why some readings on Specimen 4 and 6 are empty in Table 8. For the most part the readings from a single specimen were relatively equal when comparing one side to the other. The most variation can be seen in the gauges reading the cover plate. These gauges are encased in concrete, and even though measures were taken to protect them it is possible that the strain gauges were damaged when concrete was placed.

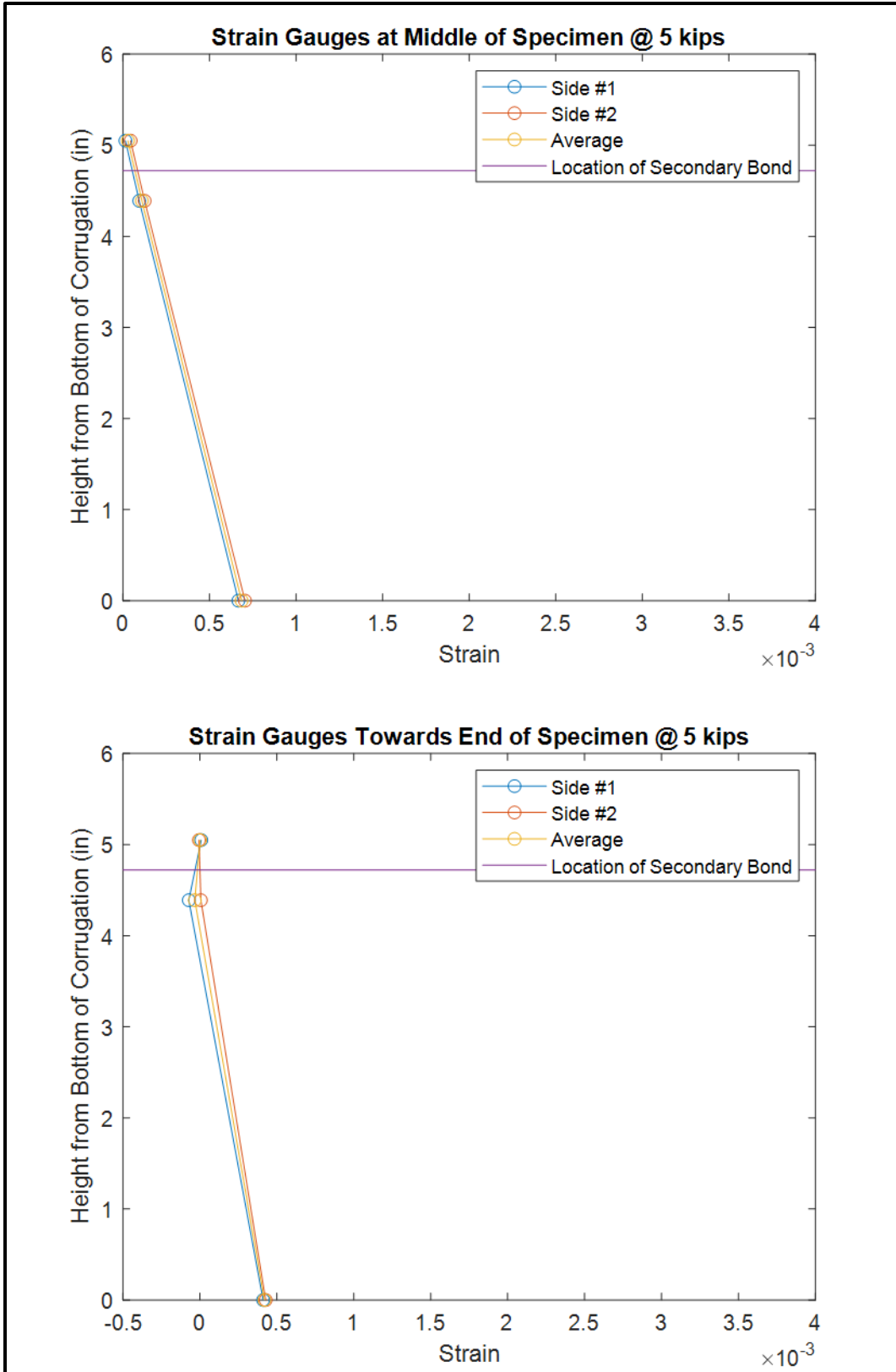


Figure 40: Specimen 3 Strain-Heights at Midspan and Beyond the Load Head at 5 kips

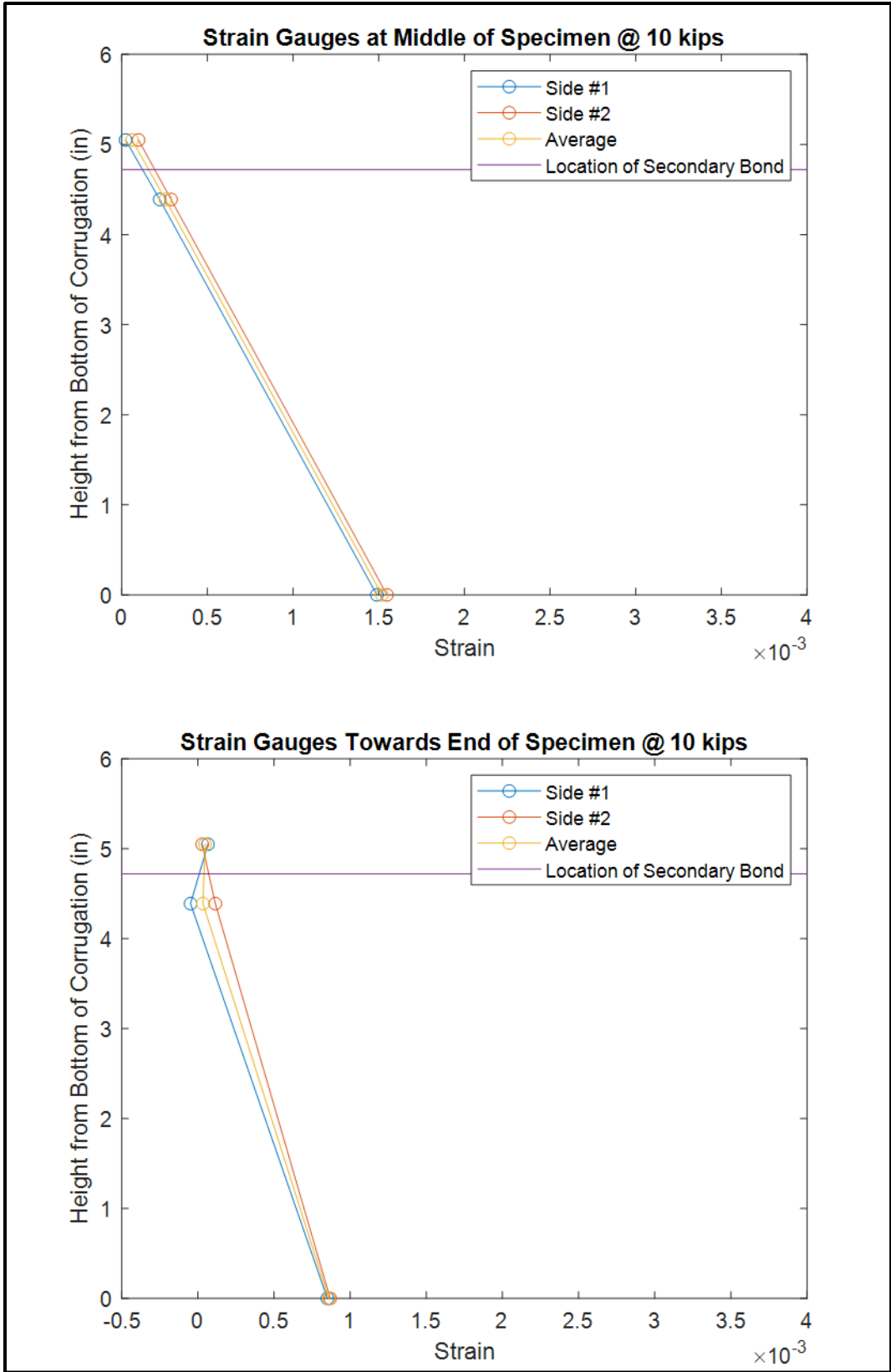


Figure 41: Specimen 3 Strain-Heights at Midspan and Beyond the Load Head at 10 kips

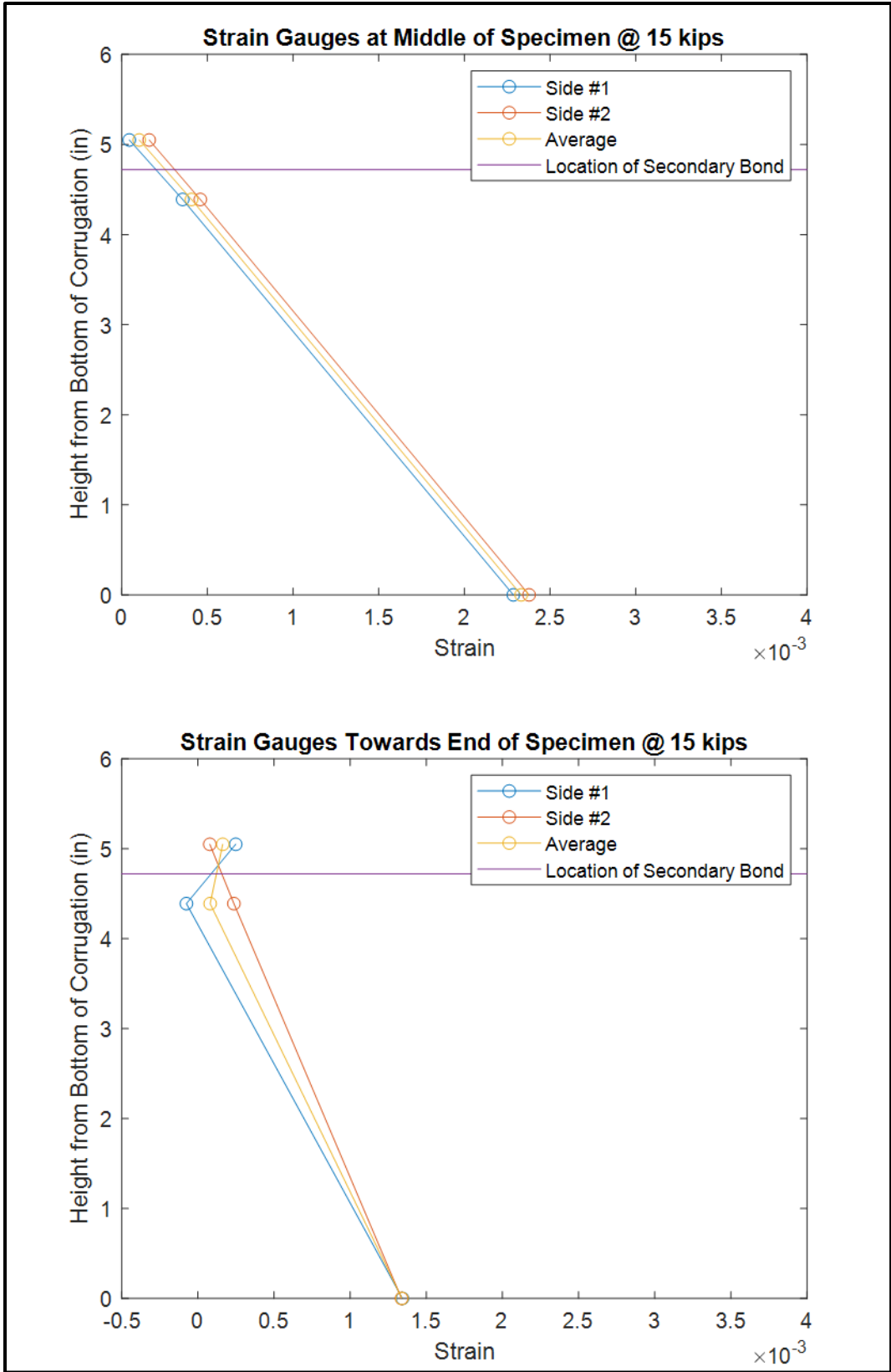


Figure 42: Specimen 3 Strain-Heights at Midspan and Beyond the Load Head at 15 kips

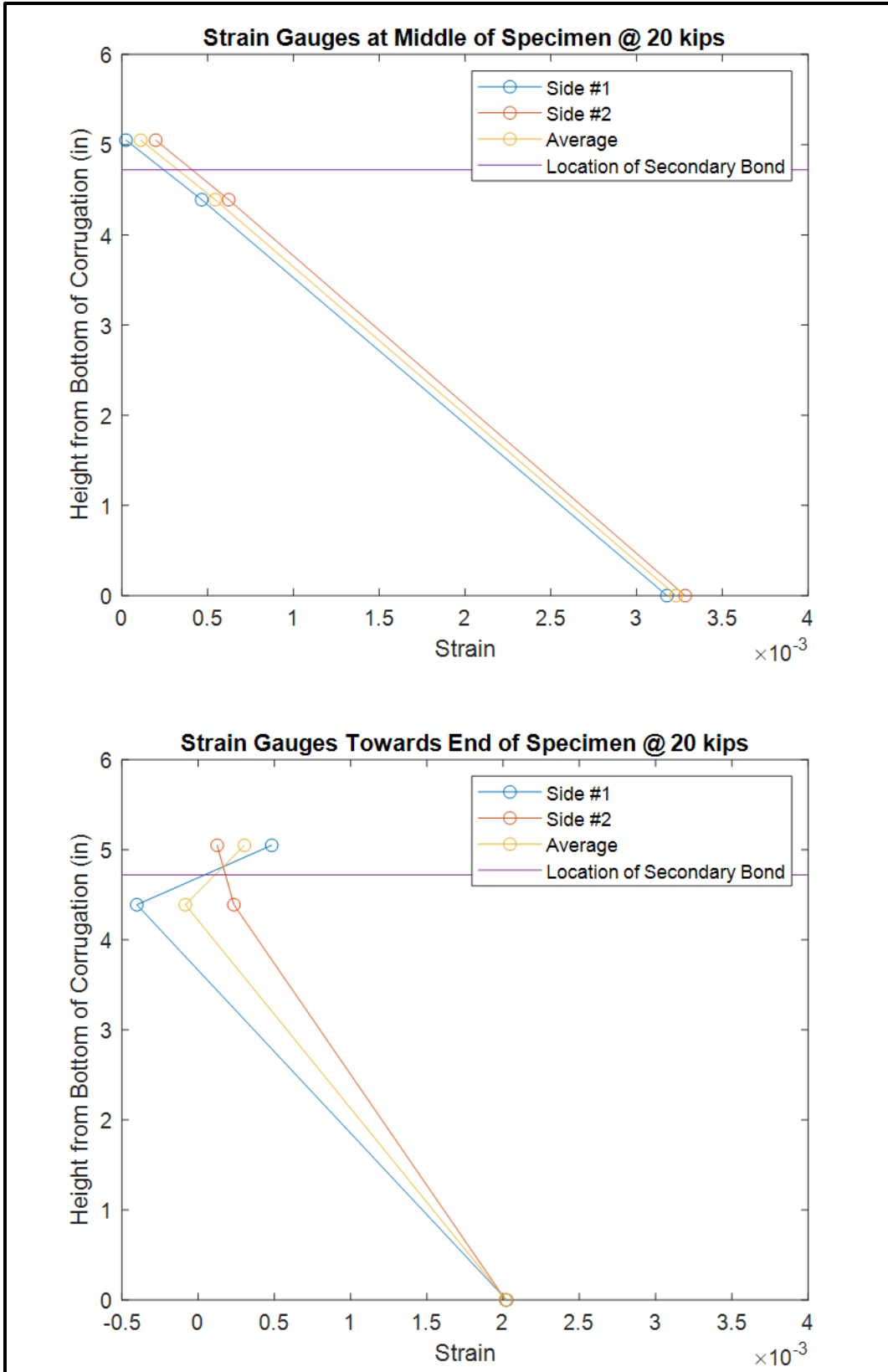


Figure 43: Specimen 3 Strain-Heights at Midspan and Beyond the Load Head at 20 kips

The strain readings at midspan also corresponds to being between the load head during the 4-point bend test, where the shear force should be zero. Because of this a linear reaction is observed throughout the loading process with no large drops in the shear stresses. But this drop is seen when looking at the strain readings towards the end of the beam, or beyond the load head, especially when looking at the heights around the bond line. This drop could point to the first sign of secondary bond failure, but since the drop is seen throughout testing it doesn't appear to be caused by a singular load resulting in bond failure. Therefore it points to being a sign of a relatively poor secondary bond of the thermoplastic parts resulting in a relative slip between the cover plate and the corrugated section.

Table 8: Summary of Strain Data – Readings at 20 kips

		Middle Gauges				End Gauges			
		Side #1	Side #2	Average	Coefficient of Variation	Side #1	Side #2	Average	Coefficient of Variation
Specimen 3	Top of Cover Plate	24.2	197.2	110.7	110.51	482.9	125.4	304.15	83.11
	Bottom of Top Flange	465.6	623.0	544.3	20.45	-401.6	234.6	-83.5	-538.76
	Bottom of Bottom Flange	3177	3283	3230	2.32	2023	2017	2020	0.21
Specimen 4	Top of Cover Plate	119.5				201.0	164.2	182.6	14.25
	Bottom of Top Flange	359.4				270.3	390.9	330.6	25.79
	Bottom of Bottom Flange	2018				1093	1074	1083.5	1.24
Specimen 5	Top of Cover Plate	148.9	81.6	115.25	41.29	390.7	369.9	380.3	3.87
	Bottom of Top Flange	574.9	532.4	553.65	5.43	463.8	448.7	456.25	2.34
	Bottom of Bottom Flange	3321	3391	3356	1.47	1524	1590	1557	3.00
Specimen 6	Top of Cover Plate		70.9						
	Bottom of Top Flange		412.7						
	Bottom of Bottom Flange		1418						

Initially using a cracked section analysis, the neutral axis was calculated to be just above the cover plate, above the strain gauges on the top of the cover plate. The data in Figures 39 to 42 are consistent with a neutral axis located above the cover plate.

3.4 Advancement Options – Secondary Bonding

The closed-corrugation cross-section and its novel approach to achieving composite action between the CFRTP and concrete is promising, but improving the strength of the secondary bond of the cover plate is necessary to achieve full capacity of the section and optimize its design for bending and shear. Ideally, the secondary bond would result in a specimen that performs similarly to a high-quality section made in a single consolidation, or using pultrusion. Coupon-level testing has been performed as discussed in the next chapter to increase understanding of the forming settings required to achieve a higher-quality secondary bond. Once high-quality secondary bonds are possible, closed-corrugation cross sections could be spliced via single, wide cover plat to give a wide deck section as shown in Figure 44.

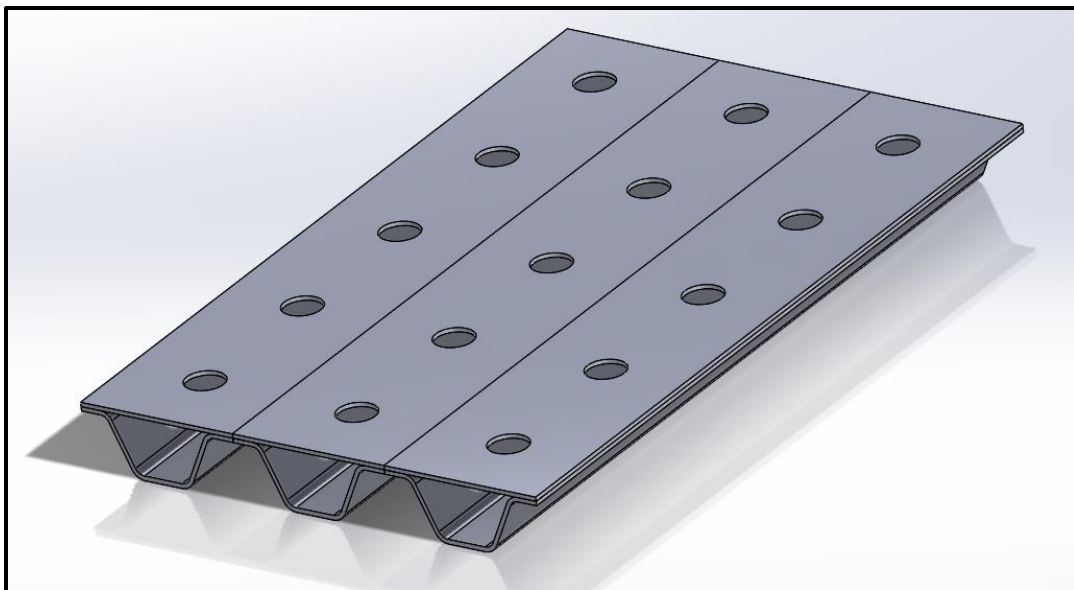


Figure 44: Multi Closed-Corrugation Spliced Panel Rendering

CHAPTER 4: SECONDARY BONDING MANUFACTURING TRIALS

4.1 Introduction

This chapter looks into options for secondary processes that go beyond simple consolidation and stamp forming of thermoplastic parts. Part of the chapter looks into possible improvements to be done to the settings used for secondary bonding of pre-consolidated plates, further outlined in Section 4.1.1. The other part of the chapter looks into possible surface manipulation using a stamp forming process for either plates or internal concrete reinforcement, further outlined in Section 4.1.2.

4.1.1 Secondary Bonding

A benefit gained from using continuous fiber reinforced thermoplastic (CFRTP) composites is the ability to modify a part through secondary bonding via heat and pressure. The ability to reshape a part has already been established in previous work like the initial corrugated section and stiffened panel by Smith [4], and additionally in the closed-corrugation sections described in Chapter 2 and 3. As previously mentioned the secondary bond was the weak point in the closed-corrugation, and where the failure occurred during testing of hybrid specimens. A portion of this chapter will outline some coupon level testing to assess secondary bond settings to be used on future work of the project. This will be done by manufacturing coupon sized lap shear specimens to evaluate the heat and pressure required to form a quality bond between two thermoplastic plates already consolidated. Testing will be adopted from ASTM 5868-01: Lap Shear Adhesion for Fiber Reinforced Plastic (FRP) Bonding [12]. An example of the specimen to be used is shown in Figure 45.

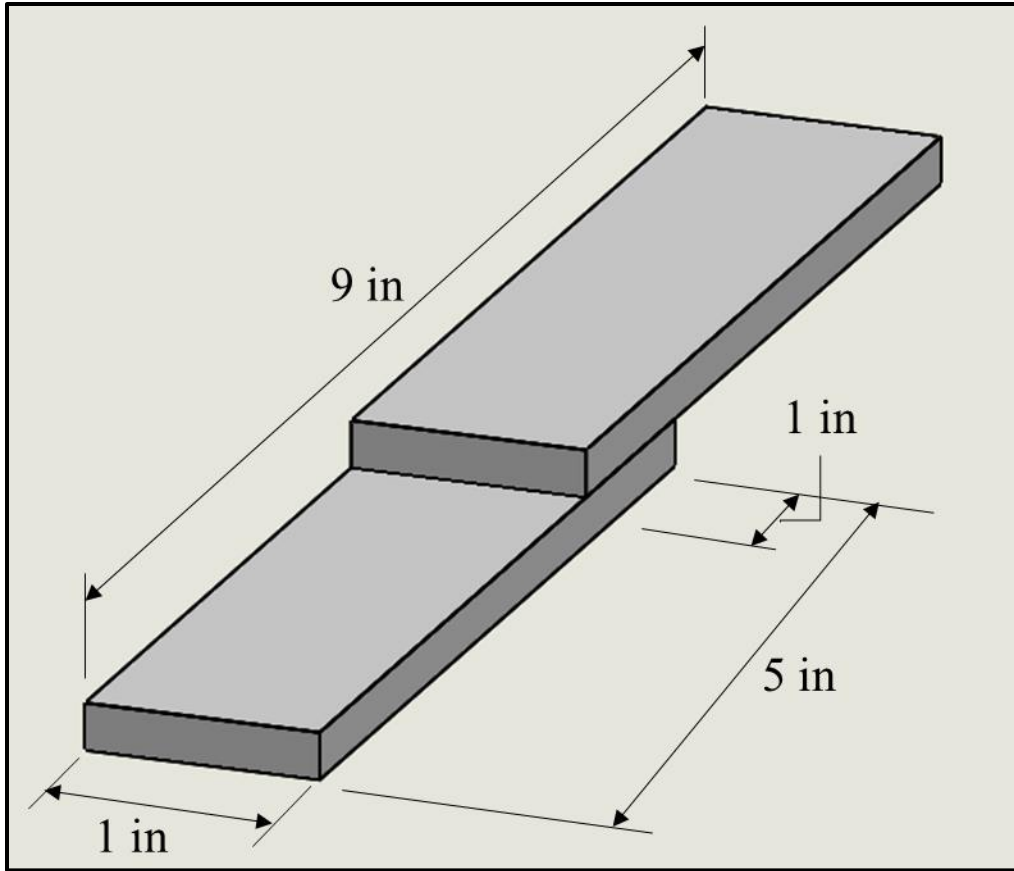


Figure 45: Secondary Bonding Lap Shear Specimen Rendering

4.1.2 Surface Manipulation

In order to develop thermoplastic composites to manufacture internal concrete reinforcement (thermoplastic composite rebar), some initial contributions were performed primarily on ways to roughen the outer surface of the bar. These included stamp forming, thermal rolling, sand or bead coating. For the first generation prototype manufacturing stamp forming was still utilized to give the bar a series of ridges pressed into outer layer. This process could be used in the stay-in-place formwork research work as well. Ridges formed on the surface of an FRP composite against which concrete is cast have been demonstrated to provide additional effective transfer of shear forces between concrete and FRP this concept has been further explored by Guzzi [13] and Davids et al (in review) [14]. The second section of this chapter looks into this surface manipulation and the first generation stamp forming strategy.

4.2 Manufacturing of Secondary Bonding Coupon Specimen

4.2.1 Tape Layup Orientation

The orientation of the corrugated plate and cover plate weren't the primary issue in the initial closed-corrugated section. Since the closed-corrugation design will be utilized as the project continues into testing a stay-in-place formwork plate, the design will build off the single closed-corrugation and be a series of closed-corrugations. Because of this it was determined that the secondary bonding testing specimen should have the same orientation. All plates have the following laminate layup sequence,

$$[0_2/\pm 45/0_2/\pm 45/0_2/\pm 45/0_2/\pm 45/0_2/\pm 45/0]_S$$

Tailored blanks were all manufactured on the Dieffenbacher Fiber Forge Relay 2000 automated tape layup machine. Sizes varied depending on the set of coupons that were going to be used to manufacture. For control specimen made using PETg spacers tailored blanks were made as 12 inches by 60 inches, and for control specimen made using an Aluminum spacers tailored blanks of 6 inches by 48 inches. After tailored blanks were created edges from the ± 45 layers that extended beyond the edge of the plate were trimmed creating the desired coupon shape. For test specimen that required plates that had already been consolidated tailored blanks of 36 inches by 60 inches were made. Larger plates allowed parent plates to be consolidated and then have multiple test specimen to be cut out with the water jet.

4.2.2 Consolidation of Control Specimen

Control specimen tailored blanks were stacked into the press following the schematic shown in Figure 46. Consolidating the tailored blanks at the same time while being set into the press where a portion of the surfaces were in contact with each other aimed to consolidate the two sides individually and together. This process should create an optimum bond identical to that

created through a traditionally consolidation. The spacers had two functions; first, they gave the correct lap shear specimen shape to the part. Second, they ensured equal pressure was applied across the part, fully consolidating each side and bonding the joint. Two different spacer materials were used; E-glass/PETg composite and aluminum. In both cases the spacers were wrapped in release film, this prevented the spacers from bonding to the part and kept chemical release agents from being added to the process and potentially being baked into the part and impacting the bond of the two sides.

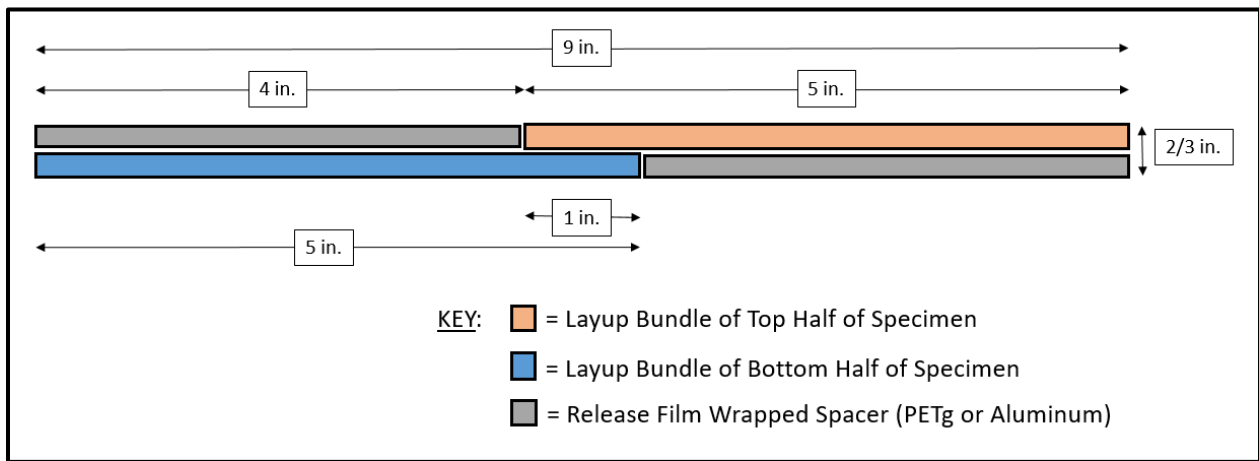


Figure 46: Cross-Sectional View of Stacking Procedure for Control Specimen

E-glass/PETg composite spacers were used first as an attempt to keep completely equal pressure across the entire part, since a spacer material other than PETg could causing unequal pressure due to both the stiffness and the thermal properties of the material of the spacer. Consolidation settings matched the settings used in previous portions of this task and others when using PETg, which is 335°F and 100 psi. However, E-glass/PETg composite spacers resulted in some shifting in the layers of the tailored blanks, since when stacked the tailored blanks are significantly thicker than the thickness and the spacers. This caused uneven surfaces and shifting of the part and the spacer as the temperature increases and the PETg material becomes malleable.

This layer shifting was seen primarily at the bond area and is highlighted and shown in Figure 47.

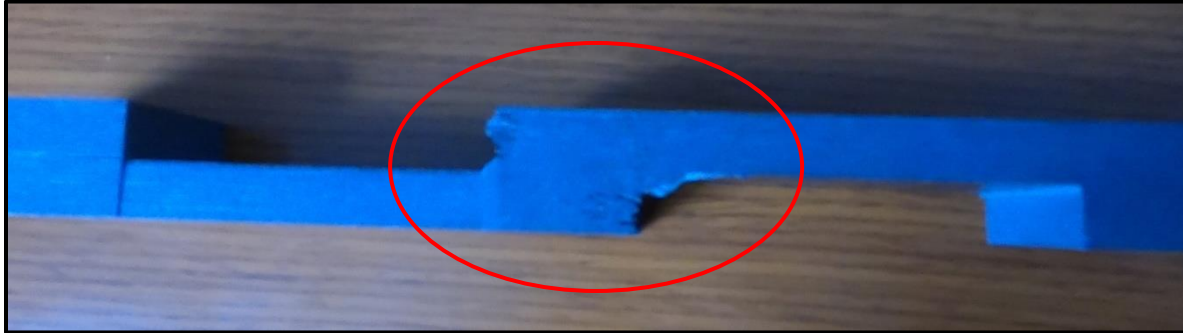


Figure 47: Side View of a PETg Spacer Control Coupon – Highlighted Bond Area

To remedy this, spacers made from aluminum were acquired. The same process was followed with these spacers. The aluminum spacers were slightly thinner than the PETg spacers and each half of the coupon. This ensures that the full pressure is applied to the bond. However, a similar shift was seen in the layers, seen in Figure 48. This result points to the shift potentially happening as pressure is applied and the tailored blanks are pressed into their final thickness regardless of the spacer used. During this process any misalignments or imperfections in the tailored blanks could cause some shifting.

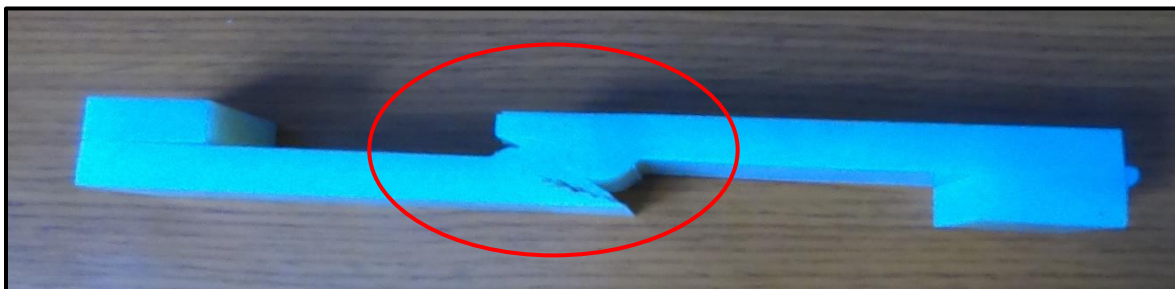


Figure 48: Side View of an Aluminum Spacer Control Coupon – Highlighted Bond Area

This shifting wasn't initially expected and visually isn't what was intended but the specimen still would serve as the control. Only testing would truly determine if this shifting would impact the

strength of the specimen. This shifting does impact the overall size of the bond area, in both cases making the bond area less than the desired one square inch.

Once parent plates were fully consolidated the plate was cut down to a width of 7 inches, which is the desired lap shear specimen length. Next strips were cut out of the parent plate creating the final control specimen. The final stage was using pligrip to attach small PETg cubes to the ends to provide loading tabs during testing.

4.2.3 Consolidation of Test Specimen

In order to test secondary bonding and splicing techniques, PETg tape layups had to be first consolidated into flat plates. In order to do this large tailored blanks (36 inches by 60 inches) were consolidated using PETg standard settings, 335°F and 100 psi. Each large plate allowed for multiple halves of lap shear specimen and spacers to be created, giving relative uniformity across the thickness of parts, resulting in pressure to be appropriately applied to the bond line. During this consolidation release film was used as a release agent in order to keep the bonding surfaces free of a chemical release agent that could possibly impact the bond quality. This measure is performed for all plates undergoing a secondary bond. From the large consolidated plates strips were cut out at 5 inches by 60 inches and 4 inches by 60 inches. The 5 inch wide strips would be used to create the lap shear specimen and the 4 inch strips were used as spacers during the secondary bonding process. A final example of a test specimen can be seen in Figure 49.

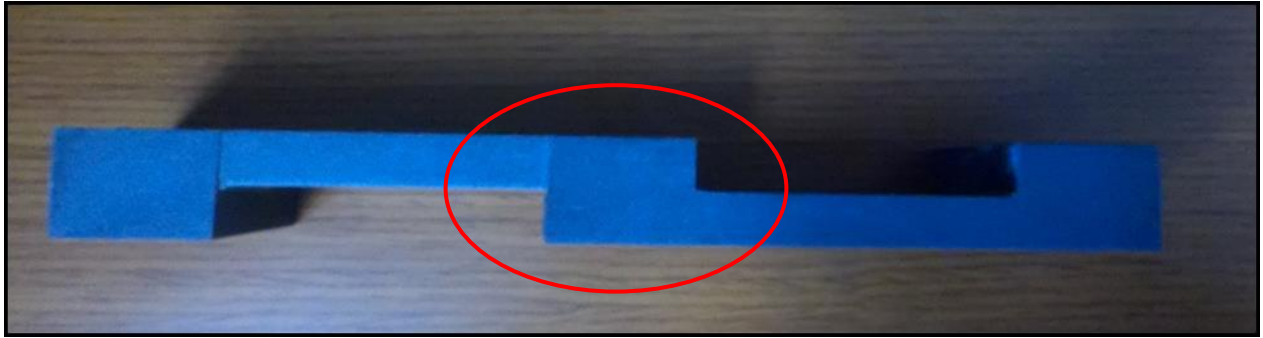


Figure 49: Side View of a Secondary Bonded Test Specimen – Highlighted Bond Area

4.2.4 Secondary Bonding Process

The procedure followed during the secondary bonding of the test specimen utilizes steps from both the secondary bonding of the single closed-corrugated sections and the control specimen for this experiment. First the substrate part and spacers were properly stacked into the press. For the secondary bonding procedure PETg spacers were used to ensure uniform pressure across the entire part. There was less fear of the spacers or part shifting during bonding since the overall temperature was lower than the consolidation temperature and since fully consolidated plates were being bonded. The stacking order is shown in Figure 50.

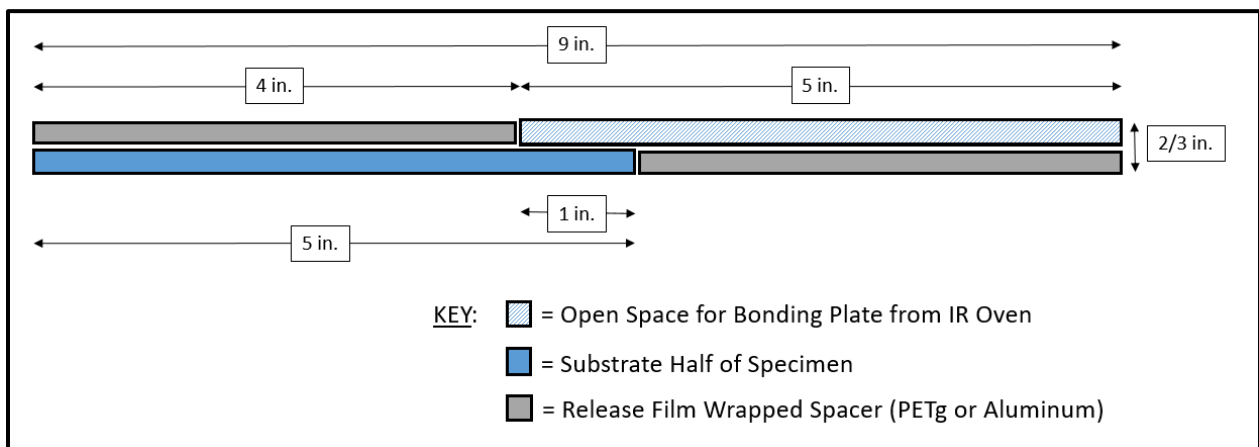


Figure 50: Cross-Sectional View of Stacking Positioning of Test Specimen

The substrate part was then heated until its bonding surface reached the desired bonding temperature. At this point the bonding plate is placed into the IR oven and flash heated to its

bonding temperature, after which it is quickly moved into the opening of the stack in the press using an automated robotic arm. The desired forming pressure is applied until the part falls least below the T_g (178°F).

There are three main settings that can be adjusted to create the experimental testing matrix: the temperature of the substrate plate in the press, the temperature of the plate heated in the IR oven, and the secondary bonding pressure. Initially, the substrate plate temperature was kept constant across all manufacturing settings at 225°F. As previously mentioned this temperature was chosen based on 3D printing parameters, where the part already on the table must be heated but is not required to be as hot as the material being pultruded out of the nozzle to create the next layer. In this case with PETg the T_g is 178°F so a temperature 225°F is a 26.4% increase above the T_g . Surpassing the T_g is important because it allows the surface of the substrate plate to become receptive of another consolidated plate, that is also properly heated, allowing the two plates to bond together.

This leaves the temperature of the part from the IR oven and the bonding pressure as being the parameters that were tested. The current settings used during consolidation of PETg used by the ASCC in the TPL are 335°F specimen temperature and 100 psi consolidation pressure. These settings were used for both consolidating control specimen and consolidating the test plates used to make the secondarily bonded lap shear specimens. The test matrix parameters were based on these two settings, ranging from an IR oven temperature of 310°F to 350°F and a pressure of 100 psi to 200 psi. These settings and the success rate of creating a bond is shown in Table 9, ‘No Bond’ refers to an unsuccessful cycle with no parent plate being produced and ‘Bond’ refers to a successful cycle that resulted in a completed parent plate.

Table 9: Tested Secondary Bonding Settings with Success Rate

		IR Oven Temperature		
		310 °F	335 °F	360 °F
Forming Pressure	100 psi	No Bond	Bond	Bond
	150 psi	No Bond	Bond	Bond
	200 psi	No Bond	Bond	Bond

After not getting a single specimen formed using a temperature of 310°F, it was decided to expand the experimental matrix and look at how adjusting the substrate temperature could impact the quality of the bond. For this the IR oven was set to 335°F and the bonding pressure was set to 100 psi. The substrate in one cycle was 280°F and the second it was increased to 335°F. The second cycle simulated a second full consolidation at the bond surface. These samples were expected to give some insight into the importance of local heating of the parts during bonding. The labeling scheme of the manufacturing trials that will be used for the remainder of Chapter 4 can be seen in Table 10.

Table 10: Labeling System with Full Manufacturing Settings

Group ID	Manufacturing Pressure (psi)	Press Temperature (°F)	IR Oven Temperature (°F)
Control - PETg Spacer	100	335	N/A
Control - Aluminum Spacer	100	335	N/A
Group A	100	225	335
Group B	150	225	335
Group C	200	225	335
Group D	100	225	360
Group E	150	225	360
Group F	200	225	360
Group G	100	280	335
Group H	100	335	335

The same final steps were performed to each test group parent plate as were done to the control parent plate. The widths of parent plates were cut down to coupon dimensions and loading tabs were attached to each end.

4.3 Secondary Bonding Coupon Testing

4.3.1 Test Setup and Procedure

It was determined that the best way to evaluate the strength of this secondary bonding process was to perform lap shear tests on coupons. In order to do this ASTM 5868-01 [12] was adapted for our specimen. There was a slight adjustment made to the geometry of the coupon. The required geometry of the standard was met first with coupons consisting of two 1 inch wide by 4 inch long plates that overlapped 1 inch. Loading tabs were added to the coupons to apply load concentrically to the specimen and minimize peeling stresses. There was a concern that peeling could compromise the bond prematurely and not truly test the tensile strength. During testing specimen were loaded at a slower rate (0.01in/min) than recommended in the standard. This was done in order to obtain a reasonable amount of data points before failure of the coupons. Using faster loading rates resulted in nearly instantaneous failure. The goal was to produce a specimen whose failure load resulted in a lap shear strength of 3000 psi, equivalent to the shear strength of the PETg given by the manufacturer of the PETg tapes. Coupons were photographed before and after with any unusual damage to the coupon being noted. Coupons first were fully measured, including thickness of loading tabs and thickness of the bond area, as well as the width and length of the bond area. Next they were carefully loaded into a 50kN Instron testing machine with only the 1 inch loading tabs being gripped on the top and bottom. The grips of the Instron had to be closed individually, this caused any improper alignment of the specimen to cause for premature failure either during the loading of the specimen or very early in the testing cycle. This further supports the idea that any peeling action could affect the overall strength of the

bond. During the test videos were used to capture the response of the coupon and the failure. A specimen loaded into the Instron is shown in Figure 51.



Figure 51: Lap Shear Coupon Loading into Instron Machine

4.3.2 Test Results

Testing concluded with a large number of data points, 7 to 15 specimen were tested for each bond setting. A brief summary of the raw test results and measurements is shown in Table 11, further analysis and displays of the data is shown in Section 4.3.3.

Table 11: Lap Shear Coupon Testing Raw Data

Group ID	Number of Successful Tests	Average Bond Area (in²)	Minimum Failure Load (lb)	Maximum Failure Load (lb)	Average Failure Load (lb)	Coeffivient of Variation (%)
Control - PETg Spacer	14	0.884	1203	1471	1288	5.5
Control - Aluminum Spacer	15	0.452	1098	1535	1335	9.2
Group A	14	0.755	28.9	576	231	62.8
Group B	15	0.977	158	547	353	28.9
Group C	7	0.948	146	503	364	31.9
Group D	15	1.000	74.4	1133	46	60.7
Group E	15	0.992	430	660	544	14.6
Group F	14	0.973	409	1593	890	40
Group G	9	0.955	19.2	195	109	62.9
Group H	13	0.807	444	1533	1004	40.2

During testing most bonded specimens exhibited complete failure of the bond directly on the bond surface, resulting in two completely separate halves. Some bonded specimens were still somewhat connected, but typically by only a few fibers. The control specimens had the most coupons that stayed connected, even after failure. Examples of failed specimens can be seen in Figure 52 to 54 – Figure 52 shows a control specimen, Figure 53 a spliced specimen with complete failure and Figure 54 a spliced specimen that did have some fibers connecting the two halves (but was later separated to examine the bond area), respectively.

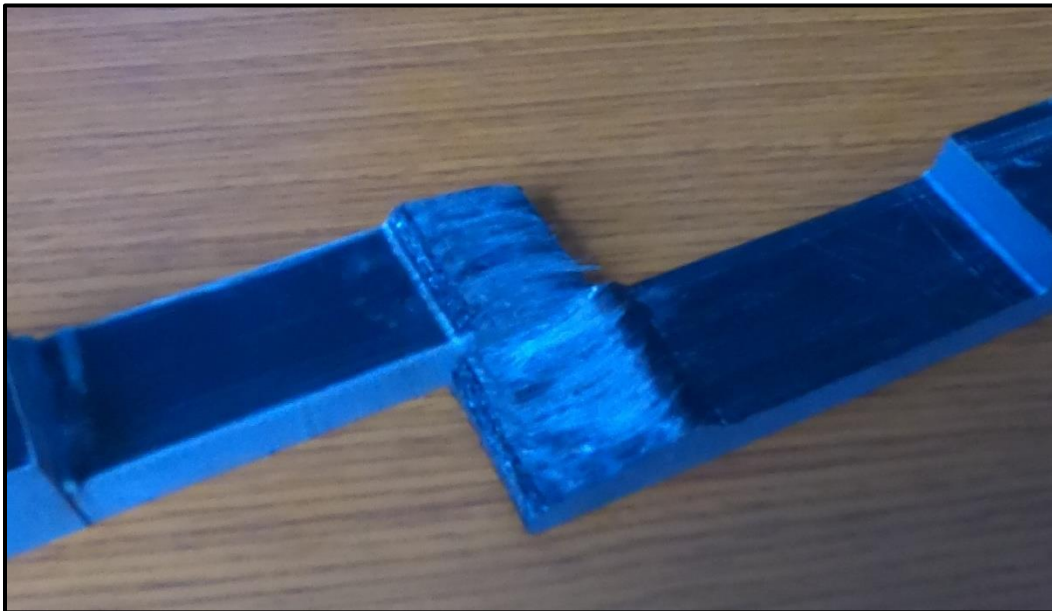


Figure 52: Failed PETg Spacer Control Coupon

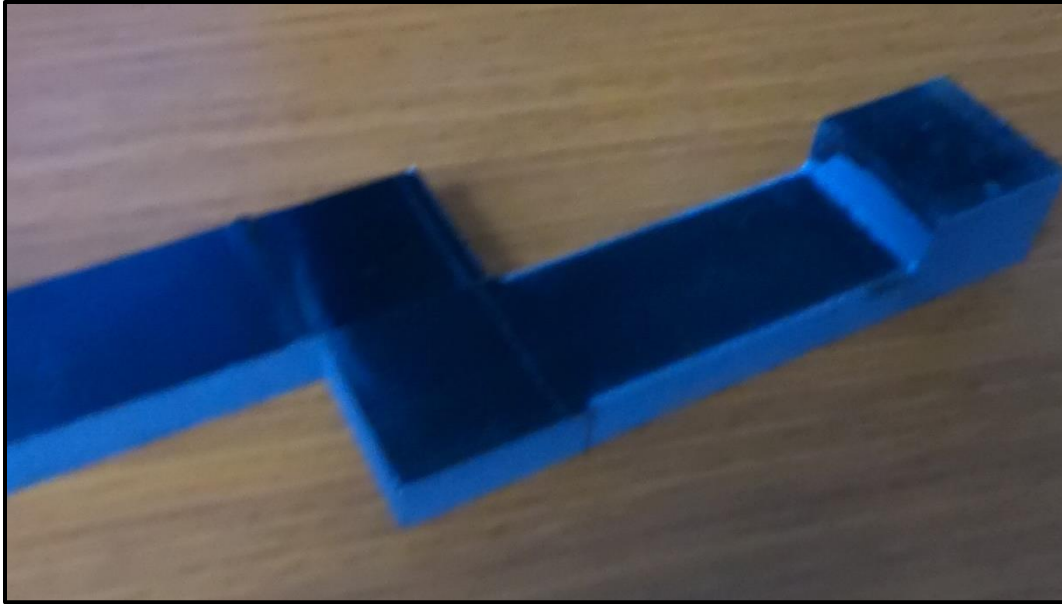


Figure 53: Failed Test Specimen – Complete Bond Line Failure

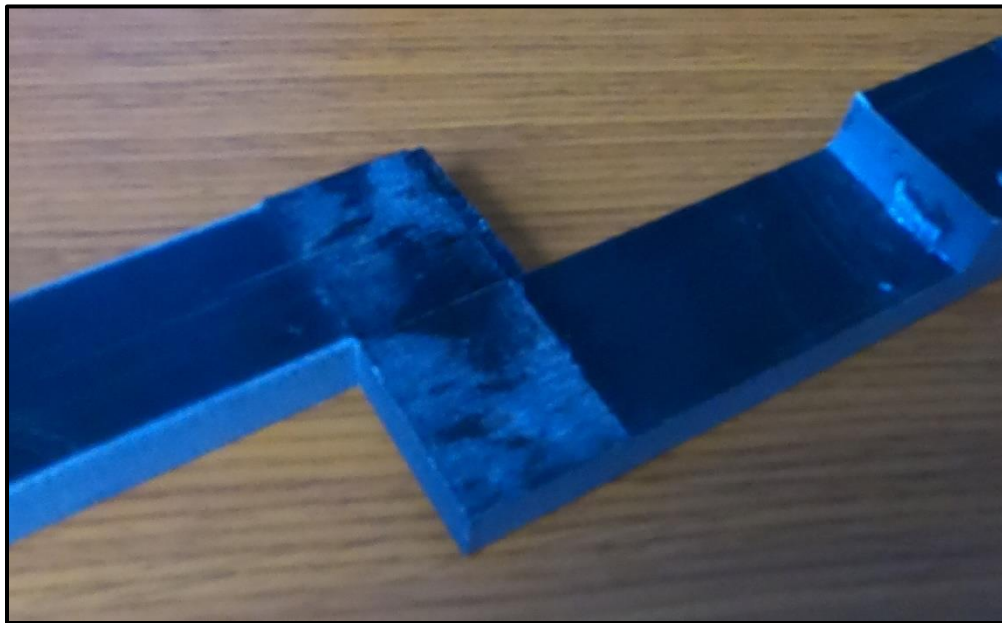


Figure 54: Failed Test Specimen – Fibers Present at the Failure Surface

The presence of fibers at the failed bond surface indicate that a bond between the two halves was formed. Fibers thus had to fail in order for coupon to fail. Coupons where fibers were not present at the failed bond surface points to a weak bond being formed at that setting and only a slight resin bond and friction were ultimately holding together the coupon.

4.3.3 Discussion of Results

Initial calculations and analysis of test data looked at the mean failure load values and the corresponding standard deviation, as well as the mean lap shear strength and its corresponding standard deviation. All of these values are shown in Table 12.

Table 12: Failure Loads and Lap Shear Strength Calculations

Group ID	Average Bond Area (in ²)	Failure Loads		Lap Shear Strength		Coefficient of Variation (%)
		Average Failure Load (lb)	Standard Deviation (lb)	Average Lap Shear Strength (psi)	Standard Deviation (psi)	
Control - PETg Spacer	0.884	1288	70.4	1457	79.5	5.5
Control - Aluminum Spacer	0.452	1335	123	2949	271	9.2
Group A	0.755	231	145	306	192	62.8
Group B	0.977	353	102	362	105	28.9
Group C	0.948	364	116	384	123	31.9
Group D	1.000	46	283	466	283	60.7
Group E	0.992	544	79.3	548	79.9	14.6
Group F	0.973	890	356	915	366	40
Group G	0.955	109	68.6	114	71.9	62.9
Group H	0.807	1004	404	1245	501	40.2

Due to the small sample size a check was performed looking at if any outliers could potentially exist. Using a Maximum Normed Residual (MNR) Method [15], it was determined if any of the trials included any data points that were outliers. The Critical MNR Value was determined using a 5% significance level. The outcomes of this review can be seen in Table 13.

Table 13: MNR Outlier Check in Data Sets

Group ID	Finding Outliers		
	Maximum Normed Residual (MNR)	Critical MNR Value (CV)	Outliers Observed?
Control - PETg Spacer	2.599	2.472	Outliers Exist
Control - Aluminum Spacer	1.929	2.518	No Outliers
Group A	2.381	2.472	No Outliers
Group B	1.915	2.518	No Outliers
Group C	1.871	1.947	No Outliers
Group D	2.357	2.518	No Outliers
Group E	1.471	2.518	No Outliers
Group F	1.971	2.472	No Outliers
Group G	1.303	2.151	No Outliers
Group H	1.387	2.422	No Outliers

This only points to the Control made with a PETg spacer to be containing outliers. However, a full look at that data set, shown in Table 14 doesn't indicate that the specimen with the maximum MNR value occurs will impact the average or standard deviation by a substantial margin when removed. Removing the maximum value data point drops the Average Lap Shear Strength to 1440.7 psi, the Standard Deviation to 54.9 psi, and results in no outliers in the updated data set. Therefore, all data were retained for all configurations.

Table 14: Control – PETg Spacer Specimen Data Set with MNR Calculation

Sample ID	Max Load (lbs)	Lap Shear Strength (psi)	Individual MNR
J12	1203	1360	1.21
J3	1216	1375	1.03
J10	1223	1383	0.93
J11	1225	1385	0.90
J9	1258	1422	0.44
J6	1271	1437	0.25
J14	1287	1455	0.02
J4	1292	1460	0.05
J8	1293	1462	0.07
J7	1300	1470	0.16
J5	1308	1479	0.28
J13	1314	1485	0.36
J1	1376	1556	1.25
J2	1471	1663	2.60

Avg. Area =	0.884
Mean =	1457
Stan. Dev. =	79.5
Sample Size =	14
Max MNR =	2.60
CV =	2.47
Outliers?	Outliers Exist

Plots were created to assess how test specimen compared to the results of the control specimen as well as each other. Figure sets are split up by IR oven temperature. Figure 55 shows specimens with an IR oven temperature of 335°F; Figure 56 shows specimens with an IR oven temperature of 360°F; and Figure 57 shows specimens with unique substrate temperatures (280°F and 335°F) and uniform pressure of 100 psi and IR oven temperature of 335°F. For each set a bar showing the average value and +/- one standard deviation is included along with all the individual lap shear strength.

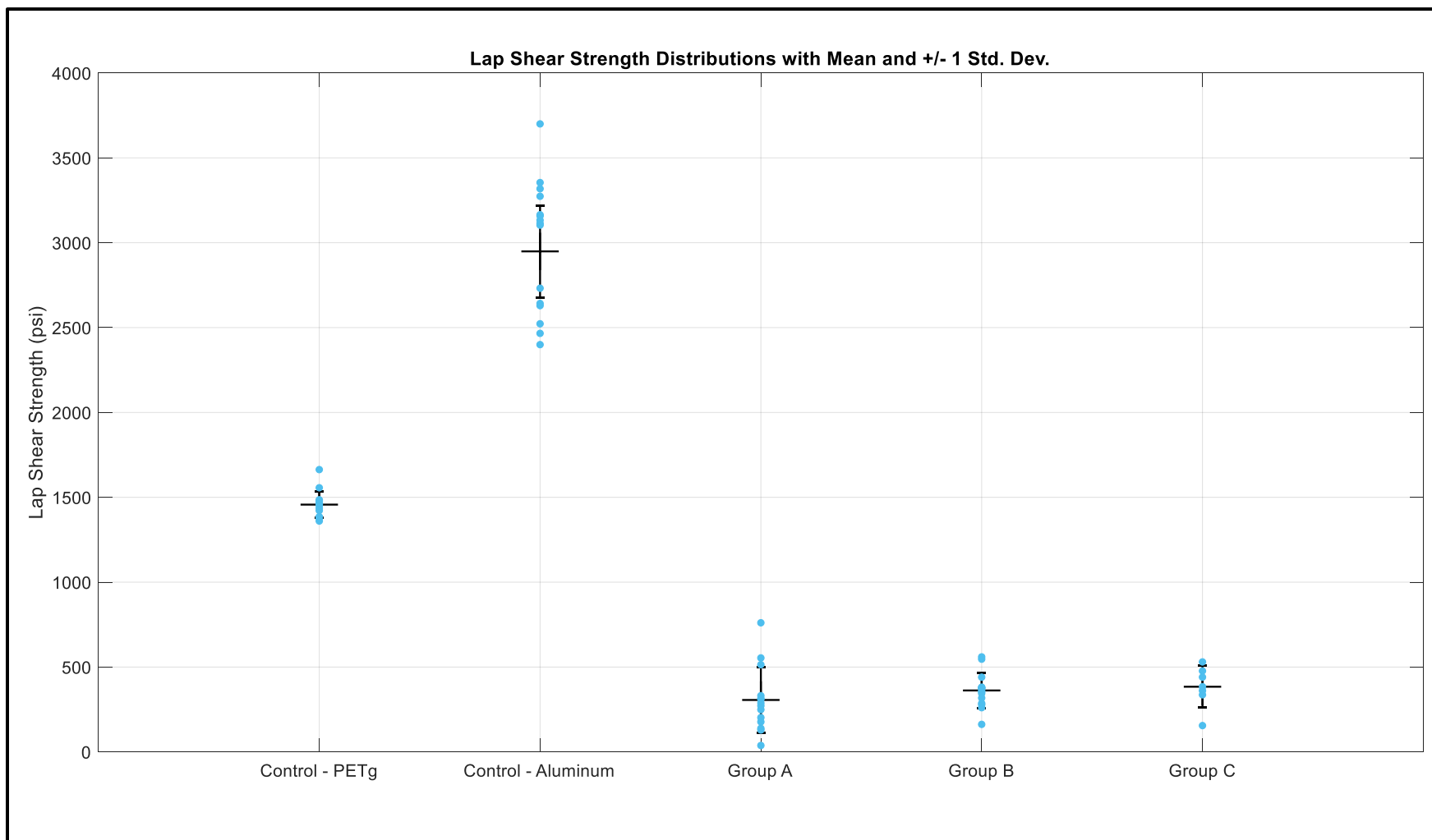


Figure 55: Lap Shear Distribution (Substrate 225°F and IR Oven 335°F)

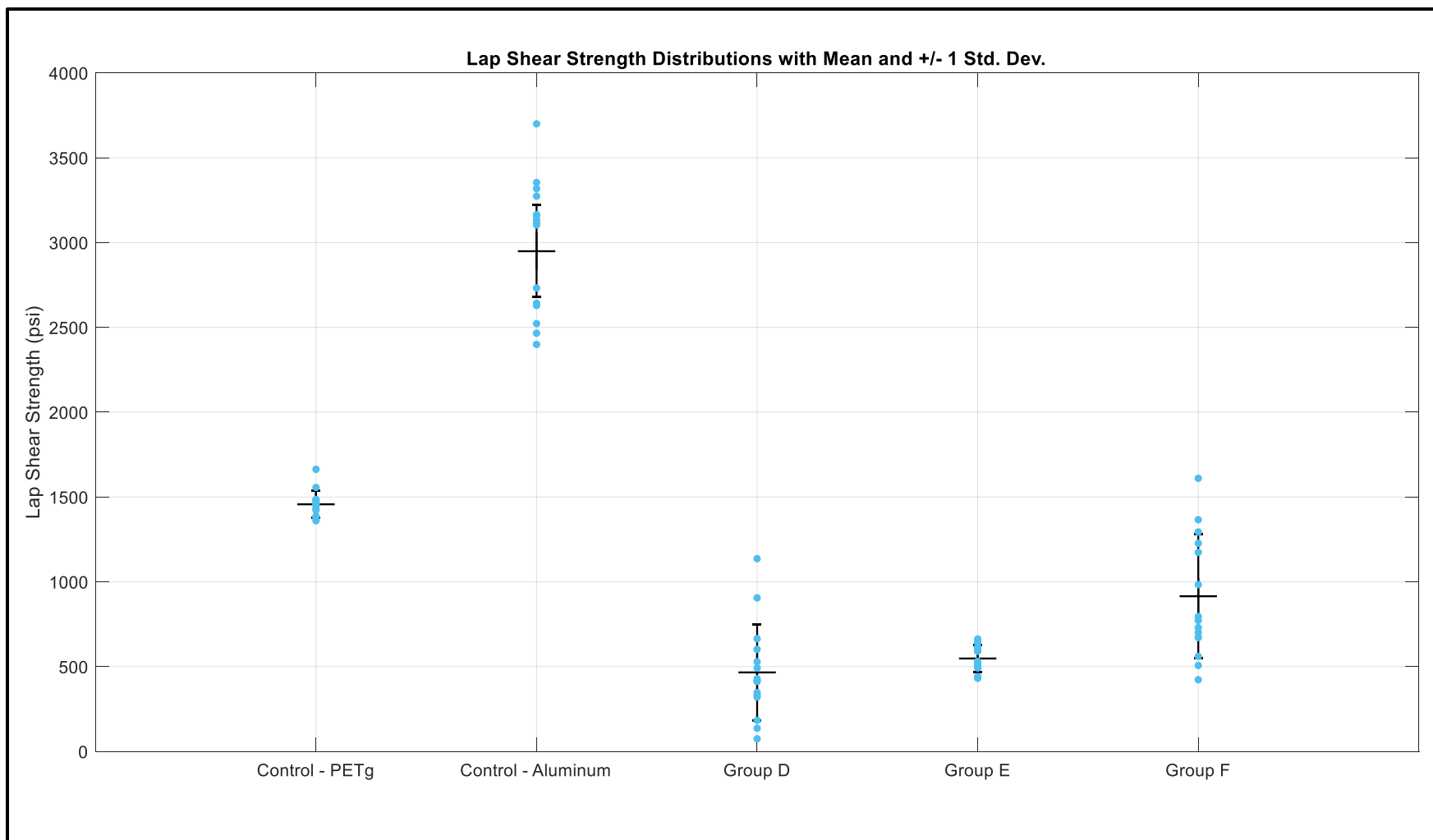


Figure 56: Lap Shear Distribution (Substrate 225°F and IR Oven 360°F)

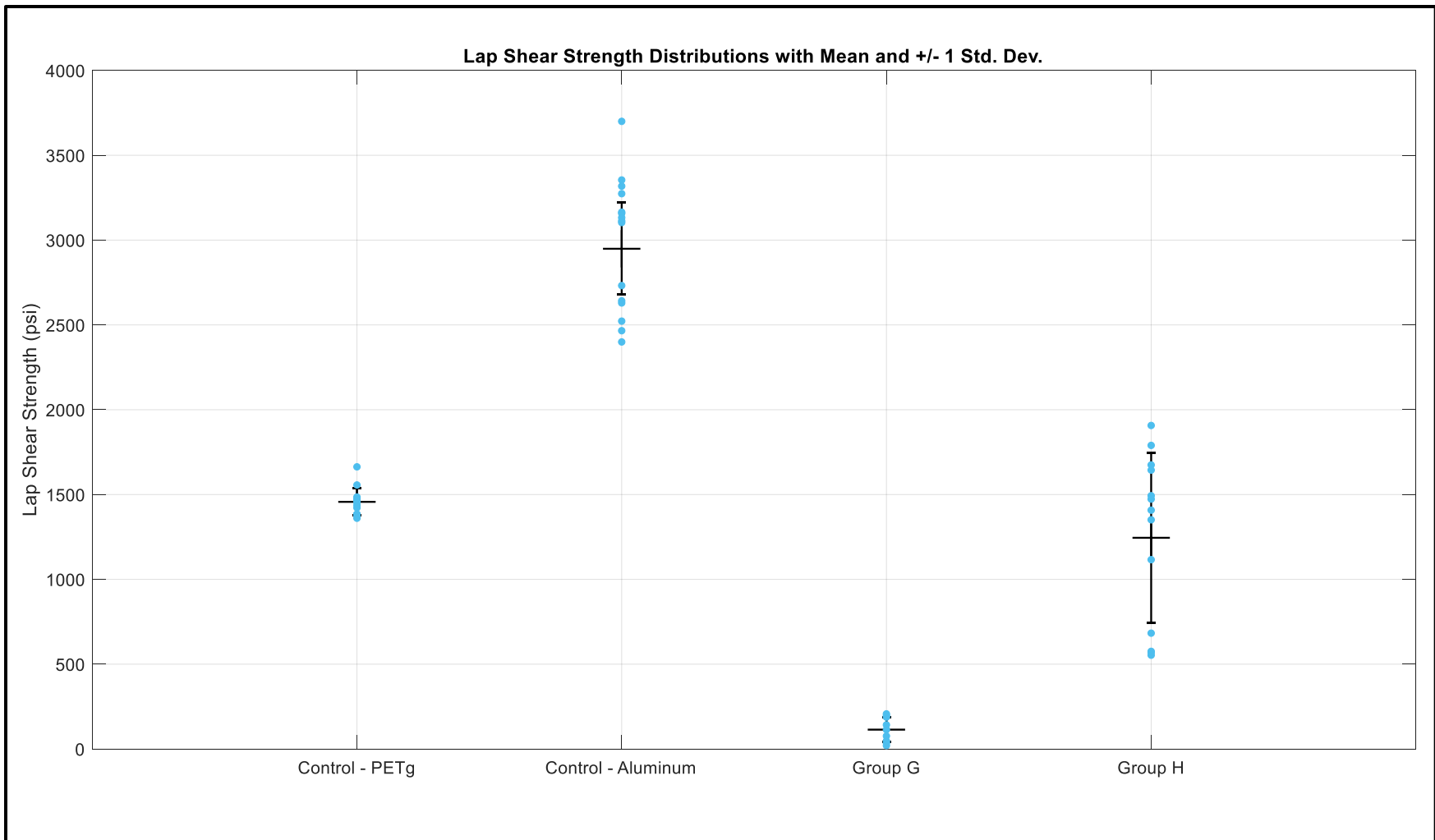


Figure 57: Lap Shear Distribution (Substrate 280°F and 335°F)

The results indicate that there are two specimen that stand out and should be considered when trying to determine the more optimum settings for creating a secondary bond. Group E had a standard deviation closest to that of the control specimens, and the smaller variability for all secondarily bonded specimens. These specimen were made with an IR Oven temperature of 360°F, a Press temperature of 225°F, and a pressure of 150 psi. The second is Group H, with a mean lap shear strength that is closest to that of the control. These specimen were made with an IR Oven temperature of 335°F, a Press temperature of 335°F, and a pressure of 100 psi.

The results from these two specimen help to narrow the field of manufacturing settings needed to ensure the strongest possible bond. Looking at the data as a whole, lap shear strength values for the most part did not reach the initially expected value of 3000 psi. The only specimen set that came close to that mark was the aluminum spacer control coupons. The effect of the shifting in the layers around the bond area of both control sets, is unclear. But due to both sets having fairly different lap shear strengths, it doesn't appear that the shifting caused any mechanical advantage. The increased strength of the aluminum spacer coupons is believed to be from the full pressure being applied to the bond area, since these spacers were slightly thinner than each half of the specimen itself. The PETg spacers being the same thickness as each half of the specimen could have prevented the bond area from getting the true pressure applied, in turn creating a weaker bond.

Indeed, the control specimen exhibited the largest average lap shear strength with the PETg spacer set being a little less than half the manufacturer's shear strength and the aluminum spacer set being just shy of the 3000 psi. Groups which shared the same temperatures but varied in pressure did show an increase in lap shear strength with increasing pressure as shown in Figure 58. Additionally the series with a hotter overall temperature; press temperature of 225°F and an

IR oven temperature of 360°F, saw a higher average lap shear strength than the specimen made at the same pressure from the other series. Taken together, the results indicate that higher lap shear strengths might be achieved with IR oven and press temperatures of 335°F or 360°F and pressures higher than 100 psi.

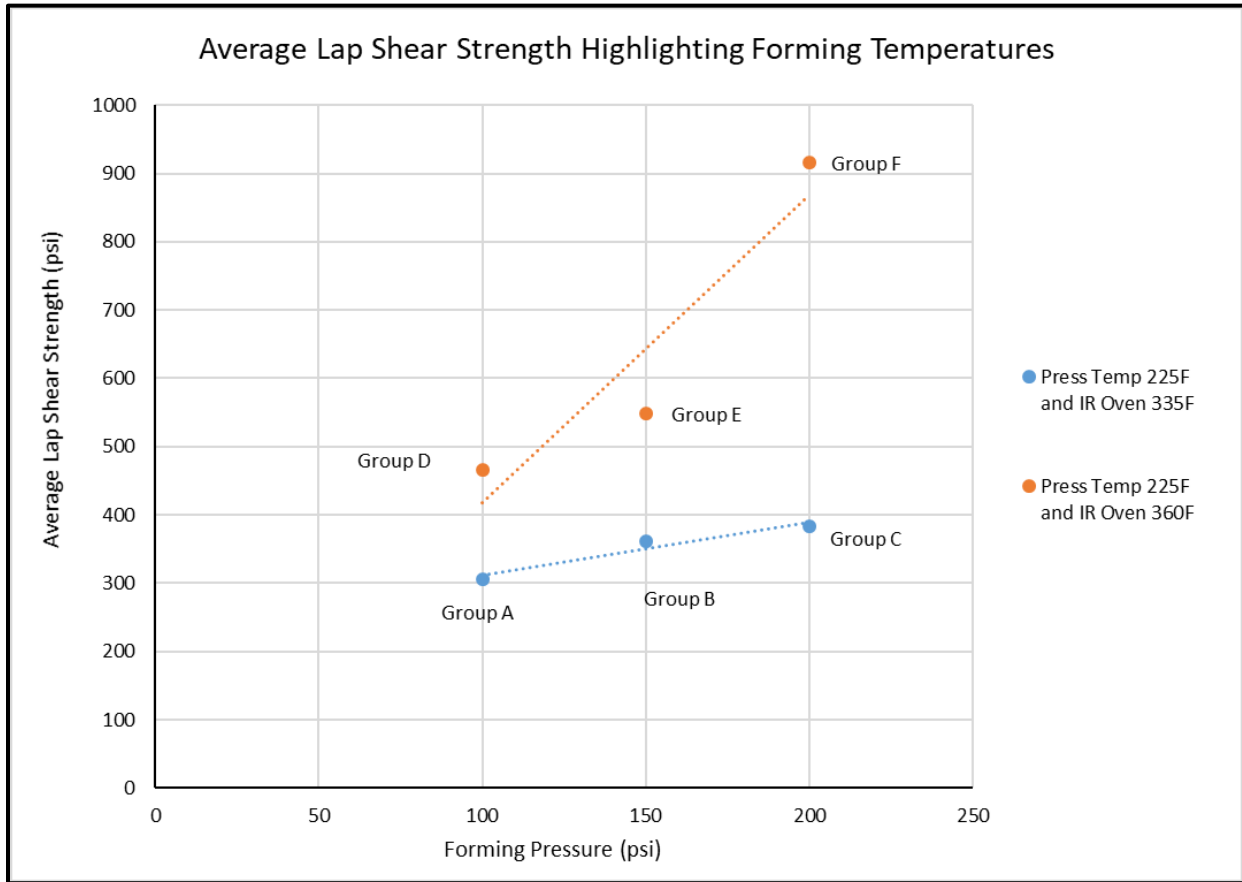


Figure 58: Plot of Specimen Series by Average Lap Shear Strength and Forming Pressure

The results also rule out the idea of heating the part in the press to slightly above the T_g of the material in a manner similar to 3D Printing, but indicate that the entire process must resemble a second consolidation cycle as much as possible. Comparing the two specimen series shows that the hotter overall temperature series saw better results. It also ensured that the temperature of the part from the IR oven that was heated to 360°F was closer to the 335°F consolidation

temperature during the secondary bonding, or when the press was closed. Even with heat loss during the transition from the IR oven to the press the part would not be able to drop more than the part only heated to 335°F in the IR oven.

It must also be noted that Group G performed significantly below expectations given the higher temperatures of both the press and oven used in its fabrication. The cause of this poor performance is unknown, but it is possible that during the manufacturing process there could have been some peeling force applied weakening the bond before it was even tested.

Based on the results shown here, secondary bond parameters will be a temperature of 335°F of the part in the press, a temperature of 335°F-360°F of the part in the IR oven, and a pressure of 100 psi or more in the press. The range of IR oven temperatures may need to be adjusted for different size plates that could deform when being removed quickly from the IR oven carriage by the robot arm. This could impact the accuracy of placement of the part onto the other part and the ability to ensure a sufficient forming temperature. While the pressure does show a positive increase in performance in the specimen series it was tested in, increasing pressure at these temperatures would require further assessment to ensure the part geometry is not compromised.

4.4 Prototype Rebar Surface Manipulation

An important consideration when it comes to developing CFRTP composites to be used as reinforcement for concrete sections is the ability to transfer loads between the concrete and the CFRTP reinforcement. This was initially achieved with holes in the cover plate for the closed corrugation sections. As research work turns to developing a CFRTP rebar, getting this same transfer is important and could be achieved through a number of different methods. This includes adhering sand to the surface, wrapping material creating a ridge, or pressing deformations into the surface. For the purposes of initial prototyping and utilizing current operations available in the lab, stamp forming grooves onto the outer surfaces was used. These

prototype specimen were manufactured as unidirectional E-glass-PETg bars. Grooves could be pressed directly into the unidirectional section, but this could damage the fibers and jeopardize the strength of the prototype rebar. In order to avoid this an outer layer for the deformation sides was developed that could be pressed and deformed, while not impacting the unidirectional core.

4.4.1 Material Used

This outer deformation layer was manufactured from neat PETg polymer sheets and E-glass chopped strand mat (CSM) produced by VectorPly [16] with a weight of 1.5 oz per square foot, a material sheet is attached in Appendix F. Utilizing the stamp-thermoforming process and a mold with grooves milled into it allowed the CSM and resin layer to be formed into a ridged shape. This deformation layer mimics the typical ridges present on the surface of steel rebar. This layer would require an initial consolidation between the CSM and PETg neat resin to ensure the CSM is fully wetted out followed by a second consolidation to complete the parent plate. In this second consolidation the unidirectional core is consolidated, the ridges are pressed into the deformation layer and the core and outer deformation layers are bonded together.

4.4.2 Manufacturing the CSM-PETg Layer

The deformation layer required an initial consolidation in order to fully wet out the CSM with the resin and create a sheet of material that could be used for the outer deformation layer. A series of trial runs were performed at a smaller scale in order to better understand the settings that would be required to best create these CSM sheets. Variables adjusted during trials were the amount of resin sheets used, maximum temperature reached during consolidation, the pressure applied to the part during the process, and the speed of part cooling.

In terms of testing the amount of neat resin needed to create the deformation layer there were two options: one considered two resin sheets with the CSM sandwiched between them, and the other considered a single sheet of resin on top of the CSM. Several regimes were tested,

including a constant temperature of 350°F which is just above the consolidation temperature used for E-glass/PETg tapes as well as temperatures of 400°F and 450°F. Increased temperature makes the resin less viscous so it can more easily flow into the CSM. Two pressure settings were assessed. The first was a constant pressure of 30 psi on the part with the press actively keeping 30 psi on the part even as the part thickness changed as resin started to flow. The second consisted of an initial pressure of 30 psi, with a fixed position of the press. This caused the pressure to gradually decrease as the part was heated and the resin started to flow and into the CSM causing the part to decrease in total thickness. Two cooling options were tested, including active cooling of the part after a dwell time at the maximum temperature and passive cooling where the press stayed closed after the heaters were turned off. In both cooling cases the press wasn't opened and the part was not removed until the temperature was well below the glass transition temperature (T_g) of the material (178°F).

The testing procedure of the manufacturing settings started by looking at temperature with a trial at 350°F. The specimen saw very little to no resin flow into the CSM. Other tests at this temperature were skipped, and trials were moved to 400°F. At this temperature different tests were run by varying the pressure settings and cooling methods. These specimen still did not have adequate resin flow into the CSM so the temperature was increased to 450°F. This temperature saw better resin flow into the CSM, and a series of tests were run to evaluate the effects of the amount of resin, pressure settings and cooling methods. An additional test was run to assess the quality of the part with no pressure applied to see if the resin would flow into the CSM freely. This produced a part that saw the worst resin flow into the CSM, supporting the idea pressure of some kind is required for this process. Figures 59-63 show some of the different trials that were run.

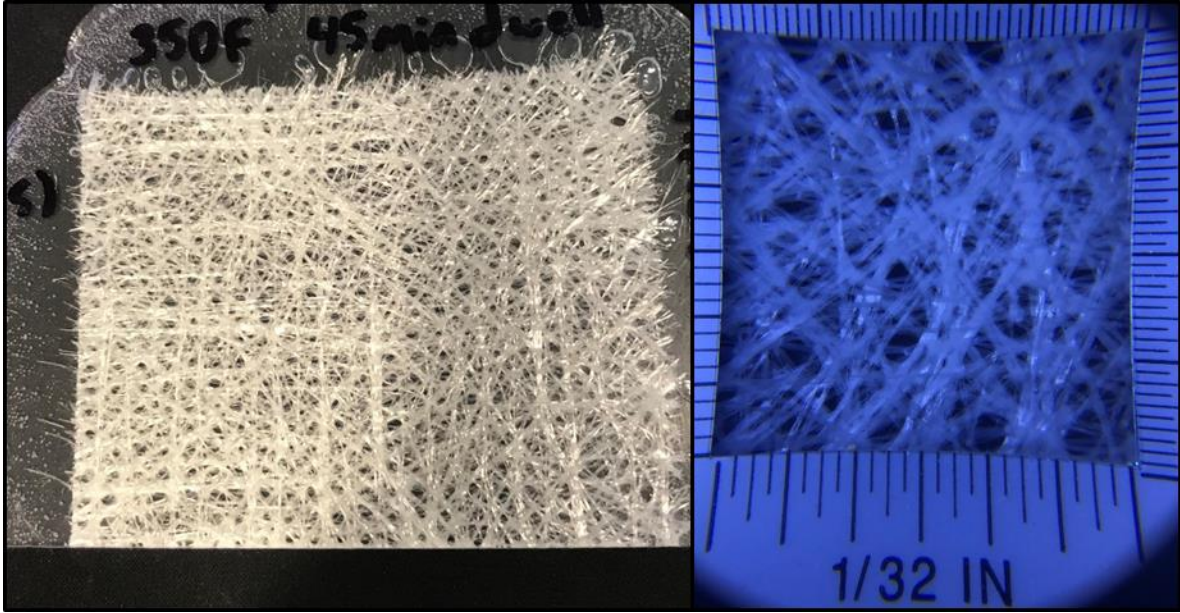


Figure 59: Trial CSM Sheet - 350°F / Constant 30 psi / 2 Resin Sheets / Passive Cooling

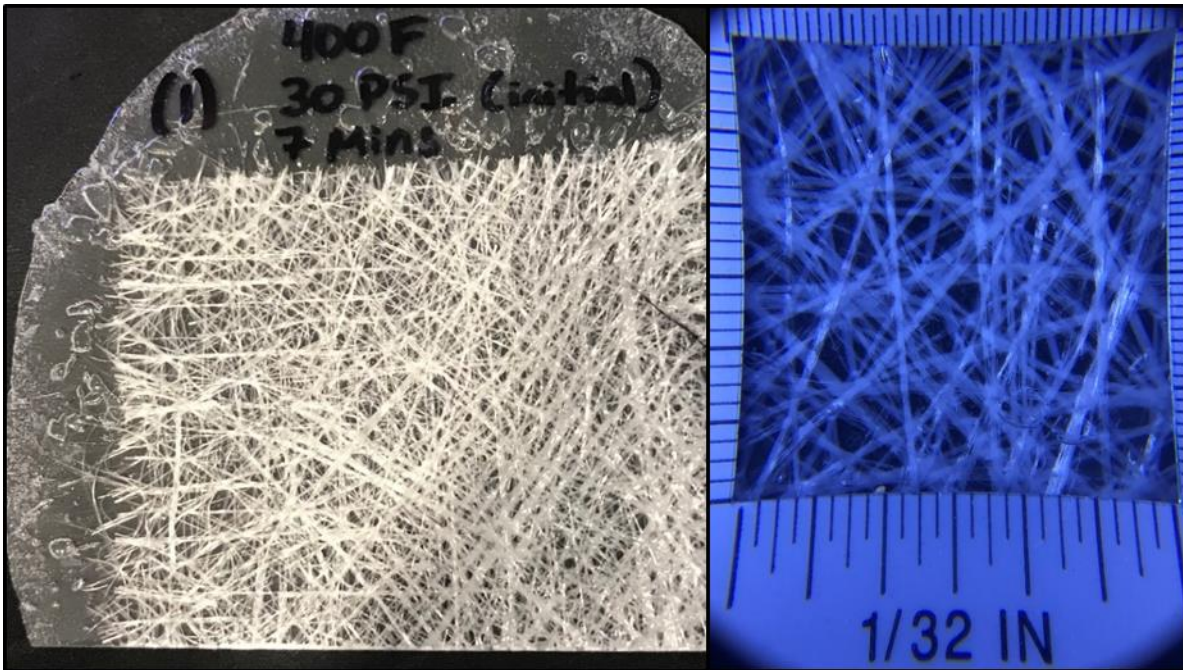


Figure 60: Trial CSM Sheet - 400°F / Initial 30 psi / 2 Resin Sheets / Active Cooling

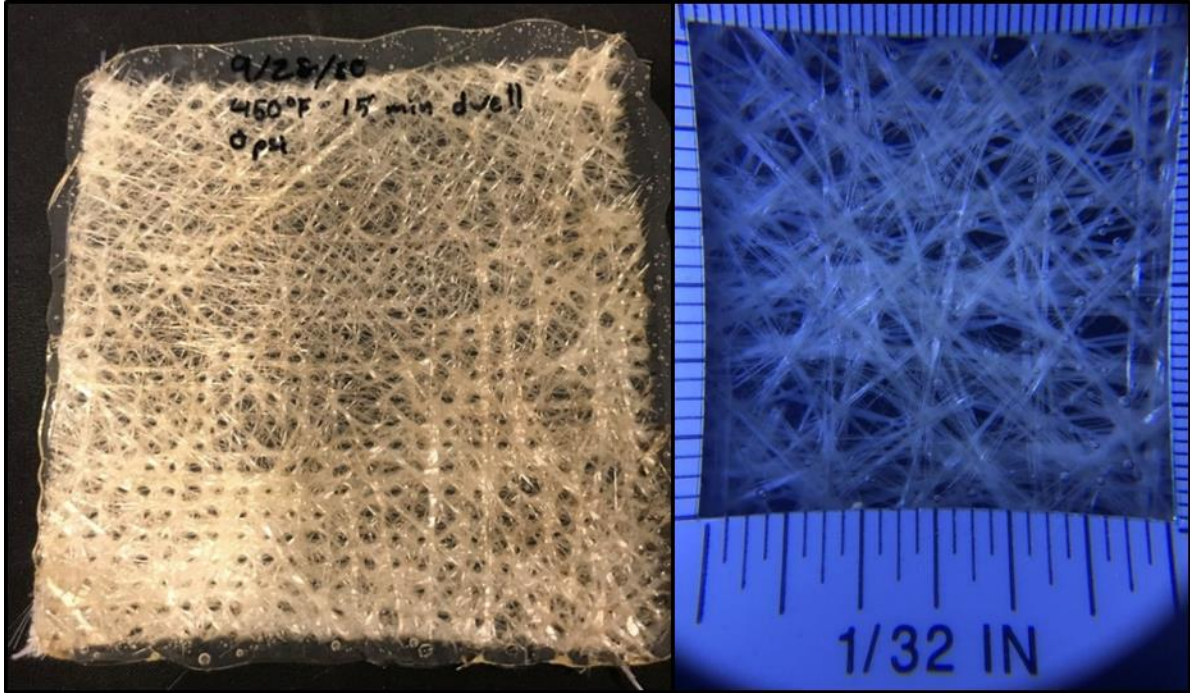


Figure 61: Trial CSM Sheet - 450°F / 0 psi / 2 Resin Sheets / Passive Cooling

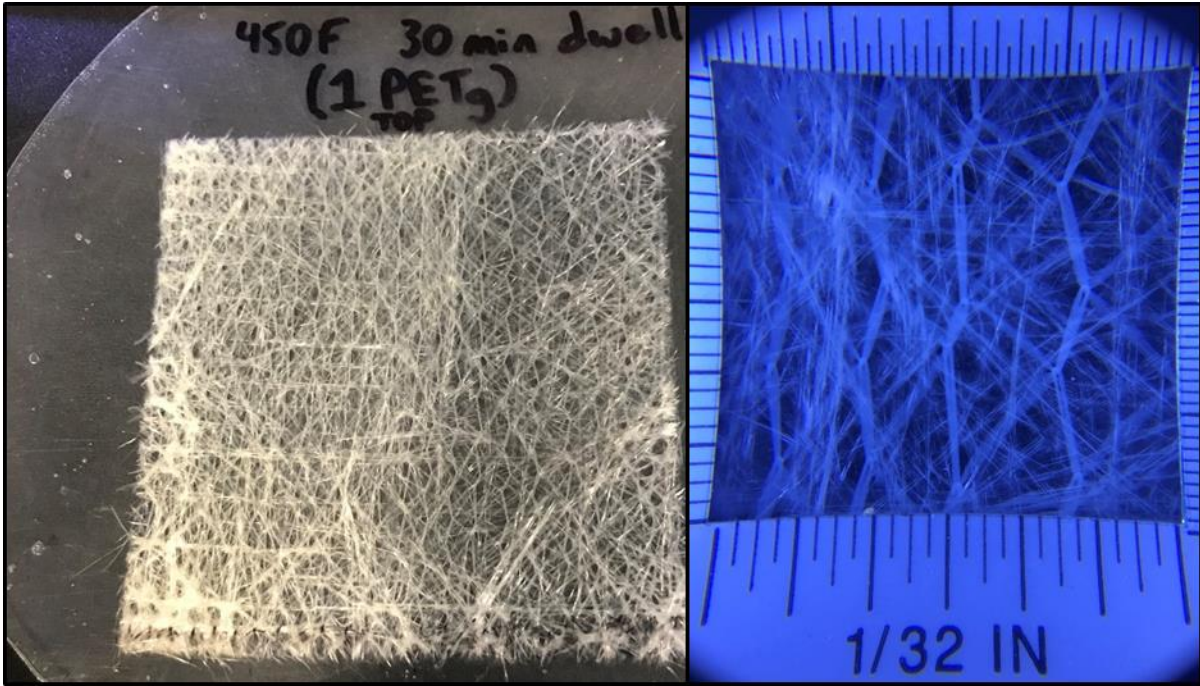


Figure 62: Trial CSM Sheet - 450°F / Constant 30 psi / 1 Resin Sheet / Active Cooling

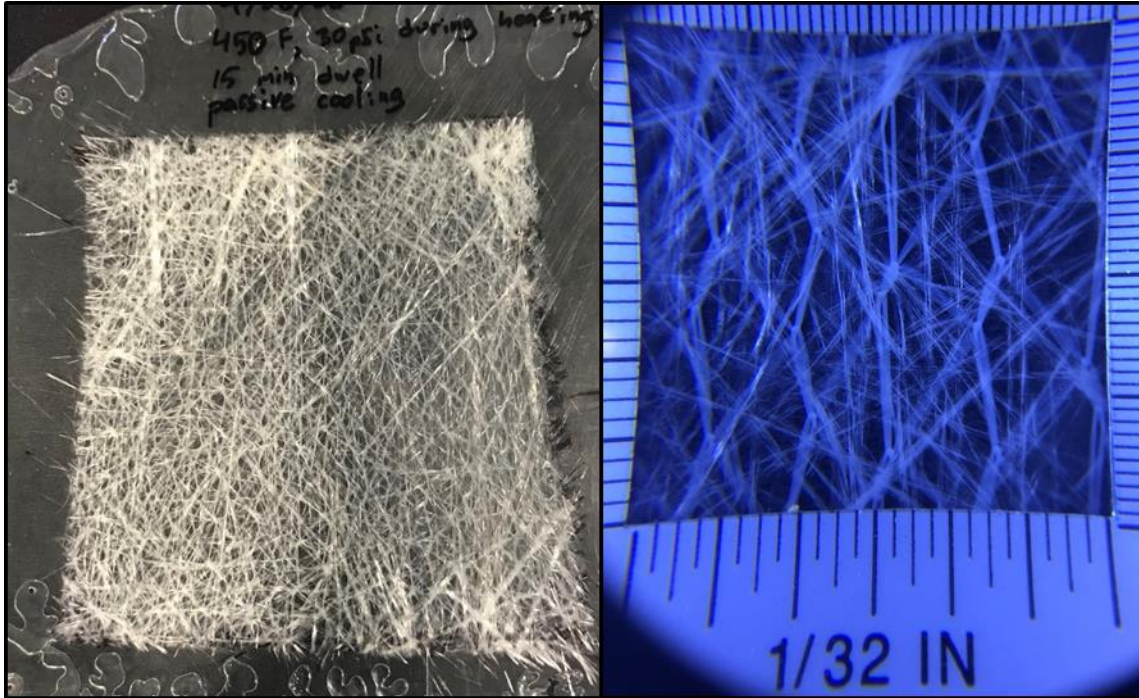


Figure 63: Trial CSM Sheet - 450°F / Initial 30 psi / 2 Resin Sheets / Passive Cooling

The final trial in Figure 63 produced what was determined to be the best impregnated CSM sheet. Primarily due to the infusion the resin had into the CSM, but also for the fact the thickness of the sheet was greater than the 1/16" height that was designed for the ridges of the prototype rebar specimen. Trials with only 1 resin sheet tended to be too thin and the other 2 resin sheet trials tended to not have proper resin infusion. Therefore the settings of the final trial were utilized (450°F, Initial Pressure of 30 psi, 2 Resin Sheets, Passive Cooling) there was a slight adjustment to produce full size sheets to be used during the manufacturing of the CFRTP rebar. The update was to the pressure, which was done by adding a thin steel caul sheet. This caul sheet was added above the part allowing for the initial pressure to be applied but once the resin starts running out and thinning pressure was slowly decreased from what was applied by the press. However, the weight of the caul sheet kept some pressure on the part, continuing to force some resin into the CSM. The stacking procedure is shown in Figure 64.

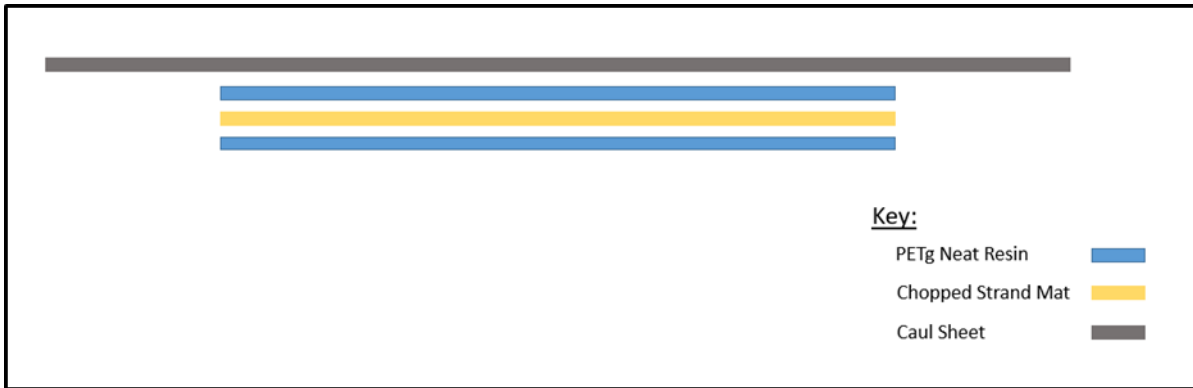


Figure 64: Stacking Procedure to Form Deformation Layer

The settings used to form the final deformation layers are as follows; first, 30 psi was applied to the part and caul sheet and the temperature was ramped up. Next the part was held under dwell settings for 15 minutes, including holding the temperature at 450°F. Because the press is set to a fixed position pressure during this time tended to decrease slightly as the part thinned due to infusion and resin flow. Pressure applied from the press was not adjusted during the dwell period. Instead, as the part thickness decreased due to infusion and resin flow, the pressure reduced to slightly less than 30 psi during and after the dwell time. Finally, after the full dwell time, the press was opened just enough to remove pressure on the part from the press. The press was held at that level so heat was still applied while it passively cooled, which took upwards of 18 hours. The part was removed once the press temperature was around 100°F, well below the glass transition temperature (T_g) of 178°F. A plot of the final forming process is shown in Figure 65.

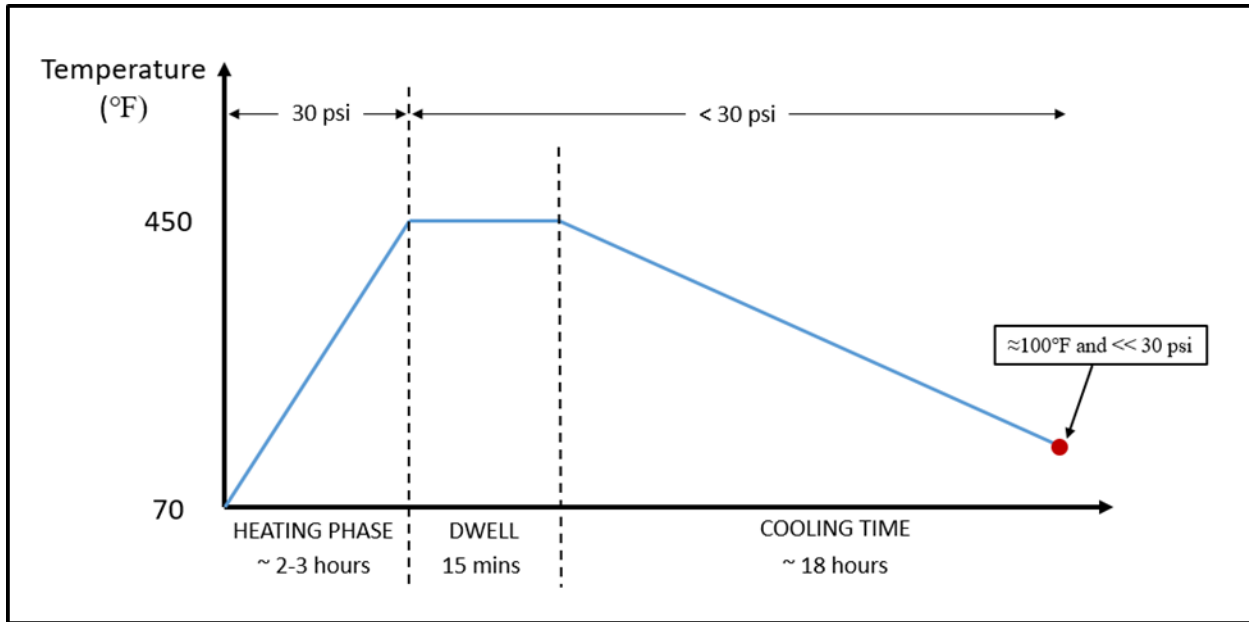


Figure 65: Forming Settings of the Deformation Layer

4.4.3 Manufacturing the Grooved Plate

The final manufacturing stage of this set of stamp-thermoformed reinforcing bars was the consolidation of the E-glass/PETg tape cores, bonding between the core and the pre-consolidated deformation outer layer, and the formation of grooves on the surface. This was all done simultaneously to form a stronger bond between the pre-consolidated outer deformed layer and the core than what would typically be achieved with a secondary bonding process.

The stacking procedure was important for this step in order to ensure that the pressure was maintained throughout the consolidation process. It was expected that the outer layers would shift and change thickness again as the part was heated, reducing part consolidation pressure. In order to combat this silicone sheets were added to the stacking procedure in an attempt to maintain pressure as the material thinned. This resulted in the following stacking sequence: silicone sheets, aluminum deformation mold, outer deformation layer of neat resin and CSM, and E-glass/PETg tape core. This was repeated on the top half to give the complete stacking set up. Figure 66 shows a schematic of the stacking set up.

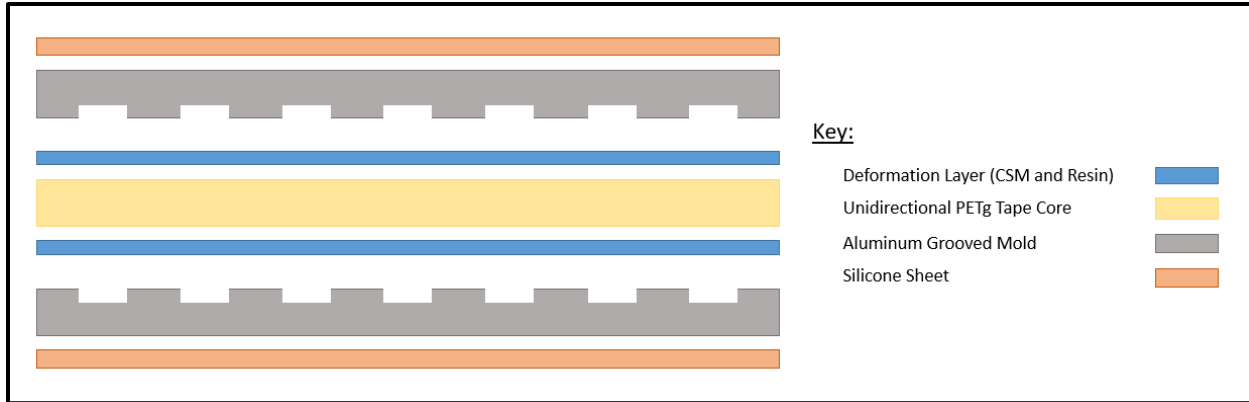


Figure 66: Schematic of Stacking Procedure of Final Consolidation

A forming temperature of 335°F and a pressure of 100 psi were used for the final consolidation, which have been shown to be effective by both the ERDC and TPL teams for consolidating PETg. Tapes were utilized during this forming process. The only alteration performed in the manufacturing process was an initial preheat to 200°F, which is just slightly above the T_g of PETg. The goal of this was to prevent fracture of the deformation layers, which can occur if pressure is applied at room temperature. This fracture might cause an uneven amount of resin through each deformation layer and discontinuities in the ridges created by the mold. Pressure was monitored and maintained by the press. However, reaching appropriate forming temperature at the core of the E-glass/PETg tapes proved to be a challenge. The temperature was monitored for each forming cycle by a thermocouple at the center of the part, and the core temperature reached a maximum of approximately 310°F, less than the target 310°F. The cause of the lower core temperature was never determined, but one possibility was that the silicone acted as an insulating layer for the mold and part. Another possibility was the aluminum mold acting as a heat sink due to its thermal mass. Despite these issues, the deformations were successfully formed and bonded to the E-glass/PETg core. Specimens were water jetted from the plate to a variety of lengths and widths. An example of one of the finished rebar prototypes is shown in Figure 67.

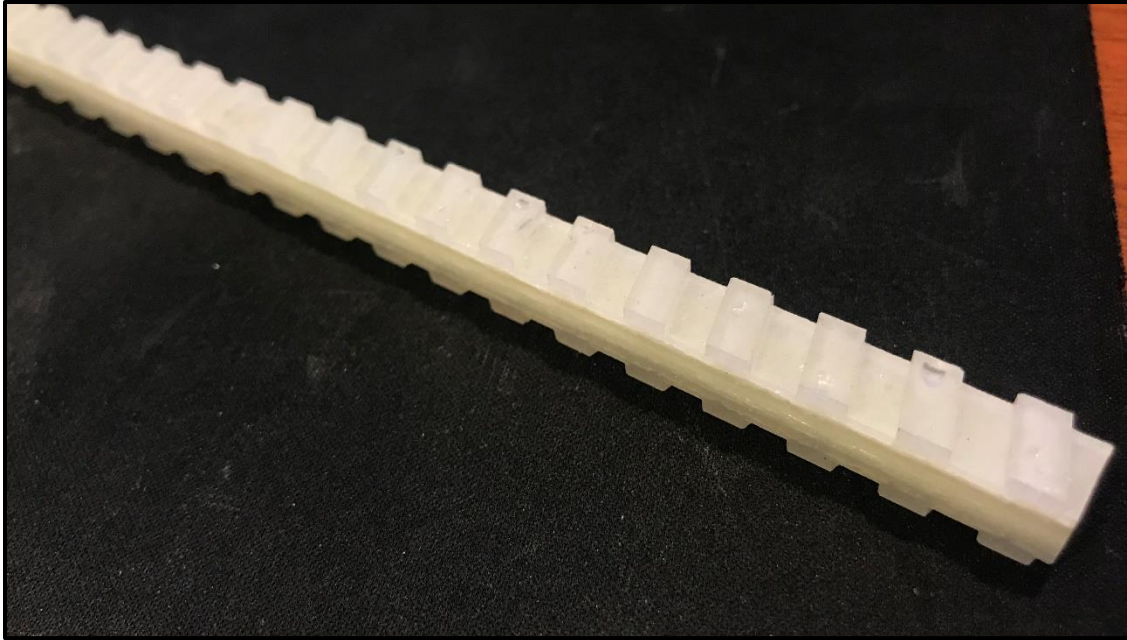


Figure 67: Completed Prototype CF RTP Reinforcing Bar

Upon inspection it was clear that the core had not been fully consolidated, most likely due to the fact the core temperature didn't reach the desired consolidation temperature and only reached 310°F. A close up of the core with an example of poor consolidation highlighted is shown in Figure 68, which indicates discoloring across the thickness of the core and small cuts into the core. This could be layers that were not consolidated and unbonded or fibers that were torn out during water jetting specimen out of the parent plate.

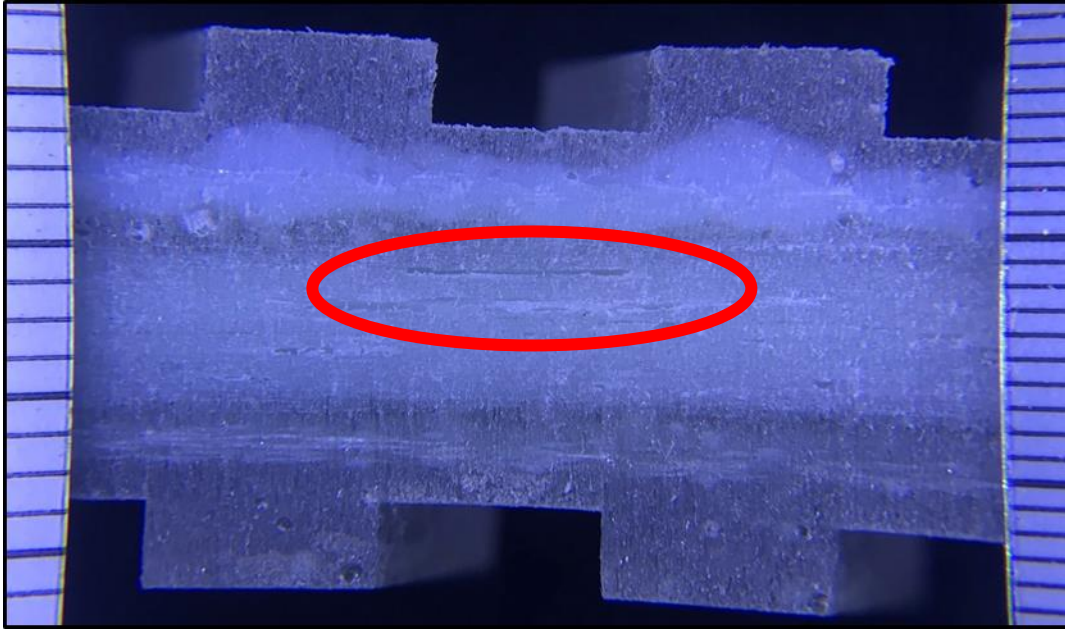


Figure 68: Close up View of Unidirectional Core

It was observed that the deformation layer was formed as intended, with the CSM present in both the ridges and in the valleys of the deformations. A close up view of the ridge itself showing the CSM bubbling up into the ridge is shown in Figure 69. While this process could be optimized in the future by potentially altering the thickness of the neat resin sheets or the thickness of the CSM, these initial results were very promising.

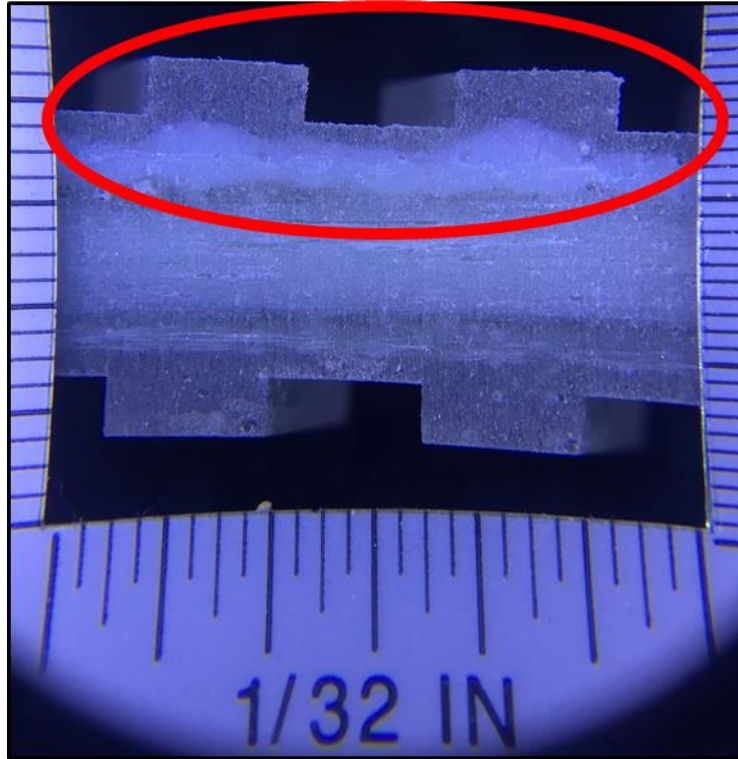


Figure 69: Close up View of CFRTP Rebar Deformation Layer

For the purpose of this thesis work the manufacturing process was the end of scope of research for internal reinforcing. Testing and further research into the internal thermoplastic rebar was continued by other graduate students.

4.4.4 Adaptions to Stay-In-Place Formwork

The aim for creating these ridges was to create a transfer of energy between the rebar itself and the concrete it looked to reinforce. This same concept could be used in stay-in-place and external reinforcement formwork. Surfaces could be stamped with ridges or coated in a sand or plastic bead to ensure shear transfer between the CFRTP and the concrete. For the closed-corrugation design this grooved surface could be added to the top of the cover plate to improve the shear transfer that was obtained through the concrete shear studs of the original design.

Similarly, the top of the corrugation troughs could have a deformed surface to better mobilize the

corrugations as tension reinforcing. A rendering of what could be created as a closed-corrugated section with secondary surface manipulation is shown in Figure 70.

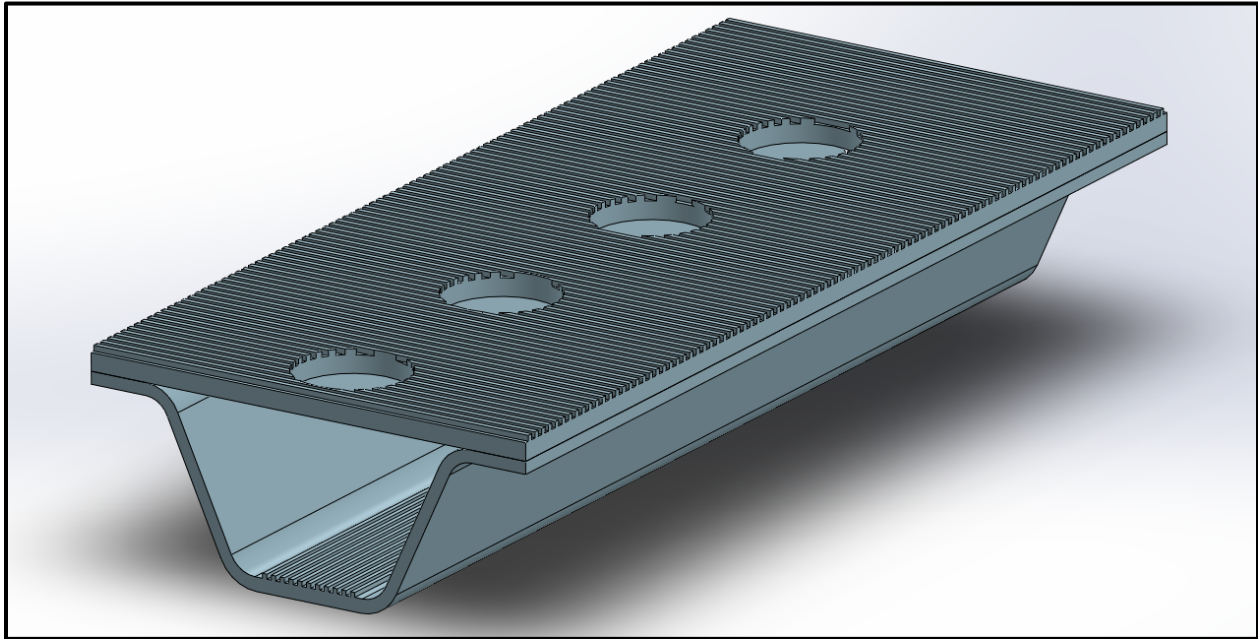


Figure 70: Section View of Closed-Corrugation with Grooved Surfaces

4.5 Summary and Conclusions

The secondary bonding processes explored in this chapter will help contribute to the manufacturing of a closed-corrugation panel of multiple single closed-corrugation sections detailed later in this thesis. The strongest secondary bond was achieved with a press and substrate temperature of 335°F, the temperature of the part from the IR oven of 335°F-360°F, and a pressure of 100 psi or more applied by the press. Adding a secondary procedure for surface texturizing could help enhance the shear transfer ability between CFRTP reinforcing plates and concrete in stay-in-place formwork, although it will likely be most beneficial for future research exploring the development of CFRTP rebar.

CHAPTER 5: CLOSED-CORRUGATION SPLICED PLATE

5.1 Introduction

5.1.1 Splicing Options for Closed-Corrugations

The concept of the closed-corrugation section being used on a commercial level would require a continuous forming or pultrusion manufacturing process. This would both allow for faster manufacturing as well as production of wider, multi-cell panels of any length. In this research, longitudinal splicing was explored to create a wider section via connecting multiple individual sections. The process of widening a single section was thought of to be done in multiple ways; through a mechanical connection, a secondary adhesive connection, or a secondary bonding connection.

For a mechanical option a tongue and groove design was developed. The design would allow closed-corrugation sections to fit into one another and be secured through bolts, an adhesive, or a secondary bonding process. This design would be the most complicated to manufacture. A concept image of the cross section is shown in Figure 71.

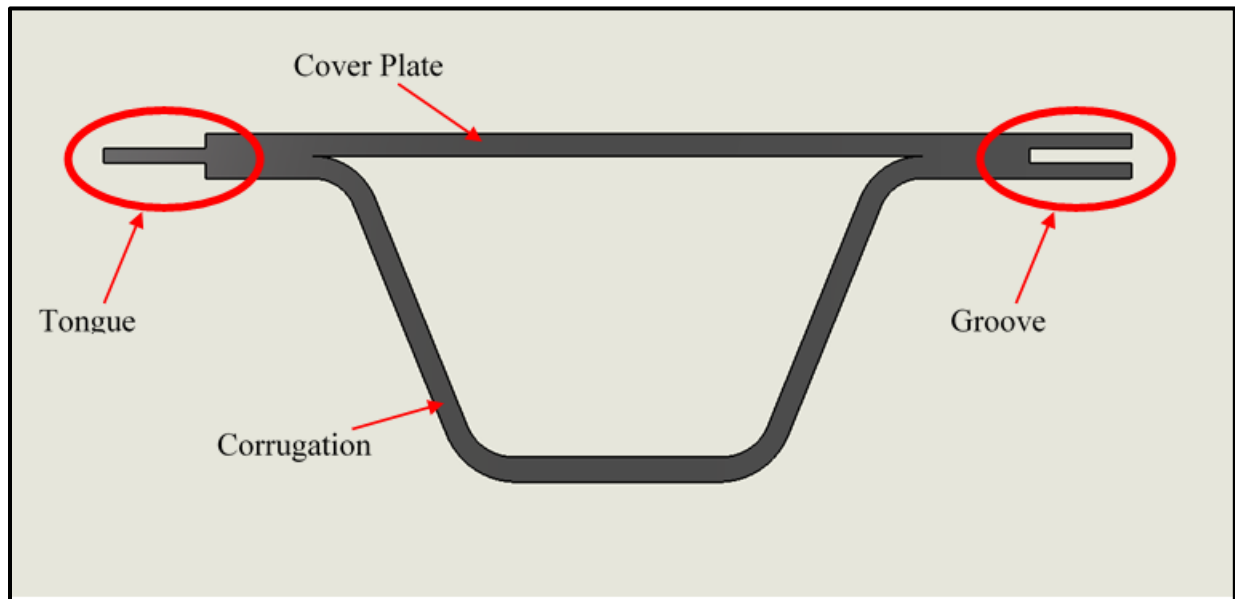


Figure 71: CF RTP Tongue-and-Groove Closed-Corrugation Design

The next design option looked to utilize the knowledge gained of secondary bonding, by creating a surface that would allow for the connection between sections to be achieved through a secondary bond. The first design is a more complicated initial manufacturing process, especially with a stamp forming manufacturing cycle. But the more complex design also has benefits to the performance of the section. From initial testing of the closed-corrugation it was seen that the connection of the top flanges of the corrugation and the cover plate were an area of interest. The first design named the implanted corrugation, and is shown in Figure 72.

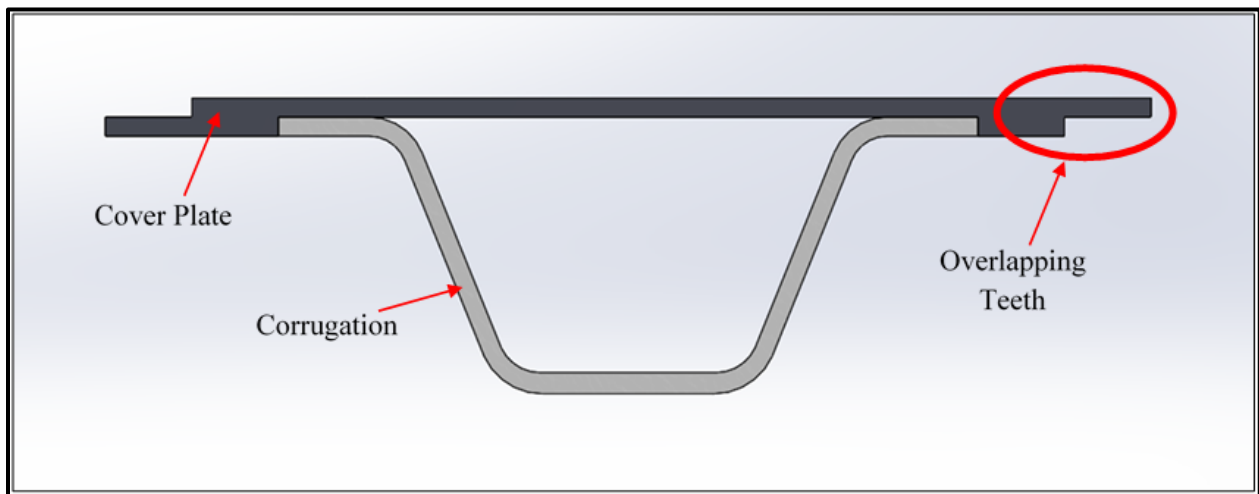


Figure 72: CF RTP Implanted Corrugation Design

This design took a single corrugation bonding it to a cover plate with a groove that is large enough for the corrugation to fit into and provide the top flanges a restraint on the sides of those top flanges, preventing them from opening up and working against the secondary bond. The design also included overlapping teeth that provided the surface for bonding. Similarly to before this design could have connection points between closed-corrugation sections that are accomplished either through a bolt, adhesive, or secondary bond. The simplicity of the overlapping however provides an ideal surface to be secondarily bonded.

The third design is very similar to the implanted corrugation and simple would be a traditional single closed-corrugation section but with a cover plate shifted to one side producing a shiplap joint. Again creating an overlapping bond area that could be connected with other single closed-corrugations either through a secondary bonding process, an adhesive, or a bolt/fastener. A cross sectional view of this design is shown in Figure 73.

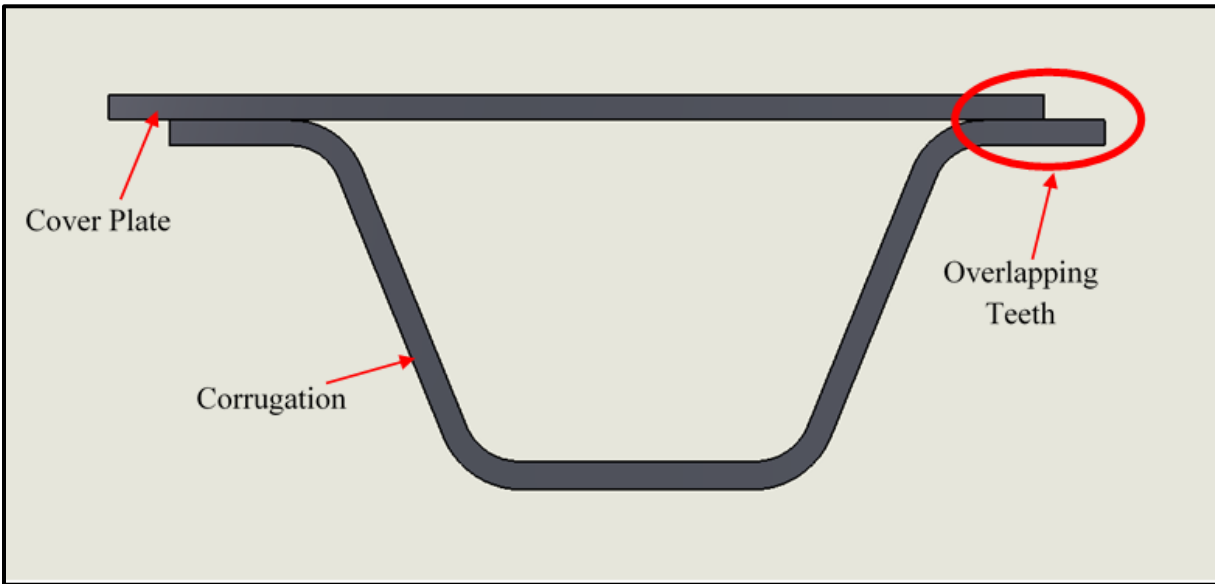


Figure 73: CF RTP Overlapping Cover Plate Design

In terms of manufacturing this is the simplest design and could be easily achievable, since the traditional manufacturing process for closed-corrugations could be slightly altered and this cross section could be produced. The main alteration would be in the size of the parts, specifically the top flanges and the cover plate. This size adjustments would help create a quality bond between sections during secondary bonding. The other adjustment to the manufacturing process would be with the molds used in order to achieve the appropriate pressure on all portions of the part to preserve the strength of the part.

The final design would be a large cover plate that could be attached to several corrugations to create a panel of closed-corrugation. This design could be scaled up to any size, with the only

requirement being to increase the size of the cover plate to meet the amount of corrugations you would like to be included in the panel. This simplifies the design even more to splice multiple closed-corrugations to create a wider section. This design is shown in Figure 74.

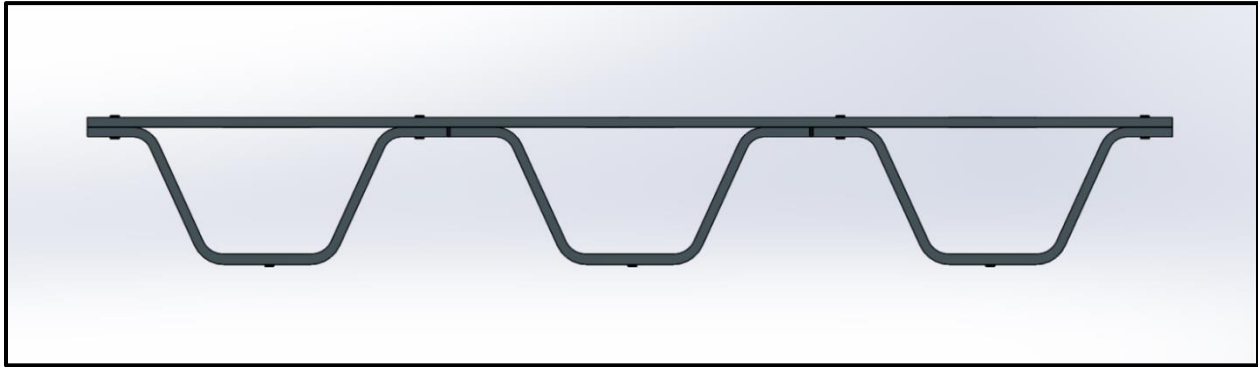


Figure 74: CF RTP Multi-Corrugation Single Cover Plate Design

This single cover plate design was used for prototype testing, as it gives preliminary insight into behavior of a closed-corrugated panel and is simpler to fabricate than the overlap or tongue and groove options.

5.2 Design of Thermoplastic Section

5.2.1 Design of Thermoplastic Section

The thermoplastic composite plates used for this closed-corrugation panel design were the same as what had been previously used for the single closed-corrugation design from Chapter 2 and 3. The performance of the thermoplastic plates of the single section was considered to be adequate and the secondary bonding was the area that needed improvement. For that reason the same layup would be used for the corrugation and the cover plate, and using information outlined in Chapter 4 an improved secondary bond was attempted. The only difference is the size of the cover plate, in this testing the cover plate was larger to cover three corrugations to form the panel for testing.


The layups are provided again in Table 15 and show the two different layups. Layup #1 is the Bottom Flange of the Corrugation and Layup #2 is the Top Flange and Web of the Corrugation. Layup #2 is also the one used for the cover plate.


Table 15: Corrugated Plate Laminate Layup Schedule

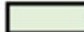
Plate Name: Corrugated Plate			
Layer:	Orientation:		Continuity Across Layups
	Layup #1	Layup #2	
1	0	0	continuous
2	0	0	continuous
3	45	45	continuous
4	-45	-45	continuous
5	0	0	continuous
6	0	0	continuous
7	0	45	
8	0	-45	
9	0	EMPTY	
10	0	0	continuous
11	0	0	continuous
12	45	45	continuous
13	-45	-45	continuous
14	0	0	continuous
15	0	0	continuous
16	0	45	
17	0	-45	
18	0	EMPTY	
19	0	0	continuous
20	0	0	continuous
21	45	45	continuous
22	-45	-45	continuous
23	0	0	continuous
24	0	EMPTY	
25	0	0	continuous
26	-45	-45	continuous
27	45	45	continuous
28	0	0	continuous
29	0	0	continuous
30	0	-45	
31	0	45	

Table 15: continued

32	0	EMPTY	
33	0	0	continuous
34	0	0	continuous
35	-45	-45	continuous
36	45	45	continuous
37	0	0	continuous
38	0	0	continuous
39	0	-45	
40	0	45	
41	0	EMPTY	
42	0	0	continuous
43	0	0	continuous
44	-45	-45	continuous
45	45	45	continuous
46	0	0	continuous
47	0	0	continuous

 **Blue Highlighted Layers** = Bottom Layup Bundle for Corrugated Plate

 **Red Highlighted Layers** = Middle Layup Bundle for Corrugated Plate

 **Green Highlighted Layers** = Top Layup Bundle for Corrugated Plate

5.2.2 Failure Prediction

Failure predictions for this closed-corrugation panel were conducted similarly to the single closed-corrugation section and can be seen here. Because the layer orientations aren't changing the same laminate strengths were used to make failure predictions as those used in Section 2.2.2. These properties are provided here in Table 16 and Table 17.

Table 16: Laminate Strength – Corrugation Top Flange and Web / Cover Plate

Corrugation Top Flange and Web / Cover Plate		
Material Property	ksi	MPa
Longitudinal Tensile Strength, F_{xt}	30.7	211.9
Longitudinal Compressive Strength, F_{xc}	27.8	191.4
In-Plane Shear Strength, F_{xy}	4.1	28.6

Table 17: Laminate Strength – Corrugation Bottom Flange

Corrugation Bottom Flange		
Material Property	ksi	MPa
Longitudinal Tensile Strength, F_{xt}	42.0	289.4
Longitudinal Compressive Strength, F_{xc}	35.9	247.3
In-Plane Shear Strength, F_{xy}	2.9	19.8

Geometric properties such as heights, cross section areas, moment of inertia and centroid values had to be calculated for the new cross section but like before were gathered through modeling. Measurement features of SolidWorks and MATLAB functions calculated moment of inertia and centroid values, these functions are provided in Appendix G. Geometric properties are displayed in Table 18.

Table 18: Geometric Properties of Multi-Corrugation Panel

Geometric Property	Variable	Value	Unit
Total Height of Cross Section	h	5.05	in
Total Width of Cross Section	w	37.05	in
Total Bond Length	b	9.42	in
Diameter of Shear Studs	d	3	in
Cross Sectional Area of Single Corrugation	A_c	5.92	in ²
Cross Sectional Area of Cover Plate	A_{CP}	12.41	in ²
Moment of Inertia	I	103	in ⁴
First Moment of Area	Q	18.8	in ³
Centroid Location of Cover Plate – from base	C_{CP}	4.886	in
Centroid Location of Full Panel – from base	Z_1	3.37	in
Centroid Location of Full Panel – from top	Z_2	1.68	in
Spacing between Applied Loads	a	18.67	in

These values allow for the three capacity checks previously calculated for the single closed-corrugation beams: flexural, shear, compression flexure adjusted for shear stud holes. An additional fourth check was completed evaluating the shear strength of the closed-corrugation panels looking at the secondary bond strength. This uses the experimental lap shear strength

gathered through testing in Section 4.3.3, for Specimen H with was at 1245 psi, instead of the In-Plane Shear Strength of the laminate. These checks solve for P , which is the load applied by a single load head and doubled to get the fully applied load. Again for the purposes of these calculations because the section has two separate layups the lower strengths were used, therefore the tensile and compressive strength are from the top flange/web/cover plate layup (Table 16) and the shear strength from the bottom flange (Table 17).

- Flexural Check:

$$M_{flex} = \min\left(\frac{F_{xt} * I}{Z_1}, \frac{F_{xc} * I}{Z_2}\right)$$

$$M_{flex} = 938.3 \text{ kip} * \text{in}$$

$$M_{max} = P * a \text{ Steel Manual [8]}$$

$$M_{max} = M_{flex} = P * a \rightarrow P = \frac{M_{flex}}{a} = 50.3 \text{ kip}$$

$$P1_{applied} = 2 * P = 100.6 \text{ kip}$$

- Secondary Bond Shear Check:

$$V_{max} = F_{xy} * \left(\frac{I * b}{Q}\right)$$

$$V_{max} = P = 64.3 \text{ kip}$$

$$P2_{applied} = 2 * P = 128.6 \text{ kip}$$

- Laminate Shear Check:

$$V_{max} = F_{xy} * \left(\frac{I * b}{Q} \right)$$

$$V_{max} = P = 149.7 \text{ kip}$$

$$P3_{applied} = 2 * P = 299.3 \text{ kip}$$

- Compression Flexure Adjusted for Shear Studs:

$$\text{Width Adjustment: } adj = \frac{w - (3 * d)}{w} = 0.757$$

$$F'_{xc} = \frac{F_{xc} * adj}{1.3} = 16.2 \text{ ksi}$$

$$M'_{flex} = \frac{F'_{xc} * I}{Z_2} = 993.2 \text{ kip}$$

$$P = \frac{M'_{flex}}{a} = 53.2 \text{ kip}$$

$$P4_{applied} = 2 * P = 106.4 \text{ kip}$$

- Predicted Failure Load:

$$P_{failure} = \min(P1_{applied}, P2_{applied}, P3_{applied}, P4_{applied}) = P1_{applied} = 100.6 \text{ kip}$$

This points to tensile failure occurring at 100.6 kip in flexure. During single corrugation testing, bare CFRTP experienced failure at about 35% below its prediction following these equations. Therefore the failure load could be seen at low as approximately 65 kip, if the same is to hold true. An additional factor of multiple secondary bonds being formed during the manufacturing process could promote specimen to fail on the lower end of the prediction. Any alignment or surface connection issues could result in a weak point to be exploited during testing.

5.3 Manufacturing of Spliced Panel

The steps to manufacture the closed-corrugation panel is similar to the single section with a few modifications specifically in the secondary bonding process. The steps are listed below.

1. Creation of the tailored blanks
2. Consolidation of the tailored blanks into flat panels
3. Water jetting panels to desired dimensions and create shear stud holes (alignment holes were also water jetted at this time)
4. Forming of the corrugated shaped panels from flat consolidated plates utilizing a machined mold
5. Manufacture 3D Printed mold with heating elements for secondary bonding.
6. Secondary bonding large flat cover panels to three corrugated panels creating the closed-corrugation panel specimen

5.3.1 Initial Manufacturing Process

The manufacturing process was identical up until the secondary bonding of corrugations to the cover plate. The manufacturing process started with a tailored blank formed with Glass fiber/PETg unidirectional tapes placed in the layup orientations and tack ultrasonic welded into position, then moved into the consolidation phase. The final two steps were the water jetting the plates down to size and the final step was the corrugation plates being stamp formed into shape using the IR Oven and single corrugation mold. These steps are detailed more in Chapter 2, Section 2.3.1 to Section 2.3.3.

5.3.2 Secondary Bonding Mold Manufacturing

Using a previously manufactured corrugation model the initial manufacturing process had already been established and was able to be followed, a current mold was used to stamp form the corrugated sections into shape. This manufacturing process began to diverge during the secondary bonding of corrugation sections to the top cover plate. Because these panels were manufactured using three corrugations a new mold was required. It was determined that 3D printing a mold was the best route to go, it would allow it to be made in house and utilizing capabilities of the ASCC, primarily the Ingersoll 3D Printer.

The mold was printed out of a Polycarbonate with Carbon Fiber reinforcement. It was selected because of its strength and thermo-properties. These thermo-properties were very important since the mold and parts it held would be heated during the secondary bonding cycle. In order to minimize the print time and ensure a quality part was printed with no substantial defects or warping in the part occurred during printing the mold was printed in three separate parts, a view of one of these parts being printed is shown in Figure 75.

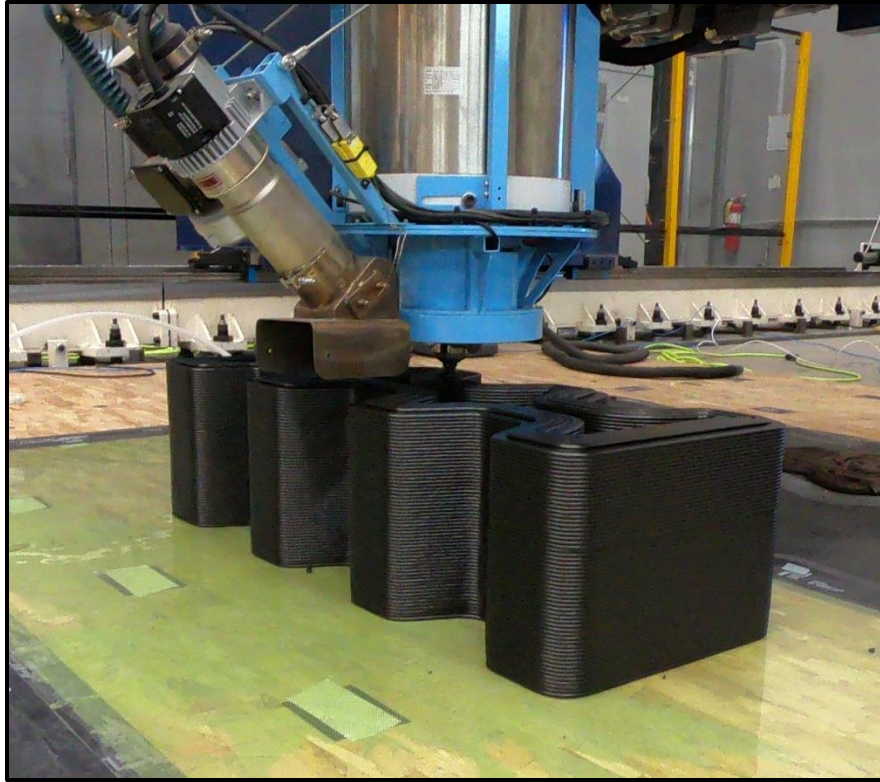


Figure 75: 3D Printing of Multi-Corrugation Mold – Single Section

These loops were then split and attached using an epoxy into the final mold orientation and prepared for machining. At this stage the mold was roughly to size in the overall dimensions, with inner geometry and features needing to be machined in. The mold ready for machining is shown in Figure 76.



Figure 76: 3D Printed Mold Ready for Machining

The design of the corrugated part being manufactured had known dimensions, since it had been used multiple times in previous work on the project. This allowed the inner geometry of the mold to be precisely machined in order to fit and support corrugations during the secondary bonding process. Additionally, part of the secondary bonding process is localized heating of the top flanges of the corrugations. To achieve this heating elements were used and needed grooves machined into the mold that allowed them to sit flat with the upper surfaces of the mold while additionally providing enough heat and supportive surface to create a quality secondary bond. Considerations additionally went into wiring and insulation that would be included in the grooves. A view of the grooves with the geometry is shown in Figure 77. The final fully machined mold with a heating bar placed into one of the grooves is shown in Figure 78.

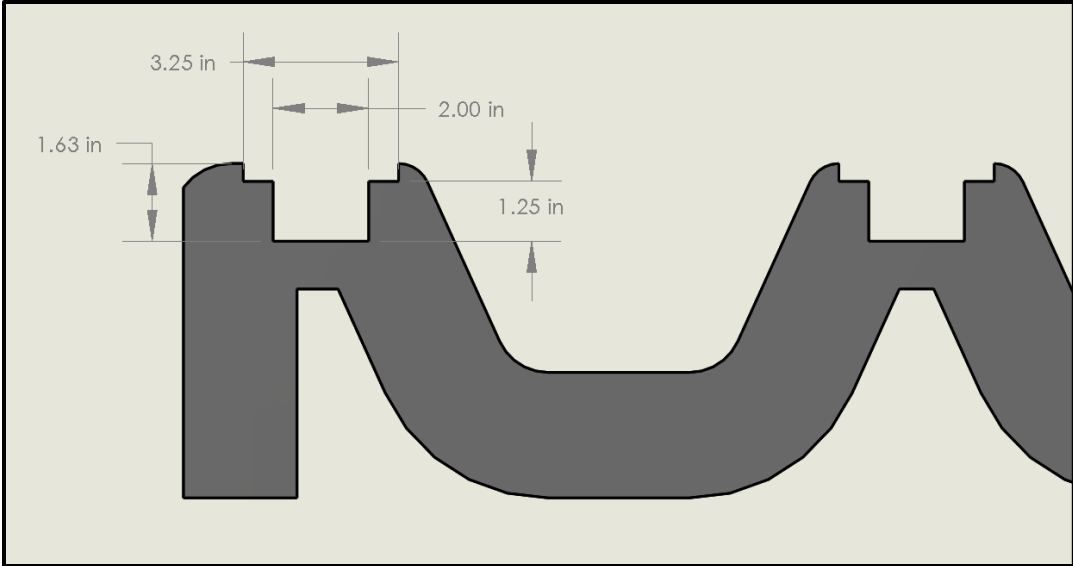


Figure 77: Dimensioning of Heating Element Groove



Figure 78: Fully Machined 3D Printed Mold

5.3.3 3D Printed Mold Manufacturing Trials

Heating elements were assembled, each element was constructed of an aluminum bar with three cartridge heaters attached to the bottom. Each element was wired to the control system which allowed heaters to be monitored and controlled during the manufacturing cycles and ensure proper heating was being applied to the part. The mold was also painted with a Digital Imaging Correlation (DIC) pattern that allowed deformation to be tracked through the manufacturing of parts process. The mold was then placed in the press of the TPL, the mold was on the bottom of the press and a platen was attached to the top.

The mold worked well enough to manufacture several spliced panels that were able to be tested, but didn't hold up as well as expected. There were two issues that came up with the mold during its use. The first issue was with the mold bending during initial heating, a diagram of how the mold bent is shown in Figure 79.

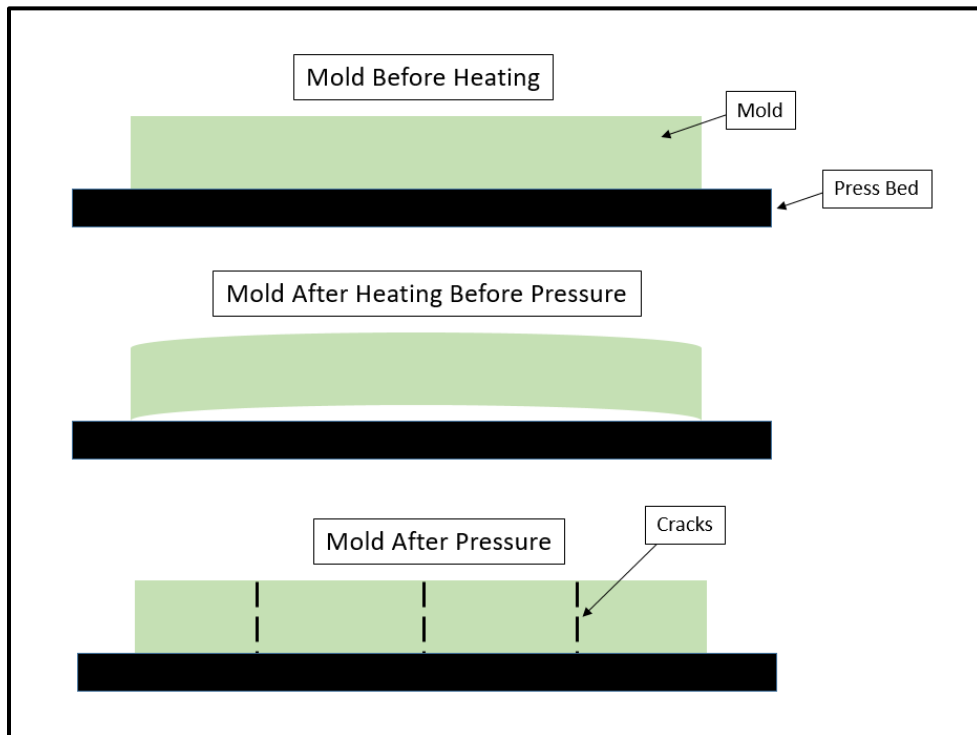


Figure 79: Bending and Cracking of Mold during Initial Heating

This caused the mold to crack after the first manufacturing cycle. The three cracks were directly at locations sections of the mold was epoxied together. What is believed to have happened is as the mold heated up and expanded the epoxy didn't heat up and expand at the same rate and when the pressure was applied it caused the epoxy to give way and crack. After the cracking occurred the mold didn't experience any bending during the pre-heating section of secondary bonding. Because this mold wasn't a forming surface and was just being used as a support system for the corrugations these cracks were ignored for the remainder of bonding cycles.

The other issue observed was with the heating element grooves. The ridges which the heating bar was supported by saw melting at locations directly next to some of the heaters, primarily in the middle two grooves. Once secondary bonding began this problem was challenging to avoid, some additional insulation was used but didn't provide the machined supports enough protection from the heating elements. This most likely impacted the support the part had since the mold was melting and very malleable, and with this being the bond area that means the bond could be jeopardized in those locations. These potentially weaker bonds can be seen when evaluating the spliced panel when the part is removed.

The mold worked well enough to manufacture the panel parts for the work of this milestone but during the manufacturing cycles damaged the mold enough to where it wouldn't be able to form many more parts. There are a few adjustments that could be made during future use of 3D printed molds.

The first adjustment would address the cracking of the mold, ideally the part would be printed as either one complete part or two halves that could be attached only at one spot. In the case of having to attach sections of a mold it would be best to use a combination of epoxy and a mechanical fastener to hold sections together.

The second adjustment would be to address localized heating. Insulation on the heating element as a whole is needed, much like was done during this manufacturing cycle, but additional insulation around the cartridge heaters themselves to ensure the material of the mold doesn't get exposed to excessive heat and lose its strength properties. This could simply be extra insulation packed in those areas or an insulated box around the cartridge heater itself.

5.3.4 Secondary Bonding of Closed-Corrugation Panel

Once all components of the Multi-Corrugation Panel, cover plate and corrugations, were the correct size and geometry the secondary bonding process began. The first step was to load the mold into the press, including placing the heating elements into their grooves and wiring up the heating system. Once the proper alignment and power checks were made the first cycle was performed. Secondary Bonding cycles started by loading three corrugations into the mold, and then placing a spring table into each. Spring tables help to support the cover plate over the openings of the corrugation, this allows for a quality secondary bond to form between corrugations and the cover plate well additionally not allowing the cover plate to droop at all over the corrugations. This setup of spring tables in the corrugations is shown in Figure 80.



Figure 80: Corrugation Prepared for Secondary Bonding with Spring Table

The initial plan was to repeat secondary bonding procedures used in the last closed-corrugation manufacturing work with the one adjustment be to the temperature the top flanges of the corrugations was required for bonding. Previously in the manufacturing of single closed-corrugations in Chapter 2 and 3 secondary bonds were formed at 225°F. The lap shear work from Chapter 4 determined 335°F would result in a stronger bond between plates. So for this work the cartridge heaters and the heating from the top platen heated the top flanges up to 335°F. At that point the cover plate would be heated in the IR Oven to 370°F for 120 seconds. Once the IR Oven heating cycle was completed the cover plate was quickly moved into the press into position on top of the corrugations and 100 psi was applied over the part. Once pressure started to be applied heating in the platen and cartridge heaters was turned off. Due to the mold appearing to give some during initial pressure trials and the press not having an active pressure seeking ability, it was decided that after the initial 30 minutes of pressure the pressure would be

reset to 100 psi and then left for the remainder of the forming cycle. The cycle concluded when the part fell to a temperature below the T_g (178°F) allowing for the panel to be removed.

During the first complete secondary bonding cycle there was an issue with moving the cover plate from the IR Oven into the press. There wasn't enough suction power in the robot arm to properly support the heated plate. This was the largest plate to be heated in the IR Oven, when the part was heated and malleable it sagged significantly enough to come in contact with the mold during placement, and completely throwing off the alignment of the cover plate onto the mold and corrugations. Because of this the process was modified. The IR Oven stage was skipped and instead the cover plate was stacked onto the corrugations before heating started. All parts were heated until the bond area reached 335°F, at this point pressure was applied at 100 psi. Pressure had to be adjusted again at the 30 minute mark since pressure since pressure typically had dropped to around 50 to 60 psi by that point. Once the pressure was reset, the press was left alone until the panels were removed about 18-20 hours later once the part was below the T_g (178°F). This new procedure would better represent a second full consolidation, which should provide a very strong secondary bond. The largest potential source of error in the process that would impact the quality of the bond would be in the rigidity of the mold when creating a support for pressure to be applied to the surfaces to create the secondary bond. The final panel will be approximately 37 inches wide, 60 inches long and 4.85 inches tall. A view of the final panel after the secondary bond is shown in Figure 81.



Figure 81: Completed Multi-Corrugation Panel

Bonded areas can be seen when looking at the cover plate. Darker areas show where a secondary bond is located and a darker color points to the bond being stronger than in the lighter areas. Some of these lighter areas in which secondary bond is expected to be worse than the darker areas is highlighted in Figure 82.

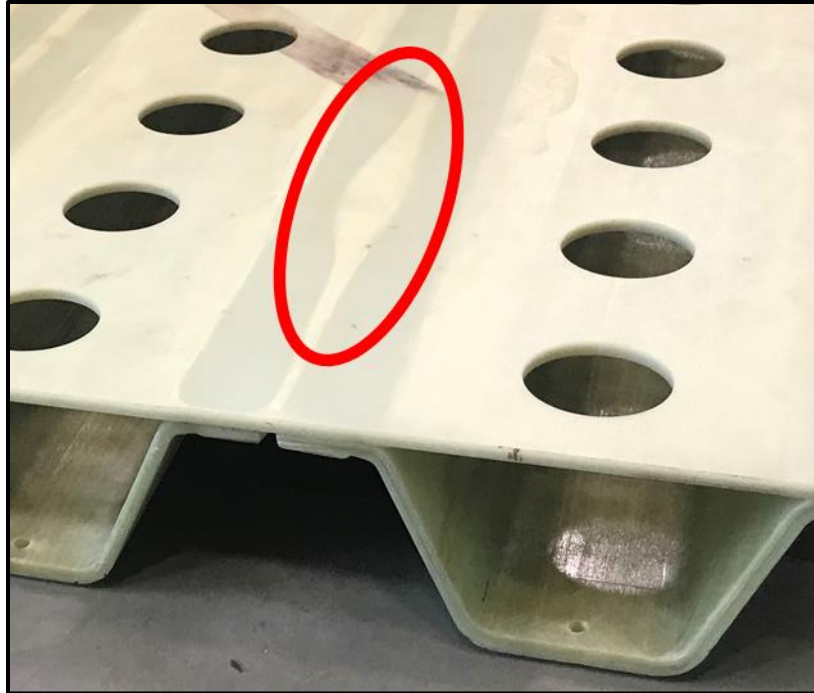


Figure 82: Assumed Poorly Bonded Area of Spliced Panel

The cause of this is most likely due to the previously mentioned concern with support the mold gave to the heating elements as the mold itself being heated and malleable during the secondary bonding process. These lighter areas are directly above the cartridge heaters on each bond section, and seemed to be the worse on the middle two bonds. This channel was observed to be impacted the most by the heat and saw the same melting in the areas directly below these lighter bond areas.

5.3.5 Instrumentation of Closed-Corrugation Panel

Panels were instrumented with the typical instrumentation for testing of thermoplastic support systems, this includes strain gauges, string potentiometers, and Linear Displacement Transmitters (LDTs). With a focus of the strain gauges being in the outer two corrugations, in an attempt to get a reading on how the panel is reacting to being loaded and if it is symmetrical. Strain Gauges were placed on the top and bottom of the secondary bonds of the two outer corrugations and on the bottom of each corrugation at both the center and 18 2/3 inches from the

center towards the edge. This results in 22 total strain gauges. The location of the strain gauges for each location is shown in Figure 83 and the two locations of each set are shown in Figure 84.

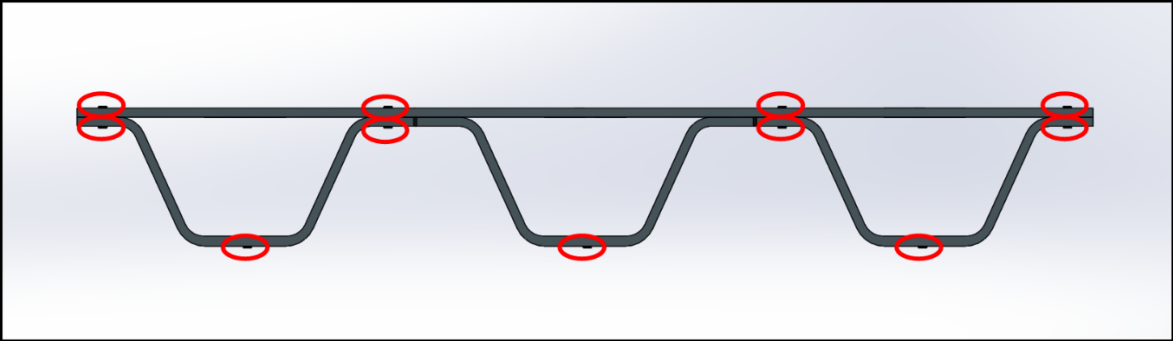


Figure 83: Location of Strain Gauges at both Center and Outer Locations

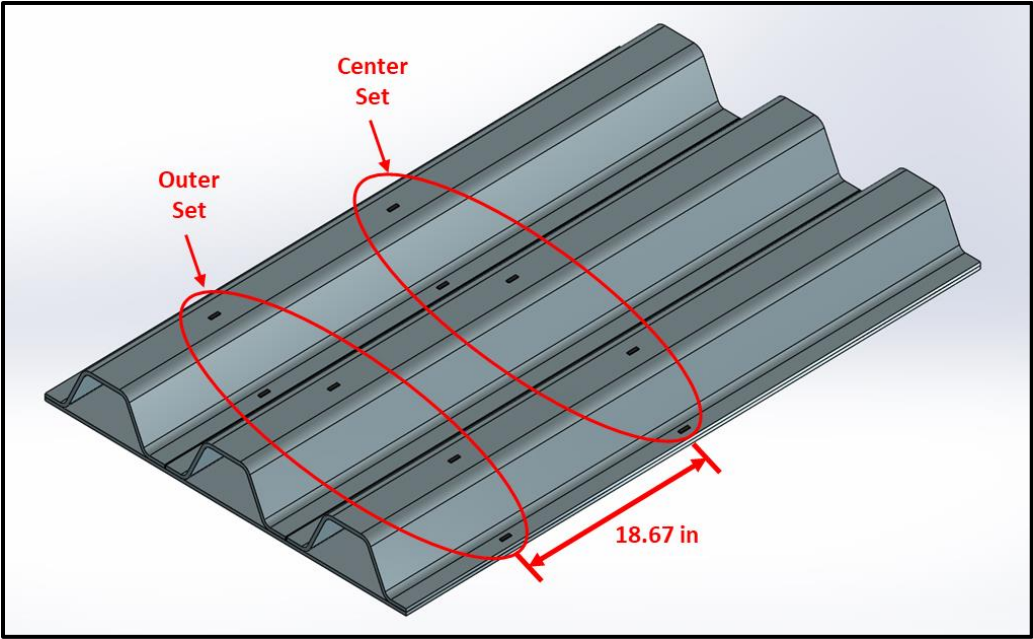


Figure 84: Location of the Center and Outer Sets of Strain Gauge

String potentiometers were attached to the underside of the center corrugation at the midspan and 9 1/3 inches towards each end, this would place the outer string potentiometers below the load heads. LDTs were mounted on each end to record the deflection at the supports.

5.4 Spliced Closed-Corrugation Panel Testing

5.4.1 Test Setup

Due to the size of a single panel testing the four point load head was assembled through three I-beams. One acted as a spreader and the other two applied the load to the panel. Reinforced concrete blocks were used as end supports topped with neoprene pads on the locations the panel comes in contact with the support. This allowed the part some ability to rotate, typically this would be done through the use of tilt tables but due to the size of the panel this adjustment was made. This setup can be seen in Figure 85 and the FBD is shown in Figure 86.

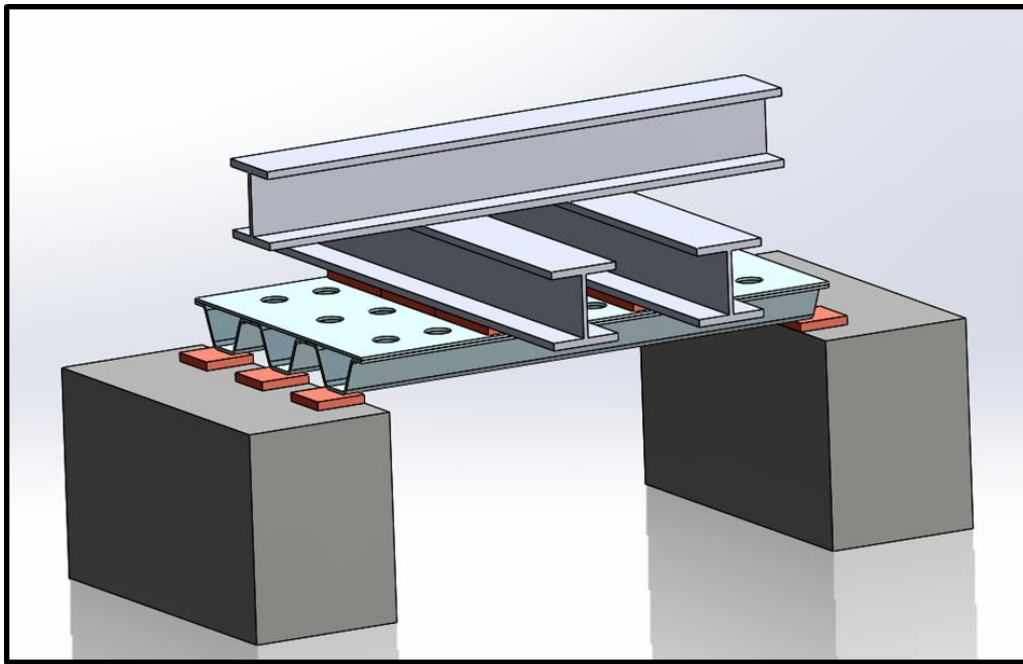


Figure 85: Multi-Corrugation Panel Test Setup

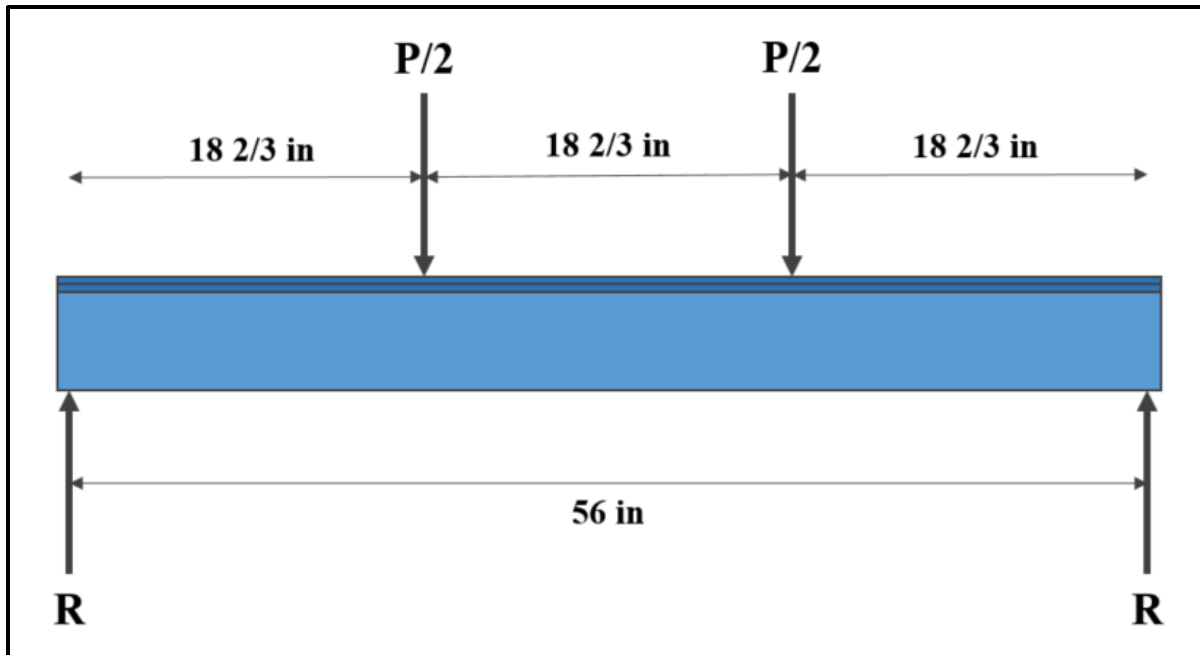


Figure 86: Free-Body Diagram of Closed-Corrugation Testing

5.4.2 Test Procedure

The testing procedures follow that previously done during testing of single section stay-in-place formwork. All testing was done as a four point bend test. Test specimens were instrumented before being moved under the frame and fully wired for data collection once properly in place under the test frame. Loading pads are placed to reduce stress concentrations and preliminary photos are taken of the test specimen. This leads to the first part of the testing, being a cyclical loading of the construction loads on the panel. The max load during this testing is calculated following the same AASHTO specifications outlined in Section 3.2. Through calculating the loads that must be withstood and then adjusting for the four point test set up it was calculated that the Construction Loading test should cycle up to a maximum of 1550 lb before being unloaded. One full cycle is from 0 lb to 1550 lb to 0 lb, this was repeated for a total of three times per test specimen. Once Construction Loading is completed the panel is checked for significant damage and then tested until failure. Video was taken during the failure test to

capture part deformation and failure during testing, additionally photos were taken at the conclusion of the test to visually record damage to the test specimen.

5.4.3 Discussion of Results

The first data produced was that for the construction loading cyclical test. All four specimens were loaded to 1550 lb and then completely unloaded a total of 3 times. This load was calculated to produce a moment equal to that required by AASHTO. Load versus midspan deflection can be seen for all specimen in Figure 87. The midspan deflection is taken from Instron position displacement, because of cross section design the webs compress during loading and cause the specimen to become thinner and impact part deflection readings. The Instron position displacement should provide an approximate top surface deflection. Early loading provided substantial noise in the data because of silicone pads deforming and limiting loads from fully being applied to the specimen, for this reason a preload of 50 lb was applied to the specimen.

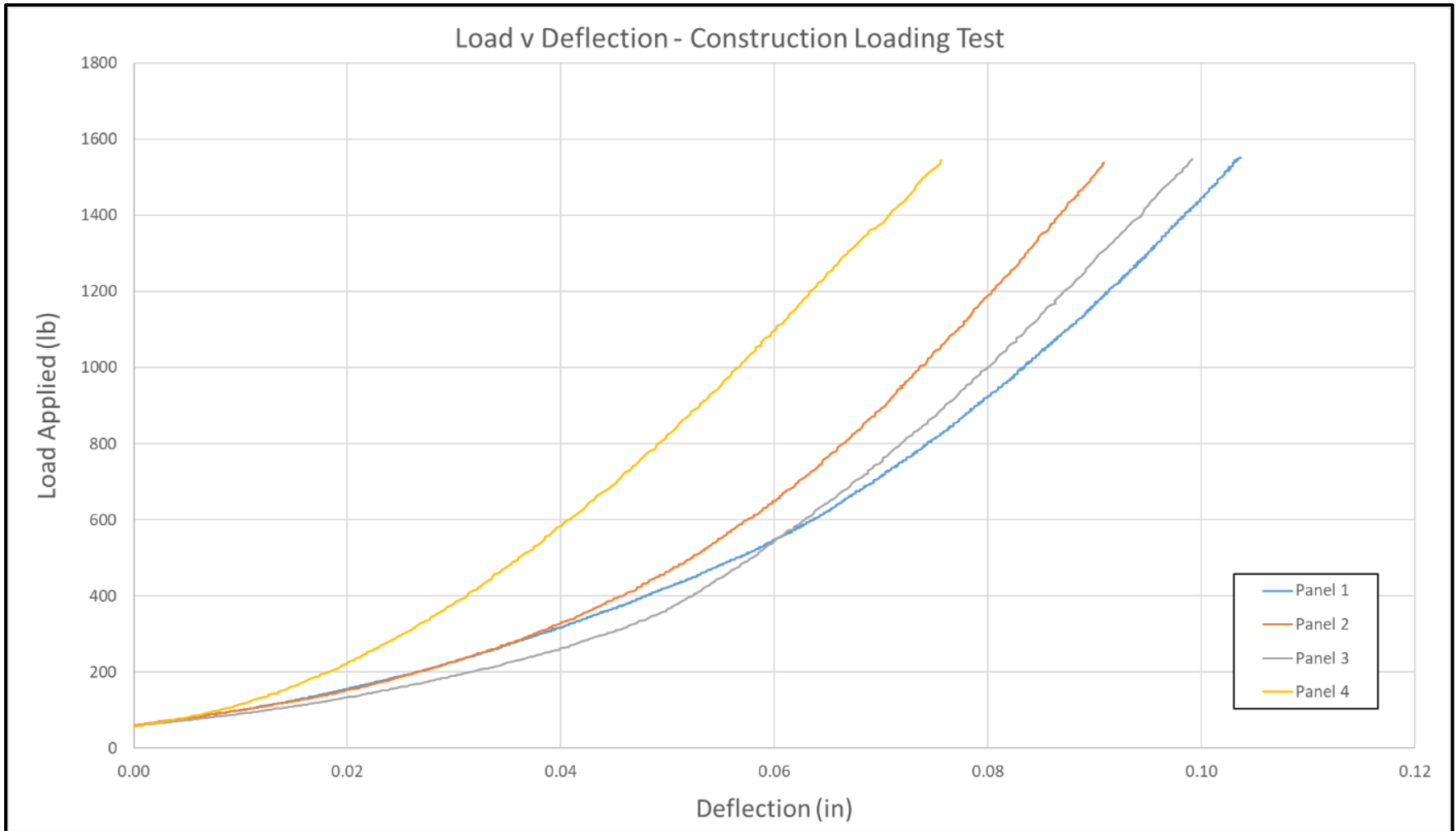


Figure 87: Load versus Deflection of Panels during Construction Loading

The drawback to this approach is that the neoprene pads that are used under the load heads introduce additional compliance into the system which is reflected in the initially soft response. This can be seen in the plot over the first section of loading where there is a large deflection at relatively low loads before the plots start becoming linear around 800 lb. Because of this the deflection taken from the underside of the specimen from the test of Panel 4 was examined and plotted along with the Instron displacement data and the calculated load deflection for a beam with the material properties and geometry of the multi-corrugation panel. These plots are shown in Figure 88.

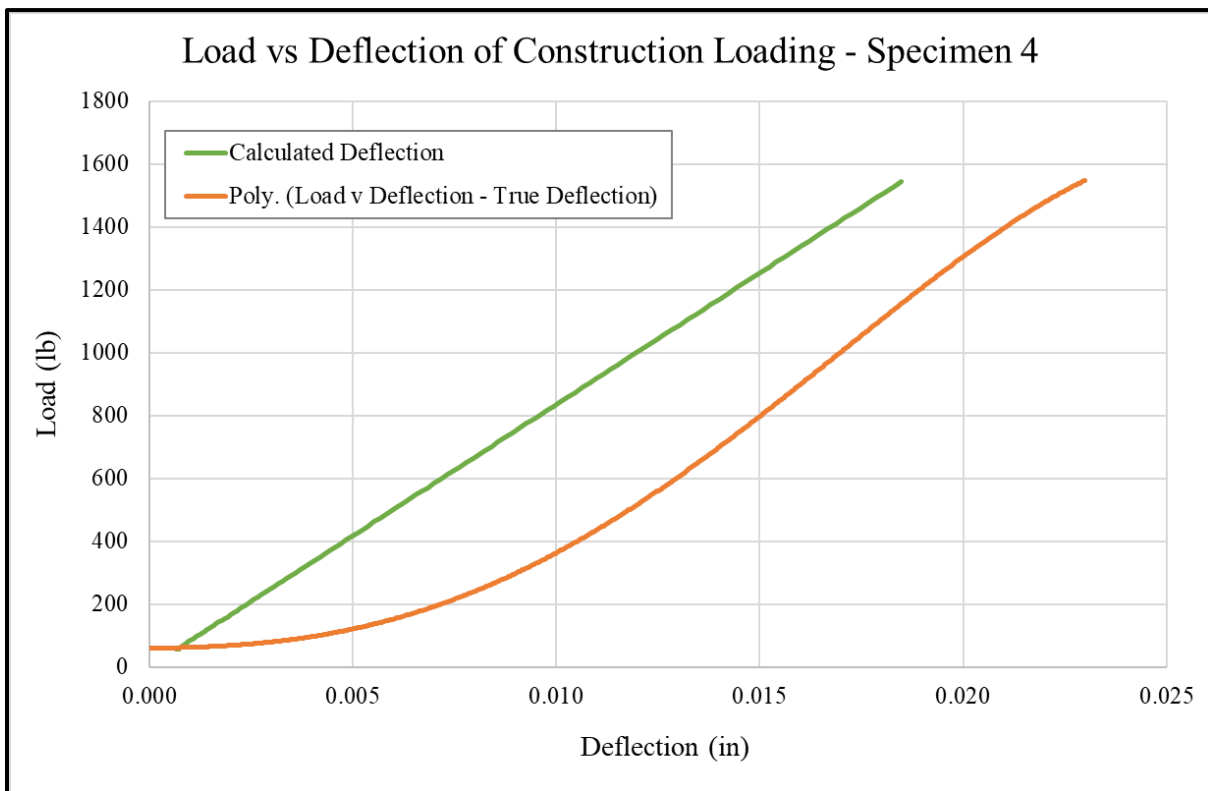


Figure 88: Load v. Deflection of Specimen 4 – Construction Loading

Looking at the data in these plots, for earlier loading it seems the deflection from the bottom of the panel corresponds better with the calculated deflection and corresponds well with the AASHTO 0.02 inch deflection limit. The underside deflection slightly exceeds that limit, which

could be due to the LDT measured end deflection being elevated due to mounting issues. One important note in terms of the construction loading test is that the loading accounts for the weight of the concrete that would be added to the corrugation channels, which would cause the loads to be distributed differently to specimen, averting an excessive compression of the webs. During the construction load cycling the parts showed very little to no permanent deflection, returning to roughly original condition. There were no visible issues in terms of damage to individual sections of the specimen or the secondary bond.

Experimental stiffness during construction test loading of the closed-corrugation panel can be calculated and be compared to the experimental stiffness of the single closed-corrugation during the same loading criteria, being an average of 38.1 kip/in, see Section 3.3.1. In the case of Specimen 4 of the closed-corrugation panels the experimental stiffness can be approximated where the plot is relatively linear, between deflections 0.01 inch and 0.0155 inch. This allows an experimental stiffness to be calculated at 131.8 kip/in. This would be an improvement of about 346% from the single closed corrugation, indicating an improvement in the strength of the secondary bond created using the new settings.

Once a panel completed construction loading and was deemed undamaged it began a failure test. Observations and analysis were made primarily through visual inspection, load vs deflection plots, and calculating the shear flow experienced by the section during testing. As previously mentioned because of the web compression and cross-sectional deformation that happened during testing it was determined the best way to display the deflection was with the Instron position. These deflections will be elevated due to the compression of the neoprene pads below the load heads but will better resemble the deflection and compression seen in the top half of the specimen. During testing the specimens were deemed failed if they saw a significant loss in load

or a part failed completely, crushed or experienced significant damage. Significant loss in load was defined as a drop of over 5000 pounds. The load deflection plots are shown in Figure 89; an important note is that Panel 2 was tested beyond the point the secondary bonds were deemed to be failed to observe how the failed section would behave when most of the secondary bonds had been broken.

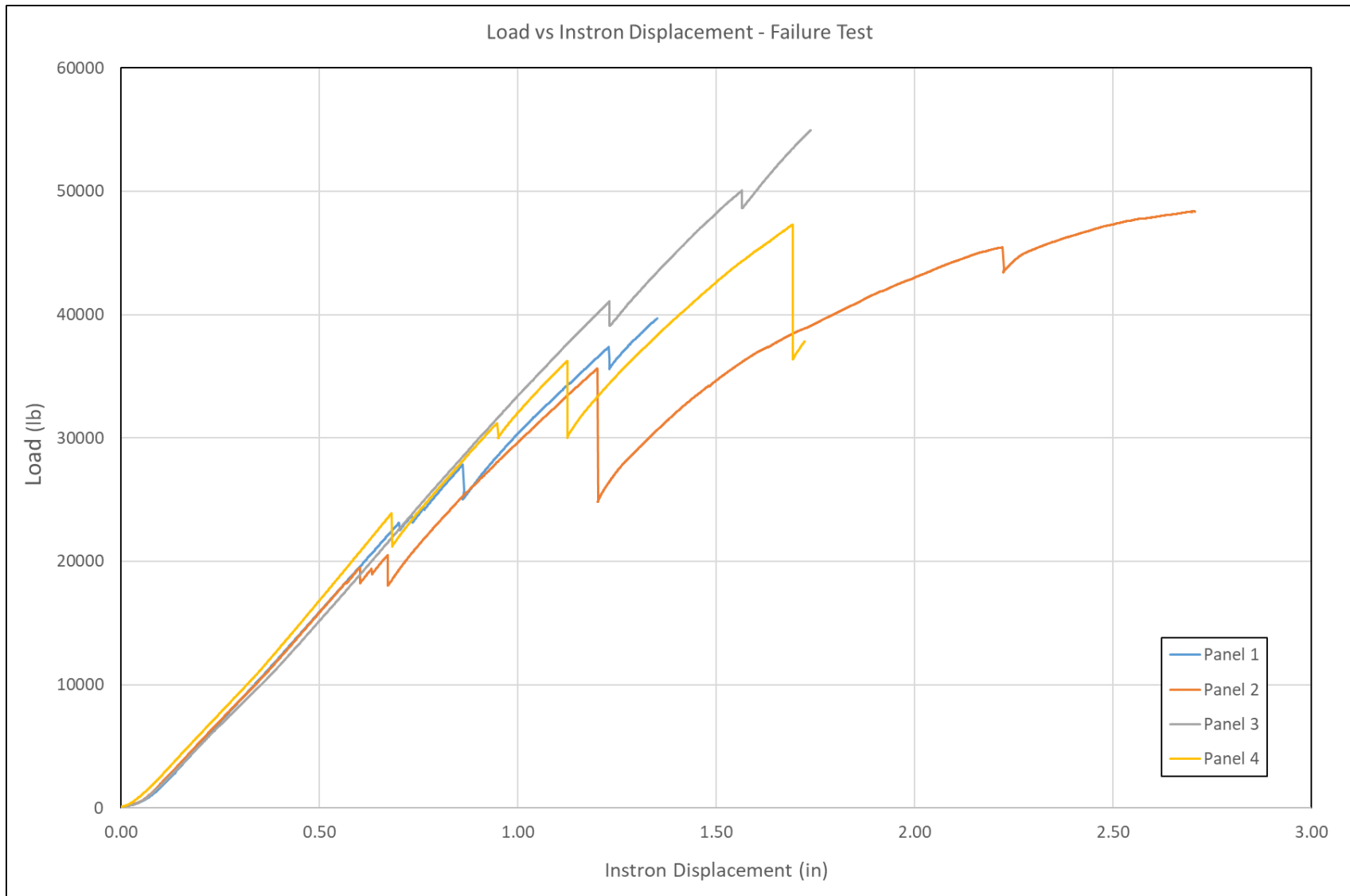


Figure 89: Failure Test Load-Deflection Plot of Multi-Corrugation Panel Specimen

None of the specimen were completely crushed or ruptured, but failure was determined to have occurred in three of the panels when there was a significant loss of applied load, with these maximum failure loads ranging from 35.6 kip to 39.7 kip. Panel 3 reached the maximum load cell limit of 55 kips. Panel 2 continued to carry increasing load even after failure was deemed after one large loss of loads, representing the secondary bonds failing. This residual strength shows that even after the secondary bonds fail the specimen can still support load. This indicates the member may does not fail suddenly and possesses some ductility.

All panels saw small drops during the loading process before continuing being able to withstand increases in load, these drops could be representative of early secondary bond failure at certain locations across the panel. The earliest of drops in load occurred in the range of 19.6 to 23.1 kips. During testing of single closed-corrugation failure testing saw secondary bond full failures occurring at approximately 20 kips, discussed in Section 3.3.1. For the Multi-Corrugation Panels these first bond failures were occurring at one of the outer most secondary bonds. For the three fully failed panels the large drop in load occurred when the middle corrugation's secondary bonds failed. Table 19 summarizes the experimental stiffness, peak load, and maximum deflection values for the panels.

Table 19: Failure, Maximum Deflection, Stiffness of Failure Test

	Manufacturing Order	Failure Load (kip)	Max Deflection (in)	Stiffness (kip/in)
Panel 1	Fourth	39.7	1.352	35.8
Panel 2	Third	35.6	1.203	28.5
Panel 3	Second	55+	1.738+	34.2
Panel 4	First	47.3	1.723	36.1
Average		44.4	1.504	33.6

Stiffness values were calculated based on the slope of the plots between 3 and 19 kips where the plots are behaving linearly before first signs of secondary bonding failure, and above loads where deflection could be more impacted by the neoprene. This provides an average experimental stiffness to be 33.6 kip/in, during failure tests of the closed-corrugation panel at the time when the load-displacement plots, Figure 88, are still acting linearly. The most likely reasoning for this would be due to the deflection value being slightly increased due to the neoprene pads having some initial compression throwing off the deflection measurements.

The failure load data indicates that the 3D printed mold used for secondary bonding could have been overheated and damaged by the multiple forming cycles. The first two panels made (Panel 4 and Panel 3) performed the best out of the manufactured set. Panel 3 performing better than Panel 4 could be due to the fact the mold was slightly modified after forming Panel 4 with some thin aluminum shims added under the heaters to the most heavily damaged areas of the mold to level out the mold surface. However, with additional cycling the mold around the heaters was damaged due to repetitive high heats and pressures, and may not have provided adequate support

to ensure the forming pressure could be maintained for Panels 1 and 2. Panel 3 is considered to be the panel that closest matched the desired manufacturing settings and did show improvements on the maximum load the specimen was able to withstand.

The shear flow plotted against the applied load for Panel 4 is shown in Figure 90.

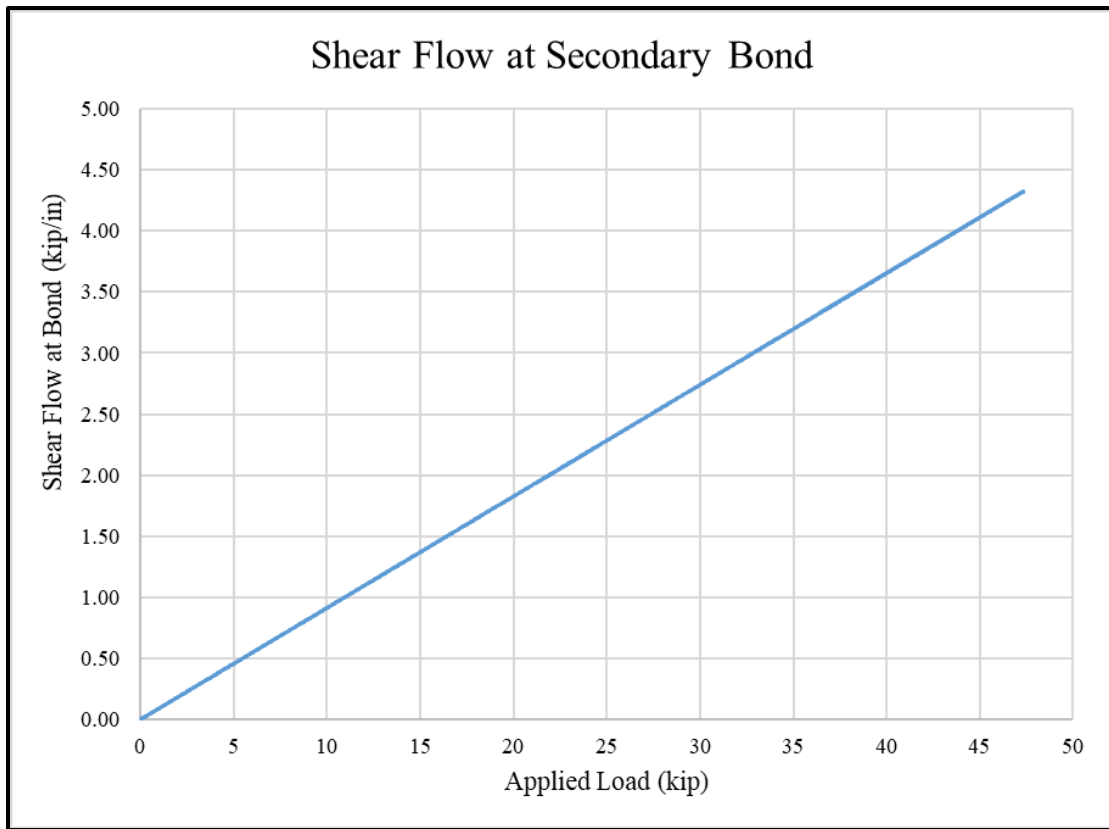


Figure 90: Shear Flow at Secondary Bond of Panel 4

The first sign of possible secondary bond failure in Panel 4 occurred at approximately 24 kips, which corresponds to a shear flow of approximately 2.25 kip/in. Similarly Panel 3, which saw the highest failure loads, a shear flow of approximately 3.7 kip/in at the first sign of possible secondary bond failure. With the data gathered in Chapter 4 about the bond strength using these secondary bonding manufacturing settings, we have a bond shear strength of 1245 psi. Accounting for the cross sectional length of the bond being 9.42 inches, this gives a shear flow at bond failure of approximately 11.7 kip/in. Based on inspection of the parts following the test

bond surfaces were very smooth. It is therefore concluded that the cover plate secondary bond is significantly less than the bond that would exist if the entire section was fabricated through a single process such as pultrusion.

All specimens experienced the same basic failure corresponding to the panels becoming detached from the cover plate. The only other clear damage was on the base of the corrugations around the supports, shown in Figure 91.



Figure 91: Inside of Corrugation at Support of Failed Panel 1

These failures near the supports are due to stress concentrations at the reactions, and would not be experienced by the panels in service. Very similar damage was seen in the testing of single closed corrugations. The only damage observed at the supports was in the bottom flange of the corrugation where the first several inches to a foot stayed deformed as the part was unloaded. This is also shown in Figure 91. However, the remainder of the part did largely recover its undeformed shape as displayed in a before, during and after image of the panel in Figures 92-94.



Figure 92: Photo before Testing of Panel 1 – No Load



Figure 93: Photo during Testing of Panel 1 - Loaded



Figure 94: Photo after Testing of Panel 1 – No Load

Figure 90 highlights how secondary bonding of the center and left most corrugations failed during this test and there was more damage to the bottom of those corrugations at the support and more permanent deformations in the center of the bottom flanges. However, overall the shape was recovered after removing the load with the exception being that the parts were not all still bonded. The only panel that saw no full secondary bond failures was Panel 3. While it did experience some secondary bonding failures as shown in the load-deflection plot, all corrugations remain attached and the permanent damage to the corrugations at the support was less than that of a failed panel as shown in Figure 95.



Figure 95: End Cross Section View after Testing of Panel 3

Strain data was recorded for all tests, but all strain data had issues that kept a full flexural analysis from being performed. The first issue was with strain gauge connectivity to the computer, every test had at least one gauge that was unresponsive because of some level of damage to the gauge. The other issue was the alignment of data between the strain recordings and load recordings. Technical issues prevented recorded points from being properly aligned. Some of these issues were resolved for the final test and allowed strain data to be recorded and then strain and load data were able to be aligned allowing strain data to be analyzed. Gauges were split into four regions per set (Midspan Set and Outer Set) and outlined in Table 20 and 21.

Table 20: Closed-Corrugation Panel Midspan Strain Gauge Regions

Midspan Set			
Western Corrugation		Eastern Corrugation	
Three Edge Gauges	Three Inner Gauges	Three Edge Gauges	Three Inner Gauges
Region 1 - M	Region 2 - M	Region 3 - M	Region 4 - M

Table 21: Closed-Corrugation Panel Outer Strain Gauge Regions

Outer Set			
Western Corrugation		Eastern Corrugation	
Three Edge Gauges	Three Inner Gauges	Three Edge Gauges	Three Inner Gauges
Region 1 - O	Region 2 - O	Region 3 - O	Region 4 - O

Figures 96-98 show the strain at each height for Specimen 4 where gauges were placed. The strain measurements correspond to a load of 15 kips, at which point the specimen load-deflection was linear.

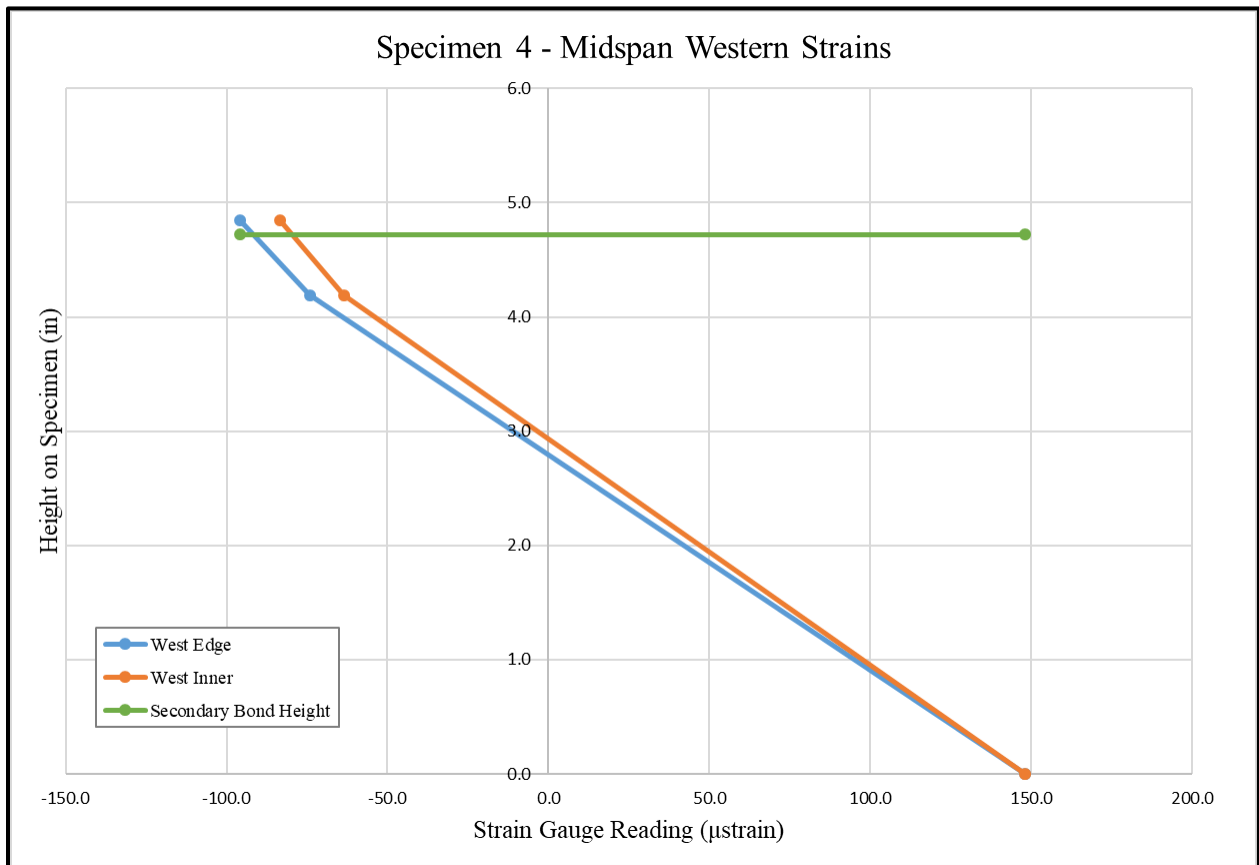


Figure 96: Strain Readings in Regions 1-M and Region 2-M at 15 kips

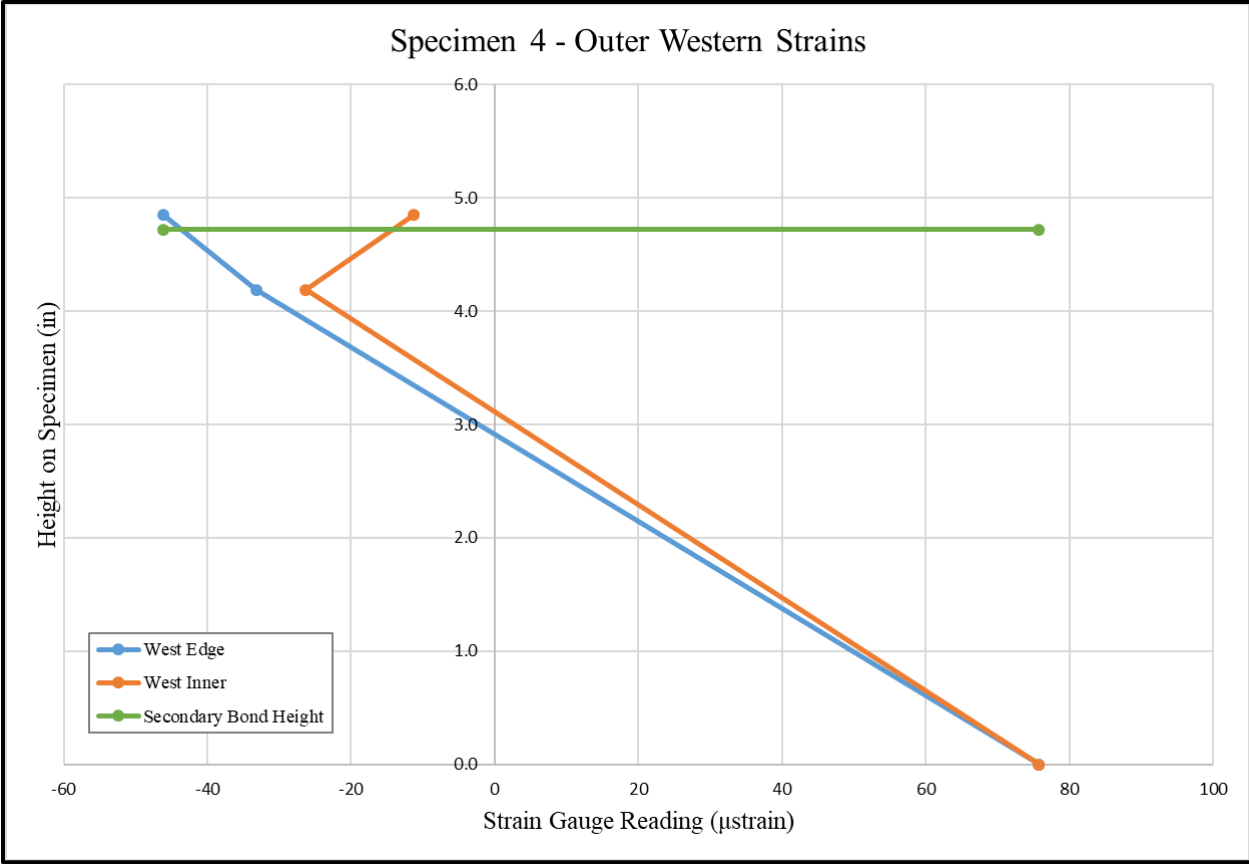


Figure 97: Strain Readings in Region 1-O and Region 2-O

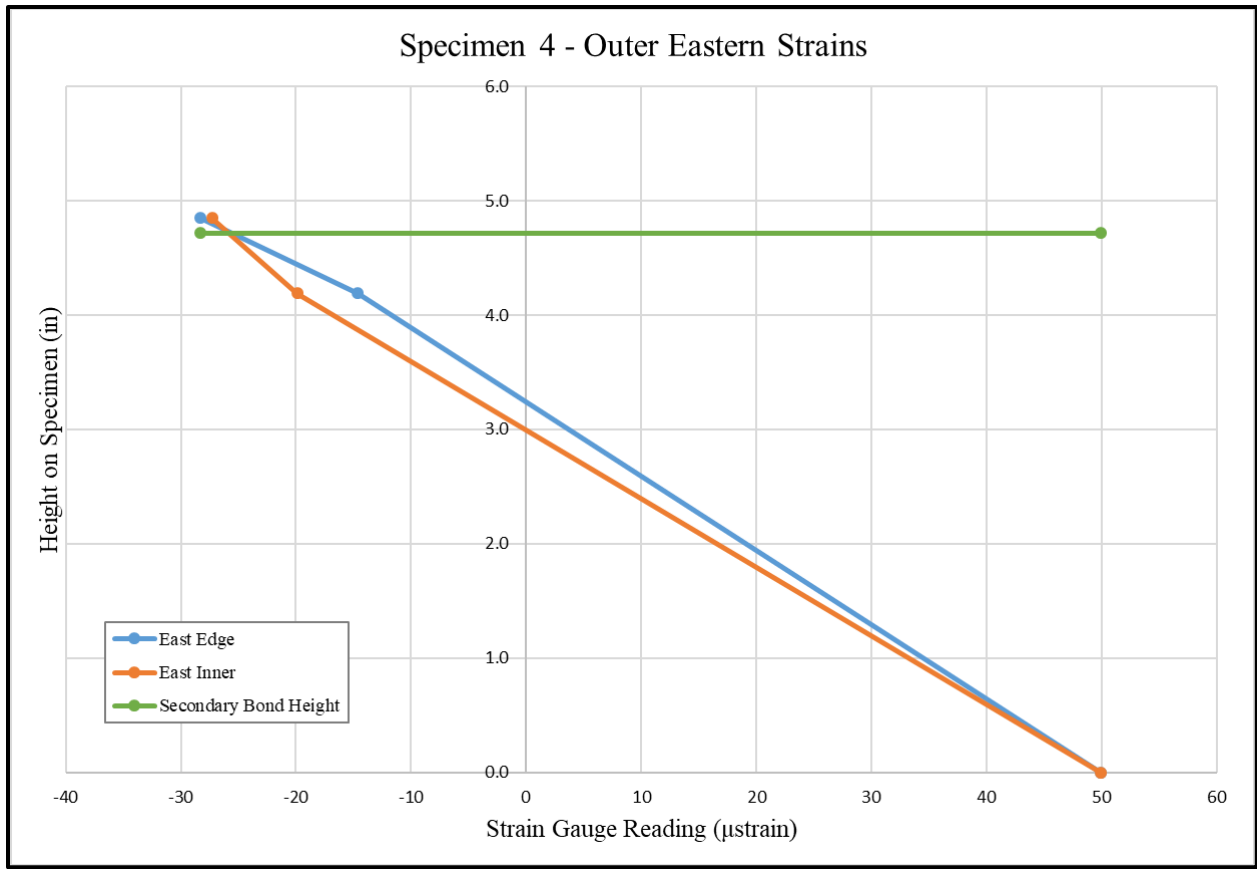


Figure 98: Strain Readings in Region 3-O and Region 4-O

A plot looking at the strain as load is applied is shown for the gauges of Region 1-M in Figure 99.

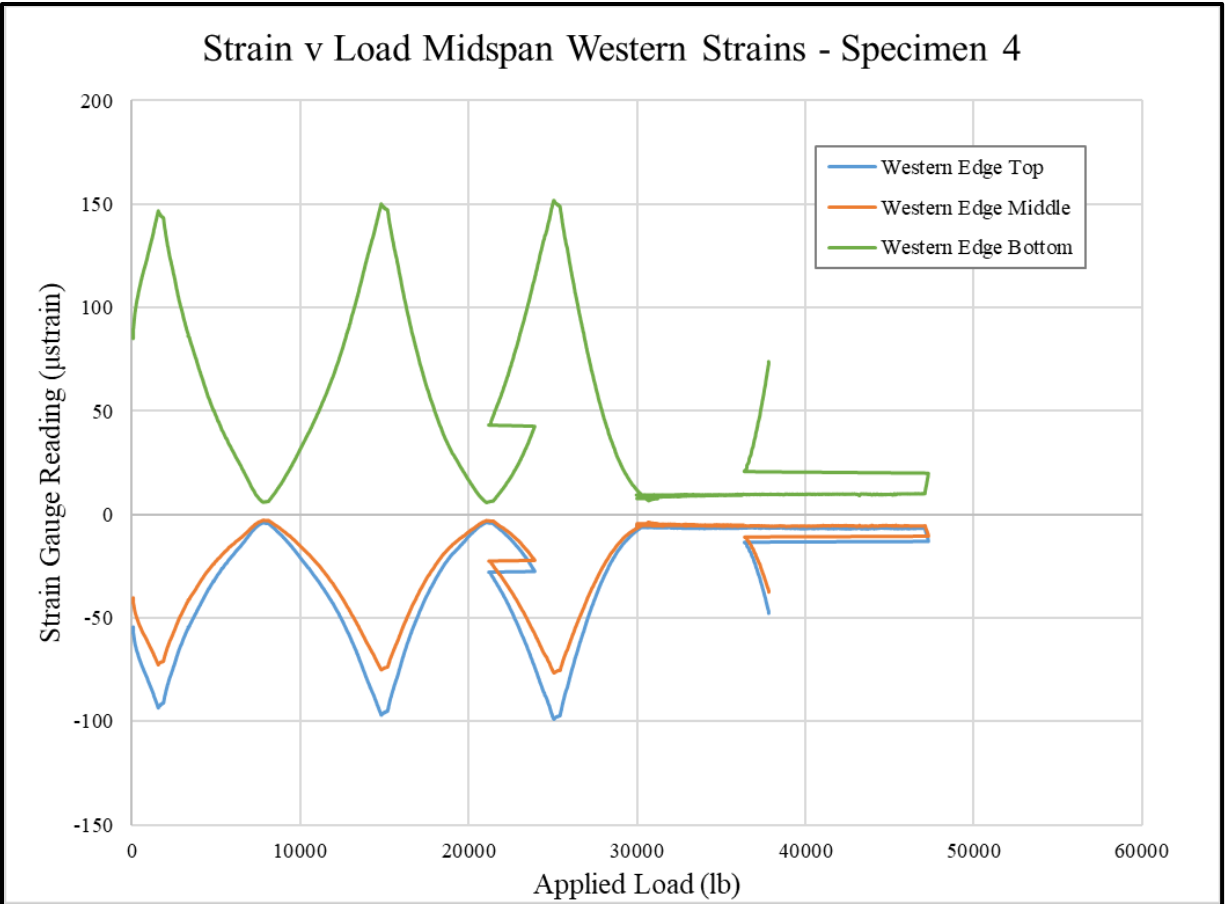


Figure 99: Strain v. Load of Midspan Western Edge – Specimen 4

This oscillating data as the applied load increases points to an issue that occurred during the strain recording process and limits the overall usability of the strain data in the analysis of the closed-corrugation panels.

5.5 Advancement Options

5.5.1 Takeaways from Spliced Closed-Corrugation Manufacturing and Testing

In-house large-format 3D printing and manufacturing equipment were used to create a mold for secondary bonding. There were issues with deformations of the mold once the part was put under repeated heating, pressure and cooling cycles for part forming, which appeared to affect the quality of the secondary bonds. It is possible that as the surface of the 3D printed mold was heated by the cartridge heaters it made the material malleable enough that when the forming

pressure was applied the mold wasn't rigid enough to hold the desired pressure against the part. While the material for this mold was chosen for its strength and thermal properties, it performed below expectations. Some simple changes could be made in either the material choice for improved thermal properties, or in the design of heating areas to increase the insulation between plastic material and heaters.

The objective of this test was to see how multiple corrugations would perform as a single panel, while also attempting to improve on the secondary bonding manufacturing settings. It can be seen that in Panel 3 when the new settings were more closely matched the part produced was much stronger and saw a higher load at which secondary bond failure initiated. However, secondary bonds in the other panels did not perform as well, and indeed were only slightly better than the initial settings used during single closed-corrugation testing.

5.5.2 Improvements of Splicing Methods

A suggestion for the appropriate next steps to advance the stay-in-place formwork is to improve inter-panel connection, which would involve longitudinally connecting multiple panels to form a full-width deck. Options could include mechanical connectors, or deformations that could be secondarily bonded to the panel flanges. Panel manufacturing should also be investigated further to determine if there are better options for forming the closed corrugation cross-section. One option could be using a separate bonding adhesive versus the stamp forming secondary bonding. Secondary bond continues to be the area of weakness that prevents the full shear and moment capacity of the panel from being developed, and this problem will be more acute once concrete is placed and the panel bending and shear strength are increased further. Another option is pultruding all or part or all of the cross-section, which would eliminate secondary bonding and also permit the fabrication of longer span panels.

CHAPTER 6: CONCLUSIONS AND RECOMMENDATION FOR FUTURE WORK

6.1 Hybrid Closed-Corrugation Beam

Work for this thesis began with the closed-corrugation beam, this design was selected on based on previous project work and provided an opportunity to look into the capabilities of secondary bonding thermoplastic plates that had already been consolidated. The goal was this design would make an improvement on the stiffness of previous stay-in-place formwork options developed under the project. The process began with constructing corrugated plates and cover plates similarly to how it had been done previously on the project, where the new developments began was with the secondary bonding of the cover plate onto the corrugation. Using concepts from 3D printing a set of heating and pressure requirements were developed, the substrate plate (corrugation) had the bonding surface heated to 225°F and the bonding plate (cover plate) was heated to 370°F in an IR oven, bonding happened under 100 psi. This process successfully manufactured a secondary bond, achieving the desired closed-corrugation cross section. Construction loading tests and failure tests were performed on bare thermoplastic specimen as well as reinforced concrete-thermoplastic hybrid specimen.

Bare specimen saw failure occur at an average of 20.2 kip, and hybrid specimen saw an average failure of 34.4 kip and an approximate average stiffness of 169 kip/in. Both of these values are improvement on the peak load and stiffness the first corrugation design by Smith [4], which had average failure load of 26.1 kip and an average stiffness of 54.6 kip/in (pulled from Smith thesis Table 16 pg. 94).

The specimen in both cases saw failure and the weak point of the design being the secondary bond, and the quality that was achieved during manufacturing. The bare specimen additionally saw flexural failure in the bottom flange of the corrugation at the supports. But with the secondary bonding being the leading cause of failure, especially in the hybrid sections it was

determined to continue research with the closed-corrugation cross section and pursue ways to improve the secondary bonding process during manufacturing with the hope of further improving the stiffness and shear transfer of the closed-corrugation design.

6.2 Secondary Bonding and Surface Manipulation

The work completed in this stage of the research was performed primarily to look into possible methods of manipulating the surfaces either of already consolidated thermoplastic plates or the surface directly during the consolidation process. This is a delicate process and if not done properly either by not achieving quality bonds or damage layers of the plate could impact the overall strength of the manufactured part. The following sections outline the two individual processes that were evaluated individually.

6.2.1 Secondary Bonding

This work was done by performing a lap shear test of coupons that were secondarily bonded under a range of settings. The purpose was to evaluate this secondary bonding settings in order to determine the best settings to use moving forward. Pin pointing these settings are important for two reasons that will be directly be utilized in future work,

1. Will allow for improvements to be made on the secondary bonding of plates when trying to achieve complex cross sections through stamp forming prototyping.
2. These same settings will need to be achieved in order to connect sections when attempting to form a spliced panel without any fasteners.

Initially secondary bonding was being completed by heating the surface of the substrate plate to 225°F and the bonding plate to 370°F and then applying 100 psi until the part is cooled below the T_g . These settings were chosen because it resembled what is done during 3D printing where the substrate is heated in order to be receptive of new material allowing a bond to form, but the substrate didn't need to be as hot of a temperature as the new material being added. But through

doing the full set of lap shear testing it was determined that the substrate needed to be much warmer, and instead a full second consolidation needed to be performed in terms of the settings achieved. Therefore future secondary bonding needed to have the substrate surface heated to 335°F and the bonding plate heated to 370°F, then have 100 psi applied until the part was below the T_g . These settings should produce a quality secondary bond.

6.2.2 Exterior Surface Manipulation

Well the work performed in this section didn't directly impact the remainder of work in this thesis is was a stepping stone for future work of the project. This partially built off of work and knowledge gained from the previous secondary bonding work. The work was looking to create a ridge surface on a prototype square rebar, giving the thermoplastic rebar a textured surface that would be able to have a connection with concrete. It primarily served as a proof of concept and a way of coming up the method of creating a ridged surface.

The finalized method was,

1. Manufacture a sheet of resin and chopped strand mat (CSM), in this work two resin sheets are sandwiched around the CSM, this sheet will become the textured surface of the rebar.
2. Stack the resin/CSM sheets and the pre-impregnated thermoplastic tape core into the mold with the desired ridge pattern and consolidate as normal.

Doing this a set of prototype thermoplastic rebar was produced with a full set of ridges, this model allowed for some preliminary material property testing and build into a full series of research work to be performed on thermoplastic rebar and its feasibility.

6.3 Spliced Closed-Corrugation Panel Fabrication and Assessment

This portion of work looked to bring together the work up to this point, taking secondary bonding information learned from the lap shear testing and construct an improved closed-

corrugation section and prototype a spliced panel that would more realistically be used in industry. The manufacturing process resembled that of the single closed-corrugation specimen, with the addition of a new 3D printed mold used for secondary bonding that consisted of heating elements and provided the needed support for the secondary bonding pressure to be applied.

These secondary bonding settings used were,

- Substrate Temperature (corrugations): 335°F
- Bonding Plate Temperature (cover plate): 370°F
- Secondary Bonding Pressure: 100 psi

Using these settings panels were able to be constructed that consisted of three corrugation plates secondarily bonded to a single cover plate. Specimen were left as bare thermoplastic specimen for testing and went under the same cyclical construction loading test and then loaded until failure. Panels were able to perform quite well when tested and were able to be compared to the single closed-corrugation bare specimen. Average failure loads and apparent stiffness from construction loading test are provided below. For closed-corrugation panels the apparent stiffness was just from Panel 4 because it was the only panel where true deflection was able to be calculated as compared to the other panels where Instron displacement was used for deflection of the panels.

- Single Closed-Corrugation:
 - Experimental Failure Load: 20.2 kip
 - Experimental Stiffness: 38.1 kip/in
- Closed-Corrugation Panel:
 - Experimental Failure Load: 44.4 kip
 - Experimental Stiffness: 131.8 kip/in

This does point to an improvement being made with the modified secondary bonding technique. However because of the limitations of the 3D printed mold being deformed under repeated heating and pressure cycles, it is truly unknown the maximum ability of the closed-corrugation panel. To obtain the true strength the process would have to be completed using a mold that would be able to withstand the manufacturing cycle.

6.4 Recommendations for Future Work

Future work could be expanded in two different paths. One path would be a continuation of the stay-in-place formwork design and the splicing capabilities to form larger panels. The other is to take a deeper dive into manufacturing of internal reinforcement in the form of CFRTP rebar. Both options will be discussed more in this section.

6.4.1 Advancement of Thermoplastic Stay-In-Place Formwork

Through completing testing of closed-corrugation beams purely on a strength criteria the cross section has shown to perform quite well. This leads to a few potential options for advancements,

1. Pursuing a manufacturing method that can create the closed-corrugation cross section through a pultrusion machine, will provide longer sections and be a good representation of what would be utilized in industry.
2. Looking into the benefit of adding ridges to the cover plate, like described in Section 4.4, and the improvement that gives to transferring shear between the concrete and CFRTP formwork.
3. Develop a feasible splicing method for in-field use, could utilize knowledge gained through this research and secondary bonding or could look into other methods with bolts or other mechanical fasteners.
4. Could further explore making adjustments to the laminate layer design and orientations to increase the formworks performance as a support to concrete decking.

5. Testing larger spans, this would require an advancement in the manufacturing process or design a method to splice sections longitudinally.

There are still many steps that need to be addressed to have the ability to manufacture a fully usable CFRTP stay-in-place formwork for concrete bridge decking applications that can both support the concrete until it is cured as well as provide tensile reinforcement. This research has taken steps towards this goal, and with additional future work this idea could be fully achieved.

6.4.2 Advancement of Internal Reinforcement

This path is something that would be of great benefit for future research to explore. There are many more applications for a thermoplastic rebar, any concrete structure requires some configuration of rebar to provide the necessary support and reinforcing to withstand loading.

Additionally a thermoplastic rebar allows for multiple advantages over traditional steel rebar,

1. Lighter weight, can help with shipping complications and be maneuvered easier onsite.
2. Being manufactured out of thermoplastics could allow for relatively easy onsite shape manipulation with proper heating and pressure applied to the bar.
3. Thermoplastic rebar have a good resistant to weather conditions, there would be little fear of thermoplastic rebar rusting or being damaged and therefore jeopardizing the strength of the structure.

The best first steps to take would be to explore manufacturing prototypes both through a stamp forming system and a pultrusion machine. This would include designing a core the can provide the reinforcing strength necessary to be comparable to steel rebar. But also include designing an outer surface that has enough texture to create a bond between the concrete and rebar. This thesis outlined the method of stamp forming physical ridges onto the bars, but this process could be accomplished many different ways.

Because of the wide range of applications for rebar, turning research to more heavily focused on manufacturing a feasible thermoplastic rebar would be a worthwhile transition that could go a long way in the advancement of concrete construction.

REFERENCES

- [1] "Freiman's Timber Construction," 2010. [Online]. Available: <https://freimans.com/timber-truss-formwork/>. [Accessed 8 February 2022].
- [2] "Tata Steel," 2022. [Online]. Available: <https://www.tatasteeleurope.com/construction/products/flooring/composite-floor-deck/comflor-51plus>. [Accessed 8 February 2022].
- [3] C. Seigars, "Feasibility of Hybrid Thermoplastic Composite-Concrete Load Bearing," University of Maine, Orono, Maine, 2018.
- [4] B. Smith, "Development of a Hybrid Thermoplastic Composite and Concrete Deck System," University of Maine, Orono, Maine, 2019.
- [5] Tangram Technology LTD, "Tangram Technology Periodic Table of Thermoplastics," August 2021. [Online]. Available: <https://tangram.co.uk/technical-information/plastics-topics/>. [Accessed 19 April 2022].
- [6] PolyOne, *Polystrand PETg IE 5842 Technical Data Sheet*, 2017.
- [7] M. W. Hyer, *Stress Analysis of Fiber-Reinforced Composite Materials*, Lancaster: DEStech Publications, Inc., 2009.
- [8] American Institute of Steel Construction, *Steel Construction Manual*, AISC, 2011.
- [9] K. Vanclooster, "Forming of Multilayered Fabric Reinforced Thermoplastic Composites," Katholieke Universiteit Leuven, Leuven, 2009.
- [10] S. Haanappel, "Forming of UD Fibre Reinforced Thermoplastics - A Critical Evaluation of Intra-Ply Shear," University of Twente, Enschede, 2013.
- [11] American Association of State Highway and Transportation Officials, *AASHTO LFRD Bridge Design Specifications*, Washington, D.C.: AASHTO, 2012.
- [12] ASTM International, *ASTM 5868-01: Lap Shear Adhesion for Fiber Reinforced Plastic (FRP) Bonding*, West Conshohocken: ASTM International, 2014.
- [13] D. Guzzi, "Shear Connectors for Hybrid Composite FRP-Concrete Bridge Girders," University of Maine, Orono, Maine, 2019.
- [14] W. Davids, D. Guzzi and A. Schanck, "Development and Experimental Assessment of Friction-Type Shear Connectors for FRP Bridge Girders with Composite Concrete Decks," University of Maine, Orono, Maine, 2022.
- [15] ASTM International, *D7290-06(2017) Standard Practice for Evaluating Material Property Characteristic Values for Polymeric Composites for Civil Engineering Structural Applications*, West Conshohocken: ASTM International, 2017.
- [16] VectorPly Corporation, *E-M 0015*, Phenix City: VectorPly Corporation, 2011.

APPENDIX A:

PolyOne

TECHNICAL DATA SHEET

Polystrand™ IE 5842

Continuous glass-reinforced thermoplastic PETG composite

Key Characteristics

Product description

Polystrand™ IE 5842 is a PETG-based thermoplastic unidirectional tape, which balances strength and toughness with excellent adhesive properties. Applications include structural components and reinforcement for wood, metal, and polymer molded or thermoformed components. The use of PETG resin imparts excellent mechanical properties, and good chemical and solvent resistance. Unidirectional tapes are available in rolls 25" wide. Custom slit widths and finished stampings are also available. Multi-ply laminates are available with plies arranged in 0 or 90 degree orientations, with maximum roll width of 125".

Technical Properties of Unidirectional Tape

Typical Properties

PROPERTY	TEST METHOD	UNITS	DATA
Glass Content	ASTM D3647	wt%	58
Areal weight	–	oz/yd ² (g/m ²)	12.0 (405)
Thickness	–	In (mm)	0.012 (0.3)
Flexural modulus	ASTM D790	MPsi (GPa)	4.18 (29)
Flexural Strength	ASTM D790	Ksi (MPa)	87 (602)
Longitudinal Tensile Modulus	ASTM D3039	MPsi (GPa)	4.14 (28.5)
Longitudinal Tensile Strength	ASTM D3039	Ksi (MPa)	82.8 (571)
In-Plane Poisson's Ratio	ASTM D3039	–	0.27
Transverse Tensile Modulus	ASTM D3039	MPsi (GPa)	0.52 (3.6)
Transverse Tensile Strength	ASTM D3039	Ksi (MPa)	1.5 (10.0)
Longitudinal Compressive Modulus	ASTM D6641	MPsi (GPa)	0.71 (4.9)
Longitudinal Compressive Strength	ASTM D6641	Ksi (MPa)	29.5 (197)
Transverse Compressive Modulus	ASTM D6641	MPsi (GPa)	0.26 (1.8)
Transverse Compressive Strength	ASTM D6641	Ksi (MPa)	5.5 (38)
In-Plane Shear Modulus	ASTM D7078	MPsi (GPa)	0.21 (1.5)
In-Plane Shear Strength	ASTM D7078	ksi (MPa)	3.0 (21)
Transverse Shear Modulus	ASTM D7078	MPsi (GPa)	0.17 (1.2)
Transverse Shear Strength	ASTM D7078	ksi (MPa)	6.7 (46)

Notes

NOTE: The data listed herein reflect typical sheet properties. They are the latest available at the time of publication and are reliable to the best knowledge of PolyOne. The properties are listed solely to give general guidance and are not to be construed as a warranty or representation for of this information or the safety and suitability of our products, either alone or in combination with other products. Users are advised to make their own test to determine the safety and suitability of each such product or product combination for their own purposes. We sell the products without

APPENDIX B:

CLT MatLab Script:

```
% -----  
%                               INPUTS  
% -----  
% User Name: Jackman  
% Date: 2/12/22  
% Design Name: Corrugation TFlange/Web and Cover Plate  
% Material Type: PETg with E-Glass Fibers  
  
% ----- MATERIAL PROPERTIES -----  
% Material Properties:  
E1 = 28.2*(10^9); %Long. Elastic Modulus (Pa)  
E2 = 4.43*(10^9); %Trans. Elastic Modulus (Pa)  
G12 = 1.48*(10^9); %In-Plane Shear Modulus (Pa)  
v12 = 0.353; %In-Plane Poisson's Ratio ()  
t = 0.2; %Single Layer Thickness (mm)  
  
% Failure Strengths:  
F1t = 623*(10^6); %Long. Tensile Strength (Pa)  
F1c = -310*(10^6); %Long. Compression Strength (Pa)  
F2t = 14.5*(10^6); %Trans. Tensile Strength (Pa)  
F2c = -65*(10^6); %Trans. Compression Strength (Pa)  
F6 = 28.8*(10^6); %In-Plane Shear Strength (Pa)  
  
% ----- LAYUP SCHEDULE -----  
layup = [0,0,45,-45,0,0,45,-45,0,0,45,-45,0,0,45,-45,0,0,-  
45,45,0,0,-45,45,0,0,-45,45,0,0,-45,45,0,0]; %Full Layup Schedule  
(degrees)  
diff_layers = [0,45,-45]; %Different Orientations (degrees)  
  
% ----- STRESS RESULTANTS -----  
%NOTE: for simplification loading only in two directions (X and Y)  
%Note: positive for tension, negative for compression  
Nx = 1; %Normal Force in X-Dir. (N/m)  
Ny = 0; %Normal Force in Y-Dir. (N/m)  
Nxy = 0; %Shear Force Parallel to Edges (N/m)  
Mx = 0; %Bending Moment in X-Dir. (N*m/m)  
My = 0; %Bending Moment in Y-Dir (N*m/m)  
Mxy = 0; %Twisting Moment on Edges (N*m/m)  
NR = [Nx;Ny;Nxy];  
MR = [Mx;My;Mxy];  
  
% ----- KNOWN MID-SURFACE STRAINS/CURVATURES -----  
%NOTE: for simplification loading only in two directions (X and Y)  
%NOTE: if stress resultants are known below should be zeros  
epsx_o = 0; %(strain)  
epsy_o = 0; %(strain)  
tauxy_o = 0; %(radian)  
kx_o = 0; %(m^-1)  
ky_o = 0; %(m^-1)  
kxy_o = 0; %(radian/m)  
m_strain = [epsx_o;epsy_o;tauxy_o];  
m_curve = [kx_o;ky_o;kxy_o];
```

```

% -----
%                               CLT MATRIX BUILDING
% -----
% ----- COMPLIANCE MATRIX -----
Sred = Build_S_red(E1,E2,v12,G12); %(Pa)
for i = 1:length(layup)
    Sbar{i} = Build_Sbar_red(Sred,layup(i)); %(Pa)
end

% ----- STIFFNESS MATRIX -----
v21 = (v12*E2)/E1;
Qred = Build_Q_red(E1,v12,E2,v21,G12); %(Pa)
for i = 1:length(layup)
    Qbar{i} = Build_Qbar_red(Qred,layup(i)); %(Pa)
end

% ----- TRANSFORMATION MATRIX -----
for i = 1:length(layup)
    T{i} = Build_T(layup(i)); %()
end
for i = 1:length(layup)
    Tinv{i} = Build_T_inv(layup(i)); %()
end

% ----- LAYER HEIGHT VECTOR -----
n = length(layup); %Number of Layers (#)
z = Build_z(n,t); %Layer Height for Top/Bottom per Layer (m)

% ----- ABD-MATRIX / abd-MATRIX -----
[A,B,D] = ABD_Matrix_Adj(Qred,Qbar,n,z); %A (N/m), B (N), D (N*m)
[a,b,bt,d] = ABDInv_Matrix_Adj(A,B,D); %a (m/N), b (1/N), d (1/N*m)

% -----
%                               LAMINATE EFFECTIVE PROPERTIES
% -----
H = (t*n)/1000; %total height of laminate (m)
Exbar = ((A(1,1)*A(2,2))-(A(1,2)^2))/(A(2,2)*H); %Eff. Extensional Modulus X-
Dir. (Pa)
Eybar = ((A(1,1)*A(2,2))-(A(1,2)^2))/(A(1,1)*H); %Eff. Extensional Modulus Y-
Dir. (Pa)
Gxybar = A(3,3)/H; %Eff. Shear Modulus (Pa)
vxybar = A(1,2)/A(2,2); %Eff. Poisson's Ratio ()
vyxbar = A(1,2)/A(1,1); %Eff. Poisson's Ratio ()

% -----
%                               STRESS AND STRAIN PER LAYER
% -----
% ----- MIDSURFACE STRAINS -----
if abs(sum(NR)+sum(MR))>0
    mid_strain = (a*NR)+(b*MR); %Midsurface Strain [strain;strain;radian]
    mid_curves = (bt*NR)+(d*MR); %Midsurface Curvature [m^-1;m^-1;radian/m]
else
    mid_strain = m_strain;
    mid_curves = m_curve;
end

% ----- STRESS/STRAIN per LAYER XY-DIRECTION -----

```

```

strain_xy = Kirchhoff_Hypo(mid_strain,mid_curves,z); %XY-Strain Top/Bottom of
Every Layer [strain;strain;radian]

count = 0; %loop counter
for i = 1:n
    stress_xy{i+count} = Qbar{i}*strain_xy{i+count}; %[Pa;Pa;Pa]
    stress_xy{i+count+1} = Qbar{i}*strain_xy{i+count+1}; %[Pa;Pa;Pa]
    count = count+1;
end

% ----- STRESS/STRAIN per LAYER 12-DIRECTION -----
count = 0; %loop counter
for i = 1:n
    strain_12{i+count} = T{i}*strain_xy{i+count}; %[strain;strain;radian]
    strain_12{i+count}(3,1) = 2*strain_12{i+count}(3,1);
    strain_12{i+count+1} = T{i}*strain_xy{i+count+1}; %[strain;strain;radian]
    strain_12{i+count+1}(3,1) = 2*strain_12{i+count+1}(3,1);
    count = count+1;
end

count = 0; %loop counter
for i = 1:n
    stress_12{i+count} = T{i}*stress_xy{i+count}; %[Pa;Pa;Pa]
    stress_12{i+count+1} = T{i}*stress_xy{i+count+1}; %[Pa;Pa;Pa]
    count = count+1;
end

% -----
%          LAYER BY LAYER TABLE - ORIENTATATION/HEIGHT/STRESSES/STRAINS
% -----
[Layer_Table_12,Layer_Table_XY] =
Layer_SS_Table(n,z,layup,stress_12,strain_12,stress_xy,strain_xy);

% -----
%          LAYER BY LAYER - STRESS and STRAIN PLOTTING
% -----
Stress_Strain_Plots(z,Layer_Table_12,Layer_Table_XY);

```

Additional Functions:

```
function [S_red] = Build_S_red(E1,E2,v12,G12)
%Build_S_red, takes the material properties of the composite and then
%builds the Reduced Compliance Matrix (S_red).
% Author: Jackman Mickiewicz      Date: 11/2021
% INPUTS:
%   E1 - Elastic Modulus in the 1-Direction (Pa)
%   E2 - Elastic Modulus in the 2-Direction (Pa)
%   v12 - Poisson's Ratio in the 12-Direction
%   G12 - Shear Modulus in the 12-Direction (Pa)
% OUTPUTS:
%           [S11 S12 S16]
%   S_red = [S12 S22 S26] (1/Pa)
%           [S16 S26 S66]
% -----

S11 = 1/E1;
S12 = (-1*v12)/E1;
S16 = 0;
S22 = 1/E2;
S26 = 0;
S66 = 1/G12;

S_red = [S11,S12,S16;S12,S22,S26;S16,S26,S66];

end

function [S_bar] = Build_Sbar_red(S,theta)
%Build_Sbar_red, takes the inputs of the Reduced Compliance Matrix(S_red)
%and the orientation of layer at question. And outputs the Transformed or
%Off-Axis Compliance Matrix(Sbar_red).
% Author: Jackman Mickiewicz      Date: 11/2021
% INPUTS:
%           [S11 S12 S16]
%   S_red = [S12 S22 S26] (1/Pa)
%           [S16 S26 S66]
%
%   theta = theta_n (degree)
%
% OUTPUTS:
%           [Sbar11 Sbar12 Sbar16]
%   Sbar_red = [Sbar12 Sbar22 Sbar26] (1/Pa)
%           [Sbar16 Sbar26 Sbar66]
% -----

m = cosd(theta);
n = sind(theta);

Sb_11 = (S(1,1)*(m^4))+((2*S(1,2))+S(3,3))*(m^2)*(n^2)+(S(2,2)*(n^4));
Sb_12 = ((S(1,1)+S(2,2)-S(3,3))*(n^2)*(m^2))+S(1,2)*((n^4)+(m^4));
Sb_16 = (((2*S(1,1))-(2*S(1,2))-S(3,3))*n*(m^3))+((2*S(1,2))-
(2*S(2,2))+S(3,3))*(n^3)*m);
Sb_22 = (S(1,1)*(n^4))+((2*S(1,2))+S(3,3))*(n^2)*(m^2)+(S(2,2)*(m^4));
```

```

Sb_26 = ((2*S(1,1))-(2*S(1,2))-S(3,3))*(n^3)*m)+((2*S(1,2))-
(2*S(2,2))+S(3,3))*n*(m^3));
Sb_66 = (2*((2*S(1,1))+2*S(2,2))-(4*S(1,2))-
S(3,3))*(n^2)*(m^2))+S(3,3)*((n^4)+(m^4));

S_bar = [Sb_11,Sb_12,Sb_16;Sb_12,Sb_22,Sb_26;Sb_16,Sb_26,Sb_66];

```

end

```

function [Q_red] = Build_Q_red(E1,v12,E2,v21,G12)
%Build_Q_red, takes the material properties of the composite and then
%builds the Reduced Stiffness Matrix (Q_red).
% Author: Jackman Mickiewicz      Date: 11/2021
% INPUTS:
%   E1 - Elastic Modulus in the 1-Direction (Pa)
%   E2 - Elastic Modulus in the 2-Direction (Pa)
%   v12 - Poisson's Ratio in the 12-Direction
%   v21 - Poisson's Ratio in the 21-Direction
%   G12 - Shear Modulus in the 12-Direction (Pa)
% OUTPUTS:
%           [Q11 Q12 Q16]
%   Q_red = [Q12 Q22 Q26] (Pa)
%           [Q16 Q26 Q66]
% -----

```

```

Q11 = E1/(1-(v12*v21));
Q12 = (v12*E2)/(1-(v12*v21));
Q16 = 0;
Q22 = E2/(1-(v12*v21));
Q26 = 0;
Q66 = G12;

```

```

Q_red = [Q11,Q12,Q16;Q12,Q22,Q26;Q16,Q26,Q66];

```

end

```

function [Q_bar] = Build_Qbar_red(Q,theta)
%Build_Qbar_red, takes the inputs of the Reduced Stiffness Matrix(Q_red)
%and the orientation of layer at question. And outputs the Transformed or
%Off-Axis Stiffness Matrix(Qbar_red).
% Author: Jackman Mickiewicz      Date: 10/27/2020
% INPUTS:
%           [Q11 Q12 Q16]
%   Q_red = [Q12 Q22 Q26] (Pa)
%           [Q16 Q26 Q66]
%
%   theta = theta_n (degree)
%
% OUTPUTS:
%           [Qbar11 Qbar12 Qbar16]
%   Qbar_red = [Qbar12 Qbar22 Qbar26] (Pa)
%           [Qbar16 Qbar26 Qbar66]
% -----

```

```

m = cosd(theta);
n = sind(theta);

Qb_11 = (Q(1,1)*m^4) + (2*(Q(1,2)+2*Q(3,3))*m^2*n^2) + (Q(2,2)*n^4);
Qb_12 = ((Q(1,1)+Q(2,2)-4*Q(3,3))*n^2*m^2) + (Q(1,2)*(n^4+m^4));
Qb_16 = ((Q(1,1)-Q(1,2)-2*Q(3,3))*n*m^3) + ((Q(1,2)-Q(2,2)+2*Q(3,3))*n^3*m);
Qb_22 = (Q(1,1)*n^4) + (2*(Q(1,2)+2*Q(3,3))*n^2*m^2) + (Q(2,2)*m^4);
Qb_26 = ((Q(1,1)-Q(1,2)-2*Q(3,3))*n^3*m) + ((Q(1,2)-Q(2,2)+2*Q(3,3))*n*m^3);
Qb_66 = ((Q(1,1)+Q(2,2)-2*Q(1,2)-2*Q(3,3))*n^2*m^2) + (Q(3,3)*(n^4+m^4));

Q_bar = [Qb_11,Qb_12,Qb_16;Qb_12,Qb_22,Qb_26;Qb_16,Qb_26,Qb_66];

```

```
end
```

```

function [T] = Build_T(theta)
%Build_T, takes an input of the orientation of fibers of the layer
%and outputs the Transformation Matrix (T) for both Strains and Stresses
%from the XY-Plane to the 12-Plane.
% Author: Jackman Mickiewicz      Date: 11/2021
% INPUTS:
%   theta = theta_n (degree)
% OUTPUTS:
%   [m^2  n^2  2mn]
%   T = [n^2  m^2  -2mn]
%       [-mn  mn  (m^2-n^2)]
% -----

```

```

m = cosd(theta);
n = sind(theta);

T = [(m^2), (n^2), (2*m*n);
      (n^2), (m^2), (-2*m*n);
      (-1*m*n), (m*n), ((m^2)-(n^2))];
end

```

```

function [T_inv] = Build_T_inv(theta)
%Build_T_inv, takes an input of the orientation of fibers of the layer
%and outputs the Inverse Transformation Matrix (T^-1) for both Strains and
%Stresses from the 12-Plane to the XY-Plane.
% Author: Jackman Mickiewicz      Date: 11/2021
% INPUTS:
%   theta = theta_n (degree)
% OUTPUTS:
%   [m^2  n^2  -2mn]
%   T_inv = [n^2  m^2  2mn]
%           [mn  -mn  (m^2-n^2)]
% -----

```

```

m = cosd(theta);
n = sind(theta);

T_inv = [(m^2), (n^2), (-2*m*n);

```

```

        (n^2), (m^2), (2*m*n);
        (m*n), (-1*m*n), ((m^2)-(n^2))];
end

function [z] = Build_z(n,t)
%Build_z, takes inputs of number of layers and thickness of each layer and
%builds a vector of z-positions. Each layer has two z-positions, for the
%top and bottom of the layer, ex. Layer #1 corresponds to z0 (bottom
%coordinate) and z1 (top coordinate), Layer #2 corresponds to z1 (bottom
%coordinate) and z2 (top coordinate), etc. Layer #1 is the bottom most
%layer and Layer N is the top most layer.
% Author: Jackman Mickiewicz      Date: 10/29/2020
% INPUT:
%   n - number of layers in the composite
%   t - thickness of each individual layer (mm)
% OUTPUTS:
%   z - vector of top/bottom coordinates of layers [z0,z1,...,zN-1,zN] (m)
% -----

num_coor = 2*n; %number top/bottom coordinates of each layer

t_con = t*(1/1000); %thickness of a single layer converted from mm to m

H = n*t_con; %total thickness of laminate (m)

%loop builds the z-vector for laminate
for i = 1:num_coor
    if i == 1
        z(i) = -H/2;
    elseif rem(i,2) == 0
        z(i) = z(i-1) + t_con;
    else
        z(i) = z(i-1);
    end
end

if rem(n,2)==0
    z(n)=0;
    z(n+1)=0;
end

end

function [A,B,D] = ABD_Matrix_Adj(Q_red,Qbar_red,n,z)
%ABD_Matrix, takes inputs of the Reduced Stiffness Matrix of the material,
%the Adjusted Stiffness Matrix by layer, the number of layers, thickness of
%the layer, and the position of the top and bottom of each layer. The
%function builds the A-Matrix/B-Matrix/D-Matrix separately, calculating
%using layer stiffness matrix and layer coordinates.
% Author: Jackman Mickiewicz      Date: 11/2021
% INPUT:
%           [Q11 Q12 Q16]
%   Q_red = [Q12 Q22 Q26] (Pa)

```



```

%           [Q16 Q26 Q66]
%
%           [Qbar11 Qbar12 Qbar16]
%   Qbar_red = [Qbar12 Qbar22 Qbar26] (Pa)
%               [Qbar16 Qbar26 Qbar66]
%
%   n - number of layers in the composite
%   z - vector of top/bottom coordinates of layers [z0,z1,...,zN-1,zN] (m)
%
% OUTPUTS:
%           [A11 A12 A16]
%   A = [A12 A22 A26] (N/m)
%         [A16 A26 A66]
%
%           [B11 B12 B16]
%   B = [B12 B22 B26] (N)
%         [B16 B26 B66]
%
%           [D11 D12 D16]
%   D = [D12 D22 D26] (N*m)
%         [D16 D26 D66]
%
% -----
A=zeros(length(Q_red(1,:)),length(Q_red(:,1)));
B=zeros(length(Q_red(1,:)),length(Q_red(:,1)));
D=zeros(length(Q_red(1,:)),length(Q_red(:,1)));
count=1;
for l=1:n
    for i=1:length(Q_red(1,:))
        for j=1:length(Q_red(:,1))
            A(i,j)=A(i,j)+round((Qbar_red{l}(i,j)*(z(count+1)-z(count))),3);
            B(i,j)=B(i,j)+round(((1/2)*(Qbar_red{l}(i,j)*((z(count+1)^2)-
(z(count)^2))))),3);
            D(i,j)=D(i,j)+round(((1/3)*(Qbar_red{l}(i,j)*((z(count+1)^3)-
(z(count)^3))))),3);
        end
    end
    count=(2*l)+1;
end

% following loop zeros out any small rounding errors
for i=1:length(Q_red(1,:))
    for j=1:length(Q_red(:,1))
        if abs(A(i,j))<=0.005
            A(i,j)=0;
        end
        if abs(B(i,j))<=0.005
            B(i,j)=0;
        end
        if abs(D(i,j))<=0.005
            D(i,j)=0;
        end
    end
end
end
end

```

```

function [a,b,bt,d] = ABDInv_Matrix_Adj(A,B,D)
%ABDInv_Matrix, takes the following inputs and computes the inverse of the
ABD
%Matrix to use to go from force and moment resultants to midsurface strain
%and curvatures.
% Author: Jackman Mickiewicz      Date: 11/17/2020
% INPUTS:
%      [A11 A12 A16]
%      A = [A12 A22 A26] (N/m)
%           [A16 A26 A66]
%
%      [B11 B12 B16]
%      B = [B12 B22 B26] (N)
%           [B16 B26 B66]
%
%      [D11 D12 D16]
%      D = [D12 D22 D26] (N*m)
%           [D16 D26 D66]
%
% OUTPUTS:
%      [a11 a12 a16]
%      a = [a12 a22 a26] (m/N)
%           [a16 a26 a66]
%
%      [b11 b12 b16]
%      b = [b21 b22 b26] (1/N)
%           [b61 b62 b66]
%
%      [b11 b21 b61]
%      bt = [b12 b22 b62] (1/N)
%            [b16 b26 b66]
%
%      [d11 d12 d16]
%      d = [d12 d22 d26] (1/N*m)
%           [d16 d26 d66]
%
% -----
abd = [A,B;B,D]^-1;

if abs(sum(sum(A)))>0
    a =
    [abd(1,1),abd(1,2),abd(1,3);abd(2,1),abd(2,2),abd(2,3);abd(3,1),abd(3,2),abd(
3,3)];
else
    a = zeros(length(A(1,:)),length(A(:,1)));
end

if abs(sum(sum(B)))>0
    b =
    [abd(1,4),abd(1,5),abd(1,6);abd(2,4),abd(2,5),abd(2,6);abd(3,4),abd(3,5),abd(
3,6)];
else
    b = zeros(length(B(1,:)),length(B(:,1)));
end

```

```

if abs(sum(sum(D)))>0
    bt =
[abd(4,1),abd(4,2),abd(4,3);abd(5,1),abd(5,2),abd(5,3);abd(6,1),abd(6,2),abd(
6,3)];
else
    bt = zeros(length(B(1,:)),length(B(:,1)));
end

if abs(sum(sum(D)))>0
    d =
[abd(4,4),abd(4,5),abd(4,6);abd(5,4),abd(5,5),abd(5,6);abd(6,4),abd(6,5),abd(
6,6)];
else
    d = zeros(length(D(1,:)),length(D(:,1)));
end

end

function [strain_xy] = Kirchhoff_Hypo(mid_strain,mid_curves,z)
%Kirchhoff_Hypo, takes the below inputs and uses the Kirchhoff Hypothesis
%to calculate the strain in the XY-Plane at the top and bottom of each
%layer.
% Author: Jackman Mickiewicz      Date: 10/29/2020
% INPUTS:
%   mid_strain = midsurface strains [eps_xo,eps_yo,gam_xyo] (microstrain)
%   mid_curves = midsurface curvatures [k_xo,k_yo,k_xyo] (m^-1)
%   z = vector of top/bottom coordinates of layers [z0,z1,...,zN-1,zN] (m)
% OUTPUTS:
%   strain_xy = strain in XY-Plane for each value of z
%               [ epsilon_x ] (strain)
%               = [ epsilon_y ] (strain)
%               [  gamma_xy ] (radians)
%
%               ***NOTE: can turn strain_xy into microstrain by
%                       multiplying strain_xy by (10^6)
% -----

%number of positions of interest, top and bottom of each layer
num_coor = length(z);

%convert the mid-surface strains from microstrain to strain
%mid_strain_adj = mid_strain*(10^-6);
mid_strain_adj = mid_strain;

%loop uses the Kirchhoff Hypothesis to calculate the strain in the XY-Plane
%of each coordinate location using mid-surfaces strain and curvatures
for i = 1:num_coor
    strain_xy{i} = mid_strain_adj + (z(i)*mid_curves);
end

end

```

```

function [Layer_Table_12,Layer_Table_XY] =
Layer_SS_Table(n,z,layup,stress_12,strain_12,stress_xy,strain_xy)
% Layer_SS_Table, this takes the inputs listed below and then builds two
% tables to summarize layer orientation, stresses and strains. One table
% is for the 12-Direction and the other is for the XY-Direction.
% Author: Jackman Mickiewicz      Date: 10/17/2021
% INPUT:
%   n - number of layers in the composite
%   z = vector of top/bottom coordinates of layers [z0,z1,...,zN-1,zN] (m)
%   stress_xy = stress in XY-Plane for top and bottom of each layer
%               [ sigma_x ] (Pa)
%               = [ sigma_y ] (Pa)
%               [ tau_xy ] (Pa)
%   strain_xy = strain in XY-Plane for each value of z
%               [ epsilon_x ] (strain)
%               = [ epsilon_y ] (strain)
%               [ gamma_xy ] (radians)
%   stress_12 = stress in 12-Plane for top and bottom of each layer
%               [ sigma_1 ] (Pa)
%               = [ sigma_2 ] (Pa)
%               [ tau_12 ] (Pa)
%   strain_12 = strain in 12-Plane for each value of z
%               [ epsilon_1 ] (strain)
%               = [ epsilon_2 ] (strain)
%               [ gamma_12 ] (radians)
% OUTPUTS:
%   Layer_Table_12 = table of layer number/orientation/stress_12/strain_12
%                   = [layer number, layer orientation, z, sig1, sig2, tau12, eps1, eps2, gam12]
%   Layer_Table_XY = table of layer number/orientation/stress_XY/strain_XY
%                   = [layer number, layer orientation, z, sigX, sigY, tauXY, epsX, epsY, gamXY]
% -----

layup_adj = zeros(n*2,1);
layer_num = zeros(n*2,1);

count = 1;
for i = 1:length(layup)
    layer_num(count)=i;
    layer_num(count+1)=i;
    layup_adj(count)=layup(i);
    layup_adj(count+1)=layup(i);
    count=(2*i)+1;
end

for i = 1:(n*2)
    sig1(i)=stress_12{i}(1); % (Pa)
    sig2(i)=stress_12{i}(2); % (Pa)
    tau12(i)=stress_12{i}(3); % (Pa)
    sigx(i)=stress_xy{i}(1); % (Pa)
    sigy(i)=stress_xy{i}(2); % (Pa)
    tauxy(i)=stress_xy{i}(3); % (Pa)
    eps1(i)=strain_12{i}(1); % (strain)
    eps2(i)=strain_12{i}(2); % (strain)
    gam12(i)=strain_12{i}(3); % (radian)
    epsx(i)=strain_xy{i}(1); % (strain)
    epsy(i)=strain_xy{i}(2); % (strain)
    gamxy(i)=strain_xy{i}(3); % (radian)

```

```
end
```

```
Layer_Table_12 =  
[layer_num,layup_adj,z',sig1',sig2',tau12',eps1',eps2',gam12'];  
Layer_Table_XY =  
[layer_num,layup_adj,z',sigx',sigy',tauxy',epsx',epsy',gamxy'];
```

```
end
```

```
function [] = Stress_Strain_Plots(z,Layer_Table_12,Layer_Table_XY)  
% Stress_Strain_Plots, takes the below described inputs and builds plots  
% for the stress and strain through the laminate. Plots have six windows  
% allowing all stress and strain plots to be displayed for each direction  
% at the same time.  
% Author: Jackman Mickiewicz      Date: 10/17/2021  
% INPUT:  
% z - vector of top/bottom coordinates of layers [z0,z1,...,zN-1,zN] (m)  
% Layer_Table_12 = table of layer number/orientation/stress_12/strain_12  
% = [layer number,layer orientation,z,sig1,sig2,tau12,eps1,eps2,gam12]  
% Layer_Table_XY = table of layer number/orientation/stress_XY/strain_XY  
% = [layer number,layer orientation,z,sigX,sigY,tauXY,epsX,epsY,gamXY]  
% OUTPUTS:  
% Stress and Strain Plots  
% -----  
  
% ----- STRESS PLOT - 12-DIRECTION -----  
figure(1)  
subplot(3,2,1)  
plot(Layer_Table_12(:,4),(z*-1000))  
title('Stress 12-Direction')  
xlabel('\sigma_1 (Pa)')  
ylabel('z (mm)')  
subplot(3,2,3)  
plot(Layer_Table_12(:,5),(z*-1000))  
xlabel('\sigma_2 (Pa)')  
ylabel('z (mm)')  
subplot(3,2,5)  
plot(Layer_Table_12(:,6),(z*-1000))  
xlabel('\tau_1_2 (Pa)')  
ylabel('z (mm)')  
  
% ----- STRAIN PLOT - 12-DIRECTION -----  
subplot(3,2,2)  
plot(Layer_Table_12(:,7)*(10^6),(z*-1000))  
title('Strain 12-Direction')  
xlabel('\epsilon_1 (\mu mm/mm)')  
ylabel('z (mm)')  
subplot(3,2,4)  
plot(Layer_Table_12(:,8)*(10^6),(z*-1000))  
xlabel('\epsilon_2 (\mu mm/mm)')  
ylabel('z (mm)')  
subplot(3,2,6)  
plot(Layer_Table_12(:,9)*(10^6),(z*-1000))  
xlabel('\gamma_1_2 (\mu radian)')  
ylabel('z (mm)')
```

```

% ----- STRESS PLOT - XY-DIRECTION -----
figure(2)
subplot(3,2,1)
plot(Layer_Table_XY(:,4),(z*-1000))
title('Stress XY-Direction')
xlabel('\sigma_X (Pa)')
ylabel('z (mm)')
subplot(3,2,3)
plot(Layer_Table_XY(:,5),(z*-1000))
xlabel('\sigma_Y (Pa)')
ylabel('z (mm)')
subplot(3,2,5)
plot(Layer_Table_XY(:,6),(z*-1000))
xlabel('\tau_X_Y (Pa)')
ylabel('z (mm)')

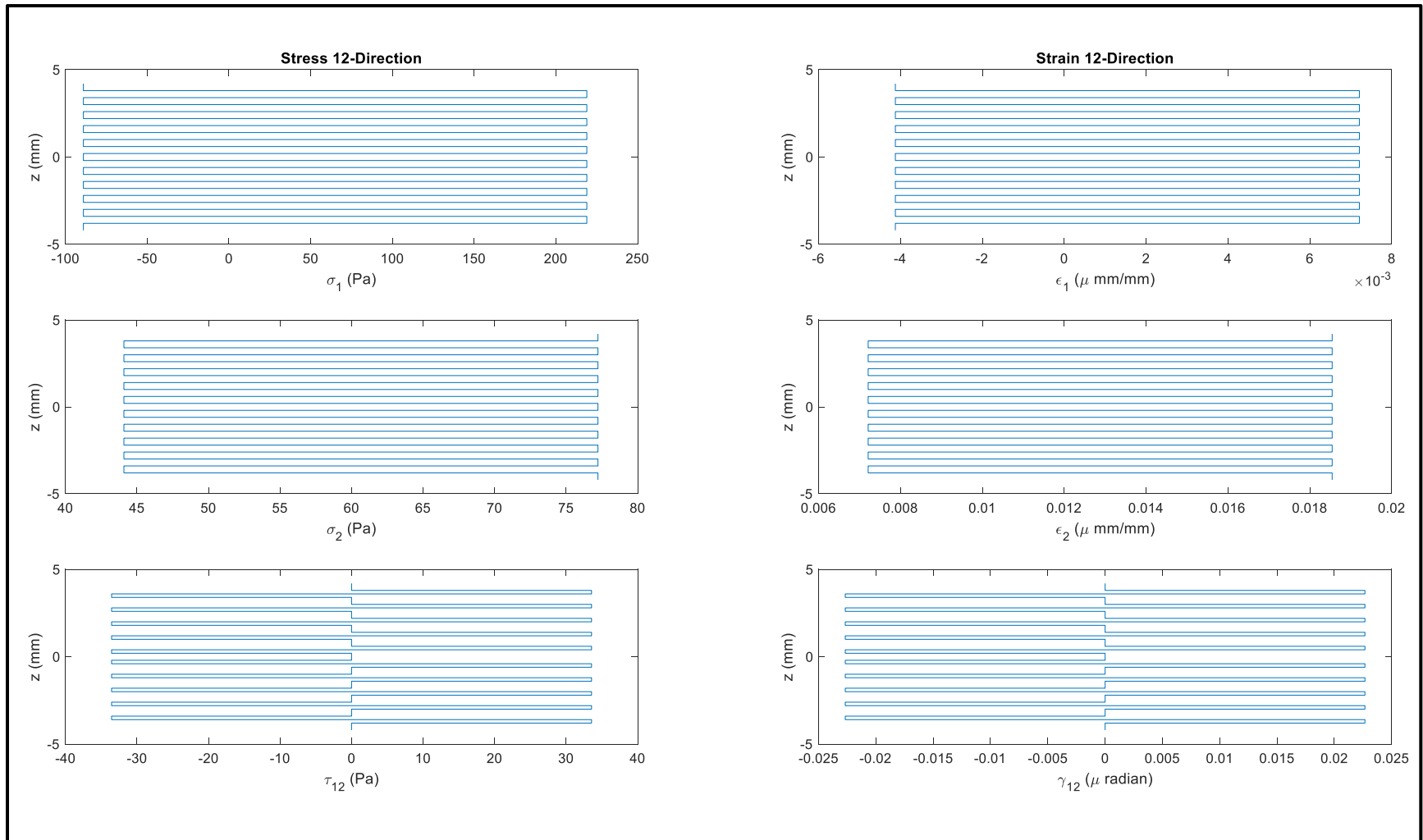
% ----- STRAIN PLOT - XY-DIRECTION -----
subplot(3,2,2)
plot(Layer_Table_XY(:,7)*(10^6),(z*-1000))
title('Strain XY-Direction')
xlabel('\epsilon_X (\mu mm/mm)')
ylabel('z (mm)')
subplot(3,2,4)
plot(Layer_Table_XY(:,8)*(10^6),(z*-1000))
xlabel('\epsilon_Y (\mu mm/mm)')
ylabel('z (mm)')
subplot(3,2,6)
plot(Layer_Table_XY(:,9)*(10^6),(z*-1000))
xlabel('\gamma_X_Y (\mu radian)')
ylabel('z (mm)')

end

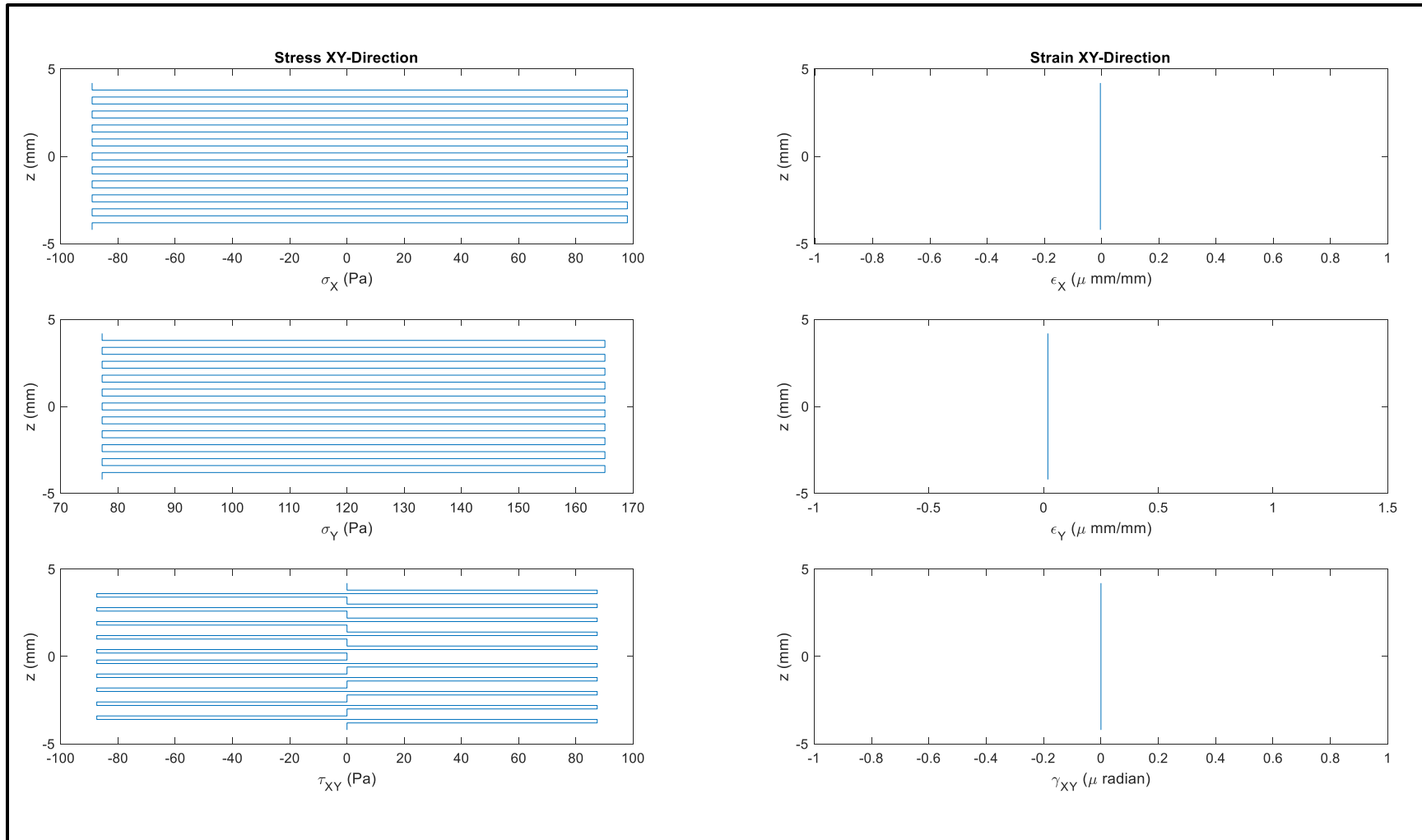
```

APPENDIX C:

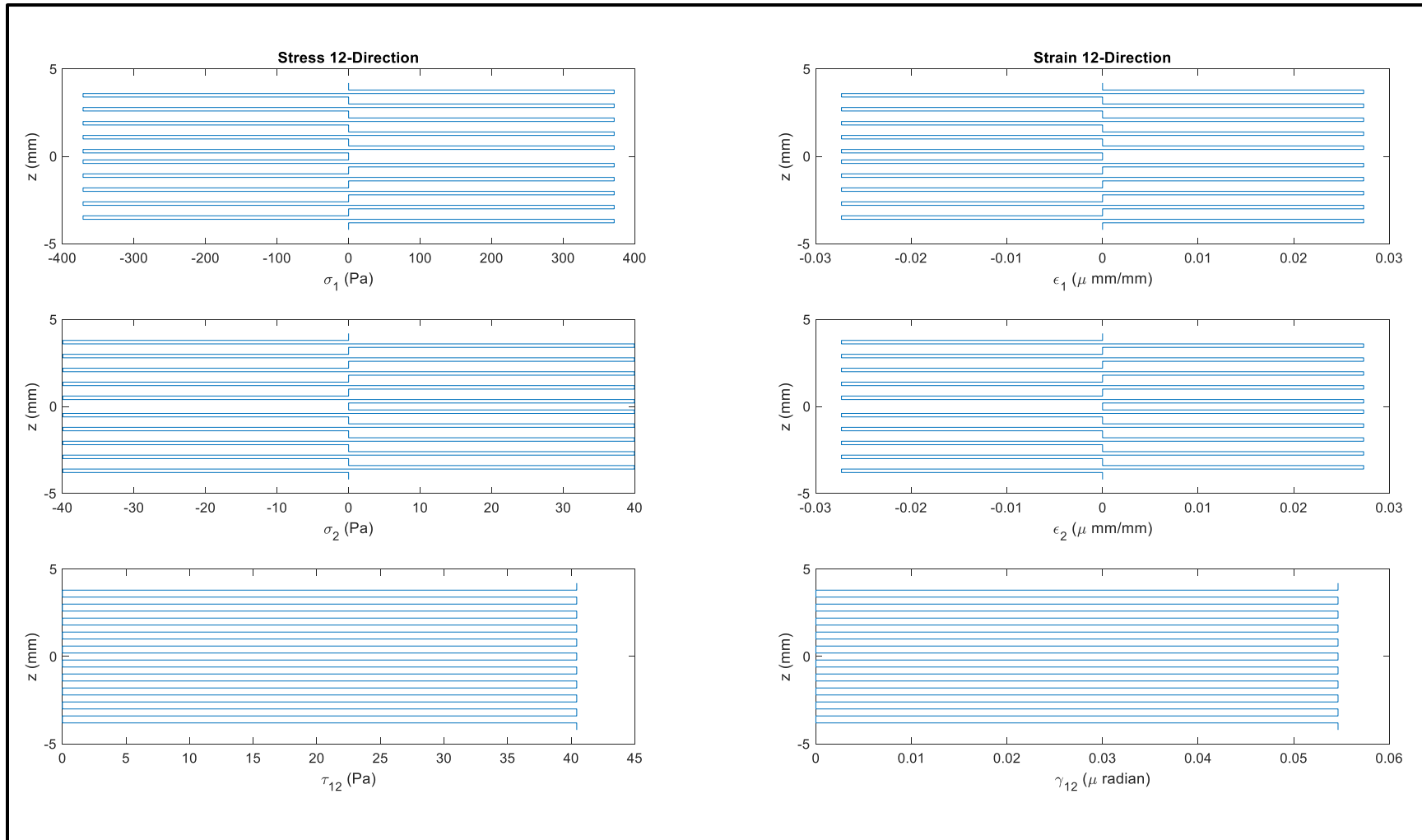
Stress-Strain Through-Thickness of Layup #2 in 12-Direction (+1 N_y Applied):



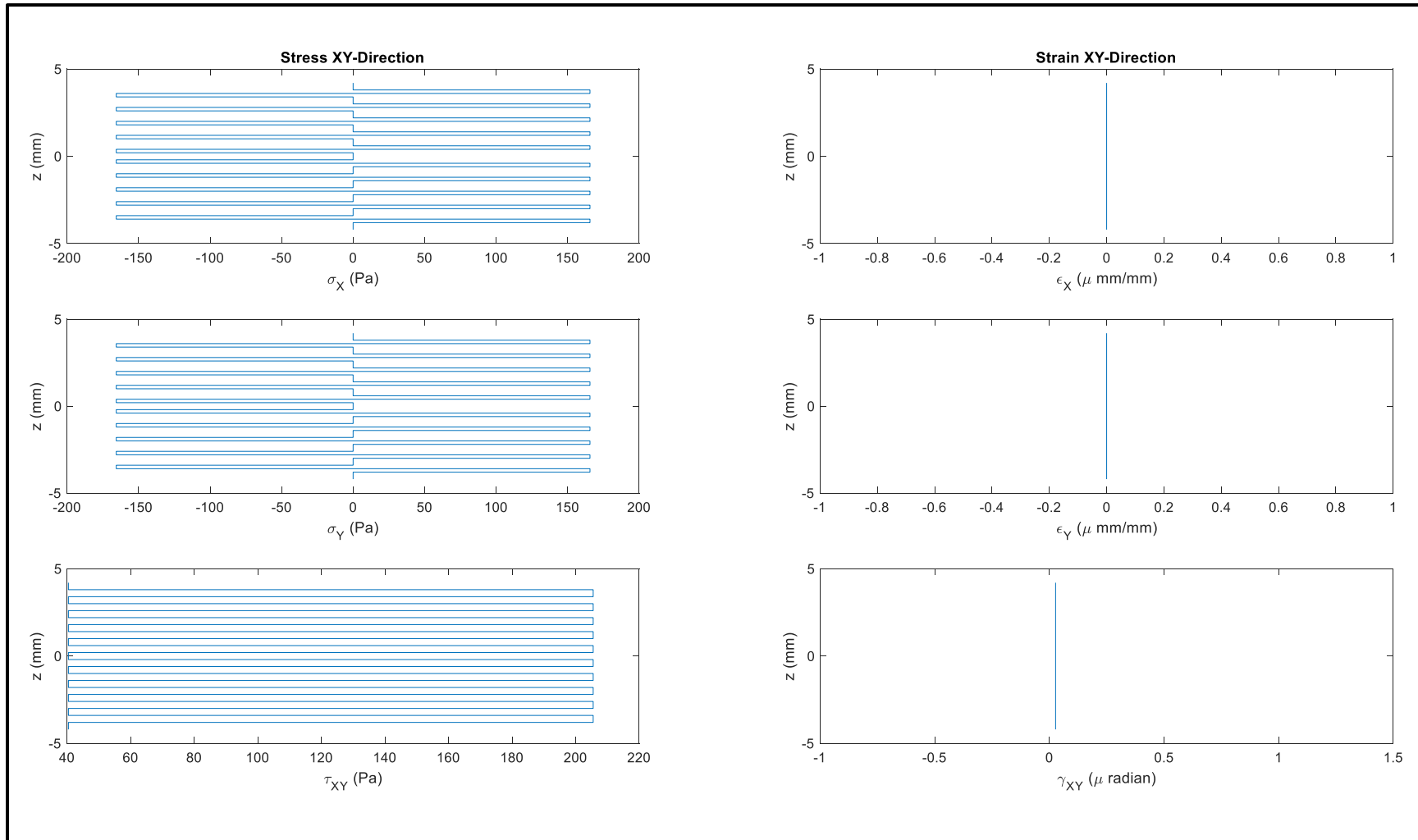
Stress-Strain Through-Thickness of Layup #2 in XY-Direction (+1 N_y Applied):



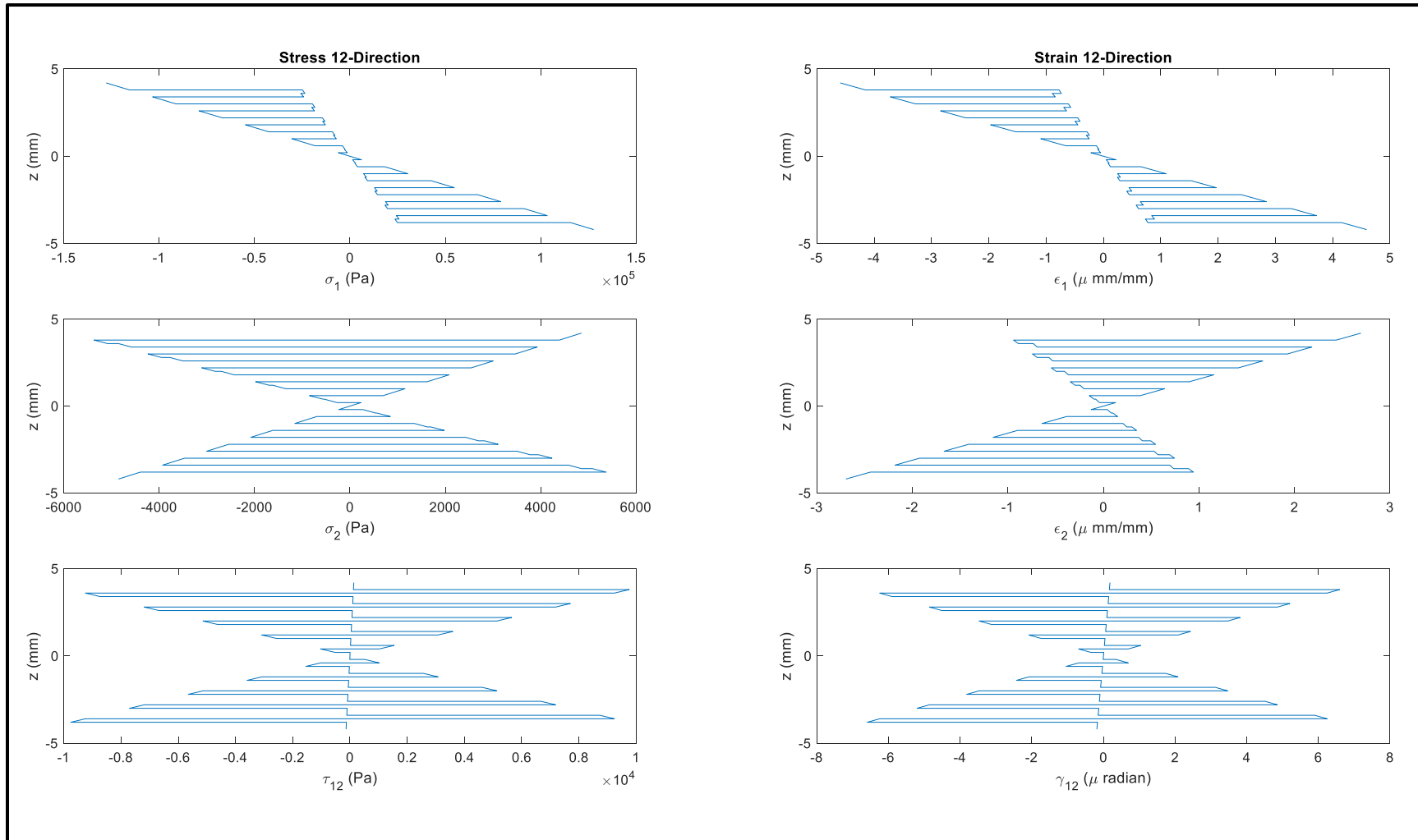
Stress-Strain Through-Thickness of Layup #2 in 12-Direction (+1 N_{xy} Applied):



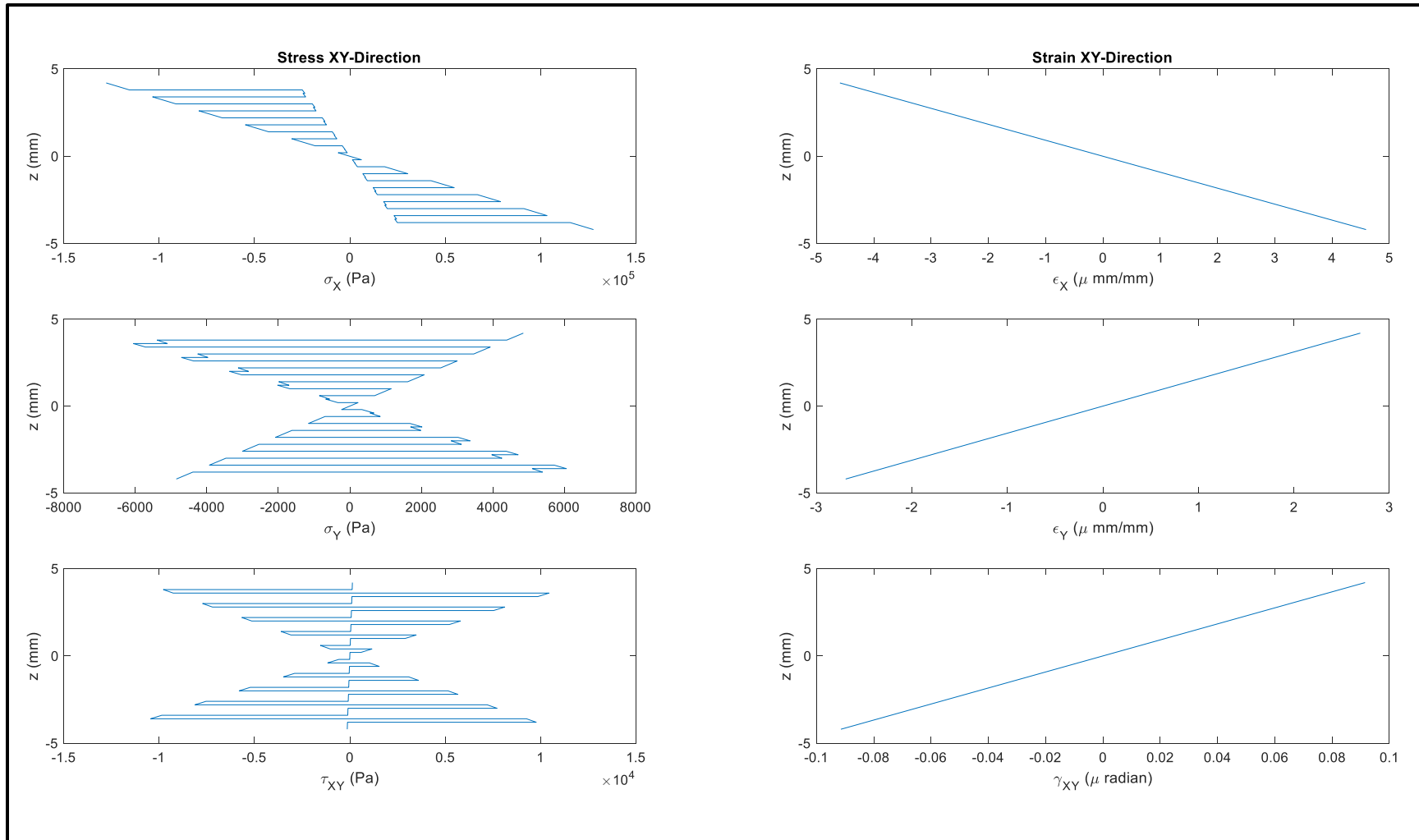
Stress-Strain Through-Thickness of Layup #2 in XY-Direction (+1 N_{xy} Applied):



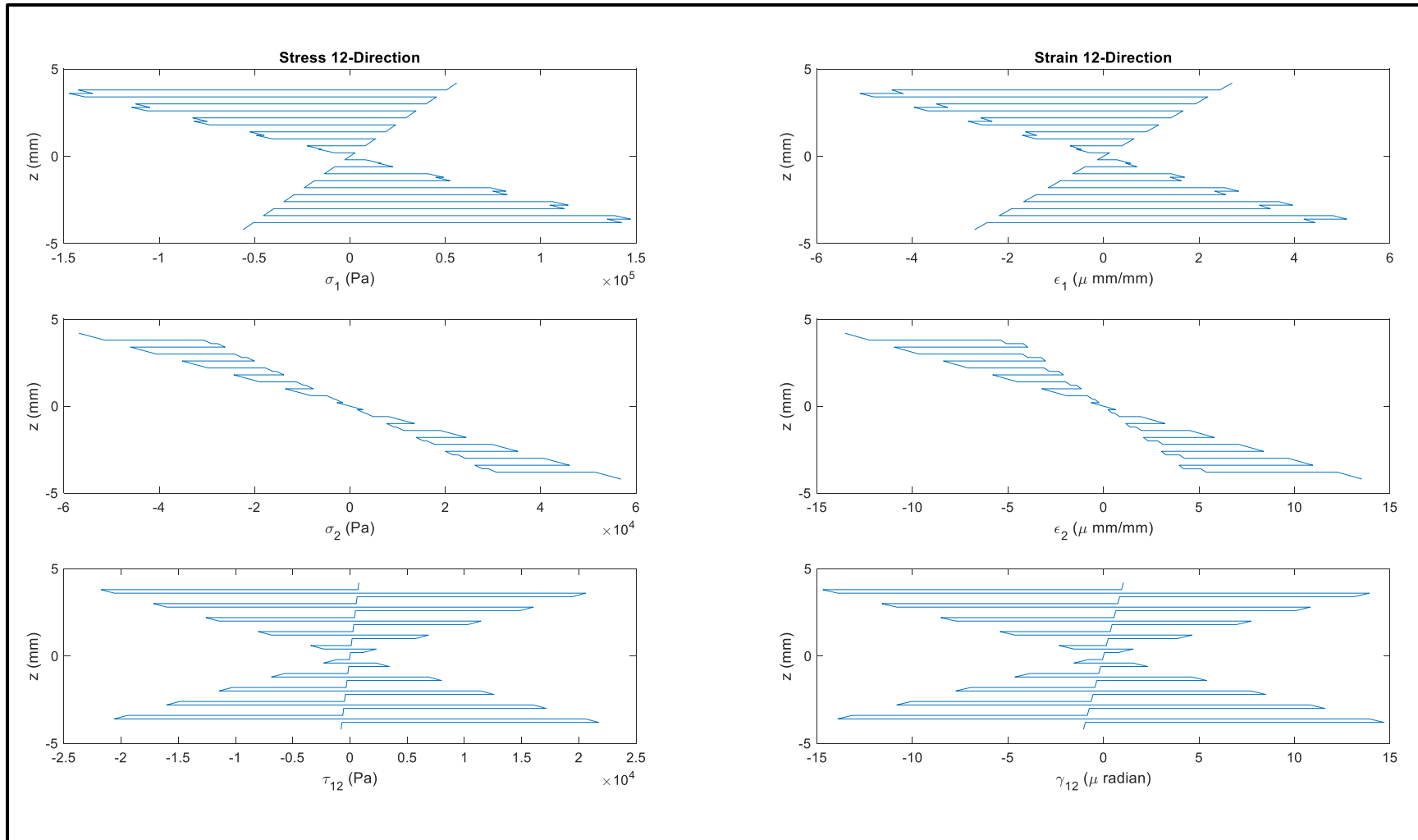
Stress-Strain Through-Thickness of Layup #2 in 12-Direction (+1 M_x Applied):



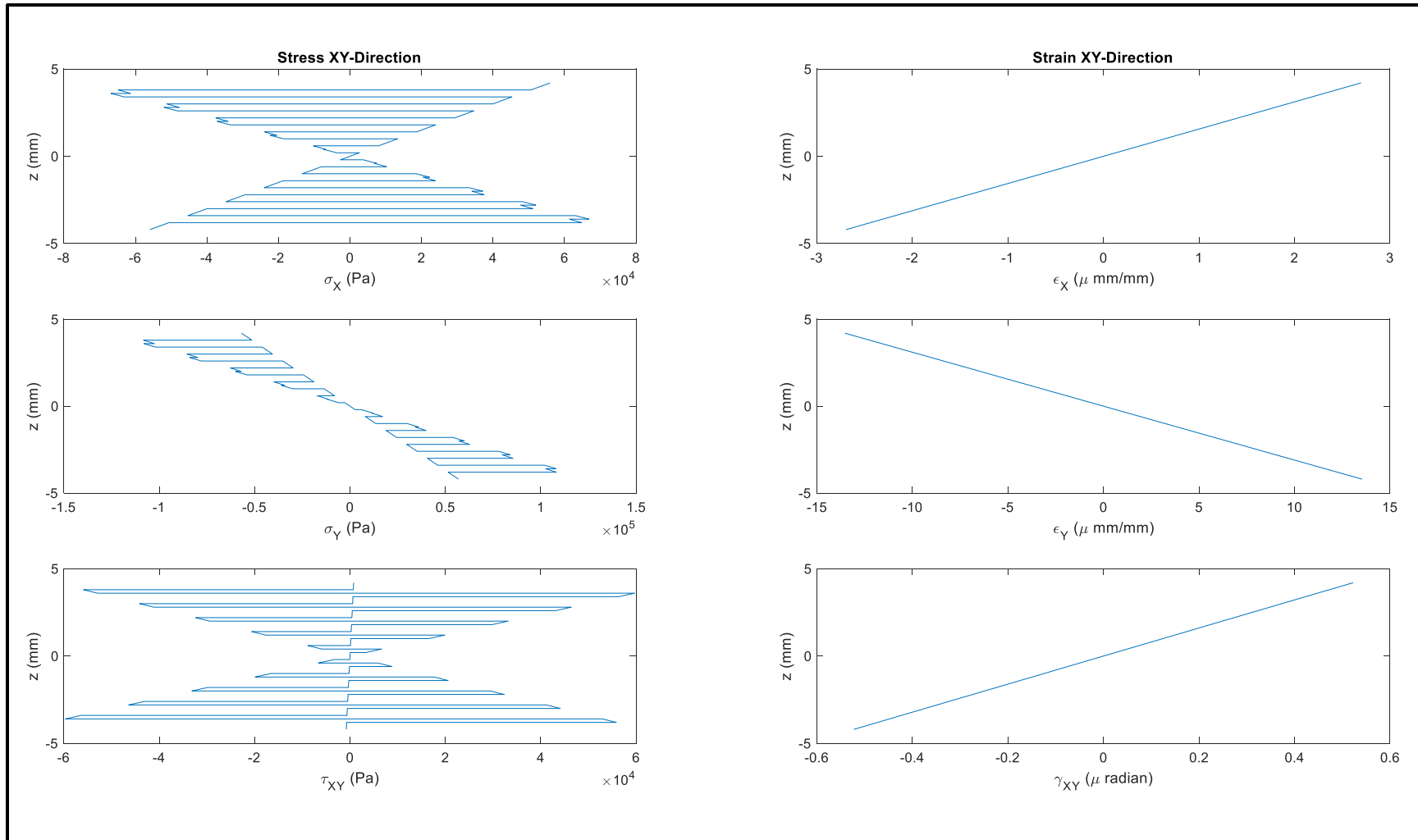
Stress-Strain Through-Thickness of Layup #2 in XY-Direction (+1 M_x Applied):



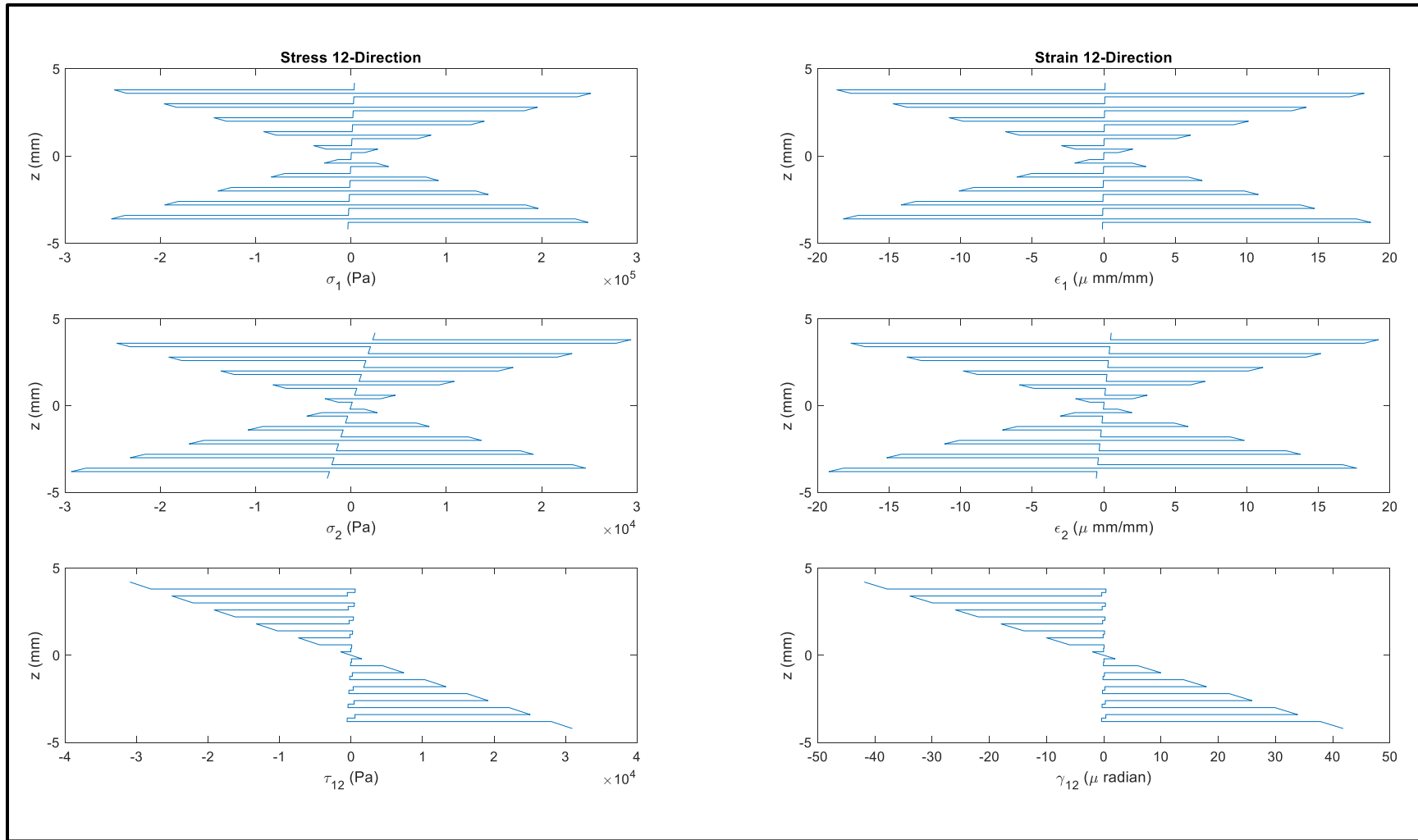
Stress-Strain Through-Thickness of Layup #2 in 12-Direction (+1 My Applied):



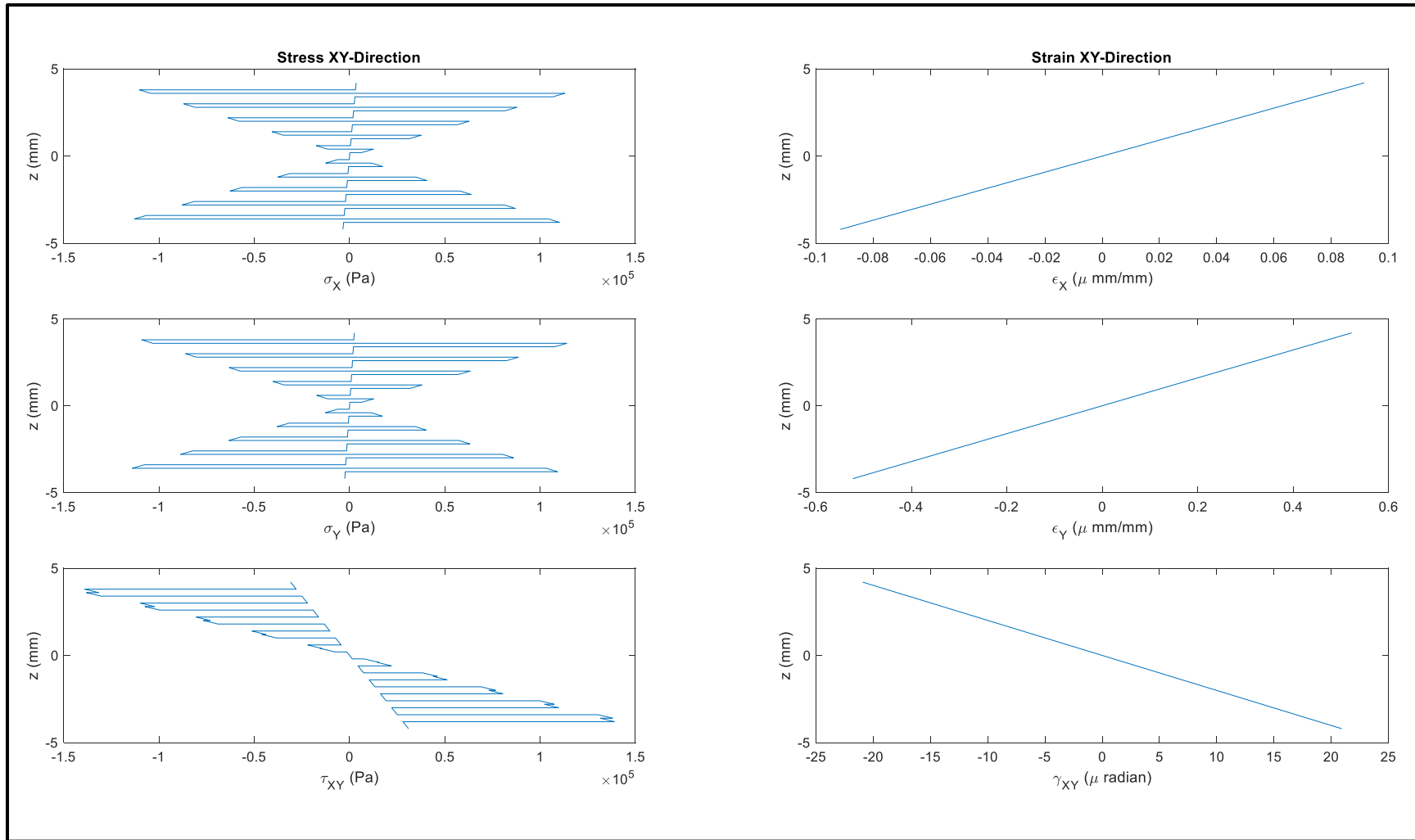
Stress-Strain Through-Thickness of Layup #2 in XY-Direction (+1 My Applied):



Stress-Strain Through-Thickness of Layup #2 in 12-Direction (+1 M_{xy} Applied):

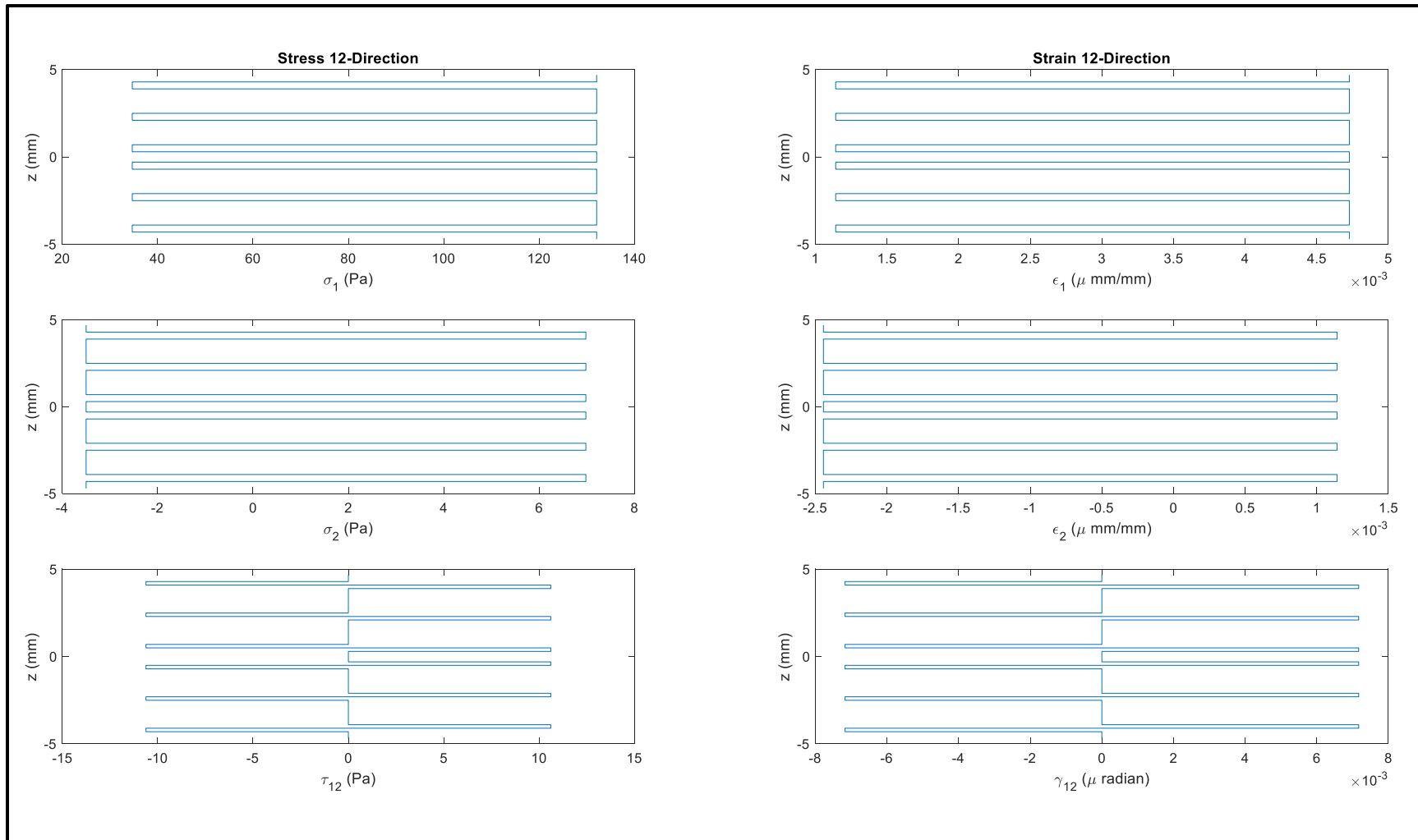


Stress-Strain Through-Thickness of Layup #2 in XY-Direction (+1 M_{xy} Applied):

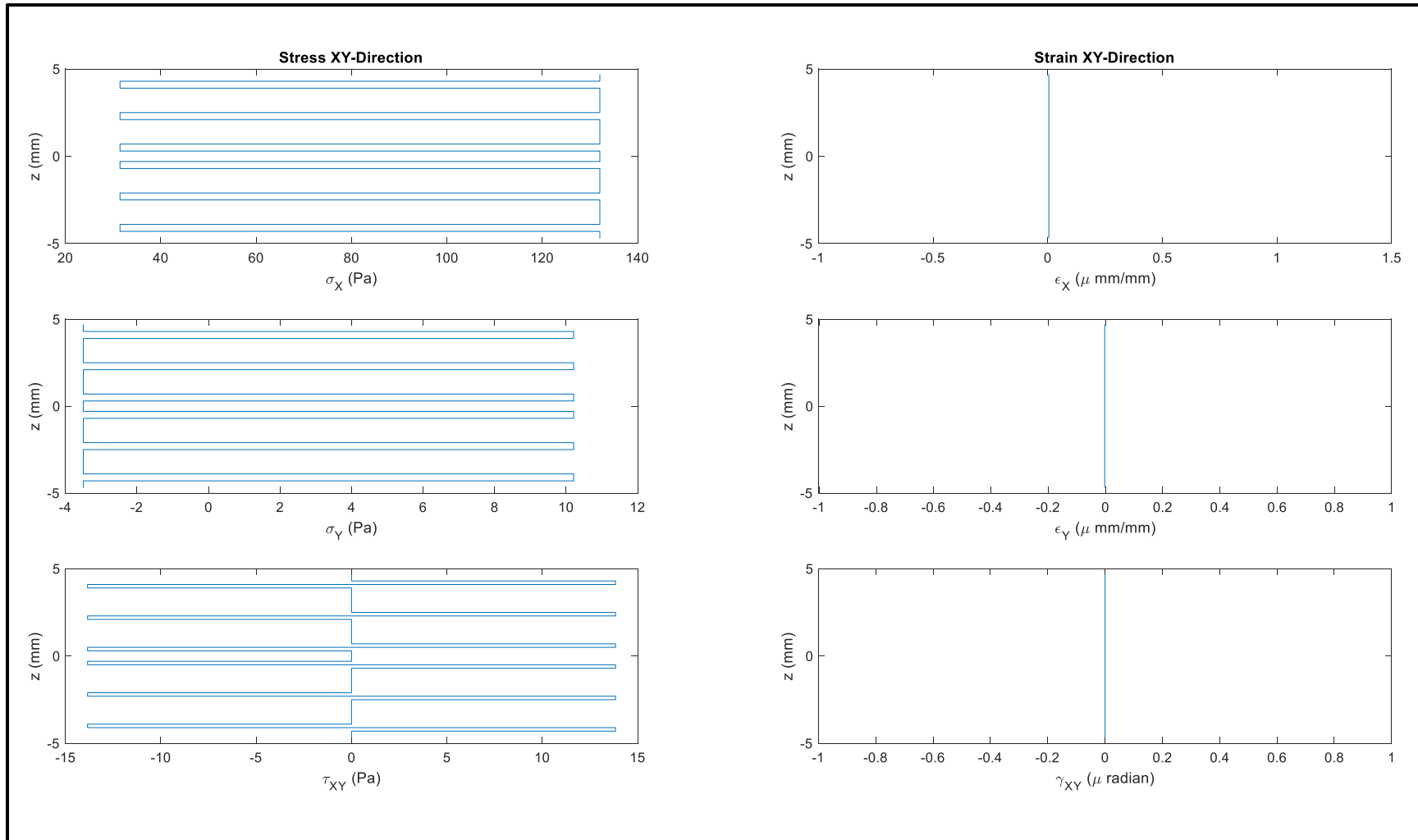


APPENDIX D:

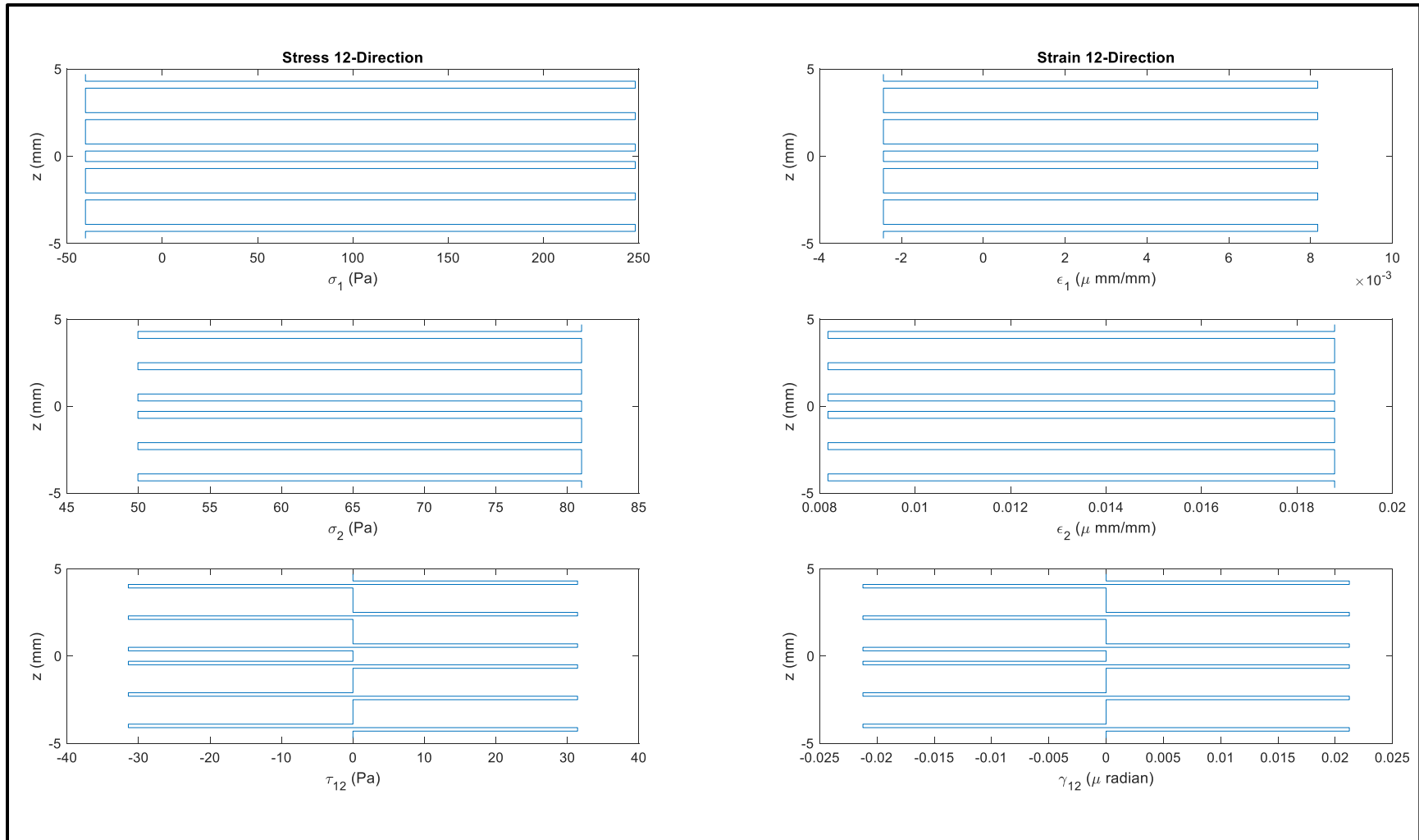
Stress-Strain Through-Thickness of Layup #1 in 12-Direction (+1 Nx Applied):



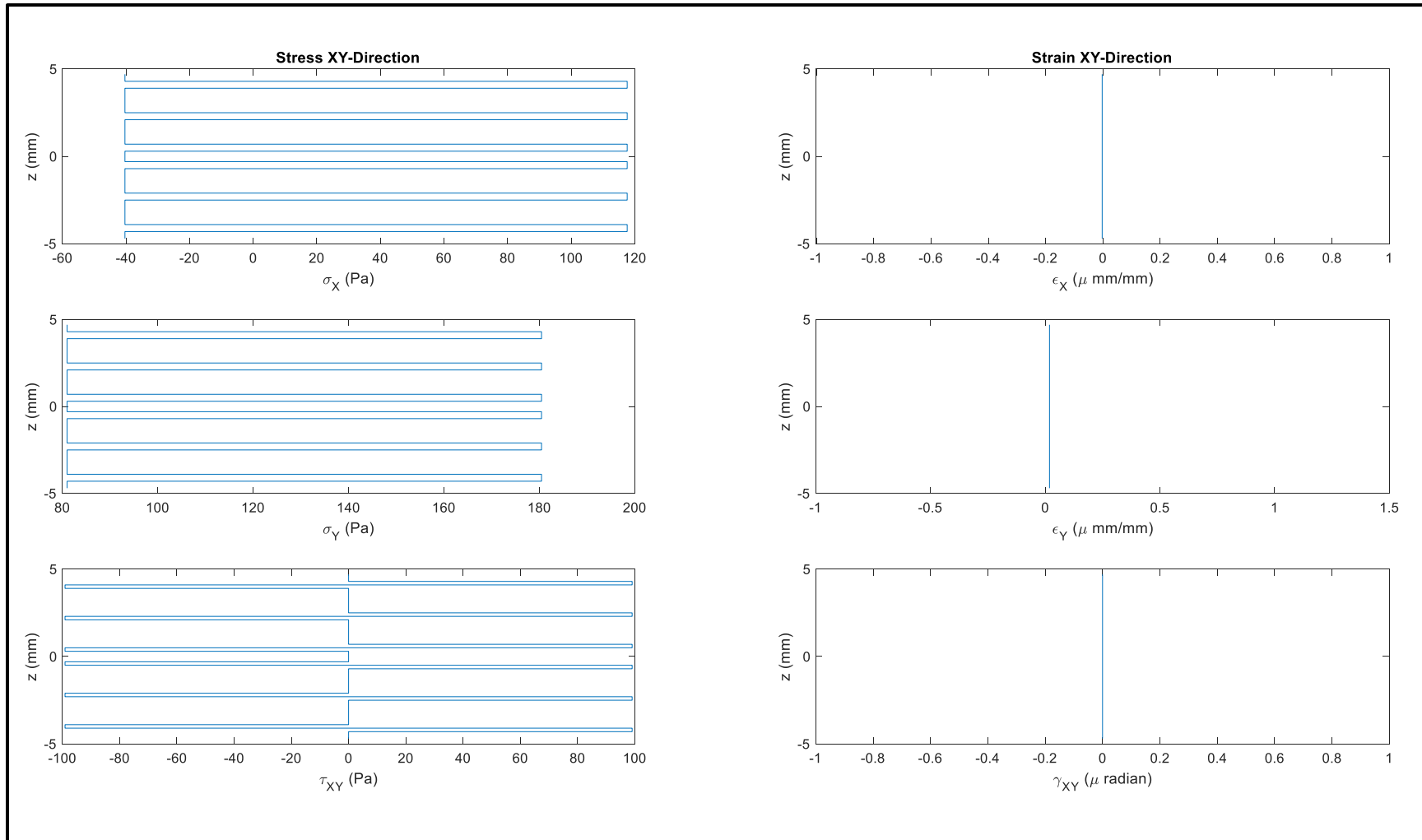
Stress-Strain Through-Thickness of Layup #1 in XY-Direction (+1 N_x Applied):



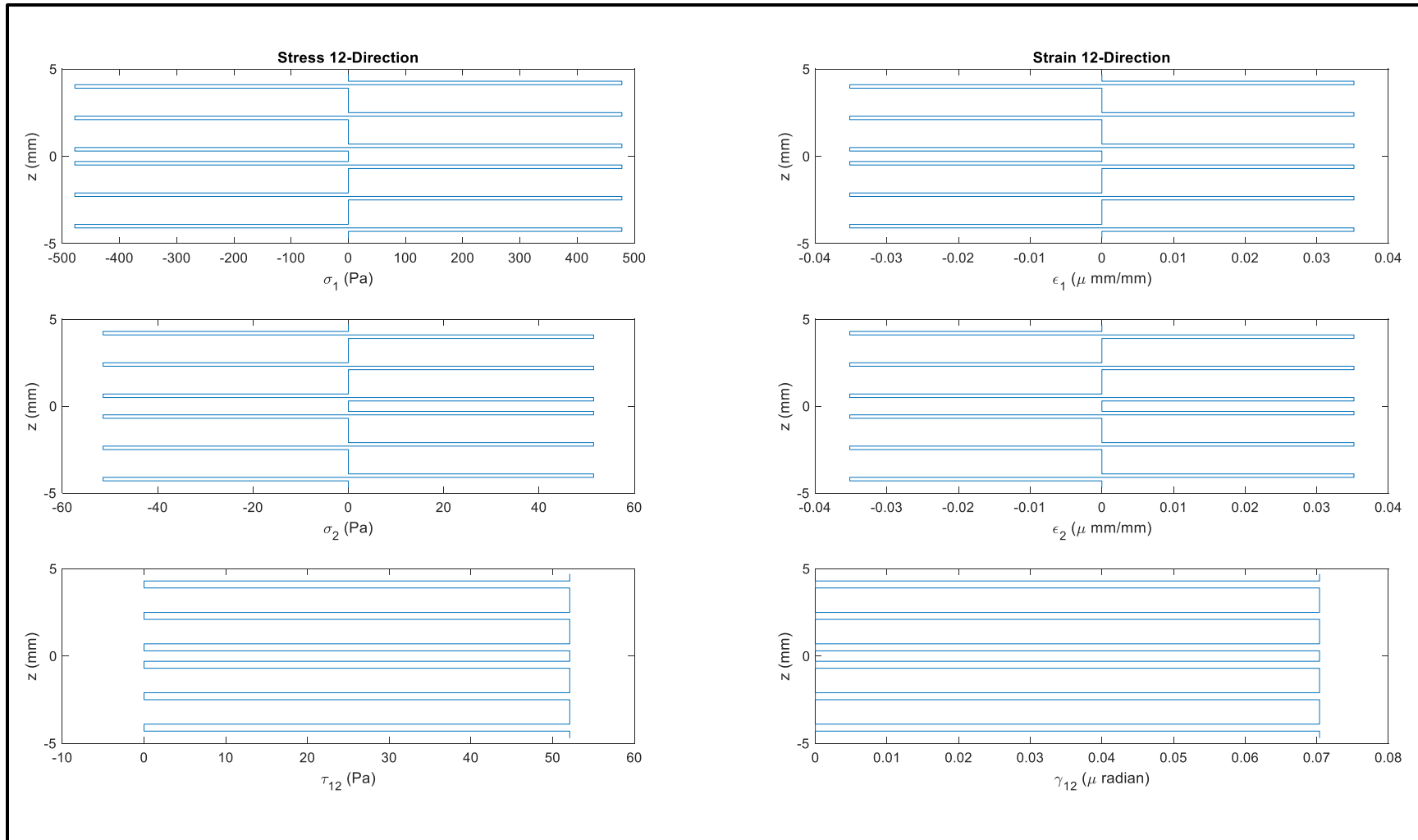
Stress-Strain Through-Thickness of Layup #1 in 12-Direction (+1 N_y Applied):



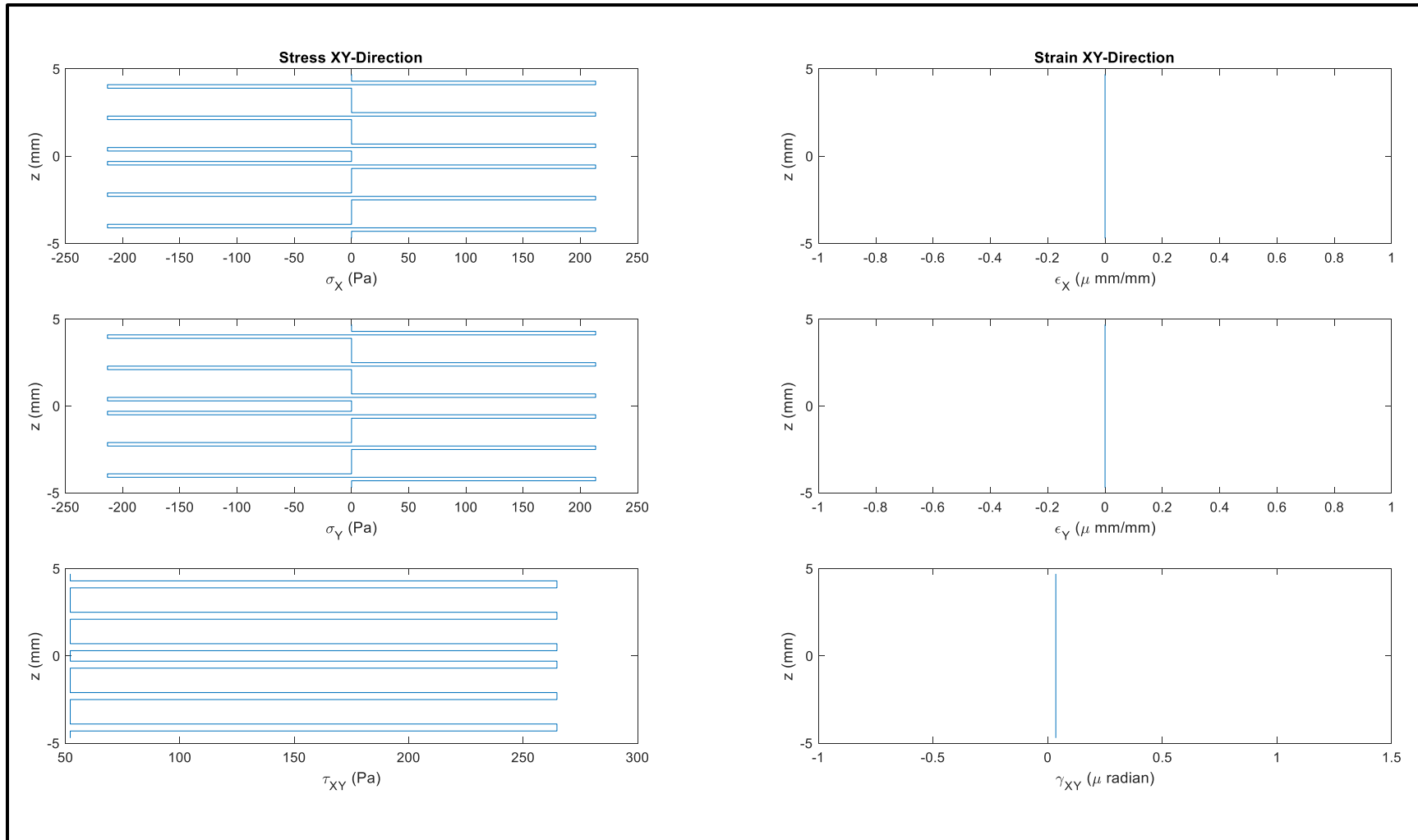
Stress-Strain Through-Thickness of Layup #1 in XY-Direction (+1 N_y Applied):



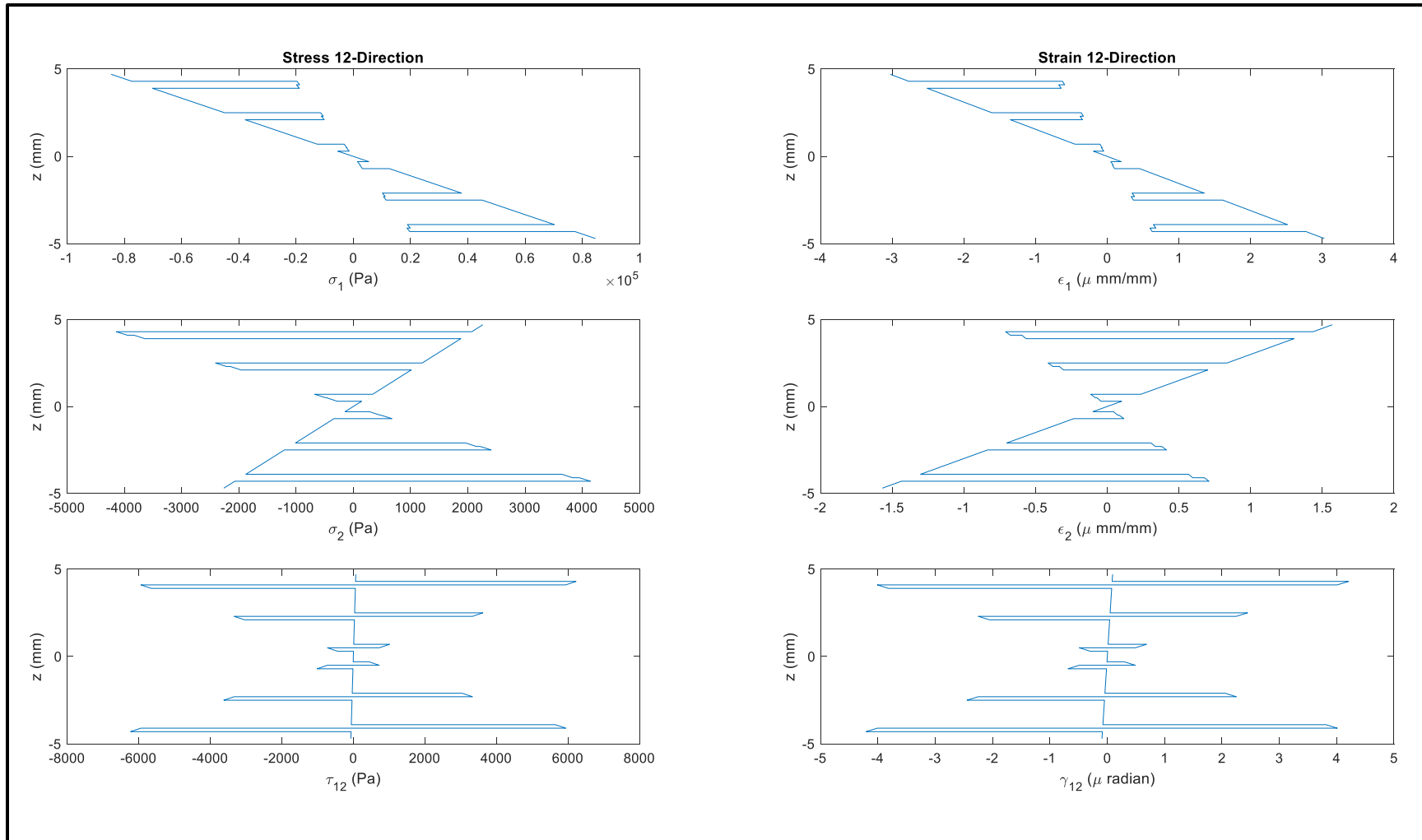
Stress-Strain Through-Thickness of Layup #1 in 12-Direction (+1 N_{xy} Applied):



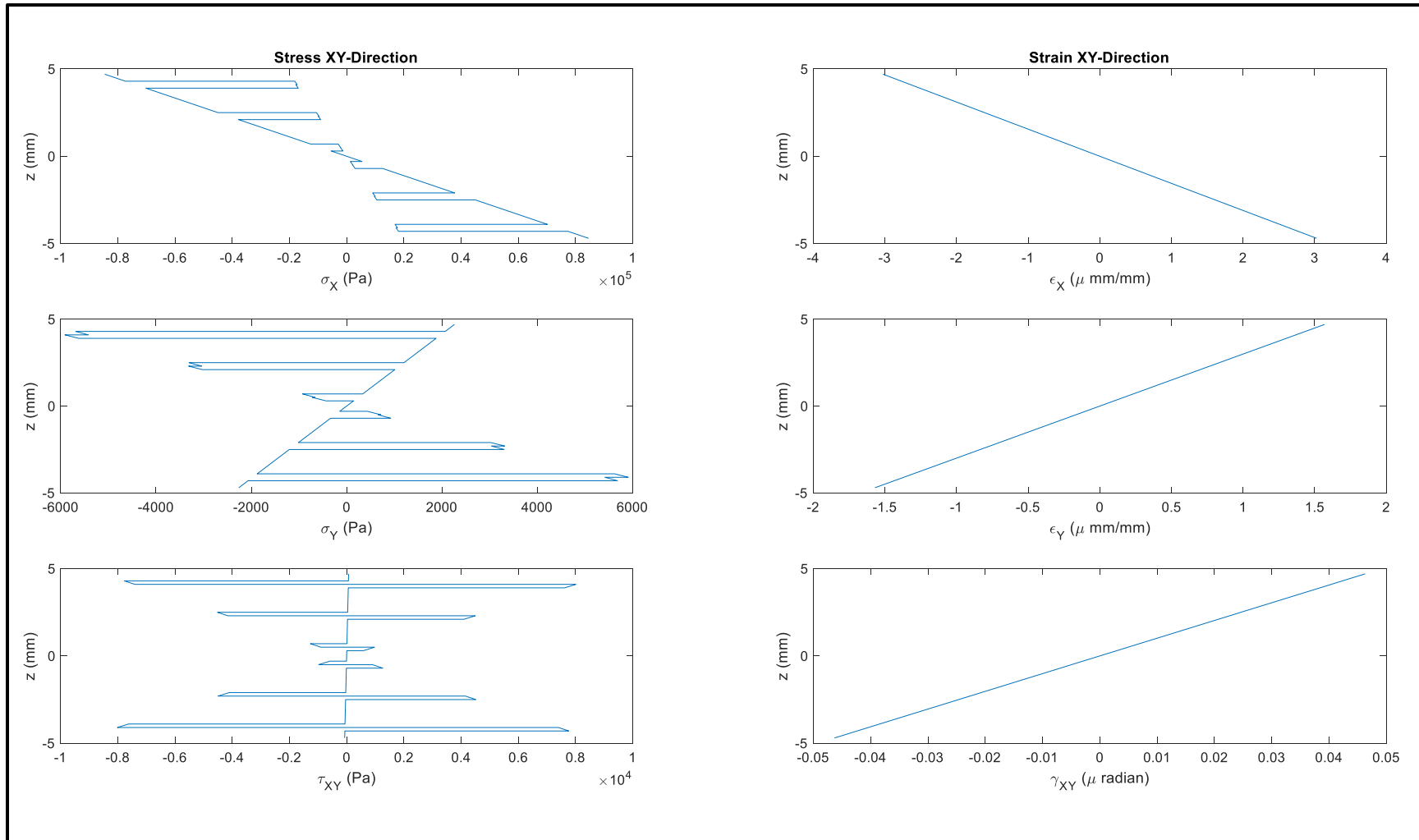
Stress-Strain Through-Thickness of Layup #1 in XY-Direction (+1 N_{xy} Applied):



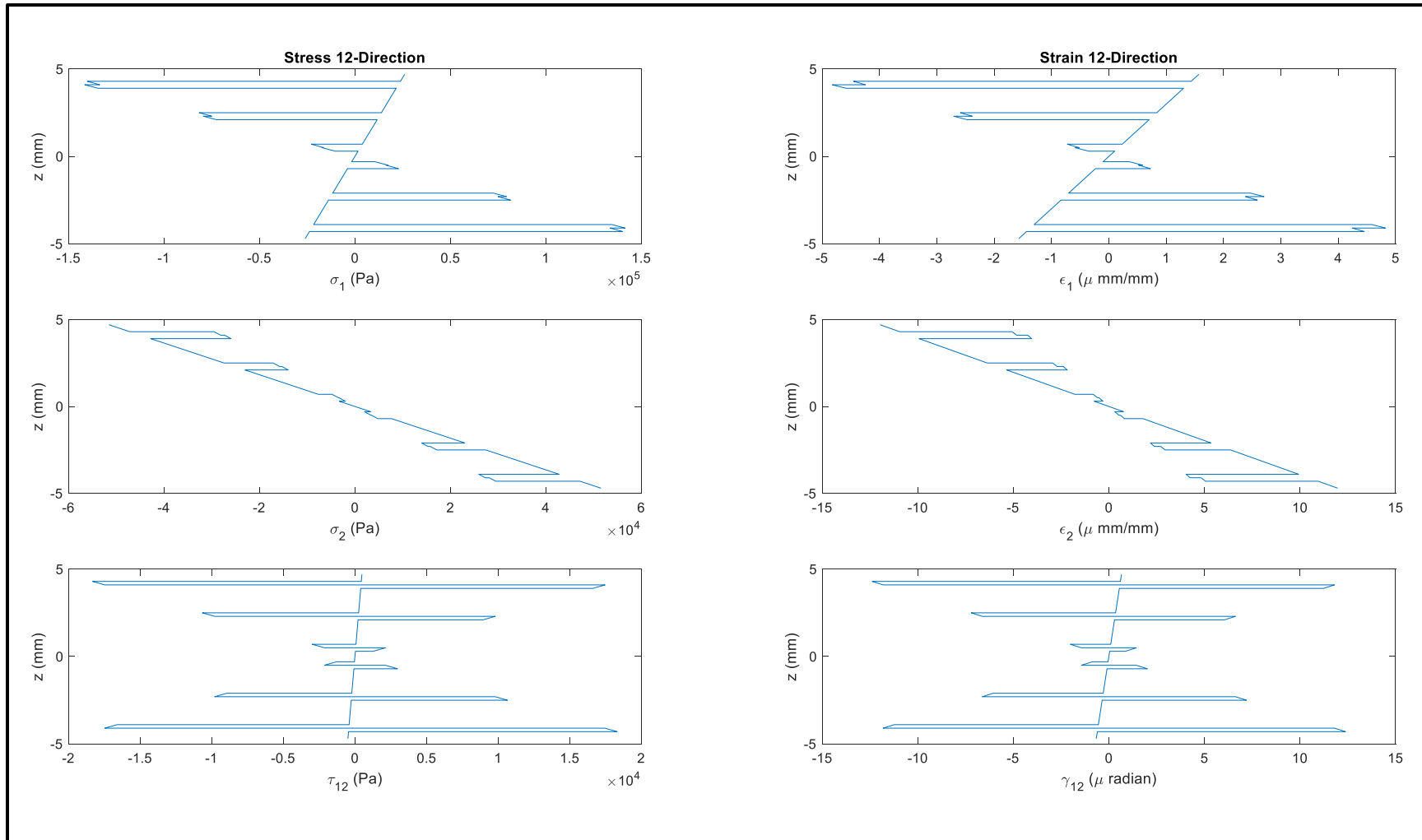
Stress-Strain Through-Thickness of Layup #1 in 12-Direction (+1 M_x Applied):



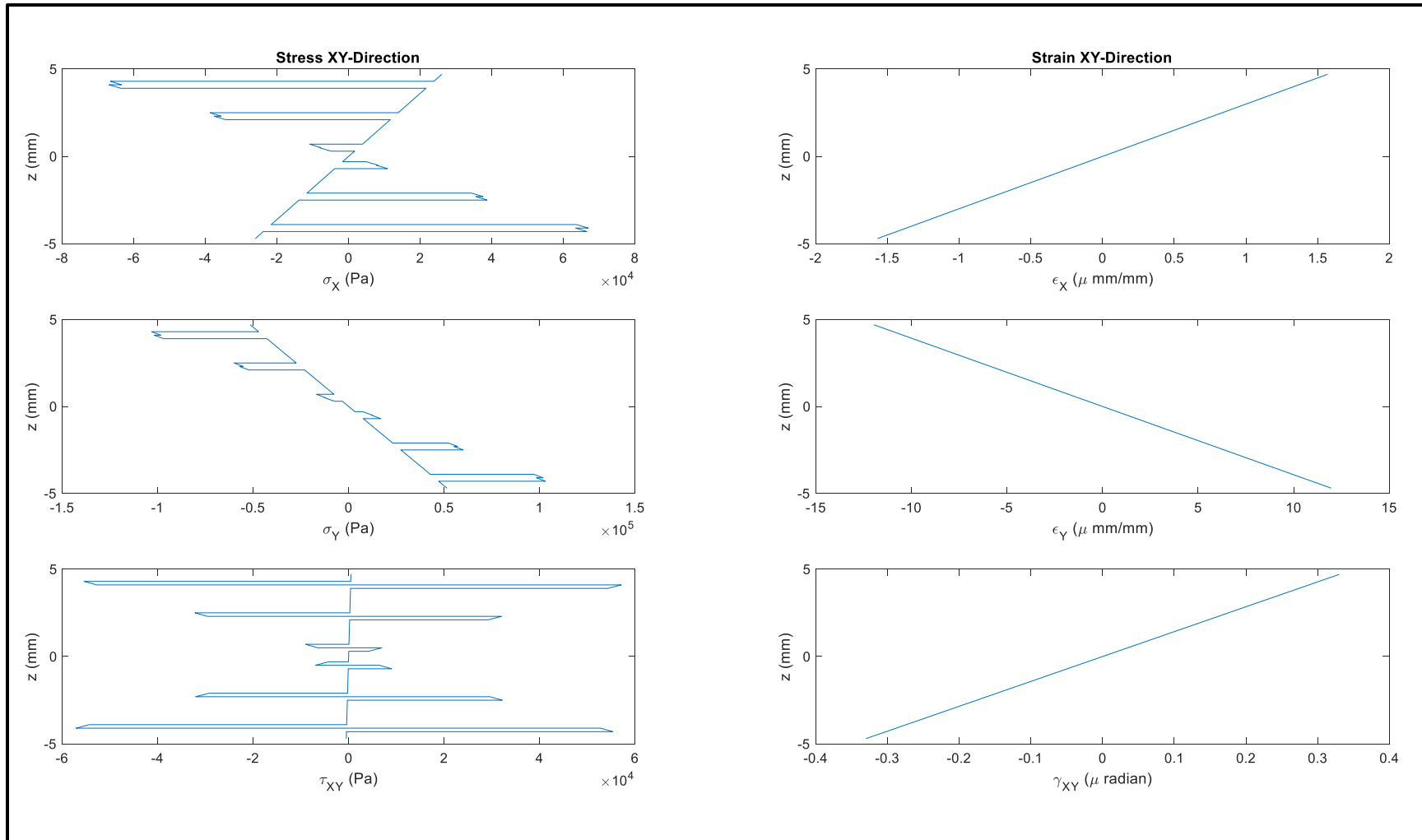
Stress-Strain Through-Thickness of Layup #1 in XY-Direction (+1 M_x Applied):



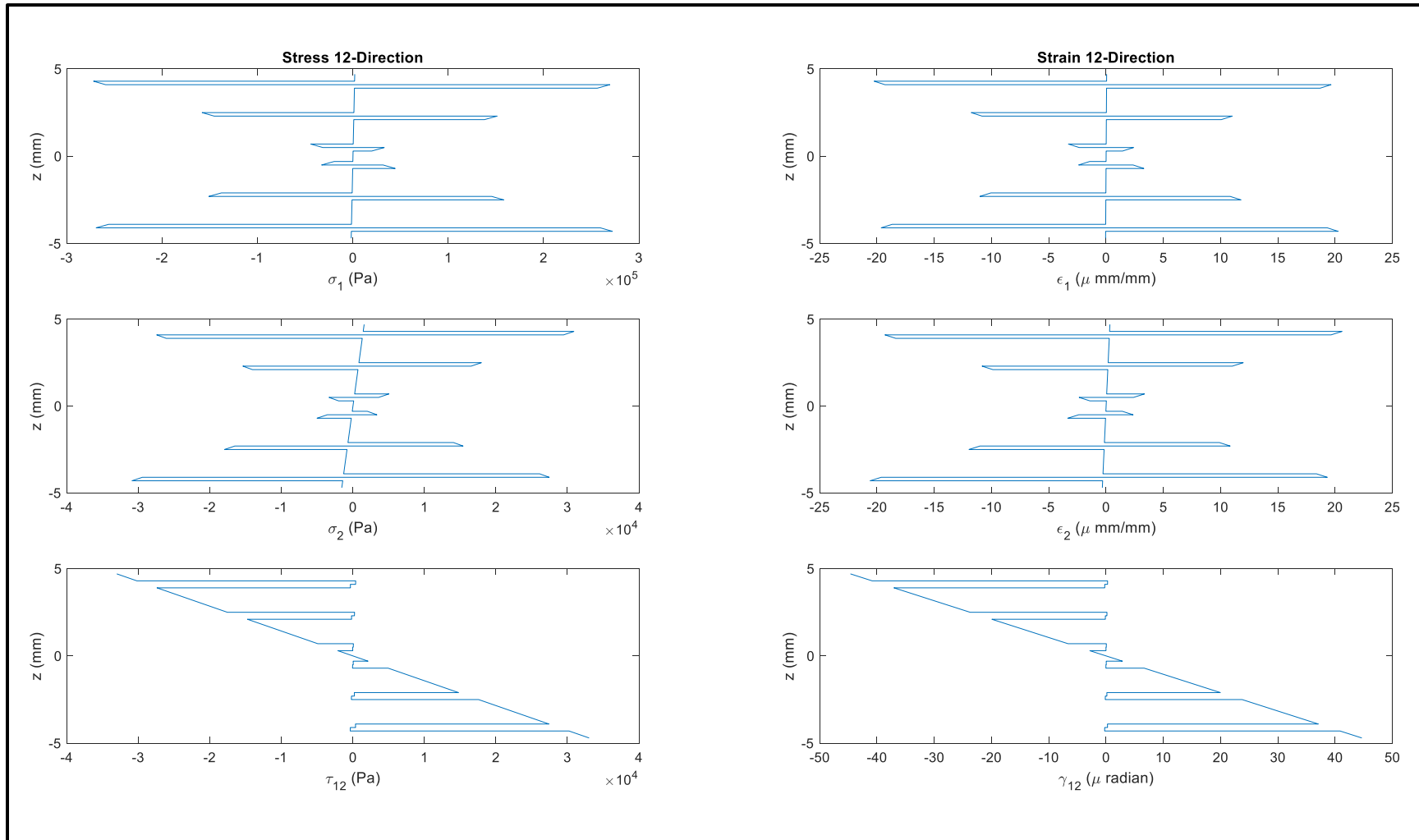
Stress-Strain Through-Thickness of Layup #1 in 12-Direction (+1 My Applied):



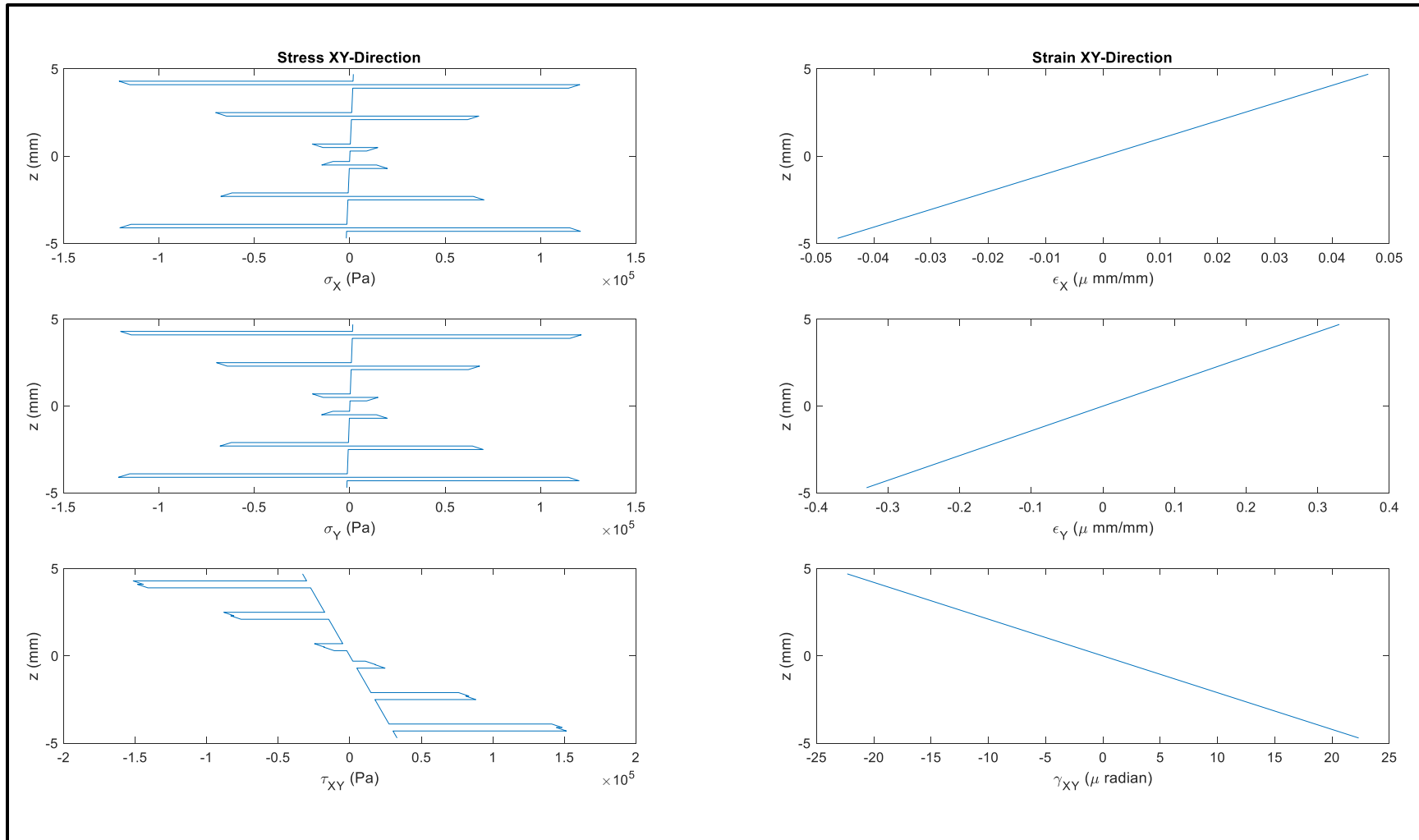
Stress-Strain Through-Thickness of Layup #1 in XY-Direction (+1 My Applied):



Stress-Strain Through-Thickness of Layup #1 in 12-Direction (+1 M_{xy} Applied):



Stress-Strain Through-Thickness of Layup #1 in XY-Direction (+1 M_{xy} Applied):



APPENDIX E:

```
function [A,NA_Bottom,NA_Top,Ix,Iy] = Single_Cgation_Geometry()
%Single_Cgation_Geometry, requires inputs from the user to input
%dimensioning of the corrugation cross section and calculates geometry
%properties

% -----
%                               INPUTS
% -----

TW = 12.34852; %Total Width (in)
TH = 4.71645; %Total Height (in)

ITW = 3.97394; %Inner Top Width (in)
IBW = 2.00035; %Inner Bottom Width (in)
IH = 4.34636; %Inner Height (in)

OTW = 1.97446; %Outer Top Width (in)
OBW = 3.98097; %Outer Bottom Width (in)
OH = 4.38645; %Outer Height (in)

plot_option = 0; %1 = plot section with NA Highlighted / 0 = no plot

% -----
%                               CALCULATIONS
% -----

% ----- AREA and NEUTRAL AXIS -----
% Solid Section: (rectangle)
AS = TW*TH; %Area of Solid Section (in^2)
yS = TH/2; %NA from Bottom of Solid Section (in)

% Outer Section Below Top Flange: (rectangle)
AOR = 2*(OTW*OH); %Area of Void, accounts for both sides (in^2)
yOR = OH/2; %NA from Bottom of Section (in)

% Outer Section Along Web: (triangle)
AOT = 2*(0.5*(OBW-OTW)*OH); %Area of Void, accounts for both sides (in^2)
yOT = (1/3)*OH; %NA from Bottom of Section (in)

% Inner Section Above Bottom Flange: (rectangle)
AIR = (2*IBW)*IH; %Area of Void, accounts for both sides (in^2)
yIR = (TH-IH)+(IH/2); %NA from Bottom of Section (in)

% Inner Section Along Web: (triangle)
AIT = 2*(0.5*(ITW-IBW)*IH); %Area of Void, accounts for both sides (in^2)
yIT = (TH-IH)+((2/3)*IH); %NA from Bottom of Section (in)

% Area of Actual Corrugated Section:
A = AS-(AOR+AOT+AIR+AIT);

% Neutral Axis of Actual Corrugated Section:
yA_sum = (AS*yS)-(AOR*yOR)-(AOT*yOT)-(AIR*yIR)-(AIT*yIT);
NA_Bottom = yA_sum/A; %NA from bottom of section (in)
NA_Top = TH-NA_Bottom; %NA from top of section (in)
```

```

% ----- MOMENT OF INERTIA -----
% (Ix about NA / Iy about Centroid X-Position)

% Solid Section: (rectangle)
SS_Ixp = (1/12)*TW*(TH^3);
SS_Ix = SS_Ixp+(AS*(abs(yS-NA_Bottom)^2));
SS_Iyp = (1/12)*(TW^3)*TH;
SS_Iy = SS_Iyp;

% Outer Void Below Flanges: (rectangle)
OR_Ixp = (1/12)*OTW*(OH^3);
OR_Ix = OR_Ixp+(AOR/2)*(abs(yOR-NA_Bottom)^2);
OR_Iyp = (1/12)*(OTW^3)*OH;
OR_Iy = OR_Iyp+(AOR/2)*(abs((TW/2)-(OTW/2))^2));

% Outer Void Along Web: (triangle)
OT_Ixp = (1/36)*(OBW-OTW)*(OH^3);
OT_Ix = OT_Ixp+(AOT/2)*(abs(yOT-NA_Bottom)^2);
OT_Iyp = (1/36)*((OBW-OTW)^3)*OH;
OT_Iy = OT_Iyp+(AOT/2)*(abs((TW/2)-(OTW+(OBW-OTW)/3))^2));

% Inner Void Above Bottom Flange: (rectangle)
IR_Ixp = (1/12)*(2*IBW)*(IH^3);
IR_Ix = IR_Ixp+(AIR*(abs(yIR-NA_Bottom)^2));
IR_Iyp = (1/12)*((2*IBW)^3)*IH;
IR_Iy = IR_Iyp;

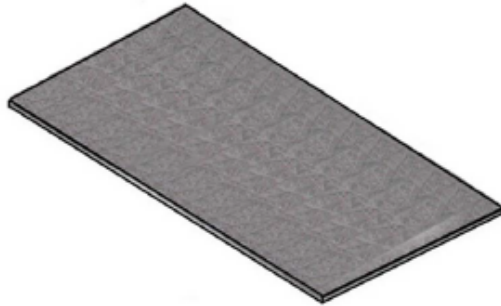
% Inner Void Along Web: (triangle)
IT_Ixp = (1/36)*(ITW-IBW)*(IH^3);
IT_Ix = IR_Ixp+(AIT/2)*(abs(yIT-NA_Bottom)^2);
IT_Iyp = (1/36)*((ITW-IBW)^3)*IH;
IT_Iy = IR_Iyp+(AIT/2)*(abs(IBW+((ITW-IBW)/3))^2));

% Moment of Inertia of Actual Corrugated Section:
Ix = SS_Ix-(2*OR_Ix)-(2*OT_Ix)-IR_Ix-(2*IT_Ix); % (in^4)
Iy = SS_Iy-(2*OR_Iy)-(2*OT_Iy)-IR_Iy-(2*IT_Iy); % (in^4)

end

```

APPENDIX F:



E-M 0015

Fiber Type: E-Glass
 Architecture: Random Mat
 Dry Thickness: 0.028 in. / 0.71 mm
 Total Weight: 13.50 oz/sq.yd / 458 g/sq.m



Roll Specifications			Fiber Architecture Data	
Roll Width:	Roll Weight:	Roll Length:	0 ° :	n/a
50 in / 1270 mm	145 lb / 66 kg	119 yd / 109 m	45 ° :	n/a
			90 ° :	n/a
			-45 ° :	n/a
			Chopped Mat :	13.50 oz/sq.yd / 458 g/sq.m

1: Packaging: box or bag.
 2: Weights do not include polyester stitching.

Laminated Properties

0 °

0 °

Laminate Weight (lb/sq.ft)	E-M 0015 Resin Infused	E-M 0015 Open Mold
Fiber	0.09	0.09
Resin	0.05	0.18
Total	0.14	0.28

Physical Properties

E-M 0015
Resin Infused

E-M 0015
Open Mold

Density (g/cc)	1.84	1.46
Fiber Content (% by Wt.)	66%	34%
Thickness (in)	0.015	0.036

Laminate Moduli		
(MSI)	E-M 0015 Resin Infused	E-M 0015 Open Mold
Ex	1.87	1.07
Ey	1.87	1.07
Gxy	0.73	0.41
Ex,flex.	1.78	1.02
Ey,flex.	1.78	1.02

Ultimate Stress		
(KSI)	E-M 0015 Resin Infused	E-M 0015 Open Mold
Long. Ten.	31	18
Long. Comp.	43	24
Trans. Ten.	31	18
Trans. Comp.	43	24
In-Plane Shear	17	9
Long. Flex.	46	26
Trans. Flex.	46	26

In-Plane Stiffness, "EA"		
10 ³ lb/in	E-M 0015 Resin Infused	E-M 0015 Open Mold
(EA)x	28	39
(EA)y	28	39
(GA)xy	11	15

Ultimate In-Plane Load		
lb/in	E-M 0015 Resin Infused	E-M 0015 Open Mold
Long. Ten.	455	638
Long. Comp.	633	886
Trans. Ten.	455	638
Trans. Comp.	633	886
In-Plane Shear	246	343

Notes:

- 1: Resin infused laminate made with a poly / vinyl ester resin blend.
- 2: Open mold laminate made with poly / vinyl ester resin blend.
- 3: All standard reinforcements should be infused with a flow aid or Vectorfusion® reinforcements.



3500 Lakewood Dr. Phenix City, AL 36867 tel. 334 291 7704 fax. 334 291 7743

REV: 5/3/2011

Disclaimer:

As a service to customers, Vectorply Corporation ("VP") may provide computer-generated predictions of the physical performance of a product using a reinforcement fabric produced by VP in combination with other materials or systems.

VP makes no warranty whatsoever as to the accuracy of any such predicted physical performance, and customer acknowledges that customer is solely responsible for determining the performance and fitness for a particular use of any product produced by customer utilizing a fabric or material produced or manufactured by VP. Specifications of reinforcements may change without notice.

APPENDIX G:

```

function [] = MultiCorr_MoI()
%MULTICORR_MOI, calculates the moment of inertia for the multicorrugation
%panel. Centroidal Calculation Origin assumed to be the bottom of the
%middle corrugation.

% -----
%                               INPUTS
% -----
%Full Panel
    Ch = 4.72; %Height of Corrugations (in)
    CP = 5.05; %Height of Full Panel (in)

%Corrugation #1 (Left Most)
    C1_Ix = 18.00; %Centroidal Moment of Inertia (in^4)
    C1_A = 5.92; %Cross-Sectional Area of Corrugation (in^2)
    C1_cx = -12.35; %Centroidal Location in X-Direction (in)
    C1_cy = 2.31; %Centroidal Location in Y-Direction (in)
%Corrugation #2 (Middle)
    C2_Ix = 18.00; %(in^4)
    C2_A = 5.92; %(in^2)
    C2_cx = 0; %(in)
    C2_cy = 2.31; %(in)
%Corrugation #3 (Right Most)
    C3_Ix = 18.00; %(in^4)
    C3_A = 5.92; %(in^2)
    C3_cx = 12.35; %(in)
    C3_cy = 2.31; %(in)
%Cover Plate
    B_Ix = 0.11; %(in^4)
    B_A = 12.41; %(in^2)
    B_cx = 0; %(in)
    B_cy = 4.886; %(in)

% -----
%                               CALCULATIONS
% -----
% Centroid of Spliced Plate (SP)
sum_A = C1_A + C2_A + C3_A + B_A; %(in^2)
sum_xA = (C1_cx*C1_A) + (C2_cx*C2_A) + (C3_cx*C3_A) + (B_cx*B_A); %(in^3)
sum_yA = (C1_cy*C1_A) + (C2_cy*C2_A) + (C3_cy*C3_A) + (B_cy*B_A); %(in^3)

x_loc = sum_xA/sum_A; %centroidal x-location from origin (in)
y_loc = sum_yA/sum_A; %centroidal y-location from origin (in)

% Moment of Inertia of Spliced Panel
C_dy = abs(y_loc-C1_cy); %(in)
B_dy = abs(y_loc-B_cy); %(in)

Ix_adj_C1 = C1_Ix + (C1_A*(C_dy^2)); %C1 contribution to the I of SP (in^4)
Ix_adj_C2 = C2_Ix + (C2_A*(C_dy^2)); %C2 contribution to the I of SP (in^4)
Ix_adj_C3 = C3_Ix + (C3_A*(C_dy^2)); %C3 contribution to the I of SP (in^4)
Ix_adj_B = B_Ix + (B_A*(B_dy^2)); %B contribution to the I of SP (in^4)

Ix_SP = Ix_adj_C1 + Ix_adj_C2 + Ix_adj_C3 + Ix_adj_B; %(in^4)

```

```

% Centroid Location from Top of Panel
Z2 = CP-y_loc; %(in)

% First Moment of Area of Spliced Panel
Q = B_A*(Z2-(B_cy-Ch)); %(in^3)

% -----
%                               DISPLAY
% -----
disp('<strong>Centrod Location of Spliced Plate: </strong>')
disp('  Origin: Bottom of Center Corrugation')
disp(['  Centrodial X-Location (in): ',num2str(x_loc,3)])
disp(['  Centrodial Y-Location (in): ',num2str(y_loc,3)])
disp('<strong>Centroid of Spliced Plate from Base: </strong>')
disp(['  Z1 (in): ',num2str(y_loc,3)])
disp('<strong>Centroid of Spliced Plate from Top: </strong>')
disp(['  Z2 (in): ',num2str(Z2,3)])
disp('<strong>Moment of Inertia of Spliced Plate: </strong>')
disp(['  Ix (in^4): ',num2str(Ix_SP,3)])
disp('<strong>First Moment of Area of Spliced Plate: </strong>')
disp(['  Q (in^3): ',num2str(Q,3)])

end

```

BIOGRAPHY OF THE AUTHOR

Jackman Mickiewicz was born in Portland, Maine on March 27, 1997. He was raised in South Portland, Maine and graduated from South Portland High School in 2015. Combining a passion for structures, math, and science he studied Civil Engineering at the University of Maine with a focus in structures. He was recognized for his academic success during his undergraduate studies by becoming a member of the engineering honor society Tau Beta Pi, where he acted as the Vice President of the University of Maine Chapter. He graduated with a Bachelor of Science degree in Civil and Environmental Engineering in 2019. Upon graduation he looked to further his education by returning to the University of Maine as a graduate student. His graduate research work was completed at the Advanced Structures and Composites Center (ASCC) and performed on behalf of the U.S. Army Engineer Research and Development Center (ERDC). He researched the feasibility of utilizing thermoplastic materials in reinforced concrete structures, primarily as a stay-in-place formwork for concrete decking. He is a candidate for a Master of Science degree in Civil Engineering from the University of Maine in May 2022.